Thesis

# Structure formation in warm dark matter cosmologies

PADUROIU, Sinziana

**Abstract**

The nature of dark matter constitutes one of the biggest questions in physics, cosmology and astronomy. This thesis explores dark matter hypothesized models, with a focus on warm dark matter models, from both theoretical and numerical simulations perspectives, with the purpose of constraining the dark matter particle candidates. Using high-resolution simulations I have studied the effect of warm dark matter properties on large-scale structure - structure formation and evolution and small-scale structure – internal properties of dark matter halos. The results show that structure formation is qualitatively different from the cold dark matter scenario and more complex than originally assumed – a hybrid between top-down and bottom-up mechanisms. Moreover, warm dark matter halos contain visible caustic and shells with shallower density profiles, depending on the free streaming length of the particles. Predictions that can be tested by observations are given. Technical aspects of warm dark matter simulations are being discussed as well.

**UNIVERSITÉ DE GENÈVE**
**Département d'astronomie**

**FACULTÉ DES SCIENCES**
**Professeur Daniel Pfenniger**

# Structure Formation in Warm Dark Matter Cosmologies

**THÈSE**

**présentée à la Faculté des sciences de l'Université de Genève pour obtenir le grade de Docteur ès sciences, mention astronomie et astrophysique**

**par**

**Sinziana PADUROIU**

**de**
**Roumanie (RO)**

**Thèse N° 4933**

**GENÈVE**
**2015**

UNIVERSITÉ
DE GENÈVE
FACULTÉ DES SCIENCES

*Doctorat ès sciences*
*Mention astronomie et astrophysique*

Thèse de *Madame Sinziana PADUROIU*

intitulée :

**"Structure Formation
in Warm Dark Matter Cosmologies"**

La Faculté des sciences, sur le préavis de Monsieur D. PFENNIGER, professeur associé et directeur de thèse (Département d'astronomie), Monsieur G. MEYLAN, professeur ordinaire (Institut de physique, Ecole Polytechnique Fédérale de Lausanne, Suisse), Monsieur Y. REVAS, docteur (Institut de physique, Ecole Polytechnique Fédérale de Lausanne, Suisse), Monsieur M. JOYCE, professeur (Université Pierre et Marie Curie, Paris, France) et Monsieur P. L. BIERMANN, professeur (Max Planck Institute for Radio Astronomy, Bonn, Germany), autorise l'impression de la présente thèse, sans exprimer d'opinion sur les propositions qui y sont énoncées.

Genève, le 4 mai 2016

**Thèse - 4933 -**

Le Doyen

N.B. - La thèse doit porter la déclaration précédente et remplir les conditions énumérées dans les "Informations relatives aux thèses de doctorat à l'Université de Genève".

**Défense de thèse: 02 Septembre 2015**

**Ce travail de thèse, a donné lieu à des publications dont la liste se trouve à la page 141.**

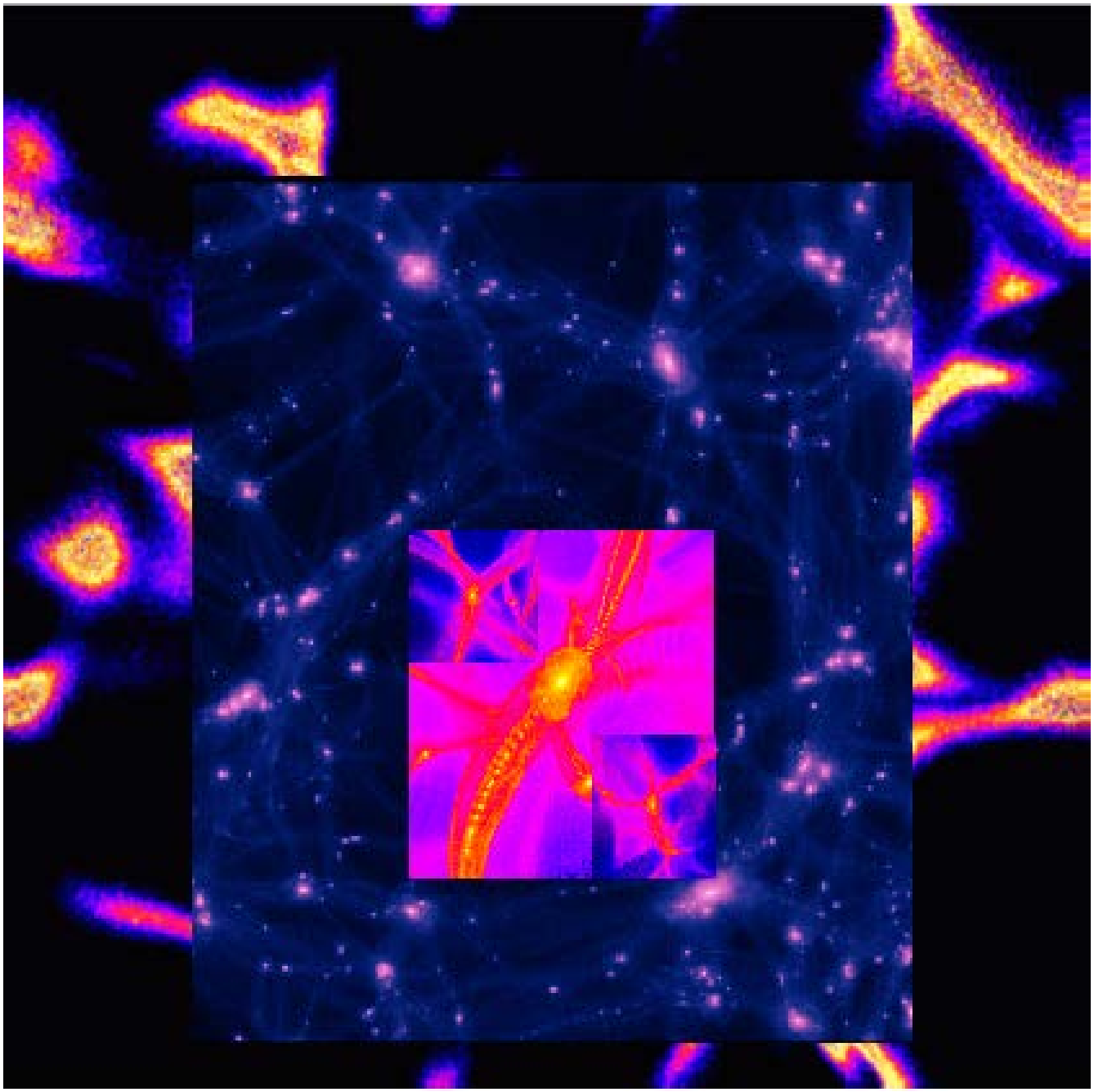

*Dedicated to my mother, Cecilia*

# Abstract


## Structure formation in warm dark matter cosmologies

The nature of dark matter constitutes one of the biggest questions in physics, astronomy and cosmology. Even though the cold dark matter model is successful in explaining many of the observations, it is still challenged by some phenomena that cannot be explained by this model alone. The warm dark matter model has been considered with an increased interest in the past few years, a viable alternative.

Computer simulations are a powerful tool for testing these models and making predictions that can be tested further with observations. In this work we focus on the implications that such models have on both large scale and small scale structure in the universe, by analyzing various $N$-body simulations that we have performed using different warm dark matter particles.

When comparing warm dark matter simulations with cold dark matter ones, we find that the formation and evolution of structures is qualitatively different in the two models. These differences come from the suppression of the power at small scales and presence of the velocity dispersion, which are properties of the warm dark matter particle candidates considered. The warm dark matter simulations performed show that structure formation is more complex than in the cold dark matter ones with different stages of evolution.

These intrinsic properties of warm dark matter particles are stretching their influence to the small scales - the internal structure of halos being different from what one would expect in the cold dark matter case. Analyzing high resolution simulations, we see that warm dark matter halos have visible caustics and shells. Depending on the free streaming length of the particle, the density profiles of halos are shallower than the cold dark matter density profiles. This is, however, not enough to explain the large cores observed in galaxies, pointing to a missing ingredient in our simulations that can either be the presence of baryonic processes or other quantum properties of warm dark matter particles.

From our results we give some predictions that can be tested by observations. Besides the results from cosmological simulations, we discuss few theoretical considerations that need to be taken into account when addressing the behavior of some warm dark matter particle candidates. Technical aspects of warm dark matter simulations are being discussed as well.

**Keywords**: cosmology, astrophysics, dark matter, numerical simulations, structure formation, internal structure of halos, density profiles

# Résumé

## La formation des structures dans matière sombre tiède comologies

La nature de la matière sombre constitue l'une des plus grandes questions de la physique, de l'astronomie et de la cosmologie. Même si le modèle de matière sombre froide avait expliqué avec succès nombreux observations, il est encore contesté par certains phénomènes qui ne peuvent pas être expliqués par ce modèle seul. Le modèle de la matière sombre tiède a été considéré avec un intérêt accru dans les dernières années, une alternative viable.

Les simulations cosmologiques sont un outil important pour tester ces modèles et pour faire des prédictions qui peuvent encore plus être testées avec les observations. En réalisant diverses simulations $N$-corps de différents modèles de matière sombre tiède, dans ce travail, nous nous concentrons sur les implications qu'un tel modèle a sur structures à grande aussi que à petite échelle de l'univers.

En comparant des simulations de matière sombre tiède avec celles de matière sombre froide, nous constatons que la formation et l'évolution des structures sont qualitativement différentes dans les deux modèles. Ces différences vient de la suppression de la puissance à petite échelle et de la présence de dispersion des vitesses, qui sont propriétées des particles candidats considérées. Nous constatons que dans les simulations de matière sombre tiède, la formation de la structure est plus complexe que dans celles de matière sombre froide, avec différents stades d'évolution.

Ces propriétés intrinsèques des particules de matière sombre tiède se étirent leur influence pour les petites échelles, la structure interne de halos étant différente que l'on pourrait prévoir dans le cas de matière sombre froide. En analysant des simulations à haute résolution, nous constatons que halos de matière sombre tiède ont caustiques et coquilles visibles. Selon la longueur de libre parcours de la particule, les profils de densité des halos sont moins piqués que les profils de densité de matière noire froide. Nous trouvons que cela ne suffit pas à expliquer les grands coeurs observées dans les galaxies, pointant vers un ingrédient manquant dans nos simulations, qui peut

être soit la présence de processus baryonique soit d'autres propriétés quantiques des particules de matière sombre tiède.

De nos résultats, nous donnons quelques prédictions qui peuvent être testées avec les observations. Outre les résultats des simulations cosmologiques, nous discutons quelques considérations théoriques qui doivent être pris en compte lorsque nous abordons le comportement de certains candidats de la matière sombre tiède. Les aspects techniques de simulations de matière sombre tiède sont aussi discutés.

**Mots clés**: cosmologie, astrophysique, la matière noire, simulations numériques, la formation de la structure, la structure interne de halos, les profils de densité

# Contents

Chapter 1

# Introduction

## 1.1 General Context

In the last century, the enormous development in physics and astronomy brought us to what one may call a fatalistic view of the universe. In almost five billion years from now the Sun will die and so will the Earth. The Andromeda galaxy will be colliding with the Milky Way galaxy. The universe may expand forever or gravity may eventually reverse this and the universe will end in a giant implosion. And yet, scientists are trying to explain the unseen and unknown.

The fact that most of the matter in the universe is unseen and of unknown origin is one of the biggest puzzles in our view of the universe. Many models have been theorized in the attempt to explain the dark side of the universe, some of them challenging our understanding of even the most fundamental concepts in physics, like gravity. That dark matter exists is now considered a fact by the majority of the scientific community. What dark matter is actually made of is a question that has yet to be answered. Agreeing that most likely non-baryonic particles are the major constituent, the nature of these particles has yet to be revealed.

In the last years, two models have been distinguished as the most promising ones. One is the cold dark matter model, with neutralino and axions as the center stage candidates, which still claims supremacy among the other models. The other is the warm dark matter model, with sterile neutrinos as the most favored candidate, which may explain many of the observational challenges that cold dark matter model presently faces.

This work focuses on the warm dark matter model and its effects and implications on the formation and evolution of structure in the universe. Bridging theory and observations, the new supercomputer technology allows the modelling and visualisation of simulated dark matter distributions. These simulations create rough replica universes using different dark matter models, which are then compared with the observed distribution of galaxies. While the main part of this study is based on results from such numerical simulations, theoretical considerations and predic-

tions are also addressed together with possible implications for detection and tests for observations.

Katherine Freese, in her book The Cosmic Cocktail: Three Parts Dark Matter, expresses her confidence that we will solve the dark matter mystery very soon. Assuming that no contribution is negligible, the following work is my humble part.

## 1.2 Thesis Outline

In Chapter 2 I will briefly present the currently adopted cosmological model and the dark matter particle candidates, focusing on the most promising ones from cold dark matter and warm dark matter models. I will discuss some of the challenges that the cold dark matter model currently faces. Since detection is the ultimate test for any dark matter model, I will summarize some detection techniques and the limits on the dark matter candidates arising from different experiments.

Chapter 3 addresses the influence of warm dark matter on structure formation. After presenting some theoretical assumptions made in describing the properties and behaviour of different warm dark matter candidates, I will focus on the signature imprinted by these particles on the structure formation in $N$-body simulations. The results will be compared with those from cold dark matter simulations.

Going from the early structure formation, in Chapter 4 I will focus on the small scale structure, mainly the internal structure of halos. Several points will be discussed, from features present in warm dark matter simulation halos like shells and caustics to the density and phase space density profiles. Our results will be compared with both cold dark matter simulations and observations.

Since the modelling of dark matter particles is in general not without its shortcomings, in Chapter 5 I will present some of the challenges that appear in warm dark matter simulations and discuss some of the techniques used.

Our findings and conclusions will be summarized in Chapter 6 together with future work prospects.

Chapter 2

# Dark Matter Models

Want a trouble-free future?
Why did you show up
in spacetime if
you didn't want trouble?

RICHARD BACH, *Messiah's Handbook*

## 2.1 A brief history of dark matter

It starts with a Big Bang - a 'Hot' one. The generally embraced model for how the universe formed is that it began in a very condensed state and rapidly expanded. The term was ironically coined by Hoyle, as a put-down for the theory of Lemaître, who believed that the universe was born from a 'primeval atom' (Lemaître 1931a). The theory was considered outrageous back then, but is now supported by many discoveries in physics and cosmology, such as the microwave cosmic background. The Big Bang, however, apart from providing the seed, is not sufficient to explain the current state of affairs as far as our universe, the observable one at least, is concerned - its existence and its evolution. Enter inflation, the exponential expansion of space just after the Big Bang, which carries the information from the beginning. But this is not enough either. One needs an explanation for the accelerating expansion of the universe: enter dark energy. Still, there is another crucial ingredient missing in this picture, mainly, a lot of matter.

Historically, however, these realizations did not happen by solving one aspect and moving on to the next challenge, nor did they follow this order chronologically. They were rather the result of solving problems that were considered unconnected and just happened to fit together.

Before the Big Bang theories were even considered, many pieces of evidence for the expansion were creeping in. Albert Einstein resisted this notion, although he had previously introduced what

is now called the cosmological constant to accommodate his general theory of relativity into the favored view of a steady state universe that is eternal and essentially unchanged, except for the local occasional cyclic birth and death of stars.

After Edwin Hubble (Hubble 1926) measured the redshift of galaxies and realized that they are moving away from us and from each other, the idea of expansion quickly became mainstream[1], while the cosmological constant simply became negligible.

In fact, it was Lemaître who in a paper published in French (Lemaître 1927) first explained the cosmological redshifts by the constant expansion of space and provided the relation of proportionality between the apparent recession velocity and the distance, known today as Hubble's law (Hubble 1929). This part, however, got lost in translation, being omitted from his 1931 paper (Lemaître 1931b) published in English[2].

A few years later, the Swiss astronomer Fritz Zwicky, while studying clusters of galaxies like the Coma cluster calculated from the velocities of the galaxies inside, the gravitational force that acts on them, which allowed him to estimate the total mass of the cluster. This mass was much larger than the mass inferred from the luminous objects inside, meaning there must be matter - a lot of it - that we just cannot see[3] (Zwicky 1933, 1937). Zwicky called this missing matter *dunkle Materie*- dark matter, but being viewed as too unconventional an idea it was not taken seriously and was ignored.

It took until the more unconventional late 60s for the dark matter conundrum to be revived. One successful attempt was made by Vera Rubin, who studied the rotation of spiral galaxies (Rubin & Ford 1970; Rubin, Ford & Thonnard 1980), and realized that the gravity exerted by the observed matter would not be able to hold the galaxies together. They just rotate too fast, requiring by her calculation[4] six times more matter to keep them from flying apart. To give a general idea, the matter close to the center of the galaxy rotates almost like a rigid rotator, like a vinyl record. As we move further away from the center, the rotational velocity of the matter is predicted to drop at a constant, proportional rate. Moving even further out, since the matter at the outskirts of the galaxies is less and less bound, we would expect this velocity to drop to zero. On the contrary, what has been observed differs from this expectation. It has been shown that the rotational velocity remains constant with the distance to the center, giving a flat rotation curve, as if there is some unseen matter keeping it together. That was enough to bring the dark matter back to the attention of the scientific community.

About the same time, the cosmological constant was to be revived. Beatrice Tinsley concluded from her study of the lifecycle of galaxies that the cosmological constant could not be zero. This

[1] Hoyle was one of the exceptions, vehemently opposing it.

[2] For a recent epistemological analysis of these developments and Lemaître's often uncredited contribution see Luminet (2015).

[3] In 1932, before Zwicky's results, the Dutch astronomer Jan Hendrik Oort concluded, after measuring the motion of the stars in the Milky Way, that the mass of the galactic plane must be higher than the mass of the observed matter.

[4] now known to be an underestimation

was discussed in 1975 in Gunn & Tinsley (1975). By this time, the cosmic microwave background had been discovered and the Big Bang model became acceptable.

It was only in 1980 that the cosmic inflation theory was proposed. The idea, as formulated by Alan Guth (Guth 1981), was that the universe went through a period of accelerated exponential expansion during its first $10^{-35}$ second of life. Many other models of inflation have been proposed since then (Linde 1982; Albert & Steinhardt 1982; Linde 1983). In the meantime, the dark matter search had gained momentum and shortly after the cosmic inflation theory, the cold dark matter model was proposed (Bond, Szalay & Turner 1982; Peebles 1982; Blumenthal et al. 1984).

Fast forwarding, the research done in the dark matter field is impressive, putting it in the top problems to be solved in physics. More than 500,000 scientific papers have now been published on dark matter - 70% of them in the last ten years.

## 2.2 The classical cosmological model

The first attempts to create a consistent cosmological model for the universe were based on the simplest assumptions regarding the large scale matter distribution. The universe was assumed to be homogeneous and isotropic. Einstein's equation is the first pillar of standard cosmology:

$$R_{\mu\nu} - \frac{1}{2} g_{\mu\nu} R = -\frac{8\pi G_N}{c^4} T_{\mu\nu} + \Lambda g_{\mu\nu}, \tag{2.1}$$

where $R_{\mu\nu}$ and $R$ are the Ricci tensor and scalar, $g_{\mu\nu}$ is the metric tensor, $G_N$ is Newton's constant, $T_{\mu\nu}$ is the energy-momentum tensor, and $\Lambda$ is the so-called cosmological constant (as expressed in Bertone, Hooper & Silk (2005), e.g.).

The second pillar is the Robertson-Walker metric. Indeed, the properties of isotropy and homogeneity imply a certain form of the metric where the line element can be written (Bertone, Hooper & Silk 2005) as follows:

$$ds^2 = -c^2 \mathrm{d}t^2 + a(t)^2 \left( \frac{\mathrm{d}r^2}{1 - kr^2} + r^2 \mathrm{d}\Omega^2 \right), \tag{2.2}$$

where $a(t)$ is the scale factor and the constant $k$, which describes the spatial curvature, can take the values $k = -1,\ 0,\ +1$. For the simplest case, $k = 0$, the spatial part of Eq. 2.2 reduces to the metric of a flat Euclidean space.

Solving the Einstein equations with this metric, one of its components leads to the Friedmann equations

$$\left( \frac{\dot{a}}{a} \right)^2 + \frac{k}{a^2} = \frac{8\pi G_N}{3} \rho_{tot}, \tag{2.3}$$

$$\frac{\ddot{a}}{a} = -\frac{4\pi G_N}{3} \left( \rho_{tot} + \frac{3p}{c^2} \right), \tag{2.4}$$

where $\rho_{tot}$ is the total average energy density of the universe.

The Hubble parameter, which describes the expansion rate of the universe is

$$H(t) = \frac{\dot{a}(t)}{a(t)} \quad . \tag{2.5}$$

We see from Eq. 2.3 that for a flat universe, the energy density equals the critical density, $\rho_c$:

$$\rho_c \equiv \frac{3H^2}{8\pi G_N} \quad . \tag{2.6}$$

In general, the abundance of a substance in the Universe (matter, radiation or vacuum energy), is expressed in units of $\rho_c$ (Bertone, Hooper & Silk 2005, e.g.). This is defined as

$$\Omega_i \equiv \frac{\rho_i}{\rho_c} \quad . \tag{2.7}$$

for a substance of species $i$ and density $\rho_i$, or

$$\Omega = \sum_i \Omega_i \equiv \sum_i \frac{\rho_i}{\rho_c}, \tag{2.8}$$

The Friedmann equation (Eq. 2.3) can be written

$$\Omega - 1 = \frac{k}{H^2 a^2} \, . \tag{2.9}$$

The sign of $k$ is thus determined by whether $\Omega$ is greater than, equal to, or less than one.

## 2.3 The new cosmological model

Over the past three decades a new, improved standard cosmology has been developed, incorporating the highly successful standard hot big-bang cosmology and extending our understanding of the Universe to times as early as $10^{-32}$ sec, when the largest structures in the Universe were still subatomic quantum fluctuations (Turner 2002a,b; Boi 2011; Cirkovic 2012).

This New Standard Cosmology is characterized by

- A flat, accelerating Universe
- An early period of rapid expansion - inflation
- Density inhomogeneities produced from quantum fluctuations during inflation
- Composition: $\sim 2/3$rds dark energy, $\sim 1/3$rd dark matter, $\sim 1/200$th bright stars
- Matter content: $\sim 29\%$ cold dark matter, $\sim 4\%$ baryons, $\sim 0.3\%$ neutrinos

The acoustic peaks in the cosmic microwave background (CMB) power spectrum measured by WMAP and Planck experiments and the evidence for a nearly scale-invariant spectrum of primeval density perturbations are in agreement with what is predicted by inflation (Turner 2001). The agreement of the Big Bang nucleosynthesis (BBN) determination of the baryon density (from D/H measurements) with recent CMB anisotropy measurements predicts a small baryon density with respect to the total matter density (Turner 2001, 2002b).

In Table. 2.1 we show the latest estimations of the cosmological parameters from the Planck Collaboration (Planck Collaboration et al. 2015).

Table 2.1: Parameter 68% confidence limits for model from Planck CMB power spectra, in combination with lensing reconstruction and external data, from Planck Collaboration et al. (2015)

| | TT+lowP | TT+lowP+lensing | TT+lowP+lensing+ext |
|---|---|---|---|
| Parameter | 68% | 68% | 68% |
| $\Omega_{\rm b}h^2$ | 0.02222±0.00023 | 0.02226±0.00023 | 0.02227±0.00020 |
| $\Omega_{\rm c}h^2$ | 0.1197±0.0022 | 0.1186±0.0020 | 0.1184±0.0012 |
| $100\theta_{\rm MC}$ | 1.04085±0.00047 | 1.04103±0.00046 | 1.04106±0.00041 |
| $\tau$ | 0.078±0.019 | 0.066±0.016 | 0.067±0.013 |
| $\ln(10^{10}A_{\rm s})$ | 3.089±0.036 | 3.062±0.029 | 3.064±0.024 |
| $n_{\rm s}$ | 0.9655±0.0062 | 0.9677±0.0060 | 0.9681±0.0044 |
| $H_0$ | 67.31±0.96 | 67.81±0.92 | 67.90±0.55 |
| $\Omega_\Lambda$ | 0.685±0.013 | 0.692±0.012 | 0.6935±0.0072 |
| $\Omega_{\rm m}$ | 0.315±0.013 | 0.308±0.012 | 0.3065±0.0072 |
| $\Omega_{\rm m}h^2$ | 0.1426±0.0020 | 0.1415±0.0019 | 0.1413±0.0011 |
| $\Omega_{\rm m}h^3$ | 0.09597±0.00045 | 0.09591±0.00045 | 0.09593±0.00045 |
| $\sigma_8$ | 0.829±0.014 | 0.8149±0.0093 | 0.8154±0.0090 |
| $\sigma_8\Omega_{\rm m}^{0.5}$ | 0.466±0.013 | 0.4521±0.0088 | 0.4514±0.0066 |
| $\sigma_8\Omega_{\rm m}^{0.25}$ | 0.621±0.013 | 0.6069±0.0076 | 0.6066±0.0070 |
| $z_{\rm re}$ | $9.9^{+1.8}_{-1.6}$ | $8.8^{+1.7}_{-1.4}$ | $8.9^{+1.3}_{-1.2}$ |
| $10^9A_{\rm s}$ | $2.198^{+0.076}_{-0.085}$ | 2.139±0.063 | 2.143±0.051 |
| $10^9A_{\rm s}e^{-2\tau}$ | 1.880±0.014 | 1.874±0.013 | 1.873±0.011 |
| Age/Gyr | 13.813±0.038 | 13.799±0.038 | 13.796±0.029 |
| $z_*$ | 1090.09±0.42 | 1089.94±0.42 | 1089.90±0.30 |
| $r_*$ | 144.61±0.49 | 144.89±0.44 | 144.93±0.30 |
| $100\theta_*$ | 1.04105±0.00046 | 1.04122±0.00045 | 1.04126±0.00041 |
| $z_{\rm drag}$ | 1059.57±0.46 | 1059.57±0.47 | 1059.60±0.44 |
| $r_{\rm drag}$ | 147.33±0.49 | 147.60±0.43 | 147.63±0.32 |
| $k_{\rm D}$ | 0.14050±0.00052 | 0.14024±0.00047 | 0.14022±0.00042 |
| $z_{\rm eq}$ | 3393±49 | 3365±44 | 3361±27 |
| $k_{\rm eq}$ | 0.01035±0.00015 | 0.01027±0.00014 | 0.010258±0.000083 |
| $100\theta_{\rm s,eq}$ | 0.4502±0.0047 | 0.4529±0.0044 | 0.4533±0.0026 |

## 2.4 Dark Matter Candidates

Dark matter does not emit light, in fact no detectable radiation. It does not absorb or diffuse light. This means that it cannot consist of dust. We know that there exists a considerable quantity of dust in our galaxy, because the light is scattered and attenuated by the intermediate clouds. But if these particles were enough to account for the entire dark matter content, they will prevent the light emitted by any large distance star from reaching us.

Other 'ordinary matter' candidates include stars that were not quite massive enough to start burning and become luminous - these are called 'Brown Dwarfs' and can be revealed by gravitational lensing. If a star like this passes in front of a brighter star, then the gravity of the small star will focus light, so that the other star would appear larger. But these phenomena are rather rare and may have other explanations. So the observations show that the number of brown dwarfs is not so large to represent the whole predicted dark matter. The EROS (Experience de Recherche d'Objets Sombres) Collaboration excludes that microlensing objects of masses in the range $5 \times 10^{-8} - 10^{-2}$ $M_\odot$ may make up more than 20% of the halo density, whereas the MACHO (Massive Astrophysical Compact Halo Objects) Collaboration delimits a likelihood contour (at 95% C.L.) for masses $\sim 10^{-1} - 1\, M_\odot$.

The non-baryonic particles are therefore the best candidates and particle physics offers a large variety of such hypothesized particles that could exist in the universe and could survive from the Big-Bang in a number sufficiently large to bring a significant contribution to $\Omega$. These heavy but chargeless particles could cross the Earth like neutrinos, but they are very hard to detect, because of their rare interactions.

Dark matter particles can be categorized by many criteria, like their production mechanism, their weak or self-interacting properties, etc. Since the purpose of this work is to study the properties and effects of warm dark matter particles, we will choose the velocity (and mass) as the main criterion in distinguishing between different particle models proposed.

### 2.4.1 What's hot and what's not

Based on the free streaming length and thus, the velocity dispersion of the particle, one can categorize (Bond et al. 1984; Primack & Blumenthal 1984) the dark matter candidates in three broad categories: cold dark matter (CDM), warm dark matter (WDM), and hot dark matter (HDM). Within each category, with names reminiscent of science fiction cartoon characters, there are specific hypothesized particles.

In principle, the higher the velocity is, the lighter the mass is, and so the hotter the particle is. By convention, particles with energies in the electron volt (eV) range and below are considered HDM. Neutrinos, for example, are fermionic particles with a mass that may lie in the meV - eV range. CDM particles are heavy, slow-moving particles. The neutralino, a hypothetical supersymmetric particle with a mass above the GeV scale, is the most favored candidate in the category of

weak interacting massive particles, generically called WIMPs. Although WDM could be anything between HDM and CDM, several constraints point to a few keV mass, with the so-called sterile neutrino as the most promising candidate. Axions, other much studied candidates, are particles theorized to be either cold or hot. In addition to the above-mentioned ones, more exotic candidates like gravitinos, axinos, Q-balls, branons, etc., have been hypothesized.

In Table 2.2 we show a list of some hypothesized dark matter candidates, the theory that predicts them and the expected masses of the particles. For similar tables and extensive discussions see Bertone, Hooper & Silk (2005) and Dekel & Ostriker (1999).

### 2.4.2 Beyond the mainstream, on stranger tides

Bolder theories are currently flirting with the idea that dark matter is not really matter, but just a reminder of our novice understanding of physics and the laws that govern the universe on different scales.

On the maverick's side of the academic realm, some scientists are arguing that Newton's law for the gravitational force becomes tricky for small gravitational accelerations, and therefore, points to the need for a Modified Newtonian Dynamics (MOND) approach (Milgrom 1983). Supporters of MOND - such as Vera Rubin, ironically - point out that certain of its predictions about the behaviour of galaxies have been confirmed by observation. MOND, as initially formulated, could be viewed as a modification of inertia or of gravity. However, critics respond that it does not explain some of the biggest discrepancies, and the evidence from gravitational lensing, which seems to show that whatever is causing the lensing is in invisible halos around a galaxy, rather than in the visible galaxy itself (which we would expect according to MOND).

Swimming against the current, other models are toying with antigravity, virtual particles and scalar-tensor-vector gravity (STVG or MOG) (Moffat 2006; Brownstein & Moffat 2006).

Probably the most controversial of theories is that we live in a computer simulation (Fontana 2006; Beane, Davoudi & Savage 2014, e.g.) and then all bets are off.

Table 2.2: Dark matter particle candidates. The table gives the mass, the theoretical model and the category in which the particle falls, whether it is cold, warm or hot.

| Candidate | Approximate Mass | Theory | Category |
|---|---|---|---|
| axion | $10^{-5}$ eV | QCD, PQ-symmetry breaking | cold |
| majoron | | | |
| Goldstone boson | | | |
| photino, axino | keV | PQ theory, SUSY | cold |
| Higgsino | MeV | SUSY/SUGRA | cold |
| heavy neutrino | | | |
| gluino | | | |
| neutralino | 100 GeV - 1 TeV | SUSY | cold |
| preon | 20-200 TeV | Composite Models | cold |
| monopole | $10^{16}$ GeV | GUTs | cold |
| Pyrgon, maximon | $10^{19}$ GeV | higher dimensional theories | cold |
| Perry pole, Newtorite | | | |
| supersymetric strings | $10^{19}$ GeV | SUSY/SUGRA | cold |
| quark-nuggets | $10^{15}$ g | QC, GUTs | cold |
| nuclearites | | | |
| primordial black holes | $10^{15-30}$ g | general relativity | cold |
| right handed neutrinos | 100 eV - keV | superweak interaction | warm |
| gravitino | 500 eV - 10 keV | SUSY/SUGRA | warm |
| Simpson neutrino | keV | | warm |
| mirror particles | keV | | warm |
| para-photon | 20-400 eV | modified QED | hot, warm |
| sneutrino | 10-100 eV | SUSY/SUGRA | hot |
| light Higgsino | | | hot |
| normal neutrinos | 10-100 eV | GUTs | hot |

## 2.5 Cold Dark Matter (CDM)

### 2.5.1 Cold dark matter candidates

Many candidates have been theorized for cold dark matter particles, but two of them stand out as the most prominent ones. These are axions and neutralinos.

**Axions**

Originally axions have been introduced in an attempt to solve the problem of CP violation in particle physics (Peccei & Quinn 1977a,b). They are expected to be extremely weakly interacting with ordinary particles suggesting that they were not in thermal equilibrium in the early universe.

The axion, like the pion, is a pseudoscalar particle. Predicted axion masses lie between $10^{-12}$ eV and 1 MeV. The calculation of the axion relic density is uncertain, depending on the assumptions made regarding the production mechanism, but it may be possible to find an acceptable range where axions satisfy all cosmological constraints and represent a possible dark matter candidate (Bertone, Hooper & Silk 2005).

Because of their small interaction with normal matter, axions have a considerable influence on the evolution of stars. Like neutrinos they easily carry off some of the energy created from the nuclear reaction from the interior of the star. The star has to adjust itself to this additional energy loss and it therefore contracts, while simultaneously increasing its central temperature and luminosity, which again leads to a shortening of its lifetime due to the quicker use of fuel. Hence, information about axion masses can be inferred from the observed nuclear burn off times in different stellar phases (Raffelt 1996, 2004; Hagiwara et al. 2002).

**Neutralinos**

In the framework of supersymmetric (SUSY) theories, the lightest supersymmetric particle, provided that is weakly interacting, is an interesting candidate for dark matter (Roszkowski 1993; Martin 1998; Steffen 2007; Bertone 2010) .

The simplest version of supersymmetry, which should be manifest at the GUT scale ($\sim 10^{16}$ GeV) and below, predicts that every kind of particle should have a supersymmetric partner particle with the same quantum numbers and interactions, except that the spin of this hypothetical partner particle should differ from that of the known particle by half a unit (Primack 1997). The model that incorporates both particles and their supersymmetric parteners is called The Minimal Supersymmetric Standard Model (MSSM).

Neutralinos are no longer relativistic at decoupling. Since their relic abundance may be considerable, at the level required to explain the total dark matter content of the universe (Bottino & Fornengo 1998), neutralinos appear as one of the most promising candidates. The interest is increased by the fact that their detection rates may be accessible to different experimental searches.

### 2.5.2 Cold dark matter challenges

The cold dark matter model has been successful in explaining many observations on cosmological scales. Indeed, the simulations match very well the large scale structure of the universe as shown by several surveys. At small scales, however, this model has been challenged. The so-called missing satellites problem (e.g. Klypin et al. 1999; Moore et al. 1999), where observations of galaxies do not map the abundance of substructures that are produced in CDM cosmologies has been considered a serious drawback of the model. The pure $N$-body cold dark matter simulations predict a much higher number of satellites than the ones observed in the Local Group and this number of satellites increases with the resolution of the simulations. One possible explanation was that the least massive satellite halos host very low surface brightness galaxies that are not observable with our present techniques. These halos get stripped of their stars and gas by interacting with the host galaxy (e.g. Kravtsov, Gnedin & Klypin 2004; Zolotov et al. 2012). While this explanation may hold for very small halos, the simulations also predict the existence of halos massive enough to be able to keep the stars and gas inside. This is usually referred to as the 'too big to fail problem' (Boylan-Kolchin, Bullock & Kaplinghat 2011).

Recent studies (Tikhonov et al. 2009; Zavala et al. 2009; Peebles & Nusser 2010) emphasized that the population of dwarf galaxies in voids is in strong contradiction with CDM predictions as well.

Furthermore, at smaller scales, the density profiles of galaxies show large cores (e.g. de Blok et al. 2001; Kuzio de Naray & Kaufmann 2011; Salucci et al. 2012) that have not been reproduced by the simulations. While for spiral galaxies the presence of the core may be attributed to the stars and gas concentration at the center of galaxies, for dwarf galaxies, which are dark matter dominated, this cannot be the case. Measurements of the stellar velocity dispersion profile of the Fornax dwarf spheroidal galaxy (Strigari et al. 2006) show that the distribution of the globular clusters inside Fornax may be explained by a large core of $\sim 1.5$ kpc, which is inconsistent with expectations from cold dark matter models.

The failure to replicate in CDM simulations pure bulgeless galaxies, which are observed in an important fraction (Kormendy et al. 2010; Kormendy 2016) adds to the problem.

Many attempts have been made in order to solve these problems by introducing baryonic processes in simulations, like star formation and supernovae feedback. The consensus as to what are the recipes for solving all these problems is far from being reached.

Because of these challenges and considering that the problems lie in the dark matter paradigm and not the baryonic physics, the attention was drawn to warm dark matter particle candidates that may be able to better reproduce our observations at galactic scales.

## 2.6 Warm Dark Matter (WDM)

Because of the aforementioned situation, where the CDM model proves deficient in explaining the observations, the WDM models, with sterile neutrinos leading as the most promising particle candidates, have been well studied and discussed in the literature in the past thirty years with an increased interest in the last few years.

Since particles in warm dark matter models have different intrinsic properties from the cold dark matter particle candidates, the effect of these particles on structure formation and evolution is expected to be qualitatively different on both large and small scales, possibly explaining some of the discrepancies between observations and the cold dark matter predictions from simulations.

### 2.6.1 Warm dark matter candidates

For warm dark matter particles, several candidates have been proposed as well.

Particles may decouple early from thermal equilibrium, while still relativistic, and may act as warm dark matter. One such particle is the right-handed neutrino added to the standard electroweak theory. Their only direct coupling is to left-handed or active neutrinos, therefore an efficient production mechanism is via neutrino oscillations (Dodelson & Widrow 1994). If the production rate is always less than the expansion rate, then these particles will never be in thermal equilibrium (Dodelson & Widrow 1994), but enough of them may be produced to account for the observed matter density (Viel et al. 2005).

Sterile neutrinos with a mass of order of few keV are the most promising WDM candidates (Peebles 1982; Colombi, Dodelson & Widrow 1996) and are in agreement with constraints from Lyman-$\alpha$ Forest, cosmic weak lensing, gamma-ray bursts, etc. (de Souza et al. 2013; Markovic & Viel 2014, e.g.). The fact that the sterile neutrino may occur naturally within extensions to the standard model of particle physics and provide a simple explanation for the neutrino flavour oscillations, increases the interest in exploring such models. Moreover, the recent detection (Bulbul et al. 2014; Boyarsky et al. 2014) of a 3.55 keV unidentified emission line both on the data from XMM spectrum of galaxy clusters and Chandra, currently undergoing scrutiny, can be a hint for sterile neutrino decay .

## 2.7 CDM vs WDM - the battle

While cold dark matter simulations describe what we observe pretty well, there are scales on which this model is encountering difficulties, as we have seen in the previous sections. The majority of the research community is, however, reluctant to give it up, sometimes because of the model's simplicity (invoking the principle of 'Occam's razor'[5]).

[5] many public and private communications

Cold dark matter is, for sure, the simplest to simulate, but it does require a complicated and extremely large energy production mechanism. Assuming that the universe was not designed to make things easier for simulators (and remembering that Occam's razor is not a law of physics), the simplicity of the model should not count as an argument in its favour[6].

Ironically, hot dark matter, which is ruled-out, is the only one that has been detected. Indeed, the only dark particle discovered is the neutrino, which is hot. Being very light and moving very fast, however, neutrinos alone would not be able to keep galaxies together and, as computer simulations show (White, Frenk & Davis 1983; Shapiro, Struck-Marcell & Melott 1983; Dekel & Aarseth 1984, e.g.) such a universe would not look anything like the real one. Moreover, neutrinos have such a tiny mass that they cannot make up all the dark matter content (Primack & Gross 2001, e.g.).

Warm dark matter models with the hypothetical 'sterile neutrino' as the centre-stage candidate cover the middle ground between cold and hot. Recent computer simulations based on warm dark matter have produced replica universes that rival those based on cold, so some are beginning to warm to that theory.

The fact that some simulations (Schneider et al. 2014) have shown no difference between warm dark matter and cold dark matter in solving some of the galaxy scale problems should not be used as an evidence against the warm dark matter models. Firstly, as we will show, the effects of warm dark matter particles strongly depend on the model. Secondly, these effects may have subtle influences on the structure formation, which escape general analysis of simulations. Last, but not least, even if warm dark matter does as badly or as well as cold dark matter, in the absence of a detected particle candidate that would validate one model or the other, there is no reason for dropping the investigation of any reasonable dark matter model.

In principle there should be no conflict between these two models, since they are not mutually exclusive, as dark matter may turn out to be made up by many species of particles. Technically, since neutrinos do exist, dark matter is already mixed[7].

## 2.8 Dark matter experiments

### 2.8.1 Dark matter direct detection

The search for techniques capable of detecting the dark matter particles (Bertone, Hooper & Silk 2005; Bergström 2012) in our galactic halo is of extreme interest for astrophysics as well as particle physics.

Assuming that the dark matter is omnipresent in the dark matter halo of the Milky Way and can traverse the Earth with galactic velocities of $\sim 200$ km/s, i.e., with $v/c \sim 10^{-3}$, one can infer

[6]Looking at evolution and genetics, we have seen that nature has a way of using the simplest initial conditions to make the most complicated things, not the other way around (although this also is not an argument).

[7]Excerpts from this introduction have been published in The Dark Side of the Universe, Sinziana Paduroiu, 2015, E-book, Brown Bear Books, Windmill Books Ltd., Kindle Edition and The Dark-Files: Dark Matter, Sinziana Paduroiu, 2014, Roostergnn, Web

from the rotation curves a local mass density of the order of $0.4$ GeV/cm$^3$ (Bergström 2012). Thus knowing the velocity and density distribution of the dark matter particles in the solar neighbourhood, for a certain scattering cross section, one can estimate the rate of scattering events expected in a detector per unit time, per unit material mass (Drukier 1984; Goodman & Witten 1985; Wasserman 1986; Jungman, Kamionkowski & Griest 1996; Bertone, Hooper & Silk 2005).

This rate is approximately:

$$R \approx \sum_i N_i n_\chi < \sigma_{i\chi} >, \tag{2.10}$$

where the index, $i$, runs over nuclei species present in the detector

$$N_i = \frac{\text{Detector mass}}{\text{Atomic mass of species } i} \tag{2.11}$$

is the number of target nuclei in the detector,

$$n_\chi \equiv \frac{\text{WIMP energy density}}{\text{WIMP mass}} \tag{2.12}$$

is the local WIMP density and $< \sigma_{i\chi} >$ is the cross section for the scattering of WIMPs off nuclei of species $i$, averaged over the relative particle velocity with respect to the detector.

Various experiments use different nuclear species, Ge, NaI, Xe, $TeO_2$ or $CaF_2$ (Donato, Fornengo & Scopel 1998; Bottino & Fornengo 1998, e.g.).

A characteristic signature for the direct detection consists in the annual modulation of the detection rate during the orbital motion of the Earth around the Sun. The change of direction of the particle velocities with respect to the detector induces a time dependence in the detection rate, which can be significant (Drukier, Freese, & Spergel 1986; Bottino & Fornengo 1998).

The experimental search undertaken by the DAMA/ NaI Collaboration (Bernabei et al. 2015) provided the indication of a modulated signal. The claimed excess of the annual modulation (predicted in Drukier, Freese, & Spergel (1986)) is approaching $9\sigma$.

Several experiments have been searching for decades for weak interacting massive particles without coming up with conclusive results. Most recently, the Large Underground Xenon detector (LUX) (LUX Collaboration et al. 2014) reported no events that could be related to the WIMPs, consolidating previous findings from experiments like XENON (Aprile et al. 2012).

In Fig. 2.1 from Aprile et al. (2012) one can see the sensitivity of the Xenon detector in comparison with many other models, for different WIMP-nucleon cross-sections and for different WIMP masses.

Meanwhile, the CoGeNt cogent detector data showed effects that can be hints of the existence of a Milky Way dark matter galactic halo, as previously shown by the DAMA (Bernabei et al. 2015) collaboration.

In the search for axions, the Axion Dark Matter Experiment (ADMX) (Asztalos et al. 2010) is yet to find the exotic particles.

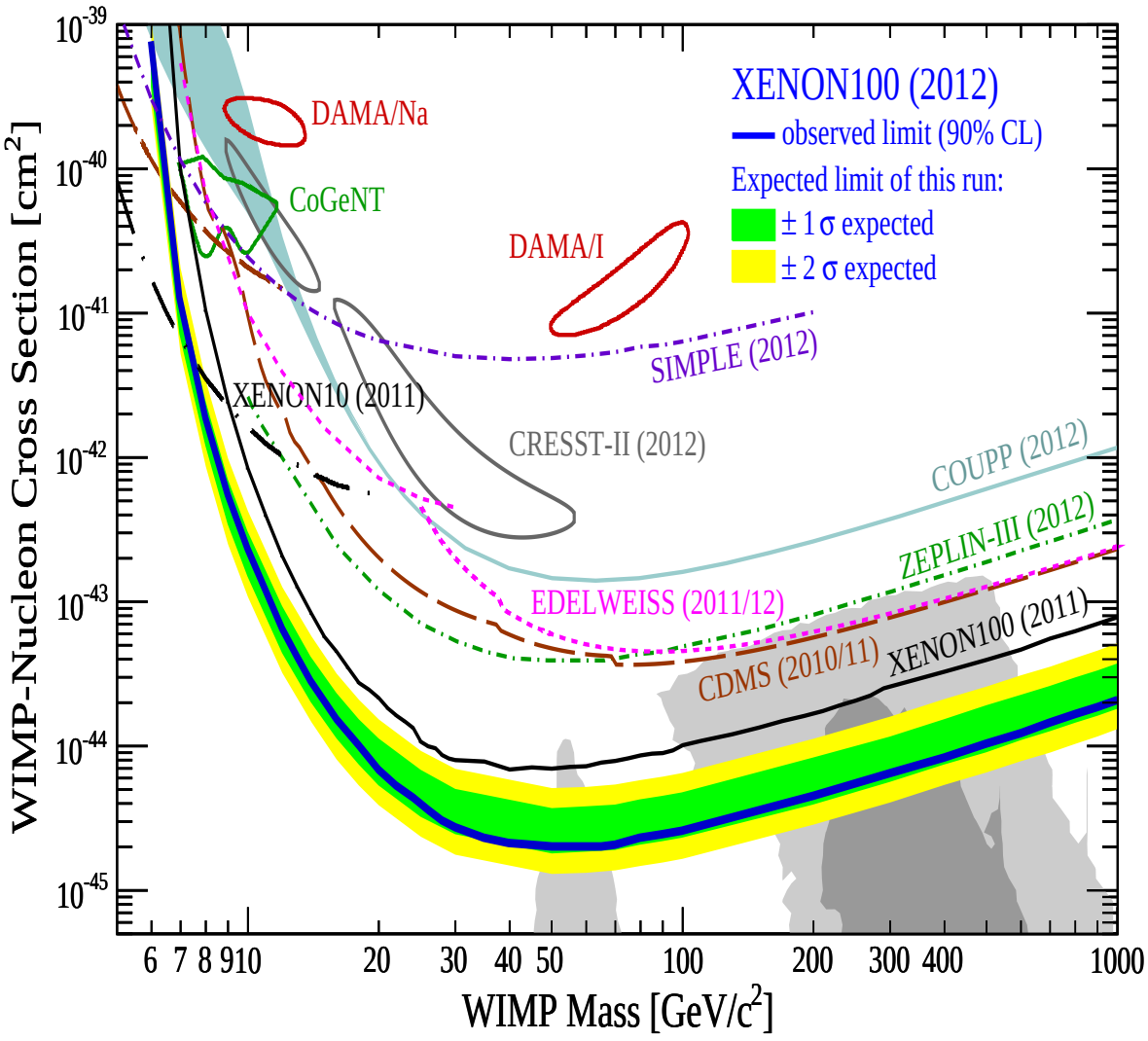


Figure 2.1: Detector sensitivity for Xenon compared to different other experiments (Aprile et al., 2012). The WIMP-nucleon scattering is shown up to 10 TeV energies together with $1\sigma/2\sigma$ regions preferred by supersymmetric models.

Probably the most ingenious detection mechanism had been proposed by Drukier et al. (2012). It involves the use of DNA and RNA as a detector material that can provide nanometer resolution tracking. The detector is made of thin fim of gold with strings of single stranded nucleic acids (ssNA). After the particle strikes one of the gold nuclei, which then traverses the strands and whenever it hits one, it breaks the ssNA. This break is easier to locate and the path of the recoiling nucleus can be tracked with nanometer accuracy.

### 2.8.2 Dark matter indirect detection

Since the present day detectors focus on very high energy particles, larger than 10 GeV, for neutrinos and sterile neutrinos, the best probe is indirect detection.

Although the neutrinos interaction with matter is weak, they play a key role in the nuclear processes through what is called the weak force. Under typical conditions, a neutrino is $10^{20}$ times less likely than light to interact with matter, so it will pass through the Earth without interaction. Nevertheless, when a massive star dies, it does so through a powerful explosion, for which the quiet neutrino is merely responsible, and a high flux of neutrinos is produced carrying off most of the enormous amount of energy released by the collapse of the core (Herant et al. 1997; Bilenky 2010) . The best way to detect these particles is from supernova explosions.

#### 2.8.2.1 Supernovae explosions

On 23 February 1987 in the Large Magellanic Cloud at a distance of about 51.4 kpc from the Earth a supernova explosion was observed (West et al. 1987). In three big underground neutrino detectors, Kamiokande II (11 events), IMB (8 events) and Baksan (5 events) at the same time neutrinos bursts with neutrino energies of about 15 MeV were observed three hours before the first optical observation of SN1987A. The observed neutrino bursts lasted for about 10 s (Alexeyev et al. 1988).

The data analysis of the supernova explosion give new insights into the physical processes that take place and may constrain the mass of the electron neutrino (Goldman et al. 1988; Jones 1994), even though a quantitative interpretation of such data poses many challenges (Vissani & Pagliaroli 2011; Dasgupta & Beacom 2011).

In January 2008, SN 2008D, a core-collapse supernova at a distance of 27 Mpc, was discovered by the Swift satellite through an associated X-ray flash. No events were observed, leading the scientists to believe that a closer to Earth, a galactic supernova explosion would be needed in order to see the events. For example, the IceCube detector is expected to see 100 events for a core-collapse supernova at 10 Mpc according with some theoretical models for supernova explosions.

#### 2.8.2.2 Indirect detection experiments

Ideally, gamma-rays detection should be done from space, outside Earth's atmosphere. Space-based telescopes like EGRET, GLAST and Fermi Space Telescope are competing in measuring the

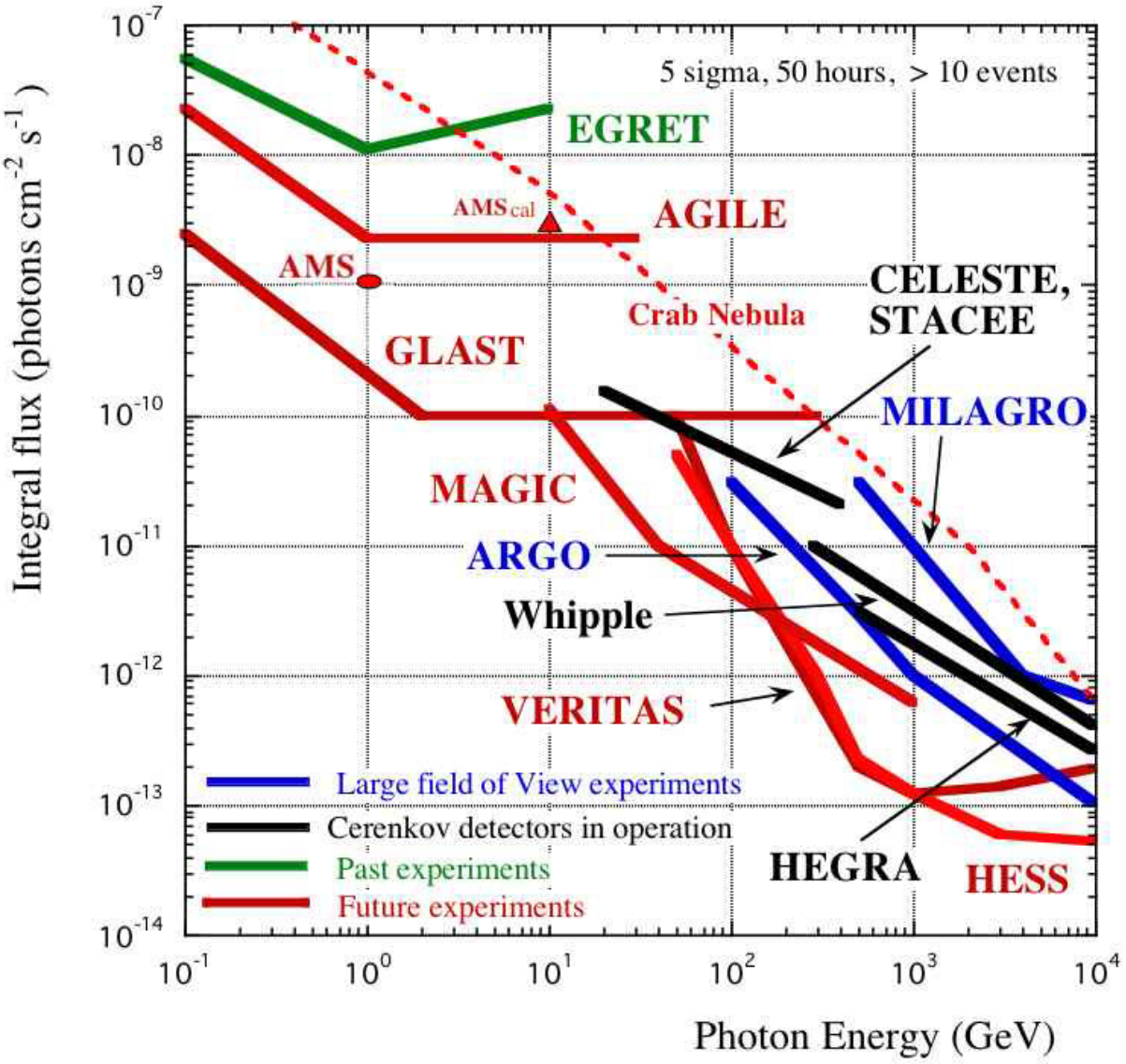


Figure 2.2: Sensitivity of gamma-ray detectors from Morselli et al. (2002)

gamma-rays. Nevertheless, efforts have been made to detect gamma-rays indirectly with ground-based telescopes. The methods rely on the fact that when radiation interacts with the atmosphere, a cascade of secondary particles is produced allowing the detection of the particles and the Cerenkov light produced. One difficulty is to distinguish between the signal coming from cosmic rays and the one from gamma rays. Such ground-based telescopes are MAGIC, HESS, VERITAS.

Recently, a significant gamma-ray signal has been detected from the newly discovered dwarf galaxy Reticulum II using Fermi-LAT Collaboration data (Geringer-Sameth et al. 2015). Since it is coming from a dark matter dominated region, such a signal could be a hint for the dark matter particles annihilation.

For the detection of neutrinos, large volume Cerenkov detectors like AMANDA and IceCube, are currently operating. The high energies neutrinos produced by the annihilation of dark matter particles are tracked by the muons, which travel through the detector emitting Cerenkov light.

Fig. 2.2 shows the previous results for the sensitivity of gamma-rays detectors (Morselli et al. 2002). Fig. 2.3 shows the most recent preliminary limits from the IceCube detector compared to several other experiments (IceCube Coll. et al. 2015).

### 2.8.3 Dark matter particle production

The quarks and gluons in the protons collided at the LHC or other colliders may annihilate in particles, which may eventually decay into WIMPs inside the detectors. The missing energy when reconstructing the chain of events, gives the signature for such particle production. There have been many attempts to figure out which processes are more likely to lead to such events (Feng, Grivaz & Nachtman 2010), but no experimental evidence has been found yet. Even if produced, the time scale on which such a particle is stable may not be sufficiently long for its evidence to be inferred (Peter 2012).

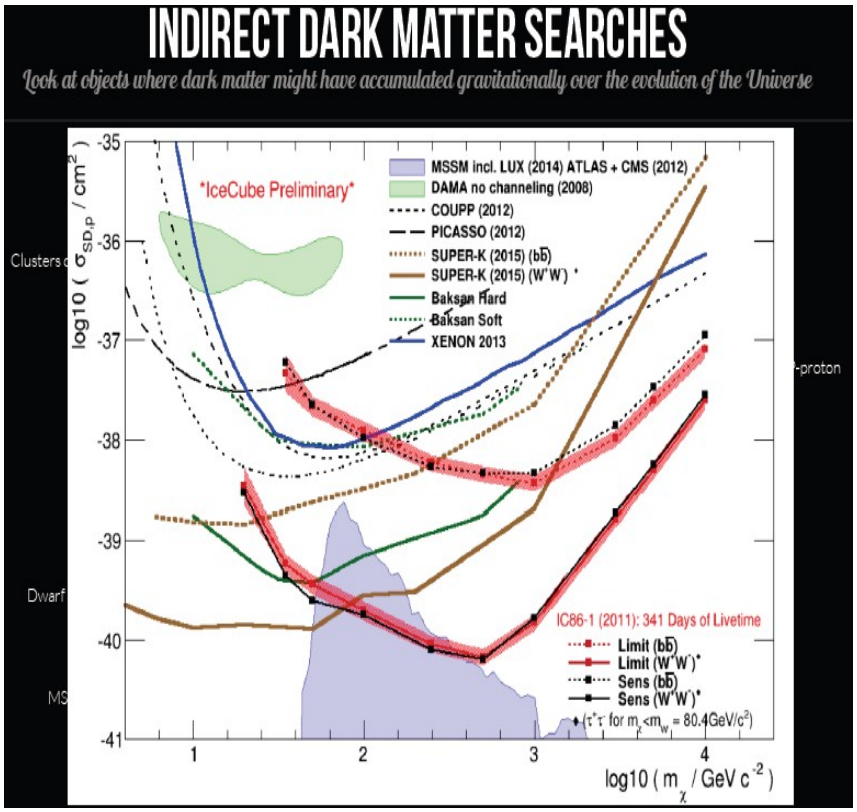


Figure 2.3: Comparison of IceCube's sensitivity and limits on the WIMP-nucleon scattering cross-section as a function of the WIMP mass with reported limits from other experiments, from IceCube Coll. (2015)

Chapter 3

# Structure Formation in Dark Matter Models

## 3.1 Large scale structure in the universe

The initial conditions for structure to form in the universe and the physics that governs the large scale structure, have been discussed in the previous chapter. For the ones who wonder how this structure actually looks like, it is through the surveys that we can get an idea. Springel, Frenk, & White (2006) show the large scale structure in the universe, displaying the results of several surveys and simulations - Fig. 3.1. The distribution of galaxies from the 2-degree Field Galaxy Redshift Survey (2dFGRS) (Colless et al. 2001), the Sloan Digital Sky Survey (SDSS2) (York et al. 2000), the Center for Astrophysics (CfA) galaxy redshift survey (Geller & Huchra 1989) together with the dark matter distribution inferred from the Millenium simulation (Springel et al. 2005), is displayed. All surveys show filaments in which the galaxies and clusters are linked together in a 'cosmic web' (Geller & Huchra 1989). One can see large scale structures like the CfA2 'Great Wall' (Geller & Huchra 1989) and the 'Sloan Great Wall' from a section of SDSS, which contains more than 10000 galaxies extending over more than 1.37 billion light years. Although the surveys are built from observations of the luminous matter in the universe, the mock catalogues constructed from dark matter simulations are obviously matching very well the distribution of galaxies and clusters over very large distances.

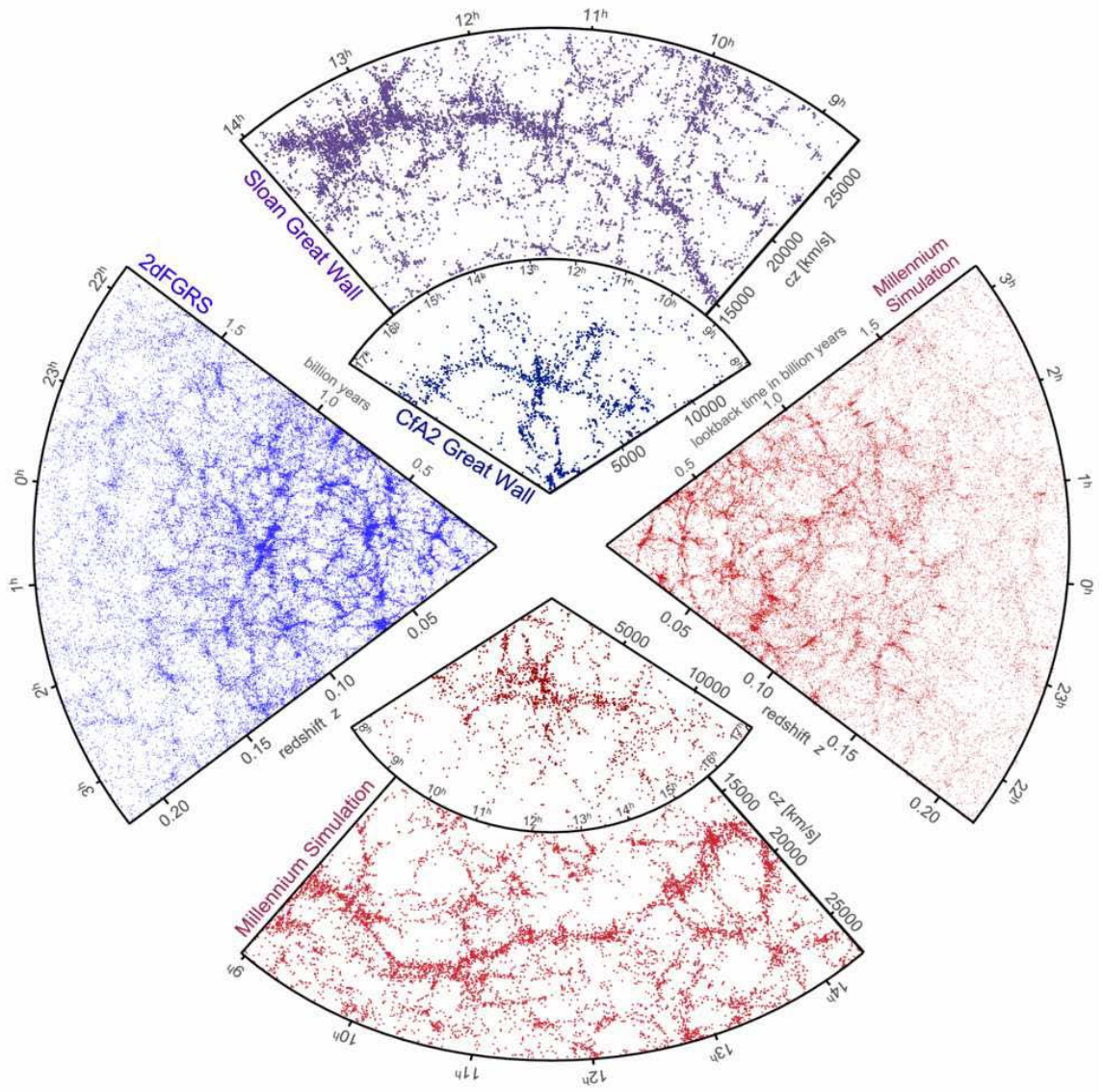


Figure 3.1: The galaxy distribution obtained from spectroscopic redshift surveys and from mock catalogues constructed from cosmological simulations, Springel, Frenk & White (2006).

Table 3.1: Several codes used for simulations depending on the method

| Codes | Particle/SPH | Grid/AMR | Hybrid |
|---|---|---|---|
| | GADGET-2 | AMIGA | Hydra |
| | PKDGRAV-2 | ART | |
| | Gasoline | RAMSES | |
| | OSPH | ENZO | |
| | VINE | Flash | |

## 3.2 Numerical simulations of structure formation

### 3.2.1 Numerical methods

To describe the dark matter behavior in simulations, one can distinguish between the collisionless and the collisional treatment. A one-dimensional analysis of gravitational clustering has been previously explored in both these cases (Melott 1982, 1983; Gheller, Moscardini & Pantano 1996, e.g.).

In general, the preferred method to describe dark matter, in both CDM and WDM scenarios, is with particles rather than as a collisional fluid, since they respond only to gravitational forces. For the collisionless case, either pure $N$-body or hydrodynamic simulations that include baryons have been used in order to explore the structure formation. Processes such as heating, cooling, possible consequences of dark matter decay (Biermann & Kusenko 2006), supersonic flow (Fialkov 2014) cannot yet all be taken into account on all length and time scales desirable in the simulations.

A different approach is the semi-analytical modeling, consisting in analytic approximations that attempt to describe the same physics. The various techniques have been reviewed in Baugh (2006). Although computationally inexpensive compared to the simulations, the degree of approximation used makes them less reliable in describing some physical processes.

In this work we will focus on the collisionless dark matter simulation methods, since we perform pure $N$-body simulations.

### 3.2.2 $N$-body codes

Depending on which numerical methods they implement, frequently used simulation codes for collisionless fluids can be cathegorized as grid, particle or hybrid, as in Table (3.1). For a detailed description of this codes, see astrosim webpage[1].

Since the simulations presented here have been performed with GADGET-2 (Springel 2005)[2] and PKDGRAV-2 (Stadel 2001)[3], we will give a short description of these two codes.

[1] https://www.astrosim.net/code/doku.php?id=home:code:nbody:multipurpose
[2] http://www.mpa-garching.mpg.de/gadget/
[3] http://hpcforge.org/projects/pkdgrav2/

GADGET-2 (Springel 2005) is a TreeSPH code (Hernquist & Katz 1989), where gravitational interactions are computed with a hierarchical multipole expansion, and gas dynamics is followed with smoothed particle hydrodynamics (SPH).

We will present here the method used for purely gravitational interactions, following Springel (2005). The dark matter particles are described by the collisionless Boltzmann equation coupled to the Poisson equation in an expanding background Friedmann-Lemaître Universe. Due to the high-dimensionality of this problem, these equations are solved with the $N$-body method, where phase-space density is sampled with a finite number $N$ of tracer particles.

The dynamics of these particles is described by the Hamiltonian (Eq. (1) in Springel (2005))

$$H = \sum_i \frac{\vec{p}_i^2}{2\, m_i\, a(t)^2} + \frac{1}{2} \sum_{ij} \frac{m_i m_j\, \varphi(\vec{x}_i - \vec{x}_j)}{a(t)}, \tag{3.1}$$

where $H = H(\vec{p}_1, \ldots, \vec{p}_N, \vec{x}_1, \ldots, \vec{x}_N, t)$. The $\vec{x}_i$ are comoving coordinate vectors, and the corresponding canonical momenta are given by $\vec{p}_i = a^2 m_i \dot{\vec{x}}_i$. The explicit time dependence of the Hamiltonian comes from the evolution $a(t)$ of the scale factor in the Friedmann-Lemaître model (Springel 2005).

Assuming periodic boundary conditions for a cubic box with length $L$, the interaction potential $\varphi(\vec{x})$ is the solution of (Eq. (2) in Springel (2005))

$$\nabla^2 \varphi(\vec{x}) = 4\pi G \left[ -\frac{1}{L^3} + \sum_{\vec{n}} \tilde{\delta}(\vec{x} - \vec{n}L) \right], \tag{3.2}$$

where the sum over $\vec{n} = (n_1, n_2, n_3)$ extends over all integer triplets. The mean density is subtracted here, so the solution corresponds to the 'peculiar potential', where the dynamics of the system is given by $\nabla^2 \phi(\vec{x}) = 4\pi G[\rho(\vec{x}) - \overline{\rho}]$. For a discretized particle system, the potential can be defined as (Eq. (3) in Springel (2005))

$$\phi(\vec{x}) = \sum_i m_i\, \varphi(\vec{x} - \vec{x}_i). \tag{3.3}$$

The single particle density distribution function $\tilde{\delta}(\vec{x})$ is the Dirac $\delta$-function combined with a normalized gravitational softening kernel of comoving scale $\epsilon$. The softening kernel employed is the spline kernel (Monaghan & Lattanzio 1985) used in SPH and set $\tilde{\delta}(\vec{x}) = W(|\vec{x}|, 2.8\epsilon)$, where $W(r)$ is given by

$$W(r,h) = \frac{8}{\pi h^3} \begin{cases} 1 - 6\left(\frac{r}{h}\right)^2 + 6\left(\frac{r}{h}\right)^3, & 0 \le \frac{r}{h} \le \frac{1}{2}, \\ 2\left(1 - \frac{r}{h}\right)^3, & \frac{1}{2} < \frac{r}{h} \le 1, \\ 0, & \frac{r}{h} > 1. \end{cases} \tag{3.4}$$

In this case, the Newtonian potential of a point mass in non-periodic space is $-G\, m/\epsilon$, as for a Plummer sphere of size $\epsilon$. This can be simplified to Newtonian space by setting $a(t) = 1$, so that the explicit time dependence of the Hamiltonian vanishes. For vacuum boundaries, the interaction potential is reduced to the usual Newtonian form, i.e. for point masses it is given by $\varphi(\vec{x}) = -G/|\vec{x}|$

modified by the softening for small separations. A detailed description of the code, tests and discussions is given in Springel (2005).

PKDGRAV-2 (Stadel 2001) is a parallel $N$-body tree code using hexadecapole multipole calculations for the forces and the Ewald summation[4] (Ewald 1921). The method for solving the Hamiltonian is based on a kick-drift method (K-D) (Bentley 1979). The peculiar potential is given by the hexadecapole expansion of the forces. Particle orbits are integrated using a symplectic leapfrog integrator. The softening kernal is a $K_3$ kernal (Dehnen 2001), not a spline kernel like in GADGET-2.

Performing the same initial conditions simulation with both these codes, we observe very small differences at very small scales, which are not important for the purpose of our work, but undoubtably hold importance for precision cosmology, as shown in Reed et al. (2013).

### 3.2.3 Initial conditions

As in any non-linear process, the initial conditions are very important (May 1976), and therefore some very elaborate codes have been developed for this purpose, like GRAFIC and GRAFIC2 package, developed by Edmund Bertschinger (Bertschinger 2001)[5], the recent MUSIC by Oliver Hahn (Hahn & Abel 2011)[6], CAMB by Antony Lewis and Anthony Challinor (Challinor & Lewis 2005)[7] for anisotropies in the microwave background, based on CMBFAST by Uros Seljak and Matias Zaldarriaga (Seljak & Zaldarriaga 1996)[8], etc.

In this work we have used GRAFIC and GRAFIC2 for generating initial conditions and refinements and we give a brief description of the method, following Bertschinger (2001).

Based on previous works of Salmon (1996) and Pen (1997) and COSMICS package (Bertschinger 1995), GRAFIC implements a standard $k$-space sampling method for generating Gaussian random fields on periodic rectangular lattices, while GRAFIC2 generates multiscale Gaussian random fields for cosmological initial conditions.

Following Bertschinger (2001) (Eq. (1) and Eq. (2)), we can write the density fluctuation field as,

$$\delta(\vec{x}\,) = \int d^3k\, e^{i\vec{k}\cdot\vec{x}}\, T(k)\xi(\vec{k}\,)\,, \tag{3.5}$$

where $\xi(\vec{x}\,)$ is Gaussian white noise with power spectrum,

$$\Big\langle \xi(\vec{k}_1)\xi(\vec{k}_2)\Big\rangle = \delta^3_{\rm D}(\vec{k}_1+\vec{k}_2)\,. \tag{3.6}$$

with $\delta_{\rm D}(\vec{k}\,)$ is the Dirac delta function assuming Euclidian space.

[4]This method for computing long-range interactions in periodic systems is a special case of the Poisson summation formula, replacing the summation of interaction energies in real space with an equivalent summation in Fourier space.

[5]http://web.mit.edu/~edbert/

[6]http://people.phys.ethz.ch/ hahn/MUSIC/

[7]camb.info

[8]http://lambda.gsfc.nasa.gov/toolbox/tb_cmbfast_ov.cfm

The function $T(k)$ is the transfer function relative to white noise, and it is related to the power spectrum $\delta(\vec{x})$:

$$T(k) = [P(k)]^{1/2} \, . \tag{3.7}$$

$\xi(\vec{k})$ and $T(k)$ are in units of [length]$^{3/2}$ and $T(k)$ is an ordinary function while $\xi(\vec{k})$ is a stochastic field - a distribution (Eq. (3) in Bertschinger (2001)).

Eq. (3.5) can be written as a convolution (Salmon 1996):

$$\delta(\vec{x}) = (\xi * T)(\vec{x}) = \int d^3x' \, \xi(\vec{x}')T(|\vec{x} - \vec{x}'|) \tag{3.8}$$

where

$$T(|\vec{x}|) = \int \frac{d^3k}{(2\pi)^3} \, e^{i\vec{k}\cdot\vec{x}} \, T(k) \tag{3.9}$$

and

$$\langle \xi(\vec{x}_1)\xi(\vec{x}_2) \rangle = (2\pi)^3 \delta^3_{\mathrm{D}}(\vec{x}_1 - \vec{x}_2) \, . \tag{3.10}$$

The spatial two-point correlation function of $\delta(\vec{x})$ is simply $(2\pi)^3(T * T)(\vec{x})$.

An arbitrary Gaussian random field can be constructed by the convolution of white noise with a convolution kernel determined by the power spectrum. The white noise process is formally divergent - $\xi(\vec{x})$ (equation (3.10)) is derived from a Gaussian distribution with infinite variance. This behavior arises because contributions from all scales are included and $\xi(\vec{x})$ is ultraviolet-divergent. Physically this divergence may be cut off by the power spectrum, although unlike the WDM spectrum, the standard CDM spectrum leads to a logarithmic divergence of the dark matter density fluctuations at small scales. In practice the integral is cut off at high wavenumber by discretizing space with a finite cell size as described in Bertschinger (2001).

Using a discretized Cartesian mesh in a finite parallelpiped with periodic boundary conditions is a standard method for generating Gaussian random fields, limiting the spatial dynamical range by the size of the largest FFT that can be performed. Aside from the condition $\xi(-\vec{k}) = \xi^*(\vec{k})$ required to enforce reality of $\delta(\vec{x})$, random variables at different points are statistically independent, so the Fourier domain is used. In the spatial domain, $\delta(\vec{x})$ has long-range correlations that are difficult to sample.

The velocity field, which is a displacement field for CDM particles, obeys similar equations and only the transfer function $T(k)$ is modified (Bertschinger 2001).

The convolution method evaluates the density and velocity fields using equation (3.8) instead of equation (3.5). Considering that the white noise is uncorrelated in the spatial domain as well as the Fourier domain, sampling $\xi(\vec{x})$ can be easily done. The algorithm used is based on multiple FFTs with appropriate boundary conditions (Pen 1997), instead of tree algorithms (Salmon 1996).

The code offers the possibility of recursive refinement to multiple levels for a zoom in simulation of cosmic structures. There are nonetheless, some issues arising in recursive refinement (Bertschinger 2001).

For a three-level refinement with refinement factors $r_1$ and $r_2$, the grid coordinates and noise fields can be written as (Eq. (29) and Eq. (30) in Bertschinger (2001))

$$\vec{x}(\vec{m},\vec{n},\vec{o}\,) = \vec{x}_o + \left(\frac{L}{M}\right)\left(\vec{m} + \frac{1}{r_1}\vec{n} + \frac{1}{r_1 r_2}\vec{o}\right) . \tag{3.11}$$

$$\xi(\vec{m},\vec{n},\vec{o}\,) = \xi_2(\vec{m},\vec{n},\vec{o}\,) + \xi_1(\vec{m},\vec{n}\,) - \bar{\xi}_2(\vec{m},\vec{n}\,) + \xi_0(\vec{m}\,) - \bar{\xi}_1(\vec{m}\,) \tag{3.12}$$

where $\bar{\xi}_2$ is obtained by averaging $\bar{\xi}_2$ over $\vec{o}$. At each level of the hierarchy there is a different grid (labeled by $\vec{m}$, $\vec{n}$, and $\vec{o}$, respectively). The variances of the white noise samples are related by $\mathrm{Var}(\xi_2) = r_2^2\mathrm{Var}(\xi_1) = r_1^2 r_2^2 \mathrm{Var}(\xi_0)$.

In order to perform recursive refinement, once a refinement has been made to level $n$ (where $n = 0$ is the periodic top grid before any refinement), the fields computed at that level serve as top-grid fields to be refined to level $n + 1$. For $n = 1$ (Eq. (31) in (Bertschinger 2001))

$$\delta(\vec{m},\vec{n},\vec{o}\,) = \delta(\vec{m},\vec{n}\,) * W + \left[\xi_2(\vec{m},\vec{n},\vec{o}\,) - \bar{\xi}_2(\vec{m},\vec{n}\,)\right] * T . \tag{3.13}$$

For multiple level refinements, the fields at the preceding level are sampled, spread to the new fine grid and convolved with the appropriate anti-aliasing filter. The short-wavelength noise is then sampled on the new fine grid and the coarse-cell means are subtracted, so that the noise is zero at every higher level of the refinement. This noise is then combined with the transfer function and added to the long wavelength field to give the high-resolution field. This procedure is repeated for all levels of the hierarchy (Bertschinger 2001).

The refinement procedure is however more complicated if one needs to refine non-regular shaped regions. In the case of cold dark matter, the particles concentrated in a region at redshift zero come from a rather confined larger region at earlier redshift. In the case of warm dark matter, however, where particles in a halo, for example, come from a large distance and different regions of the simulation, the high resolution refinements are more difficult to achieve.

## 3.3 Structure formation in warm dark matter models

The damping of the fluctuation spectrum and the presence of thermal velocities as properties of warm dark matter particles imprint a distinct signature found from the structure formation mechanisms to the internal structures of halos. Using warm dark matter simulations we explore these effects on the structure formation for different particle velocities. From both theoretical considerations and the analysis of the simulations, we discuss the impact of the thermal velocities on structure formation. Re-examining the assumptions considered when estimating the velocity dispersion for warm dark matter particles that have been adopted in previous works for more than a decade, we identify some inconsistencies in previous published results. Giving an independent estimation for the correspondence between the mass and the velocity of a warm dark matter particle, we point out how strongly model dependent this relation is and consequently, how weak are

the constraints on the particle mass from the simulations. Our results are presented in Paduroiu, Revaz & Pfenniger (2015)[9], at the end of this section.

### 3.3.1 Simulation methods for WDM

Both $N$-body and hydrodynamical collisionless cosmological simulations of warm dark matter models begin by generating the initial conditions with a cutoff in the power spectrum.

To compute the transfer function for WDM models, the fitting formula suggested by Bode, Turok and Ostriker (2001) gives:

$$T^2(k) = \frac{P^{\rm WDM}}{P^{\rm CDM}} = [1 + (\alpha k)^{2\nu}]^{-10/\nu} \tag{3.14}$$

where $\alpha$, the scale of the break, is a function of the WDM parameters, which are function of the velocity, while the index $\nu$ is a constant. It is common practice however (Macciò et al. 2012; Schneider et al. 2013, e.g), to quote the mass dependence instead of the velocity one, using Eq. (4.17) (Eq. (A3) in Bode et al. (2001)), as a conversion. In the next section we will inspect the theoretical derivation of this particular equation and the caveats of its use, but for the moment it is important to stress that the transfer function depends, in fact, on the particle velocity.

Viel et al. (2005) (see also Hansen et al. (2002)), using a Boltzmann code simulation, found that $\nu = 1.12$ is the best fit for $k < 5\ h\ {\rm Mpc}^{-1}$, and they obtained the following expression for $\alpha$:

$$\alpha = 0.049 \left(\frac{m_x}{1\,{\rm keV}}\right)^{-1.11} \left(\frac{\Omega_\nu}{0.25}\right)^{0.11} \left(\frac{h}{0.7}\right)^{1.22} {\rm Mpc}\ h^{-1}. \tag{3.15}$$

In the case of warm dark matter particles, the streaming velocity suppresses the matter power spectrum $P(k)$ and the formation of structure, on scales smaller than their free-streaming scale. A rough estimation of the free-streaming scale is given by Bond, Efstathiou & Silk (1980):

$$k_{\rm FS} = \frac{2\pi}{\lambda_{\rm FS}} \sim 5\,{\rm Mpc}^{-1} \left(\frac{m_x}{1\,{\rm keV}}\right) \left(\frac{T_\nu}{T_x}\right)\ , \tag{3.16}$$

An example of how the linear power spectrum cutoff dampens the small scales power for several warm dark matter particles, with respect to the cold dark matter power spectrum, is shown in Fig. 3.2, from Smith & Markovic (2011).

Depending on the model for the properties of a certain particle, there can be different expressions for the damping of the power spectrum (Abazajian & Koushiappas 2006, e.g.). For the purpose of our present work and for easier comparison with previous studies we use the expression given in Eq. (3.15) with the corresponding thermal velocities.

This approach used for cutting the power spectrum is only valid however, for a scenario in which the whole dark matter content is made up by one specific dark matter particle of a certain velocity as we will show in the next section.

[9] from here on Paduroiu et al. (2015)

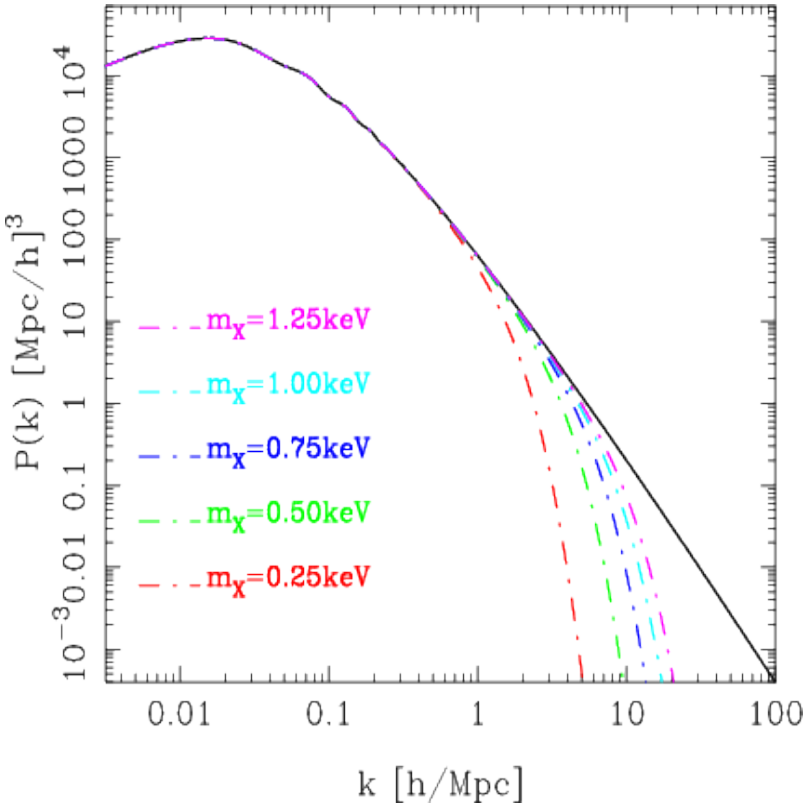


Figure 3.2: Linear mass power spectra as a function of the wavenumber for CDM and WDM scenarios for several particle masses from Smith & Markovic (2011). The solid line shows the CDM. The lighter the WDM particle, the more the power is damped on small scale.

### 3.3.2 Thermal velocities for warm dark matter particles

Besides the cutoff in the power spectrum, the warm dark matter particles assumed in simulations do have in fact a non-zero velocity dispersion. Several numerical approaches have been used to address the implementation of velocity dispersion in $N$-body simulations and to study their impact. The numerical resolution is admittedly limited with respect to the physics, making the phase space density distribution sampling poor in space as well as in the velocity space.

This reason is not sufficient for dropping entirely the velocity sampling by neglecting the thermal velocity, while keeping nonetheless the power spectrum cutoff implied by the same non-zero velocity. Nor is the fact that for some warm dark matter particles the thermal velocities are comparable or smaller than the bulk Zel'dovich velocities, since the first implies a velocity dispersion, while the latter is a bulk velocity. Based on these arguments, many simulations have ignored the thermal velocity component (e.g. Schneider et al. 2013; Governato et al. 2015). Also analytical studies, like (Valageas 2012, e.g.), argue that for a 1 keV particle, for example, the late-time velocity dispersion has a negligible effect on the power spectrum on perturbative scales and on the halo mass function, although they do acknowledge the lower redshift significant impact on the probability distribution function of the density contrast, on scales smaller than 0.1 Mpc/h.

On the contrary, even though it has been considered difficult to accurately prescribe initial thermal velocities in dark matter simulations, the importance of using them regardless, has been emphasized in previous studies like Colombi, Dodelson & Widrow (1996), Bode et al. (2001) and Melott (2007).

In this section we will show why the velocity dispersion should be used, what velocities should be used depending on the particle model assumed and how velocities are actually implemented in simulations, recalling and revising some previous arguments and presenting new ones.

#### 3.3.2.1 The 'Why'

The distribution of warm dark matter particles in velocity space is most important, as stressed by (Colombi, Dodelson & Widrow 1996, e.g.). Taking a strictly zero thermal velocity is numerically inconsistent with the description of a collisionless fluid of finite phase space density $f$. Integrating Newton's equation of motion for a set of particles in a force field $\vec{g}$ is equivalent to solving in a Lagrangian way the collisionless Boltzmann equation with discrete mass particles with the characteristics method. In conventional notations the Eulerian description of the phase space volume conservation reads,

$$\frac{\partial f}{\partial t} + \vec{v} \cdot \frac{\partial f}{\partial \vec{x}} + \vec{g} \cdot \frac{\partial f}{\partial \vec{v}} = 0, \tag{3.17}$$

where $\vec{g}$ is the force field.

The projection of the phase space density on velocity space is the mass density $\rho$:

$$\rho(\vec{x}, t) = \int d^3v \, f(\vec{x}, \vec{v}, t). \tag{3.18}$$

The mass density $\rho$ generates the force field $\vec{g}$ by Newton's gravity. In a cosmological setup the mean density $\rho_0$ is subtracted,

$$\begin{aligned} \vec{g} &= G \int d^3x' \, \left[\rho(\vec{x}', t) - \bar{\rho}_0(t)\right] \frac{\vec{x} - \vec{x}'}{|\vec{x} - \vec{x}'|^3} \\ &= G \int d^3x' \, d^3v \, \left[f(\vec{x}', \vec{v}, t) - \bar{f}_0(\vec{v}, t)\right] \frac{\vec{x} - \vec{x}'}{|\vec{x} - \vec{x}'|^3}. \end{aligned} \tag{3.19}$$

So in this context using vanishing small thermal velocity already poses a consistency problem since $f$ is of the form $\delta(\vec{v} - \vec{v}_0(\vec{x}))\rho(\vec{x})$. This implies representing the system with a diverging $f$ in a vanishing fraction of the phase space volume, in other words, mass belongs only to an infinitesimally thin 3D sheet in 6D phase space. As $f$ is conserved along characteristics, it implies that this singularity must persist at all subsequent times.

Several methods have been proposed in order to conserve arbitrarily high phase space density (Abel 2012; Hahn & Angulo 2015), but this is not necessarily sufficient. Ideally a physically sound solution $f_0$ to this Boltzmann-Poisson system should not be numerically sensitive to the initial condition discretization. In practice it is known that the gravitational $N$-body problem is exponentially sensitive to perturbations (Miller 1964), so the best that can be expected in such simulations is that over an ensemble of simulations with identical statistical initial conditions, results follow a reproducible statistical distribution.

When $f_0$ is finite and differentiable everywhere, in other words when $f_0$ mathematically exists, the sound situation that should be used, a slight variation of $f_0$, a fluctuation, will also follow the same set of equations. For $f = f_0 + f_1$, $\vec{g} = \vec{g}_0 + \vec{g}_1$, where $f_1$ and $\vec{g}_1$ are the differences between the reference $f_0$ and the perturbed solution $f$, and using the fact that $f_0$ is a solution of the system, we obtain the exact equations for the differences $f_1$, and $\vec{g}_1$:

$$\frac{\partial f_1}{\partial t} + \vec{v} \cdot \frac{\partial f_1}{\partial \vec{x}} + \vec{g}_0 \cdot \frac{\partial f_1}{\partial \vec{v}} = -\vec{g}_1 \cdot \frac{\partial f_0}{\partial \vec{v}} - \vec{g}_1 \cdot \frac{\partial f_1}{\partial \vec{v}} \tag{3.20}$$

$$\vec{g}_1 = G \int d^3x' \, d^3v \; f_1(\vec{x}', \vec{v}, t) \frac{(\vec{x} - \vec{x}')}{|\vec{x} - \vec{x}'|^3} \tag{3.21}$$

So we see that $f_1$ follows the same left-hand side equation as $f_0$ in the unperturbed field $\vec{g}_0$, except that now the right-hand side contains a source term whose first term $\vec{g}_1 \cdot \frac{\partial f_0}{\partial \vec{v}}$ is the product of the force fluctuations $\vec{g}_1$ times the gradient of the original $f_0$ in velocity space. Thus a vanishing zero thermal velocity for a set of particles supposed to represent a physical $f_0$ is not only suspicious since it corresponds to a delta function in velocity space, but also because the gradient $\frac{\partial f_0}{\partial \vec{v}}$ is at least as singular as $f_0$. In other words a zero initial thermal width is inconsistent with the initial assumptions, and susceptible to arbitrary strong amplification of perturbations, since the variational equations contain a diverging source term to first order when the initial thermal velocity is small. The only possibility to cancel this diverging term is either to have vanishing force fluctuations $\vec{g}_1$, which is exceptional when $f_1$ is non-zero, or that $\vec{g}_1$ is orthogonal to $\frac{\partial f_0}{\partial \vec{v}}$, which is also exceptional. The second order term $\vec{g}_1 \cdot \frac{\partial f_1}{\partial \vec{v}}$ on the right-hand side can cancel the first term

only when $f_1$ is proportional and opposite to $f_0$, which is also exceptional. In summary dealing with diverging $f_0$ is inconsistent with the implicit assumption of regularity of the mathematical problem.

While the implementation of velocities has been shown (Melott 2007) to be of importance even for the CDM simulations, for WDM it becomes even more relevant (Colombi, Dodelson & Widrow 1996), since the particles do have intrinsic non-zero velocity dispersion.

Furthermore, Heisenberg's inequality sets a maximum limit for the phase space density

$$\Delta x \Delta p_x \geq \frac{\hbar}{2} \tag{3.22}$$

which in turn gives a minimum particle velocity dispersion, taking $\Delta x = n^{-1/3}$ and $m$ the particle mass,

$$\Delta v \geq \frac{\hbar}{2} \frac{n^{1/3}}{m} \approx 0.003 \left[\frac{1\,\mathrm{keV}/c^2}{m}\right] \left[\frac{n}{1\,\mathrm{cm}^{-3}}\right]^{1/3} \mathrm{km/s}\,. \tag{3.23}$$

Considering a velocity dispersion smaller that this value violates Heisenberg inequality, while taking only a slightly larger one, moves the problem from the classical realm, which is the case in cosmological $N$-body simulations, into the realm of quantum physics.

We conclude that using the thermal velocity component is the correct and more 'physical' way of describing the particles, avoiding the numerical problem posed by a singular phase space density. Apart from the 'correctness' argument, while for some studies, the velocity dispersion has a negligible effect, we will see that this effect becomes important at small scales, for structure formation, as well as for the internal structure of halos, not only in phase space, but also in real space.

#### 3.3.2.2 The 'What'

The parameter used to distinguish between CDM and WDM particles in the simulations is the velocity dispersion, although usually, the mass of the particle is the one cited in the literature. The velocity, which is connected to the streaming length of the particle, is the parameter that dictates where the power spectrum should be cut off. For this reason one has to be consistent in choosing a value for the thermal velocity that corresponds to the power spectrum cutoff.

How the velocity relates to the mass is strongly dependent on the model assumed for a certain WDM particle. Several studies have been evaluating this mass to velocity correspondence, but in most of the simulations the adopted relation is the one given in Bode et al. (2001). In Paduroiu et al. (2015) we are inspecting those results (Bode et al. 2001) in detail, emphasizing some implications of the assumptions made[10]. Moreover, we give an alternative calculation based on different premises and we point out how sensitive the mass-velocity relation is to the initial model of particle production and the physics describing the behavior of the hypothesized particle.

In this section, the mass-velocity relation from several studies will be evaluated, including not just thermalized particles like thermal sterile neutrinos, but also neutrinos produced through a Non-Resonant Production (NRP) mechanism.

[10]We have also found a misprint in the value for the rms velocity factor

Let us commence by a brief[11] assessment of the frequently cited derivation of WDM particle velocities as a function of mass and redshift from Bode et al. (2001). In their Appendix A, they recall that for a thermal relict particle X that decouples when relativistic, the abundance $n_x$ relative to photons is:

$$\frac{n_X}{n_\gamma} = \left(\frac{43/4}{g_{\rm dec}}\right)\left(\frac{4}{11}\right)\frac{g_X}{2} \tag{3.24}$$

where $g_{\rm dec}$ is the number of relativistic species present at decoupling and $g_X$ is the number of spin states of the particle. To connect the particle mass density $\rho_X = m_X n_X$ with the cosmological parameters $\Omega_X \equiv \rho_x/\rho_c$ and $h$, where the critical universal density $\rho_c \equiv 3H^2/8\pi G$, and the Hubble constant $H \equiv 100h\,{\rm km\,s^{-1}\,kpc^{-1}}$, they derive,

$$\Omega_X h^2 \approx \frac{115}{g_{\rm dec}}\frac{g_X}{1.5}\frac{m_X}{\rm keV}\,. \tag{3.25}$$

Assuming that the distribution function scales as the non-thermal distribution $(\exp(v/v_0)+1)^{-1}$, for a redshift $z$, the velocity $v_0$ (in their Eq. (A3)) is given,

$$\frac{v_0(z)}{1+z} = \mathbf{.012}\left(\frac{\Omega_X}{0.3}\right)^{\frac{1}{3}}\left(\frac{h}{0.65}\right)^{\frac{2}{3}}\left(\frac{1.5}{g_X}\right)^{\frac{1}{3}}\left(\frac{\rm keV}{m_X}\right)^{\frac{4}{3}}{\rm km\,s^{-1}}\,. \tag{3.26}$$

Eliminating $\Omega_X h^2$ in this previous equation using Eq. (3.25) (their Eq. (A2)), we obtain for a $m_X = 1$ keV particle (rounding also to 2 significant digits),

$$\frac{v_0(z)}{1+z} \approx \mathbf{0.12}\left(\frac{1}{g_{\rm dec}}\right)^{1/3}\frac{\rm keV}{m_X}\,{\rm km\,s^{-1}}\,. \tag{3.27}$$

Thus we find $g_{\rm dec} = \mathbf{1000}\,(g_X/1.5)^{1/3}$ for a 1 keV particle.

This is a very high value for the number of species at decoupling. In the minimal standard model the number of the full set of particles is $\sim 107$ while in the minimal supersymmetric standard model, the value is increased to $\sim 229$ (Pierpaoli et al. 1998). Previous studies quote a much smaller value for $g_{\rm dec}$. Pierpaoli et al. (1998) assume a conservative reference value of 150 for both gravitino and a standard warm dark matter candidate like the massive neutrino, while Colombi, Dodelson & Widrow (1996) use a value of $\sim 100$ for right-handed neutrinos decoupling before the electroweak phase transition at very high temperatures, to give just two examples.

A similar derivation to the one in Bode et al. (2001) is given by Destri (2014). Assuming a freezed-out dimensionless distribution

$$\rho_M\, f_{\rm i}\,(\mathbf{v}) = \frac{g}{1+e^{\epsilon/T}}\frac{m^4}{(2\pi\hbar)^3}\,, \tag{3.28}$$

where $\epsilon = mc|\mathbf{v}|$ is the kinetic energy and $T$ is the (comoving) decoupling temperature and using $\rho_M = \Omega_M \rho_{\rm crit}$, the velocity dispersion $\sigma_0$ at reshift zero is given by

$$\sigma_0 = 0.025\left(\frac{h}{0.7}\right)^{2/3}\left(\frac{\Omega_{\rm M}}{0.3}\right)^{1/3}\left(\frac{2}{g}\right)^{1/3}\left(\frac{\rm keV}{mc^2}\right)^{4/3}{\rm km\,s^{-1}}, \tag{3.29}$$

[11] For a detailed discussion please refer to Paduroiu et al. (2015) at the end of this chapter

with a correction for the distribution of

$$\left[\frac{5\,\zeta(5)}{\zeta(3)}\right]^{1/2} = 2.07680\,, \tag{3.30}$$

where $\zeta(x)$ is Riemann's $\zeta-$function. This gives an expression for the $v_0$ velocity

$$v_0 = 0.012\left(\frac{h}{0.7}\right)^{2/3}\left(\frac{\Omega_{\rm M}}{0.3}\right)^{1/3}\left(\frac{2}{g}\right)^{1/3}\left(\frac{\rm keV}{mc^2}\right)^{4/3}\,{\rm km\,s^{-1}}, \tag{3.31}$$

citing a value of $g = 2$ or $g = 4$, depending on the specific model[12], for a -1/2 spin sterile neutrino (Dodelson & Widrow 1994; Shi & Fuller 1999; Shaposhnikov & Tkachev 2006).

Considering different assumptions than the ones previously used, we provide a different mass-thermal velocity correspondence based on number conservation and a non-entropy production, while taking into account the quantum pressure, but assuming a thermalization caused by the exchange potential.

The Fermi-Dirac and Bose-Einstein full distribution is the following (e.g., Padmanabhan 2002)

$$f(\vec{p}) = \frac{g}{(2\pi\hbar)^3}\frac{1}{\exp((\epsilon-\mu)/kT)\pm 1}\,, \tag{3.32}$$

where $\vec{p}$ is the particle momentum, $g$ the spin-degeneracy factor (of order 1 or 2), $\mu$ the chemical potential, $\epsilon = \sqrt{p^2c^2+m^2c^4} - mc^2$ the particle energy, $m$ the particle mass and $T$ the particle temperature.

The entropy $S$ expressed as a function of other thermodynamical variables reads (e.g., Padmanabhan 2002, Vol. I, Eq. 5.73),

$$S = \frac{1}{T}\left(E + PV - \mu N\right)\,, \tag{3.33}$$

where $E$ is the total thermal energy, $P$ the pressure, $V$ the volume, $\mu$ the chemical potential and $N$ the number of particles. The specific entropy $s \equiv S/N$ divided by Boltzmann's constant $k$ is a pure number

$$\frac{s(T,\mu)}{k} = \frac{1}{kT}\left(\frac{e+P}{n} - \mu\right)\,, \tag{3.34}$$

where $e = E/V$ is the specific energy density and $n = N/V$ is the number density.

The thermodynamical quantities for fermions and bosons at all regimes can be calculated accurately by evaluating numerically the relativistic Fermi-Dirac or Bose-Einstein integrals for particle density $n$, energy density $e$, and pressure $P$ (e.g., Padmanabhan 2002, Vol. II, p. 216) as functions of temperature $T$ and chemical potential $\mu$:

$$n(T,\mu) = \frac{4\pi g}{h^3}\int_0^\infty \frac{p^2}{\exp((\epsilon-\mu)/kT)\pm 1}\,dp\,, \tag{3.35}$$

$$e(T,\mu) = \frac{4\pi g}{h^3}\int_0^\infty \frac{p^2\epsilon}{\exp((\epsilon-\mu)/kT)\pm 1}\,dp\,, \tag{3.36}$$

[12] In many studies the value used is $g = 1.5$

$$P(T,\mu) = \frac{4\pi g}{h^3}\int_0^\infty \frac{p^2}{\exp((\epsilon-\mu)/kT)\pm 1}\frac{1}{3}\frac{c^2p^2}{\epsilon+mc^2}\,dp\,, \tag{3.37}$$

where $g$ is the number of distinct particle states and $\epsilon = \sqrt{p^2c^2+m^2c^4} - mc^2$ the particle energy. In the integrands the $+$ sign is for fermions, the $-$ sign for bosons.

Here we give the final expression for velocity, in the case of fermions[13]. This expression is independent on the cosmological parameters:

$$\frac{v}{1+z} = \mathbf{0.22}\left(\frac{n}{115\,\mathrm{cm}^{-3}}\frac{1}{g}\right)^{1/3}\left(\frac{\mathrm{keV}}{\mathrm{mc}^2}\right)\,\mathrm{km\,s}^{-1}\,. \tag{3.38}$$

Other examples in the literature give different correspondences between the particle mass and its velocity dispersion.

Assuming a homogeneous isotropic distribution with no chemical potential, Ringwald & Wong (2004) estimate a mass-velocity relation for neutrinos[14]

$$\frac{v_0(z)}{1+z} = \mathbf{0.16}\left(\frac{\mathrm{keV}}{m_X}\right)\,\mathrm{km\,s}^{-1} \tag{3.39}$$

with the present neutrino temperature[15]

$$T_0 = 1.614\times 10^{-4}\mathrm{eV}. \tag{3.40}$$

Distinguishing between thermal relics (TR) and neutrino produced through a Non-Resonant Production (NRP) mechanism, non-resonant oscillations with active neutrinos (Dodelson & Widrow 1994; Dolgov & Hasen 2002; Asaka, Laine, & Shaposhnikov 2007), Boyarsky et al. (2009) give the following expressions for the velocity dependence on temperature and mass

$$\langle v_{\mathrm{TR}}\rangle = \frac{3.151\,T_{\mathrm{TR}}(z)}{m_{\mathrm{TR}}} = 8.07\left(\frac{1+z}{100}\right)\left(\frac{\mathrm{kev}}{m_{\mathrm{TR}}}\right)\left(\frac{T_{\mathrm{TR}}}{1\,\mathrm{K}}\right)\,\mathrm{km\,s}^{-1} \tag{3.41}$$

and

$$\langle v_{\mathrm{NRP}}\rangle = \frac{3.151T_\nu(z)}{m_{\mathrm{NRP}}} = \frac{3.151(4/11)^{1/3}(1+z)T_{\mathrm{CMB}}}{m_{\mathrm{NRP}}} = 15.7\left(\frac{1+z}{100}\right)\left(\frac{\mathrm{kev}}{m_{\mathrm{NRP}}}\right)\,\mathrm{km\,s}^{-1} \tag{3.42}$$

with the parameter $T_{\mathrm{TR}}$ (for TR) inferred from $(T_{\mathrm{TR}}/T_\nu)^3 = \Omega h^2(94\ \mathrm{eV}/m)$. Considering that the whole dark matter content is made up by one type of particles, giving $\Omega h^2 = 0.12$, the expression derived for the velocity dispersion in the thermal case at redshift zero is

$$\frac{v_0}{1+z} = \mathbf{0.03}\left(\frac{\mathrm{kev}}{m_{\mathrm{TR}}}\right)^{4/3}\,\mathrm{km\,s}^{-1}\,. \tag{3.43}$$

One can see that depending on the model assumed and the parameters considered, the correspondence between the mass of the particle and its velocity is not universal, but it can differ by an important factor. In the Table 3.2 we give the different values of velocities corresponding to different studies for particles with the mass 0.2, 1 and 3.5 keV respectively.

[13]The detailed calculation for both fermions and bosons can be found in Paduroiu et al. (2015).

[14]They do mention that the chemical potential should not necessarily be zero. In their paper, the formula is used to study the clustering for neutrinos with masses below 1 eV.

[15]Note that in the paper the temperature is given in eV units, not $\frac{\mathrm{eV}}{m_X}K$.

Table 3.2: Correspondence between particle mass $m$ and rms velocity dispersion in the literature for 0.2, 1 and 3.5 keV. The first column shows the value originally given in Bode et al. (2001), the second column shows the value obtained using $g_{\rm dec} = 150$ (Pierpaoli et al. 1998) in Eq. (4.17), the third one, the value given by our derivation and the fourth and fifth, the value given by Boyarsky et al. (2009) for thermal and non-resonant produced neutrinos respectively. All the values are given at redshift z=0.

| Mass | Bode et al. $v_0 \times 3.571$ | Pierpaoli et al. | Paduroiu et al. | Boyarsky et al. TR | Boyarsky et al. NRP |
|---|---|---|---|---|---|
| keV/$c^2$ | km/s | km/s | km/s | km/s | km/s |
| 0.2 | 0.366 | 0.4032 | 1.113 | 0.29 | 0.785 |
| 1.0 | 0.0429 | 0.0225 | 0.223 | 0.034 | 0.157 |
| 3.5 | 0.00806 | 0.0230 | 0.0636 | 0.0064 | 0.00448 |

The different values for the velocities that depend on the cosmological parameters have been obtained assuming that there is only one species of particles that contribute to the dark matter content in the universe. For the simulations that include several species of particles, one needs to correct in the expression for the velocity, not only the fraction, but also the $g_{dec}$ number, which will give a different correspondence with the mass. This correction was missed in several previous studies in the literature. This is important not just for the simulations with thermal velocities, but for all the simulations, since the power spectrum is in fact directly depending on the streaming velocity of the particles and not the mass.

These differences in the velocities estimations are cumulative in their effect at the starting high redshifts of the simulations and are crucial not only for phase space density studies, but also for structure formation. Constraints on the mass of a particle from the simulations are thus not robust.

While we have referred mainly to particles like sterile neutrinos that are thermalized with velocities from hundreds of eV to few keV and which do not decay, we already found how strongly dependent on the model the impact of these particles is on structure formation and how difficult it is to constrain the properties of such particles from the simulation results. The warm dark matter picture can contain, from the point of view of particle physics, a large variety of particles, with different properties and behaviors than the case we have considered. Just for the sterile neutrino family there are a number of models that differ significantly that the ones we presented. For example, heavy sterile neutrinos with rest masses in the few hundred MeV that decay nonthermally (Fuller, Kishimoto & Kusenko 2011) have been considered, or particles with masses less than 10 MeV that remain in equilibrium with neutrinos until becoming non-relativistic, reheat the neutrinos with respect to the electromagnetic plasma and therefore lead to extra energy density in the early universe (Boehm, Dolan & McCabe 2012). Light sterile neutrinos, which decouple shortly after the QCD phase transition with a highly non-thermal distribution function, may explain for

example the 3.55 keV line and the cores in dwarf galaxies, as shown in Lello & Boyanovsky (2015). Also, axions that thermalize from gravitational interactions and rethermalize when falling in a galactic potential, may give an explanation for the presence of caustic rings (Erken et al. 2012). Whether or not the thermalized axions can be considered particles in the warm dark matter model is another discussion.

Giving just few examples to illustrate the variety of what the warm dark matter particles may be and what their impact on the structure in the universe they may have, to constrain or rule out warm dark matter in general based on simulations not without their shortcomings, is naive.

#### 3.3.2.3 The 'How'

Given the importance of correctly including thermal velocities for a chosen model that one would like to explore and test with simulations, the actual implementation of the velocities is not trivial, although it is usually simplified.

After generating the cosmological initial conditions, with the cutoff in the power spectrum corresponding to a certain velocity, one can add the thermal velocity component that corresponds to that particular velocity. The commonly used method for adding the velocity dispersion is to randomly generate velocities from a chosen distribution and then assign them to the particles in the simulation. It is important to take into account the fact that the rms velocity depends on the distribution assumed.

This method is as simplified as it sounds and far from ideal, since the particles in the simulations are usually of the order of several powers of 10 $M_\odot$ (off by a factor of roughly $10^{70}$) and it is one of the main reasons for choosing not to use thermal velocities in many simulations. It is however the compromise that one has to make when wanting to simulate such particles. Even when the numerical value for the thermal velocity is comparable to that for Zel'dovich velocities, the latter is a bulk velocity and not a dispersion velocity. This distinction is important not only for describing the evolution of a system of particles in a simulation, but even more so in phase space, where it makes a fundamental difference. This problem becomes more complicated in the hydrodynamic simulations, where together with the dark matter particles, gas particles and other baryonic physics processes are introduced. If and how the velocities should be treated for other particles than dark matter is a question that has not been properly addressed so far.

### 3.3.3 WDM simulation parameters

We have performed several suites of cosmological $N$-body simulations, using for each simulation both pkdgrav-2 and Gadget-2 codes. The initial conditions have been generated with grafic2.

For the WDM case we have performed simulations that cover a large range of velocities from 0.01 km/s to 10 km/s (corresponding to 3.5 keV to 15 eV in Bode et al. (2001)). We show here the analysis of a few of those simulations, where different structure formation mechanism are easier to explore with our resolution. These simulations have an initial power spectrum consistent with

Table 3.3: Details of the simulations

| Label | velocities $z_i$ | cutoff | box size | N | softening |
|---|---|---|---|---|---|
| | km/s | keV | Mpc/h | | kpc |
| CDM | no | - | 40 | $300^3$ | 1 |
| WDM1 | no | 0.2 | 40 | $300^3$ | 1 |
| WDM2 | 36.6 | 0.2 | 40 | $300^3$ | 1 |
| WDM3 | no | 1 | 40 | $300^3$ | 1 |
| WDM4 | 4.6 | 1 | 40 | $300^3$ | 1 |
| WDM5 | 36.6 | 0.2 | 30 | $256^3$ | 2.5 |

the initial velocities and for comparison we performed simulations with the same initial power spectrum without initial velocities.

The simulation parameters are summarized in Table 3.3[16]. The starting redshift for the simulations is $z_i = 100$ in order to ensure a proper treatment of the non-linear growth of cosmic structures. The cosmological parameters used are given by the WMAP7 results: $\Omega_\Lambda$=0.72, $\Omega_m$=0.28, $\Omega_b$=0.05, $h = 0.7$ and $\sigma_8 = 0.821$.

We start with running large scale simulations in cosmological box of 40 Mpc/h, using $300^3$ dark matter particles and one 30 Mpc/h box with $256^3$ particles. We then select a region where the top-down halo formation is predominant and re-simulate it with an eight times higher mass resolution.

## 3.4 Simulations analysis and results

From the number of simulations performed, with velocities in a range from 0.01 km/s to 10 km/s (3.5 keV to 15 eV in the Bode et al. (2001) estimation) at redshift zero, we have chosen the ones summarized in the previous section, as they illustrate best the qualitative differences in the structure formation. The results of our analysis on large scale structure, as well as structure of halos, are presented in Paduroiu et al. (2015), (Section 2.6). In this section we will concentrate, however, on structure formation, leaving the implications on the internal structure of halos for the next chapter.

The visualization of the outputs of the simulations, a crucial method for discovering the subtle aspects of the structure formation in warm dark matter models in particular, has been done using Tipsy[17] developed by Neal Katz and Tom Quinn and pNbody[18] developed by Yves Revaz.

[16]Other parameters used are MaxSizeTimestep = 0.0048, ErrTolForceAcc = 0.005 and MaxRMSDisplacementFac = 0.25
[17]http://www-hpcc.astro.washington.edu/tools/tipsy/tipsy.html
[18]http://obswww.unige.ch/ revaz/pNbody/

### 3.4.1 Structure formation in WDM from the numerical simulations

Traditionally, structure formation is described as 'top-down' when the biggest halos are the ones formed first, which then grow through the accretion of matter from the filaments, which in turn break into smaller halos. At redshift zero, the biggest halos would then be the earlier formed ones. The 'bottom-up' structure formation, on the other hand, decribes a structure that grows via mergers, starting with small halos formed from fluctuations on the smallest scales. These halos are merging into big halos, merging into large clusters, leading to a higher concentration of particles into these structures at low redshift. However, the small structures are forming throughout the entire simulation, resulting in the presence of a larger number of small halos at redshift zero, generally called satellites. While both these mechanisms of structure formation are hierarchical, with the hierarchy reversed in one model with respect to the other, the term 'hierarchical' has been used in the literature to rather describe the bottom-up scenario.

In earlier studies (Bode et al. 2001; Knebe et al. 2003, e.g.) of warm dark matter numerical simulations, the structure formation was associated with a top-down mechanism, meaning that the biggest structures are forming first via gravitational collapse in the highest density regions, and then continue growing through the accretion of matter from the filaments.

This mechanism differs from the monolithic collapse mechanism (Larson 1975; Tinsley & Gunn 1976) originally proposed by Eggen, Lynden-Bell & Sandage (1962) to describe how a galaxy forms through the collapse of a cloud of gas. Although in both these scenarios the structures are formed via collapse, in the monolithic case, a halo forms from a cloud of matter, while in the WDM case it forms at the intersection of filaments, where the density reaches a peak. Later studies, using much colder particles, in the few keV range, have seen that the simulation outputs do not look much different to the ones in cold dark matter, with the exception of fewer small satellites in the WDM case, and concluded that the structure formation is hierarchical.

As shown in our paper, the structure formation mechanism is not as simple as previously assumed, but it rather has different stages where both these mechanisms compete.

Performing simulations in a large range of values for the velocities, from cold to hot dark matter, we could see how the top-down and bottom-up trends manifest themselves. In the hot dark matter case, as shown in Fig.1 Paduroiu et al. (2015) (Section 3.6), the formation is essentially top-down in the classical sense, sometimes with the larger halos at redshift zero being the earlier ones formed, simply because that is when they collapse. In the simulations with colder particles, the structure formation is very similar to the bottom-up description.

We have chosen an intermediate transient regime, of particles with velocity dispersions around 0.3 km/s (corresponding to 200eV in the (Bode et al. 2001) approximation), where we can better explore these effects. This is indeed in an area otherwise ruled out by many observational constraints as being solely accounting for the whole dark matter content, mainly because the structure formation is very much delayed. This delay, however, and the slow evolution allows for a better examination of the mechanisms of stucture formation. The best way to view, especially the early

features of structure formation, is by watching the movies that show how the structure forms. The movies are made from the snapshots of almost 500 simulation outputs, starting from redshift z=20, much early than when the first collapse occurs, around redshift z=10. Several movies of WDM structure formation, filament collapse and halo formation from this study can be found on youtube [19].

From analyzing the simulations we can see that the structure formation scenario is more 'colourful' than it has been previously assumed.

- At first there are sheets, which collapse into filaments, which collapse into halos.
- The first halos form top-down in high density regions found at the intersection of well-contoured filaments. After the collapse, the newly formed halo begins accreting matter from the disrupted filaments.
- Depending on the morphology of the region, some of these halos can become very massive very fast, just by accretion (Paduroiu et al. (2015) Fig. C1 Appendix A, Section 3.6).
- Later on, in medium density regions and depending on the spatial distribution of filaments in that region, some not so massive halos merge into bigger ones, signalling the beginning of a bottom-up growth scenario (Paduroiu et al. (2015) Fig. C2 Appendix A, Section 3.6).
- In lower density regions, usually situated in voids, collapse is even more delayed. We see filaments being formed and collapsing very late. This favours the survival without any mergers of a top-down formed halo up to redshift zero (Paduroiu et al. (2015) Fig. C3 Appendix A, Section 3.6).
- In a more complex scenario, massive halos formed early are violently merging together at late times, forming a large cluster (Paduroiu et al. (2015) Fig. C4 Appendix A, Section 3.6).

Although the first halos are forming through top-down gravitational collapse, most of them are then merging into more massive ones. The statement that the most massive halos are the earliest formed ones is not valid for all regions in our simulations at redshift zero, but at a much higher redshift, around z=6, meaning the structure formation is not best described by the top-down mechanism, in the conventional sense. Also, since in the lowest density regions, in voids, the structure forms top-down via collapse at later stages, those halos will not grow as much until redshift zero and will be lower in mass in comparison with most of the halos at that redshift. The hierarchical build-up that follows the formation of the first halos does not begin from fluctuations at the smallest scale as in the bottom-up classical scenario.

[19] All the HD movies are on this playlist on youtube `https://www.youtube.com/playlist?list=PLnGS4wkStJ1aqi3M9hTDaUzuZ-vs-Qg6i` and can be watched individually on this channel `https://www.youtube.com/channel/UCEmQi8hDNW2emqGn-urtvpg`. Remember to adjust your settings to HD quality.

The mechanism of structure formation is thus a hybrid mechanism, where both long-range and short-range effects are present, from long distance to nearest neighbours, from top-down to bottom-up. Why one trend is more prominent in a certain region at a certain time, depends only on the morphology and architecture of the analyzed region. Some of our findings confirm those of previous studies like (Bode et al. 2001, e.g), agreeing that the formation of structure evolves differently at different scales.

While previously we have referred to the analysis of the WDM2 simulation in Table 3.3, in the WDM5 simulation we see similar trends in the fashion in which structure is formed. In Fig. 3.3 we show the full simulation box at different redshifts, encircling three regions of interest. One can see the evolution of a halo formed top-down at the intersection of large filaments, a halo formed late in a low density 'isolated' region and finally a region where several smaller halos that formed top-down are approaching each other for merging. In Fig. 3.4 we show the full box of WDM5 and CDM simulations at redshift zero, plotting only regions with a density 100 times higher than the mean density in order to emphasize the contrast in the distribution of high density regions.

Comparing the structure formation in WDM simulations with that in CDM simulations, one can immediately see, for a particle with a high enough velocity dispersion, several differences:

- In terms of density, there is a difference between how the high density regions are distributed in the simulations. In the WDM case one can see that large high density regions are more isolated by even larger low density ones, as shown in Paduroiu et al. (2015) (Fig.2, Section 3.6).
- The structure formation is delayed depending on the streaming velocity of the particles - the higher the velocity is, the later the collapse happens (Fig.2, Section 3.6).
- The filamentary looking structure is more apparent in the WDM case, with the filaments being preserved longer.
- The number of small halos formed in WDM is smaller than in CDM (Fig.1, Section 3.6).

When counting the number of small halos, however, taking into consideration the numerical limitations is required. We need to distinguish between two ways in which the filaments are breaking or fragmenting. After the large halos are formed at the intersection of the filaments and begin accreting matter from them, the filaments will break and in the regions that are not accreted new filaments will develop, which will then collapse into halos. This is different from the case in which a filament fragments along its main central line into equally spaced halos with similar masses. The latter case describes an artificial process, strongly dependent on the resolution of the simulation, as we will show in Chapter 5. Therefore, inside the filaments, the way the halos are formed is influenced by the fragmentation and hence, by the resolution of the simulation. Since the filaments are fragmented in small periodically distributed halos, some of these may merge and form bigger ones. This 'contamination' may propagate until redshift zero; these halos being

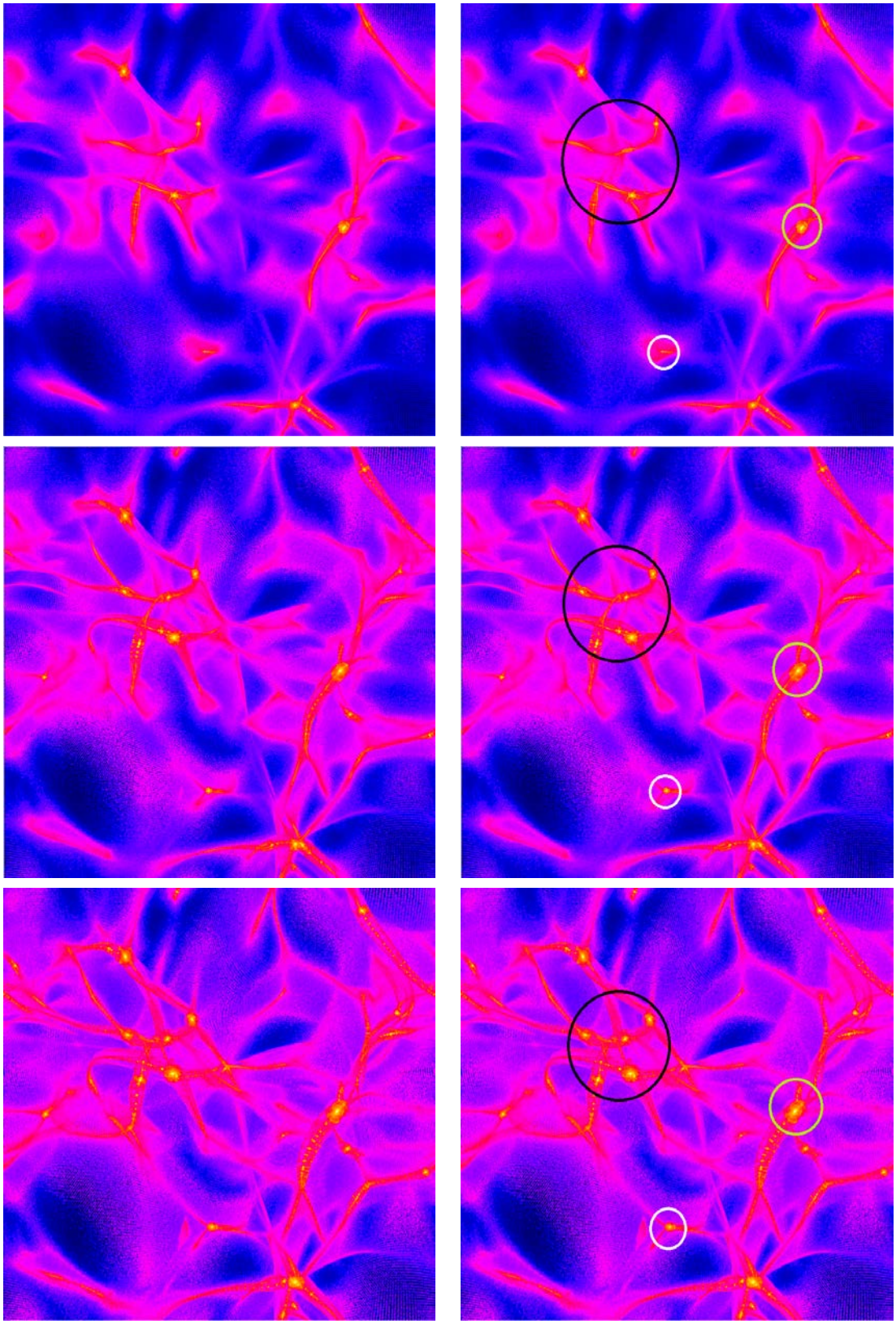

Figure 3.3: Structure formation in WDM5 simulation at redshift z=2 (upper panel) z=1 (middle panel) and z=0 (lower panel). On the right panels different regions corresponding to different mechanisms are encircled. A region where a large halo forms top-down, in green, a region where several halos are approaching merging, in black, a halo forming late in an isolated region, in white.

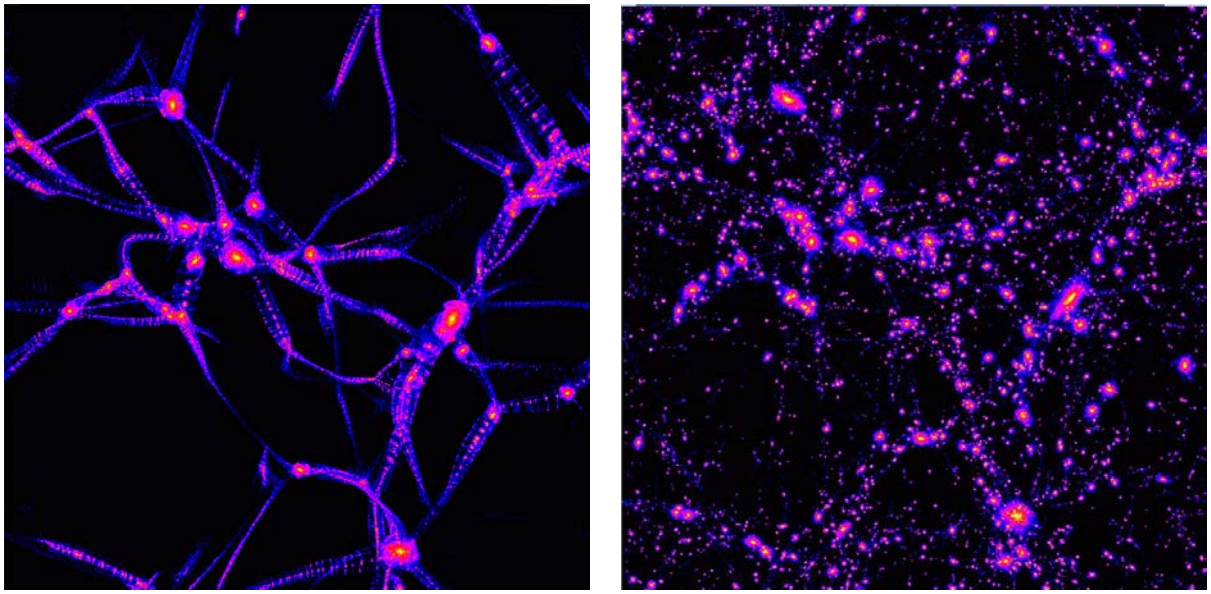

Figure 3.4: WDM5 full box (left panel) and CDM full box (right panel). Only regions with a density 100 times higher than the mean density are plotted.

hard to distinguish from the 'genuinely' formed halos because their mass will be higher than that of those initial ones formed artificially. Stressing again the fact that the number of these small artificial halos depends on the resolution of the simulation, one can conjecture that for an 'ideal' resolution and therefore in a real warm dark matter universe, the number of satellites will be even smaller at redshift zero. Since in the few keV regimes mergers are more predominant and happen at earlier redshift, the elimination from the present day sample of all the halos that are formed artificially or formed from artificial halos is impossible. This again, gives an overestimation of the number of small satellites at redshift zero.

### 3.4.2 Impact of the thermal velocities

The top-down structure formation can be seen in both simulations, with or without the added thermal velocities, and is not an effect of the velocity dispersions, but of the free streaming of particles and the suppression of power at small scales. For illustration purposes, we show in Fig. 3.5 the redshift zero outputs from simulations with no cutoff in the power spectrum, but with thermal velocities of 1 km/s, 10 km/s and 200 km/s respectively. The structure formation in this case does not happen top-down at any scale.

In Fig. 3.6 we show the differences at redshift zero between simulations with the thermal velocity component (WDM2) and without it (WDM1). The full box is displayed, together with a small ($\sim 1/9$ box) low density region[20]. A side by side movie of the evolution of structure in these two simulations can be watched on youtube[21]. One can see that these differences become important

[20] For a different zoom in region, which includes both low density and structure formation regions, please refer to Fig. 5 in Paduroiu et al.

[21] The movie can be watched here: `https://www.youtube.com/watch?v=5txGwBRNC1U`

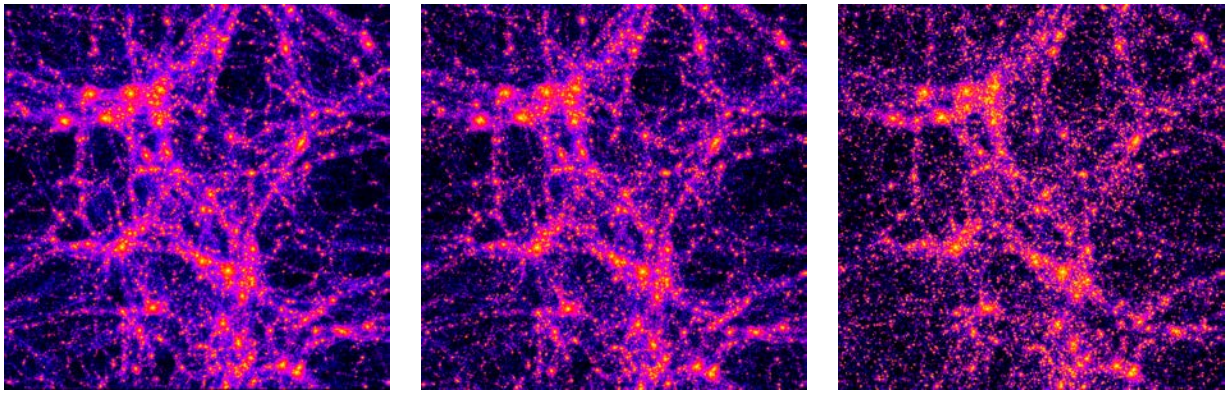

Figure 3.5: Redshift zero simulation outputs with no cutoff in the power spectrum and initial velocities of 1 km/s, 10 km/s, 200 km/s respectively

at very small scales. In the simulation where we have included thermal velocities the structure is smoothed, while in the simulation without thermal velocities the fragmentation is more prominent and the number of very small halos is slightly larger.

In the next chapter we will show how the thermal velocities affect the internal structure of halos. In particular we will see that for any phase space density studies, the use of the velocity dispersion is crucial, since in phase space the warm dark matter particle has a maximum density, different from the cold dark matter particles with infinite phase space density.

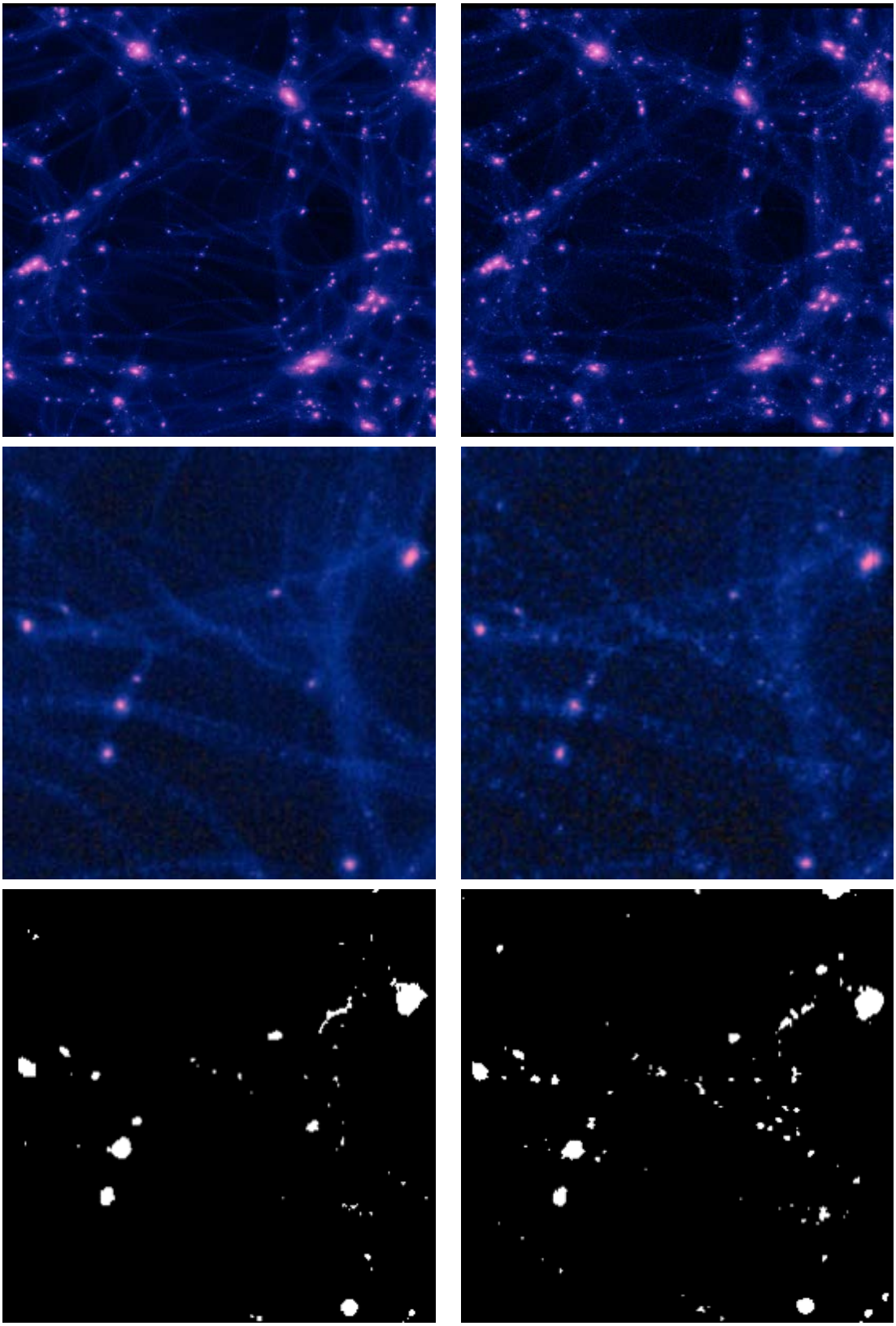

Figure 3.6: Side by side projection of redshift zero simulation outputs with thermal velocities - WDM2 (left) and no thermal velocities - WDM1 (right). The upper panel shows the whole simulation box, the middle panel shows a low density region and the lower panel shows the same zoom in region in black and white, 25% saturation, for a better view of the small scale differences.

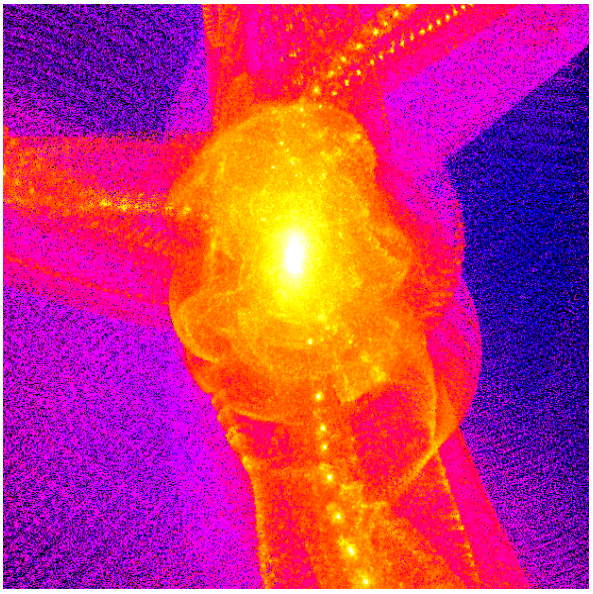

Figure 3.7: A zoom in a high resolution refined halo, formed top-down. Caustics and shells are clearly visible. Several other projections emphasizing these features are shown in Paduroiu et al. (2015) and will be discussed in the next chapter.

### 3.4.3 A refined top-down halo

From the WDM5 simulation we have chosen a region where a large halo forms top-down at the intersection of filaments and grows through the accretion of matter from the filaments. We have performed several levels of refinement. These highest resolution runs are $8^3$ times more resolved in mass than the initial ones: the dark matter particle mass is $M_{dm}$=2.72$\times 10^5$ $M_\odot$, where each dark matter particle has a gravitation softening of 355 pc. The $7\times 10^{12}$ $M_\odot$ halo has 18 million particles in its $r_{200}$ radius. Using 450 outputs we have created movies that show the formation and growth of the halo[22]. The infall material is wrapped in shells and caustics around the center of mass, as can be seen in Fig. 3.7, and the halo does not virialize by redshift zero, having a $r_{200}$ radius of about 600 $\mathrm{kpc}$ , much larger than that of a cold dark matter halo of similar mass. In Fig. 3.8 one can see projections of the region where the halo forms and a zoom in on the halo on all three axes at redshift zero. This gives an idea of the 3D morphology of the region and the architecture of filaments that favor such a structure formation mechanism. The halo was formed at the intersection of very large filaments. Besides accreting matter from the filaments and eventually breaking some of them, the halo is pulling in filaments from a larger distance, which were not originally connected to the collapse region.

Some properties of this halo will be analyzed in the next chapter, which is focused on the internal structure of warm dark matter halos.

[22]The movie can be found on youtube `https://www.youtube.com/watch?v=s_H4dSOP27I`. A zoom in the halo can be watched at `https://www.youtube.com/watch?v=zqVi9SSWmXM`

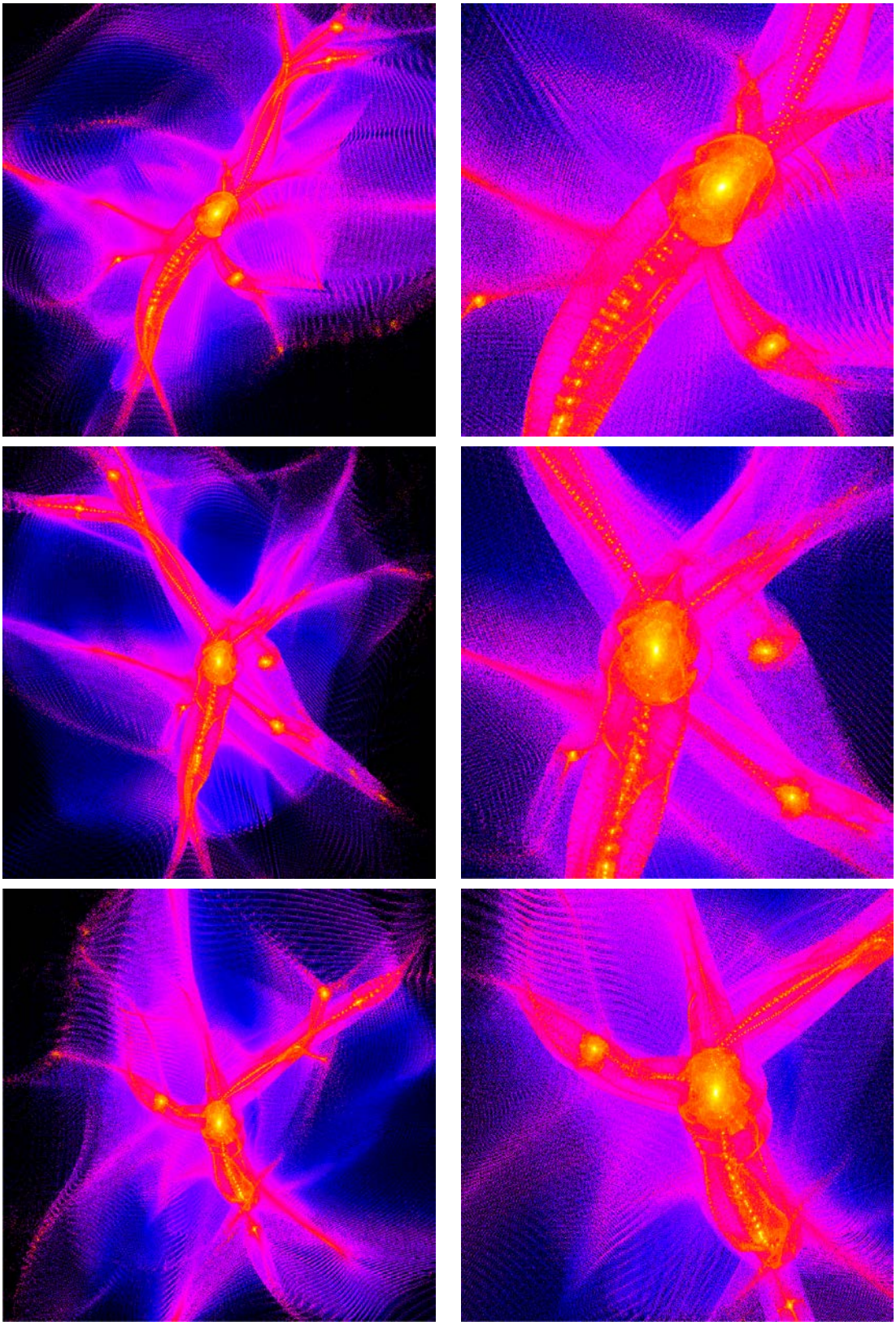

Figure 3.8: Projections of the high resolution region where a halo from WDM5 forms top-down (left panel) and a zoom in (right panel) on x (upper panel), y (middle panel) and z (lower panel) axis at redshift zero.

## 3.5 Discussion and prospects

Our conclusions are presented in Paduroiu et al. (2015) (Section 3.6). We comment here further on the implications of these results and other studies in the literature.

Although the large scale structure formation is dominated by the dark matter clustering effects, baryonic processes offer important hints towards a better comprehension of the way in which structure forms and evolves. In the tapestry of various phenomena that are happening in the universe, it is hard to disentangle with high confidence, the effect that each individual process will have on the structure at observable scales. Simulations represent our best tool at hand for testing such predictions and models, but they are far from giving accurate predictions on the myriad of physical processes that occur in nature. Nevertheless, in the past few years, important developments in the implementation of some physical processes in the cosmological simulations have been made. Alas, most of the studies have been done from the cold dark matter perspective.

From the small sample of warm dark matter simulations that include baryonic physics, one result stands out as intriguing. Gao & Theuns (2007) used high resolution simulations with dark matter particles and gas to study the very early formation of stars in both CDM and WDM case. For the WDM particles, they used a 3 keV gravitino type particle, otherwise considered in the literature to be indistinguishable from the CDM in simulations, and analyzed the behavior of gas in a 3 kpc filament from a high redshift $z \sim 23$. Comparing this simulation with a cold dark matter one, they found a remarkable difference. In the WDM case, due to the free streaming of the particle, the filament is preserved for a longer time. The gas inside the filament has time to heat as it gets compressed, but then cools due to the formation of molecular hydrogen, cooling also the center of the filament. This indicates that in such a context, stars can be formed inside the filament, before the filament collapses and forms halos. The cooling of the filament can act back as a factor of delay in the collapse of the filament. In the case of cold dark matter, the filament fragments into small halos, where the gas is then accreted, reaching the optimal conditions for star formation much later.

This is not a surprising result, since we know that structure forms differently in WDM with respect to CDM. More far reaching implications of this result are in explaining, for example, the early presence of super massive black holes. A scenario in which the filament eventually collapses along its axis, and a high number of collisions between cold cores and stars occur, providing the seed for such massive objects, seems plausible. The caveat of exploring the scenario further, is that it requires enormous resolution. Even for performing the simulation with gas until redshift z=13, very high resolution was needed, $M_{dm}$ = 272.6 $M_\odot$ and $M_{gas}$ = 41.9 $M_\odot$ in a comoving box with a Lagrangian radius of 600 kpc. A recent study confirmed that the trend in which stars form inside the filaments continues for 1.5 keV particles up to redshift $z \approx 2$ resulting in stringy "chain" galaxies that remain to be confirmed by observations (Gao, Theuns & Springel 2015).

In Fig. 3.9 (Gao & Theuns (2007), Figure 1) the density structure of the filament at redshift z=15 is shown. The filamentary pattern in density is produced by both CDM and WDM, but the CDM

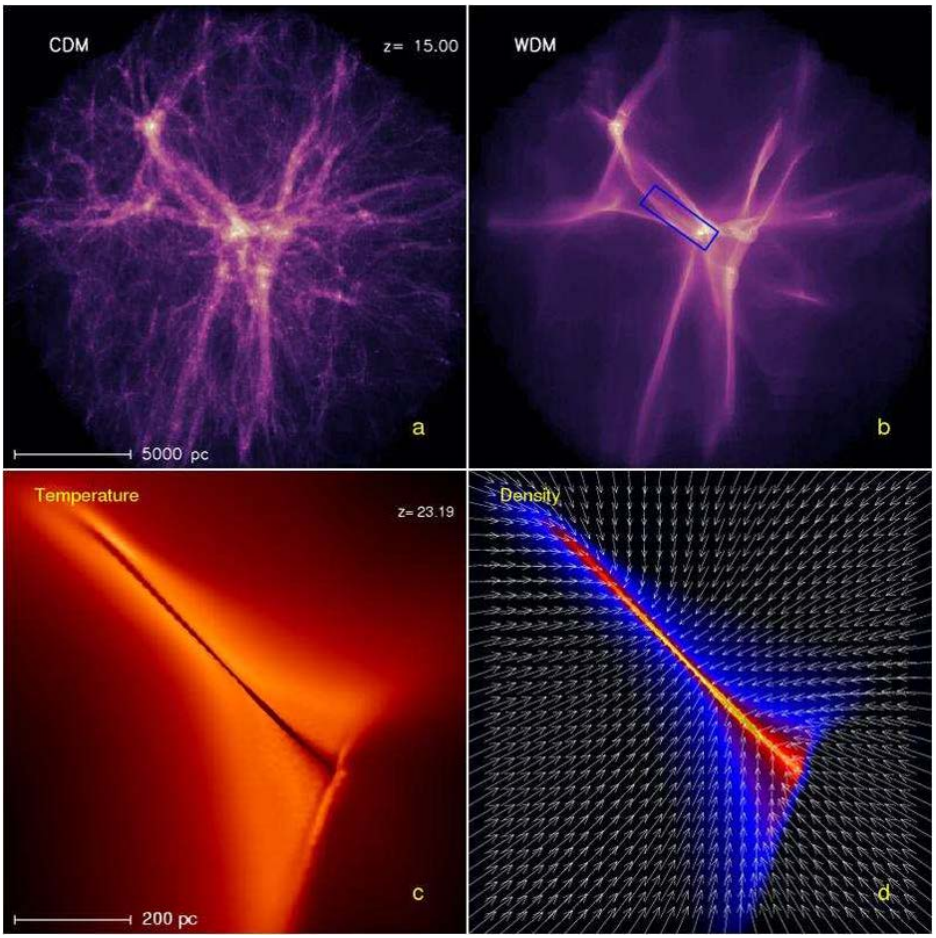


Figure 3.9: Dark Matter density structure at redshift z=15 of the progenitor of a massive cluster of galaxies from Gao & Theuns (2007). Panel a shows how the filament fragments into halos in CDM, while panel b shows the well preserved filament in WDM. Panel c shows the temperature at the redshift when the filament is formed in WDM. Panel d shows the density in the same filament.

filament fragments into small halos, while this is not the case in WDM, as shown in the same Fig. 3.9.

Other studies that do not benefit of the same resolution (Governato et al. 2015) claim that on the contrary, the structure formation is simply delayed in the warm dark matter simulations.

As we argue in Paduroiu et al. (2015), even though we explored the structure formation in a warmer regime, the top-down trend is present also in simulations using a particle corresponding to few keV (in the Bode et al. (2001) estimation), but it is more difficult to see with the common used resolution, because is rapidly overtaken by the hierarchical growth. Without using a sensitive enough time step, for example, this can be completely missed. Therefore, simulating WDM with the same parameters as CDM, especially when including baryonic processes, does not justify strong claims, constraints and conclusions.

An important fact that emerged from surveys, but is overlooked in the CDM community, is that observations show that a large fraction of galaxies do not suffer major mergers by redshift zero (Kormendy et al. 2010; Kormendy 2016). Also there are a large number of pure disk galaxies, which have been observed, but which have not been fully reproduced in simulations. These two observational pieces of evidence may in fact be connected, since we know that mergers destroy the disk. While in CDM there is no way to avoid mergers, we have seen that in WDM there are halos that survive this process. Furthermore, the smoother space distribution in the warm dark matter scenario may allow baryons to condense coherently in a smooth potential halo, providing favorable conditions for forming disk-like galaxies.

To explore these scenarios in a comprehensive manner, a much higher resolution will be needed together with a better and more specific implementation of the baryonic physics in simulations, for models like warm dark matter.

Mon. Not. R. Astron. Soc. **000**, 000–000 (0000) Printed 24 June 2015 (MN LATEX style file v2.2)

# Structure formation in warm dark matter cosmologies Top-Bottom Upside-Down

Sinziana Paduroiu[1⋆], Yves Revaz[2], Daniel Pfenniger[1]
[1] *Geneva Observatory, University of Geneva, CH-1290 Sauverny, Switzerland*
[2] *Laboratoire d'Astrophysique, École Polytechnique Fédérale de Lausanne (EPFL), 1290 Sauverny, Switzerland*



24 June 2015

**ABSTRACT**
The damping on the fluctuation spectrum and the presence of thermal velocities as properties of warm dark matter particles like sterile neutrinos imprint a distinct signature found from the structure formation mechanisms to the internal structures of halos. Using warm dark matter simulations we explore these effects on the structure formation for different particle energies and we find that the formation of structure is more complex than originally assumed, a combination of top-down collapse and hierarchical (bottom-up) clustering on multiple scales. The degree on which one scenario is more prominent with respect to the other depends globally on the energy of the particle and locally on the morphology and architecture of the analyzed region. The presence of shells and caustics in warm dark matter halos is another important effect seen in simulations. Furthermore we discuss the impact of thermal velocities on the structure formation from theoretical considerations as well as from the analysis of the simulations. We re-examine the assumptions considered when estimating the velocity dispersion for warm dark matter particles that have been adopted in previous works for more than a decade and we give an independent estimation for the velocities. We identify some inconsistencies in previous published results. The relation between the warm dark matter particle mass and its corresponding velocity dispersion is strongly model dependent, hence the constraints on particle mass from simulation results are weak. Finally, we review the technical difficulties that arise in warm dark matter simulations along with possible improvements of the methods.

**Key words:**
Dark matter: N-body simulations – galaxies, warm dark matter, structure formation.

## 1 INTRODUCTION

Independent studies and observations of both small and large scale structure are presently challenging the otherwise widely embraced CDM model. The so-called missing satellites problem (e.g. Klypin et al. 1999; Moore et al. 1999), where observations of galaxies do not map the abundance of substructures that are produced in CDM cosmologies is a serious drawback of the model. Furthermore, at smaller scales, the density profiles of galaxies show large cores (e.g. de Blok et al. 2001; Salucci et al. 2012; Kuzio de Naray & Kaufmann 2011) that have not been reproduced by the simulations. The failure to replicate in CDM simulations pure bulgeless galaxies which are observed in an important fraction (Kormendy et al. 2010) adds to the problem.

While several recipes have been proposed in the attempt of ameliorating these issues (e.g. Navarro et al. 1996; Martizzi et al. 2013; Mashchenko et al. 2008; Pontzen & Governato 2012), most of them introducing baryonic physics processes, current studies conclude that even including repeated baryonic outflows, large cored galaxies are not found in the simulations (Marinacci et al. 2014), although this is still highly debated in the literature.

The aforementioned situations, where the CDM model proves deficient in explaining the observations, are demanding further investigation. The WDM models, with sterile neutrinos leading as most probable particle candidates have been well studied and discussed in the literature in the past thirty years with an increased interest in the last few years (see the highlights of Daniel Chalonge workshops and Colloquiums 2011-2013 for latest developments in the WDM field (de Vega & Sanchez 2011; de Vega, Falvella & Sanchez 2012)).

It has been shown recently (Destri, de Vega & Sanchez 2012) that modeling the quantum pressure of fermionic particles (Weinberg 1962; Muccione & Pfenniger 2006) on the

⋆ E-mail: sinziana.paduroiu@unige.ch

other hand, one can reproduce the expected cores in dwarf galaxies, known to be dark matter dominated.

Moreover, the recent detection (Bulbul et al. 2014; Boyarsky et al. 2014) of a 3.55 keV unidentified emission line both on the data from XMM spectrum of galaxy clusters and Chandra can be a hint of sterile neutrino decay.

Since particles in warm dark matter models have different intrinsic properties from the cold dark matter particle candidates, the effect of these particle on structure formation and evolution is expected to be qualitatively different on both large and small scales.

Notwithstanding the difficulties in modeling properly the neutrino particle, several attempts (e.g. Colombi, Dodelson & Widrow 1996; Bode et al. 2001; Macciò et al. 2012; Kamada et al. 2013; Schneider et al. 2013) have been conducted with a successful outcome in solving some of the cases where CDM comes to an impasse. While the methods of CDM simulations have been accurately improved over the last decade, the WDM simulations encounter a number of difficulties in accurately describing the effect of such particles on both large and small scales. In addition to the resolution limitations that are met in the CDM case as well, WDM particles like neutrinos, for example, have a phase space density limit, a Fermi-Dirac distribution and a thermal velocity dispersion. Referring merely to sterile neutrinos, these particles decouple whilst relativistic.

The effects of the initial velocities of the warm dark matter particle are expected to manifest themselves on small scale structure formation. The free streaming exponentially dampens the power spectrum of density fluctuations such that very few structures are formed below the damping scale. Conservation of the fine grained phase space density is expected to set a maximum density that cannot be exceeded during the formation of structures with collisionless particles. For a fermionic WDM particle, we can crudely define the coarse-grained phase-space density $Q \equiv \rho/\sigma^3$, where $\rho$ is the density and $\sigma$ is the velocity dispersion. This definition is only a good approximation for locally isotropic velocities where the density of particles is not strongly varying.

Different numerical approaches have been used to address the impact of warm dark matter particles thermal velocities. Since the numerical resolution is strongly limited with respect to the physics, one knows that the phase space distribution sampling is anyway poor in space as well as in velocity space. The best compromise is to imprint the physical particle velocity to the simulation particle, as common practice in galactic dynamics. The particle limited sampling is not a sufficient reason to entirely drop the velocity sampling by neglecting the thermal velocities as done in some previous works, while keeping nonetheless the power spectrum cutoff implied by a non-zero thermal velocity (e.g. Schneider et al. 2013; Governato et al. 2015). Nor is the fact that for some dark matter particles the thermal velocities are comparable or smaller than the bulk Zel'dovich velocities. Even though it has been considered difficult to prescribe accurately initial thermal velocities in dark matter simulations, the importance of using them has been emphasized in previous studies like Colombi, Dodelson & Widrow (1996), Bode et al. (2001) and Melott (2007).

In the absence of a tested universal mechanism of production for the warm dark matter particle, the relation between the particle mass and its corresponding thermal velocity is strongly dependent on the specific model adopted. The widely used formula for generating velocities (Bode et al. 2001) which sets such a relation is based on an assumption that overestimates the number of species at decoupling and in effect underestimates the value of thermal velocities. We will take the opportunity to discuss these assumptions and we will also provide a method for estimating thermal velocities for fermionic, maxwellian and bosonic particles in both relativistic and non-relativistic regimes based on a different set of premises that takes quantum physics into consideration.

Several analyses of warm dark matter simulations in the keV range conclude that the formation of structure is hierarchical, like in cold dark matter simulations. Traditionally, top-down structure formation means forming chronologically the biggest structures first and the smaller ones later, while bottom-up or hierarchical structure formation means the reverse scale order, making it difficult to describe a scenario in which both coexist. In fact it is well known since, e.g., Lin, Mestel, & Shu (1965) and Zel'dovich (1970) that typical structure formation proceeds in time first along pancakes, then filaments and then halos, mixing the large and small spatial scales at all times with different proportions. If we use this terminology in a broader sense, top-down describes the dominant long range effects on structure formation: sheets collapsing into filaments, collapsing into halos. Bottom-up hierarchical structure formation, on the other hand, describes dominant short scale effects, mergers of both early formed and later formed halos. We will examine how both of these mechanisms of structure formation show up in the warm dark matter simulations presented here.

Additional constraints coming from peculiar features may be considered. In cold dark matter models, during the hierarchical evolution caustics are being wrapped inside earlier generations of the merging history, making them invisible in some cases even at high resolutions. However, Cooper et al. (2010) show using cold dark matter simulations that accretion mechanisms of stars and dark matter clumps and disruption of the latter can produce concentering shells that resemble those observed in NGC 7600. In the warm dark matter simulations, as we will see, the shells and caustics are more visible, especially at high redshift, where the top-down formation occurs.

Constraints on the mass of a warm dark matter particle from Lyman-$\alpha$ Forest, cosmic weak lensing, gamma-ray bursts, etc. (e.g. Markovic & Viel 2014; de Souza et al. 2013) give a lower limit in the few keV range. To study the effects of warm dark matter on structure formation, we have, however, explored a larger mass interval, focusing on the region where these effects are more prominent while fairly balanced by the resolution.

The paper is structured as follows: in Section 2 we explain the theoretical reasons for using the thermal component of velocities in the simulations. Subsection 2.2.1 shows how the common used formula for generating velocities in warm dark matter simulations (Bode et al. 2001) is conjectured from hypothetical assumptions. Section 2.2.2 presents a different approach in estimating thermal velocities from the particle mass. In Section 2.3 we discuss some of the inconsistencies found in previous studies. Section 3 describes the parameters used in our simulations while Section 4 shows

the results found from analyzing the simulations. At last, we present our conclusions in Section 5.

## 2 INITIAL CONDITIONS OF COSMOLOGICAL SIMULATIONS

### 2.1 Velocities in the initial conditions of cosmological simulations

The initial conditions of most CDM and WDM cosmological simulations have often initial thermal velocity taken as strictly zero, with the argument that at the finite initial redshift the thermal velocity of CDM particles is small in regard of the bulk flow following from Zel'dovich's prescription. We argue below that this practice is numerically inconsistent with the actual problem of describing a collisionless fluid of finite phase space density $f$. For structure formation, the distribution of the dark matter particles in velocity space is most important, as stressed by Colombi, Dodelson & Widrow (1996).

Indeed, integrating Newton's equation of motion for a set of particles in a force field $\mathbf{g}$ is equivalent to solving in a Lagrangian way with discrete mass particles the collisionless Boltzmann equation with the characteristics method. In conventional notations the Eulerian description of the phase space volume conservation reads,

$$\frac{\partial f}{\partial t} + \mathbf{v}\cdot\frac{\partial f}{\partial \mathbf{x}} + \mathbf{g}\cdot\frac{\partial f}{\partial \mathbf{v}} = 0, \tag{1}$$

where $\mathbf{g}$ is the force field. The mass density $\rho$ is the projection of the phase space density on velocity space:

$$\rho(\mathbf{x},t) = \int d^3v\, f(\mathbf{x},\mathbf{v},t). \tag{2}$$

The mass density $\rho$ generates the force field $\mathbf{g}$ by Newton's gravity. In a cosmological setup the mean density $\rho_0$ is subtracted,

$$\begin{aligned}\mathbf{g} &= G\int d^3x'\,\left[\rho(\mathbf{x}',t)-\bar{\rho}_0(t)\right]\frac{\mathbf{x}-\mathbf{x}'}{|\mathbf{x}-\mathbf{x}'|^3}\\ &= G\int d^3x'\,d^3v\,\left[f(\mathbf{x}',\mathbf{v},t)-\bar{f}_0(\mathbf{v},t)\right]\frac{\mathbf{x}-\mathbf{x}'}{|\mathbf{x}-\mathbf{x}'|^3}.\end{aligned} \tag{3}$$

So in this context using vanishing small thermal velocity already poses a consistency problem since $f$ is of the form $\delta(\mathbf{v}-\mathbf{v}_0(\mathbf{x}))\rho(\mathbf{x})$. This implies representing the system with a diverging $f$ in a vanishing fraction of the phase space volume, in other words, mass belongs only to an infinitesimally thin 3D sheet in 6D phase space. As $f$ is conserved along a characteristics, it implies that this singularity must persist at all subsequent times. Methods to conserve arbitrarily high phase space density have been set up (Abel 2012; Hahn & Angulo 2015), but this is not necessarily sufficient. Ideally a physically sound solution $f_0$ to this Boltzmann-Poisson system should not be numerically sensitive to the initial condition discretization. In practice it is known that the gravitational $N$-body problem is exponentially sensitive to perturbations (Miller 1964), so the best that can be expected in such simulations is that over an ensemble of simulations with identical statistical initial conditions, results follow a reproducible statistical distribution. Detailed evolution of particles is sensitive to perturbations, but the average evolution of an ensemble of particles is predictable.

When $f_0$ is finite and differentiable everywhere, in other words when $f_0$ mathematically exists, the sound situation that should be used, a slight variation of $f_0$, a fluctuation, will also follow the same set of equations, so, writing $f = f_0 + f_1$, $\mathbf{g} = \mathbf{g}_0 + \mathbf{g}_1$, where $f_1$ and $\mathbf{g}_1$ are the differences between the reference $f_0$ and the perturbed solution $f$, and using the fact that $f_0$ is a solution of the system, we obtain the exact equations for the differences $f_1$, and $\mathbf{g}_1$:

$$\frac{\partial f_1}{\partial t} + \mathbf{v}\cdot\frac{\partial f_1}{\partial \mathbf{x}} + \mathbf{g}_0\cdot\frac{\partial f_1}{\partial \mathbf{v}} = -\mathbf{g}_1\cdot\frac{\partial f_0}{\partial \mathbf{v}} - \mathbf{g}_1\cdot\frac{\partial f_1}{\partial \mathbf{v}} \tag{4}$$

$$\mathbf{g}_1 = G\int d^3x'\,d^3v\; f_1(\mathbf{x}',\mathbf{v},t)\frac{(\mathbf{x}-\mathbf{x}')}{|\mathbf{x}-\mathbf{x}'|^3} \tag{5}$$

So we see that $f_1$ follows the same left-hand side equation than $f_0$ in the unperturbed field $\mathbf{g}_0$, except that now the right-hand side contains a source term whose first term $\mathbf{g}_1\cdot\frac{\partial f_0}{\partial \mathbf{v}}$ is the product of the force fluctuations $\mathbf{g}_1$ times the gradient of the original $f_0$ in velocity space. Thus a vanishing zero thermal velocity for a set of particles supposed to represent a physical $f_0$ is not only suspicious since it corresponds to a delta function in velocity space, but also because the gradient $\frac{\partial f_0}{\partial \mathbf{v}}$ is at least as singular as $f_0$. In other words a zero initial thermal width is inconsistent with the initial assumptions, and susceptible to arbitrary strong amplification of perturbations, since the variational equations contain a diverging source term to first order when the initial thermal velocity is small. The only possibility to cancel this diverging term is either to have vanishing force fluctuations $\mathbf{g}_1$, which is exceptional when $f_1$ is non-zero, or that $\mathbf{g}_1$ is orthogonal to $\frac{\partial f_0}{\partial \mathbf{v}}$, which is also exceptional. The second order term $\mathbf{g}_1\cdot\frac{\partial f_1}{\partial \mathbf{v}}$ on the right-hand side can cancel the first term only when $f_1$ is proportional and opposite to $f_0$, which is also exceptional. In summary dealing with diverging $f_0$ is inconsistent with the implicit assumption of regularity of the mathematical problem.

It is instructive to compare how simulating collisionless fluids is differently approached in the fields of stellar and galactic dynamics. While in cosmology the physical collisionless fluids is assumed to consist of elementary particles, in galactic dynamics the fluid is composed of stars. In both cases the numerical simulation particles are order of magnitudes more massive than the physical particles. In the CDM context a simulation particle velocity is seen as representing the bulk flow of a large ensemble of CDM particles, explaining why zero velocity dispersion has been assumed. In galactic dynamics in contrast it is well known that doing so would immediately cause huge gravitational instabilities, and that the correct way to perform collisionless galaxy simulations is to ascribe to the simulation particles the same velocity dispersion as the stars. This is also required for respecting the virial theorem. While the use of velocities has been shown (Melott 2007) to be of importance for the CDM simulations, in WDM it becomes even more relevant (Colombi, Dodelson & Widrow 1996) since the particles do have intrinsic non-zero velocity dispersion. Collisionless fluids are particle mass agnostic, when the particle mass starts to be important is when the 2-body relaxation time is shorter than the system age. Recalling the Chandrasekhar 2-body relaxation time in an arbitrarily large homogeneous medium (Chandrasekhar

1942; Hénon 1973),

$$\tau_{\rm rel} = \frac{v^3}{8\pi G^2 m \rho \ln N}, \quad (6)$$

where $v$ is the velocity dispersion of $N$ particles of mass $m$ with average density $\rho$, it is obvious that this relaxation time is proportional to $v^3$, $1/m$, and $1/\ln N$, so is exactly zero when $v = 0$. Thus CDM simulations with initial zero $v$ are technically collisional until numerical noise heats the particles to larger $v$.

From a completely different side of physics, the maximal phase space density constraint set by Heisenberg's inequality,

$$\Delta x \Delta p_x \geqslant \frac{\hbar}{2} \quad (7)$$

gives a minimum particle velocity dispersion, taking $\Delta x = n^{-1/3}$ and $m$ the particle mass,

$$\Delta v \geqslant \frac{\hbar}{2}\frac{n^{1/3}}{m} \approx 0.003 \left[\frac{1\,{\rm keV}/c^2}{m}\right] \left[\frac{n}{1\,{\rm cm}^{-3}}\right]^{1/3} {\rm km/s}\ . \quad (8)$$

Taking a velocity dispersion lower than this value violates Heisenberg inequality, while taking it only slightly larger means that the particles behaviour is governed by quantum physics, not classical mechanics as assumed in all cosmological $N$-body simulations.

In summary, adopting even a slight non-zero velocity dispersion in cosmological simulation is certainly a safer and more correct physical assumption than taking strictly cold initial conditions associated with a mathematically singular and inconsistent state leading to situations not under control on the numerical viewpoint due to singular phase space density.

### 2.2 Thermal velocities of warm dark matter particles

Depending on the WDM particle physics and properties, different scenarios can be considered regarding the particle velocity dispersion as function of redshift. In many scenarios, particles are copiously created in ultra-relativistic conditions and very good thermal equilibrium. As the Universe expands they may subsequently decouple on the thermal point of view because their collisional relaxation rate becomes lower than the expansion rate, while still interacting with the rest of matter by gravitational coupling. If the particles do not decay their comoving number density is conserved, and if they follow the collisionless Boltzmann equation their phase space density is conserved too. But this later assumption is more fragile because some residual elastic collisional relaxation processes can still decrease the effective phase space density by coarse graining.

#### *2.2.1 Inspection of a commonly used result*

A frequently cited derivation of WDM particle velocities as function of mass and redshift can be found in Bode et al. (2001). In their Appendix A they recall that for a thermal relict particle X that decouples when relativistic, the abundance $n_x$ relative to photons is:

$$\frac{n_X}{n_\gamma} = \left(\frac{43/4}{g_{\rm dec}}\right)\left(\frac{4}{11}\right)\frac{g_X}{2} \quad (9)$$

where $g_{\rm dec}$ is the number of relativistic species present at decoupling, and $g_X$ is the number of spin states of the particle. Connecting then the particle mass density $\rho_X = m_X n_X$ with the cosmological parameters $\Omega_X \equiv \rho_x/\rho_c$ and $h$, where the critical universal density $\rho_c \equiv 3H^2/8\pi G$, and the Hubble constant $H \equiv 100h\,{\rm km\,s^{-1}\,kpc^{-1}}$, they derive,

$$\Omega_X h^2 \approx \frac{115}{g_{\rm dec}}\frac{g_X}{1.5}\frac{m_X}{\rm keV}\ . \quad (10)$$

We confirm this equation when using $n_\gamma = 413\,{\rm cm}^{-3}$. Then the authors proceed to derive a velocity formula. Since the distribution function of fermions without chemical potential $\mu$ is proportional to $(\exp(\epsilon_x/kT_X)+1)^{-1}$, they point out that if the particles decouple from photons when still relativistic $\epsilon_X = \left(p_X^2c^2 + m^2c^4\right)^{1/2} - mc^2$ can be replaced by $p_X c$ where $p_X$ is the particle momentum. To keep phase space density constant clearly in the relativistic regime $p_X$ must stay proportional to $T_X$. But obviously as the regime passes to non-relativistic this argument does not hold, the exact formula valid at all $T_X$ is

$$p_X^2 \propto \left(\frac{kT_X}{c}\right)^2 + 2kT_X\ . \quad (11)$$

Therefore it seems incorrect to assume that $p_X$ is proportional to $T_X$ also at low $T_X$. The exact scaling from Eq. (11) becomes $p_X^2 \propto 2\,kT_X$, or $0.5\,m_X v_X^2 \propto kT_X$, that is, the kinetic energy $\epsilon_X$, not the momentum, scales as temperature at all redshifts.

Another problem is the derived constant for velocity. They assume that the distribution function scales as the non-thermal distribution $(\exp(v/v_0)+1)^{-1}$, and give without detail $v_0$ (in their Eq. (A3)),

$$\frac{v_0(z)}{1+z} = \mathbf{.012}\left(\frac{\Omega_X}{0.3}\right)^{\frac{1}{3}}\left(\frac{h}{0.65}\right)^{\frac{2}{3}}\left(\frac{1.5}{g_X}\right)^{\frac{1}{3}}\left(\frac{\rm keV}{m_X}\right)^{\frac{4}{3}}\ {\rm km\,s^{-1}} \quad (12)$$

where $z$ is the redshift. But eliminating $\Omega_X h^2$ in this previous equation using Eq. (10) (their Eq. (A2)), we obtain for a $m_X = 1\,{\rm keV}$ particle (rounding also to 2 significant digits),

$$\frac{v_0(z)}{1+z} \approx \mathbf{0.12}\left(\frac{1}{g_{\rm dec}}\right)^{1/3}\frac{\rm keV}{m_X}\,{\rm km\,s^{-1}}\ . \quad (13)$$

Thus we find $g_{\rm dec} = \mathbf{1000}\,(g_X/1.5)^{1/3}$. This is too high a value for $g_{\rm dec}$ to be endorsed, as mentioned by the authors, by large entropy producing processes. Since the value for $g_{\rm dec}$ varies linearly with the mass of the particle in the given cosmological model (Eq. 10), it allows the elimination of $g_{\rm dec}$ from the final expression for velocity[1]. This high value used for $g_{\rm dec}$ leads to a significant decrease in the particle velocities, as shown in Table 1.

In the minimal standard model the number of the full set of particles is $\sim 107$ while in the minimal supersymmetric standard model, the value is increased to $\sim 229$ (Pierpaoli et al. 1998). Previous studies like Colombi, Dodelson &

[1] The authors cite a value of 688 for the number of relativistic degrees of freedom at the time of decoupling of a 1 keV particle, while then using the value of 1000. In Viel et al. 2005 this latter value is used, although a rigorous calculation gives 903 as the exact value.

Widrow (1996)[2] use a value of $\sim 100$ for right-handed neutrinos decoupling before the electroweak phase transition at very high temperatures, while Pierpaoli et al. (1998) assume a conservative reference value of 150 for both gravitino and a standard warm dark matter candidate like the massive neutrino.

The lower value for the velocity adopted by Bode et al. (2001) has been used in most WDM simulations thereafter. This value for $g_{\rm dec}$, however, is valid for a 1 keV particle only if we assume that dark matter is made entirely by these type of particles, as shown in Eq. (10). For the cases in which a certain warm dark matter particle represents only a fraction of the total dark matter content, this value is different and Eq. (12) needs to be scaled accordingly. This aspect has been overlooked in some simulation studies of mixed dark matter, providing misleading results as we will show in Section 2.3.

The next line following Bode et al. (2001) Eq. (A3) states: "The rms velocity is $3.571 v_0$". Recalculating the rms velocity of the adopted distribution function $f = (e^{v/v_0} + 1)^{-1}$ we find a slightly larger factor:

$$\langle v^2 \rangle = \frac{\int_0^\infty 4\pi v^4 f \, dv}{\int_0^\infty 4\pi v^2 f \, dv} = 15 \frac{\zeta(5)}{\zeta(3)} v_0^2 \approx (3.5\mathbf{9}714 v_0)^2 \ , \quad (14)$$

where $\zeta$ is Riemann's function. The slight discrepancy (the 9 digit) appears thus as a misprint.

In Appendix A we find that the largest correction factor for the rms speed of a Fermi-Dirac distribution with respect to a Maxwellian distribution is 1.07, not $\approx 3.6$ as stated in Macciò et al. (2012). The difference comes entirely from the very non-thermal distribution.

### 2.2.2 *Another scenario for quantum semi-degenerate particles*

In the previous Bode et al. (2001) scenario, WDM particles are treated as localized mass bullets following Boltzmann's equation. However, at creation time they are also assumed to be ultra-relativistic and in thermal equilibrium with radiation and the rest of matter, typically following a Fermi-Dirac distribution since the known stable particles are fermions. This entails that their quantum nature does play a role at birth, they are at least semi-degenerate. Phase space density is high enough for the distinction between classical and quantum particles to play a role. The non-local Pauli principle applies then, each particle "knows" about the state of each other. Now if phase space density is approximately conserved then particles remain semi-degenerate at all times, which is inconsistent with the usual assumptions applied at low redshifts that they behave as classical particles.

The known neutrinos offer a good example that particles are quantum objects instead of localized mass objects. Real neutrinos are in addition of being fermions also in a superposition of three mass states. Since mass states propagate at different velocities, with time relict neutrinos are actually in a superposition of entangled mass states increasingly spread apart. How gravitational interaction with matter structures can destroy the coherence of these entangled states is a question that will need to be addressed in future works.

Here we develop a procedure to calculate precisely the particle velocity valid in all relativistic regimes for fermions or bosons. The full distribution Fermi-Dirac or Bose-Einstein distribution reads (e.g., Padmanabhan 2002)

$$f(\mathbf{p}) = \frac{g}{(2\pi\hbar)^3} \frac{1}{\exp((\epsilon - \mu)/kT) \pm 1}, \quad (15)$$

where $\mathbf{p}$ is the particle momentum, $g$ the spin-degeneracy factor (of order 1 or 2), $\mu$ the chemical potential, $\epsilon = \sqrt{p^2c^2 + m^2c^4} - mc^2$ the particle energy, $m$ the particle mass, and $T$ the particle temperature. The comoving number density is calibrated according to a neutrino-like scenario where the particles are once coupled to the photon background and in thermal contact, at a time where gravitational perturbations are still linear.

First, the assumption that the chemical potential $\mu$ is constant and negligible is not necessarily valid for identical fermions which are created in a half-degenerate state. The Pauli principle has for effect that identical fermions, even with negligible interaction (like the weak nuclear force for neutrinos), possess an effective *exchange potential*, also sometimes called *exchange-correlation potential* (e.g., Atkins & Friedman 2005). In quantum chemistry and Density Functional Theory (DFT) the exchange potential is well known to be essential in the Hamiltonian describing electrons around a nucleus, or electrons in materials, although the exact form in different contexts is sometimes not well known. In the cosmological context the exchange potential changes the chemical potential as the spatial density of identical fermions changes. This effective repulsive interaction for fermions makes the collisionless assumption of free fermions much less obvious. In Pfenniger & Muccione (2006) the effective interaction of free fermions was illustrated by solving exactly the time-dependent Schrödinger equation for two free but identical fermions in 3D space starting as Gaussian wave packets. In the quantum regime (high phase space density) these wave packets effectively interact and are scattered due to the repulsive exchange potential. In the classical regime (low phase space density) the wave-packets follow, as expected, a straight trajectory.

In quantum statistical mechanics (Huang 1987) the exchange potential between two particles has a well known form dependent on temperature and distance $r$

$$\phi(r) = -kT \log\left(1 \mp \exp\left(-mkT\frac{r^2}{\hbar^2}\right)\right) \quad (16)$$

$$= -kT \log\left(1 \mp \exp\left(-2\pi\frac{r^2}{\lambda^2}\right)\right), \quad (17)$$

where the $-$ sign applies for fermions and $+$ for bosons, and $\lambda$ is de Broglie wavelength. For semi-degenerate particles $\lambda$ is of order of $n^{-1/3}$, so in a semi-classical description fermions "feel" a rapidly varying repulsive force from neighbouring particles, while bosons an attractive force. The reality of the exchange potential can be invoked to cast a doubt that the commonly assumed collisionless approximation for semi-degenerate particles is valid in the cosmological context. Instead one should expect a local thermalization of identical particles on a short time-scale.

To calculate the chemical potential evolution in the cosmological context, one needs therefore an additional assump-

[2] Interestingly this is the paper cited by Bode et al. (2001) as reference for production mechanisms of WDM and their relation to cosmology

tion, besides number conservation. The particle momentum and kinetic energy can not be assumed conserved due to the global gravitational interaction. A reasonable assumption (Trodden & Caroll 2004) is that the expanding medium proceeds adiabatically, at least as long as gravitational clustering is linear. This means that the particle specific entropy can be taken as a conserved quantity.

The entropy $S$ expressed as a function of other thermodynamical variables reads (e.g., Padmanabhan 2002, Vol. I, Eq. 5.73),

$$S = \frac{1}{T}\left(E + PV - \mu N\right) \ , \tag{18}$$

where $E$ is the total thermal energy, $P$ the pressure, $V$ the volume, $\mu$ the chemical potential, and $N$ the number of particles. The specific entropy $s \equiv S/N$ divided by Boltzmann's constant $k$ is a pure number

$$\frac{s(T,\mu)}{k} = \frac{1}{kT}\left(\frac{e+P}{n} - \mu\right) \tag{19}$$

where $e = E/V$ is the specific energy density and $n = N/V$ is the number density.

The thermodynamical quantities for fermions and bosons at all regimes can be calculated accurately by evaluating numerically the relativistic Fermi-Dirac or Bose-Einstein integrals for particle density $n$, energy density $e$, and pressure $P$ (e.g., Padmanabhan 2002, Vol. II, p. 216) as functions of temperature $T$ and chemical potential $\mu$ [3] :

$$n(T,\mu) = \frac{4\pi g}{h^3}\int_0^\infty \frac{p^2}{\exp((\epsilon-\mu)/kT)\pm 1}\,dp \ , \tag{20}$$

$$e(T,\mu) = \frac{4\pi g}{h^3}\int_0^\infty \frac{p^2\epsilon}{\exp((\epsilon-\mu)/kT)\pm 1}\,dp \ , \tag{21}$$

$$P(T,\mu) = \frac{4\pi g}{h^3}\int_0^\infty \frac{p^2}{\exp((\epsilon-\mu)/kT)\pm 1}\frac{1}{3}\frac{c^2p^2}{\epsilon+mc^2}\,dp \ , \tag{22}$$

where $g$ is the number of distinct particle states, and $\epsilon = \sqrt{p^2c^2 + m^2c^4} - mc^2$ the particle energy. In the integrands the $+$ sign is for fermions, the $-$ sign for bosons. The conserved particle density $n(T,\mu)$ is related to universal expansion by the scale factor $a = 1/(1+z)$, thus

$$n(T(z),\mu(z)) = n_0(1+z)^3 \ , \tag{23}$$

while the constant particle entropy gives

$$\frac{s(T(z),\mu(z))}{k} = \frac{s(\infty,0)}{k} = 4.20183245 \ , \tag{24}$$

For Fermi-Dirac particles the solution of this system for $n_0 = 115\,\mathrm{cm}^{-3}$, $m = 1\,\mathrm{keV}$, $g = 1$ in the non-relativistic regime is :

$$\frac{\mu}{kT} = -1.6202, \quad \frac{mc^2}{kT} = 5.6186\cdot 10^{12} \ . \tag{25}$$

For a graphical illustration of these functions behaviour, see Fig. B1 in Appendix B. For a couple of dex around this solution the scaling with $n$, $g$ and $m$ for $T$ and $v$ goes with good approximation as follow [4] :

$$\begin{aligned} T &= 2.0654\cdot 10^{-6}\left(\frac{n}{115\,\mathrm{cm}^{-3}}\frac{1}{g}\right)^{2/3}\left(\frac{mc^2}{\mathrm{keV}}\right)^{-1}\ \mathrm{K} \\ v &= 0.2226\left(\frac{n}{115\,\mathrm{cm}^{-3}}\frac{1}{g}\right)^{1/3}\left(\frac{mc^2}{\mathrm{keV}}\right)^{-1}\ \mathrm{km\,s}^{-1} \ . \end{aligned} \tag{26}$$

When the regime becomes relativistic this approximation is no longer accurate. One can solve the pair of equations (23) and (24) in any situation.

In comparison, for Bose-Einstein particles the solution for the same parameters is:

$$\frac{\mu}{kT} = -1.2451, \quad \frac{mc^2}{kT} = 8.1348\cdot 10^{12} \ . \tag{27}$$

Around this solution the scaling with $n$, $g$ and $m$ for $T$ and $v$ goes approximately as:

$$\begin{aligned} T &= 1.4265\cdot 10^{-6}\left(\frac{n}{115\,\mathrm{cm}^{-3}}\frac{1}{g}\right)^{2/3}\left(\frac{mc^2}{\mathrm{keV}}\right)^{-1}\ \mathrm{K} \\ v &= 0.1768\left(\frac{n}{115\,\mathrm{cm}^{-3}}\frac{1}{g}\right)^{1/3}\left(\frac{mc^2}{\mathrm{keV}}\right)^{-1}\ \mathrm{km\,s}^{-1} \ . \end{aligned} \tag{28}$$

If Maxwell-Bolzmann particles are used in simulations one can also calculate the solution, replacing the $\pm 1$ in integrals by zero, and taking $s(\infty,0)/k = 4$. The velocity coefficient is found to be $0.20592\,\mathrm{km\,s}^{-1}$, intermediate between the Fermi-Dirac and Bose-Einstein cases. The correction of quantum statistics with respect to a Maxwellian distribution remains thus small, as demonstrated in Appendix A.

### 2.3 Power spectrum of the warm dark matter simulations

Since collisionless physics does not depend on the particle mass, the power spectrum must directly depend only on the velocity distribution of the particles, which results from the particle production mechanism. Colombi, Dodelson & Widrow (1996) and Bode et al. (2001) also emphasize this point.

To compute the transfer function for WDM models the fitting formula suggested by Bode, Turok and Ostriker (2001) gives:

$$T^2(k) = \frac{P^{\mathrm{WDM}}}{P^{\mathrm{CDM}}} = [1 + (\alpha k)^{2\nu}]^{-10/\nu} \tag{29}$$

where $\alpha$, the scale of the break, is a function of the WDM parameters, which are function of the velocity, while the index $\nu$ is fixed. People prefer however, to use the mass dependence instead of the velocity, using Eq. (13) as a conversion.

[3] This part follows closely the calculations made in Pfenniger & Muccione (2006), but correct a mistake where the used entropy expression was only valid in the ultra-relativistic regime, or when $\mu = 0$.

[4] An astute reader might notice that for classical massive neutrinos ($0.01 < mc^2/\mathrm{eV} < 2$) the found temperature is much lower than the commonly quoted temperature of 1.9 K. Actually the 1.9 K value is valid for massless neutrinos only. The difference comes from the misleading use of temperature as an equivalent concept for energy and vice versa, while the neutrino rest mass energy does not contribute to thermal energy. The proper meaning of temperature is the quantity that would be measured, in the case of real neutrinos, by a cosmic sized thermometer able to thermalize with the neutrino background.

Viel et al. (2005) (see also Hansen et al. (2002)), using a Boltzmann code simulation, found that $\nu = 1.12$ is the best fit for $k < 5\ h\ \mathrm{Mpc}^{-1}$, and they obtained the following expression for $\alpha$:

$$\alpha = 0.049 \left(\frac{m_x}{1\,\mathrm{keV}}\right)^{-1.11} \left(\frac{\Omega_\nu}{0.25}\right)^{0.11} \left(\frac{h}{0.7}\right)^{1.22} h^{-1}\mathrm{Mpc}. \tag{30}$$

In the case of warm dark matter particles, the streaming velocity supresses the matter power spectrum $P(k)$ and the formation of structure, on scales smaller than their free-streaming scale. A rough estimation of the free-streaming scale is given by Bond et al. (1980):

$$k_{\mathrm{FS}} = \frac{2\pi}{\lambda_{\mathrm{FS}}} \sim 5\,\mathrm{Mpc}^{-1} \left(\frac{m_x}{1\,\mathrm{keV}}\right) \left(\frac{T_\nu}{T_x}\right) , \tag{31}$$

Depending on the model for the properties of a certain particle, there can be different expressions for the damping of the power spectrum (Abazajian & Koushiappas 2006, e.g.), but for the purpose of our present work and for easier comparison with previous studies we use the expression given in Eq. (30) with the corresponding thermal velocities.

This approach used for cutting the power spectrum is only valid however, for a scenario in which the whole dark matter content is made up by one specific dark matter particle of a certain velocity.

### 2.4 Caveat Emptor

In this section we would like to summarize the findings of previous sections and discuss some of their implications. We want to stress that the assumed particle production model and physics strongly impact on the ascribed particle mass, while the initial velocity distribution and its corresponding power spectrum is the only really important initial parameter influencing the simulation results. As far as the physics behind the origins of the dark matter particles is concerned, the assumptions found in the literature can widely differ.

Previously on section 2.2.1. we showed how the Bode et al. (2001) result for estimating velocities for neutrino like particles is based on arguments like entropy production and negligible chemical potential. The expression for velocities in Eq. (12) is based on a dependence of the number of species on the mass of the particle, such as to preserve the equivalence in Eq. (10). For the models with cold plus warm dark matter, or models with different particle mass, the value of the number of species should be adjusted accordingly. Many papers that study mixed particles simulations have omitted this readjustment for velocities (e.g. Anderhalden et al. 2012). Eq. (12) has been reduced by the fraction with which a certain particle contributes to the total density, therefore leading to inconsistencies like having for a certain mass of a particle, different thermal velocities, depending solely on that fraction. Moreover, since the power spectrum cutoff depends on the velocity of the particle (not the mass), studies that use the cutoff for a velocity, but a different thermal velocity, given by a different model of particle production are not consistent. These results, although used for constraining the mass of a particle in terms of detection experiments, should not be considered as accurate.

As an alternative, we provide a different energy-thermal velocity correspondence based on number conservation and a non-entropy production while taking into account the quantum pressure, but assuming a thermalization caused by the exchange potential. Entropy conservation by particles in the hot Big Bang is invoked by many authors, such as Padmanabhan (2002) or Weinberg (2008). From Eq. (26) which estimates the thermal speed of WDM particles, independent of the cosmological parameters, we have the following velocity dependence with the redshift:

$$\frac{v}{1+z} = \mathbf{0.2226} \left(\frac{n}{115\,\mathrm{cm}^{-3}}\frac{1}{g}\right)^{1/3} \left(\frac{mc^2}{\mathrm{keV}}\right)^{-1} \mathrm{km\,s}^{-1} . \tag{32}$$

**Table 1.** Correspondence between particle mass $m$ and rms velocity dispersion in literature for 0.2, 1 and 3.5 keV. The first column shows the value originally given in Bode et al. (2001), the second column shows the value obtained using $g_{\mathrm{dec}} = 150$ (Pierpaoli et al. 1998) in Eq. (12), and the third one, the value given by our derivation.

| Mass | Bode et al. Eq. (11)×3.571 | Pierpaoli et al. | This work Eq. (25) |
|---|---|---|---|
| keV/$c^2$ | km/s | km/s | km/s |
| 0.2 | 0.366 | 0.4032 | 1.113 |
| 1.0 | 0.0429 | 0.0225 | 0.223 |
| 3.5 | 0.00806 | 0.0230 | 0.0636 |

The difference between our and Bode et al. (2001) estimations is showed in Table. (1) for 0.2, 1 and 3.5 keV respectively, at redshift zero. The Bode et al. (2001) speed for 1 keV fermions out of equilibrium, used in most WDM simulations, is 5 times lower than the value derived here. In general these differences cumulate their effect if simulations are started at higher redshifts, and are crucial not only for phase space density studies, but also for structure formation.

Our finding affects the results and conclusions of previous papers which were using Eq. (12) to constrain the mass of sterile neutrinos. This extends even to papers which did not include thermal velocities. The power spectrum studies based on the velocity of the particle are subject to the same difference in the velocity estimation (see Section 2.3). Also, when comparing the thermal velocities to the Zeldovich velocities, these factors weaken correspondingly the reason for ignoring the thermal velocities, against all the arguments presented in Section 2.1.

Since our aim here is to describe typical qualitative effects on structure formation present in a broader range of energies, we will refer to the particles in terms of their velocity dispersion instead of their mass. Indeed the thermal velocity of a particle as its decoupling temperature at a certain redshift depends on the specific physics of particle production. That influences the ascribed mass of that particle. More complex analysis of the decoupling theories for a certain particle may give a slightly different dependence between the thermal velocity at a certain redshift and the particle mass.

## 3 SIMULATIONS SETUP

We conducted several suites of $N$-body simulations. All simulations have been performed once with PKDGRAV-2, a treecode written by Joachim Stadel and Thomas Quinn

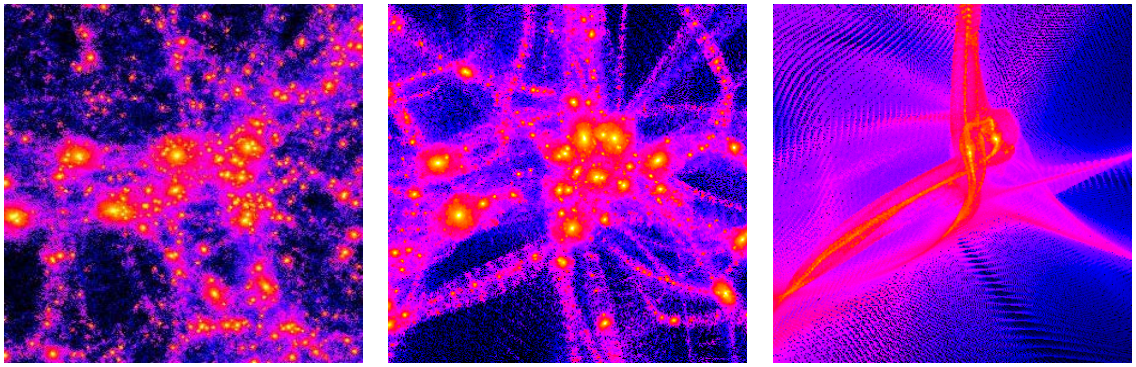

**Figure 1.** Illustrative density map of structure formation regions at redshift zero, from left to right, in CDM, WDM (0.3 km/s) and HDM (2.3 km/s). For a similar illustration of a full box see Macciò et al (2012). These simulations have not been used in this paper.

**Table 2.** Details of the simulations

| Label | velocities $z_i$ km/s | cutoff eV | box size Mpc/h | N | softening pc |
|---|---|---|---|---|---|
| CDM | no | - | 40 | $300^3$ | 50 |
| WDM1 | no | 200 | 40 | $300^3$ | 50 |
| WDM2 | 36.6 | 200 | 40 | $300^3$ | 50 |
| WDM3 | no | 1000 | 40 | $300^3$ | 50 |
| WDM4 | 4.6 | 1000 | 40 | $300^3$ | 50 |
| WDM5 | 36.6 | 200 | 30 | $256^3$ | 100 |

(Stadel 2001)[5] and then using Volker Springel's Gadget-2 (Springel 2005)[6]. The initial conditions are generated with Ed Bertschinger's GRAFIC2 package (Bertschinger 2001)[7]. Although some differences have been spotted between the two different codes, those differences are not qualitatively important where structure formation is concerned, there can be minimally spotted at very small scales.

The simulations we have performed cover a range of velocities from 0.01 km/s to 10 km/s (3.5 keV to 15 eV) at redshift zero. For illustration purposes, in Fig. 1 we show generic density maps of structure formation regions in CDM, WDM and HDM simulations. Particles that have $\sim 0.1$ km/s velocity dispersion are in a transient regime from a predominant top-down structure formation scenario to a hierarchical one, showing both these trends. We have chosen one such simulation and compared it to a simulation of a colder particle more favored by the observational constraints and with a cold dark matter simulation. For the warm dark matter the simulations have been prepared with initial power spectrum consistent with initial velocities, and, for comparison, the same initial power spectrum without initial velocities.

The simulation parameters are summarised in Table 2. The starting redshift for the simulations is $z_i = 100$ in order to ensure a proper treatment of the non-linear growth of cosmic structures.

The cosmological parameters used are given by the WMAP7 results: $\Omega_\Lambda$=0.721, $\Omega_m$=0.279, $\Omega_b$=0.0463, $h = 0.7$ and $\sigma_8 = 0.821$,

We start with running large scale simulations in cosmological box of 40 Mpc/h, engaging $300^3$ dark matter particles and one 30 Mpc/h box with $256^3$ particles. We then select a region where the top-down halo formation is predominant and re-simulate it with an eight times higher resolution.

## 4 SIMULATIONS ANALYSIS AND RESULTS

### 4.1 Structure formation in WDM simulations

Free streaming causes a delay in the formation of structure in the warm dark matter simulations. This delay depends on the energy, hence the velocity of the particle. The higher the thermal velocity of the particle, the later the filaments will reach the collapse, making it impossible for structures to be formed by redshift zero in hot dark matter scenarios, as illustrated in Fig. 1, right panel.

The fragmentation of the filaments is observed in all N-body simulations of warm dark matter where the collapse is stimulated by the noise in the particle distribution (Bode et al. 2001; Götz & Sommer-Larsen 2002; Wang & White 2007). This is especially observable at the characteristic grid or glass spacing. Above the free streaming scale the mass function is flattened to a value that closely matches the luminosity function of galaxies (assuming mass traces light). The length and the lifetime of the filaments depend on the energy of the particle. The higher the velocity dispersion of the particle, the larger will be the filaments and the longer they will be preserved. These can reach 20 Mpc in a 40 Mpc box and survive until redshift zero in the case of velocities of few km/s and above.

In Fig. 2 the difference between high density regions in a CDM simulation, versus WDM at redshift 2.3 is shown. The picture displays the 2D projection of the 3D density map of the full simulation box. One can see that due to the free streaming, particles are concentrated in large spatial structures, delimited from each other by large low density regions, or voids, as opposed to the crowded web present in the cold dark matter simulation.

It is well known that in CDM models, smaller halos

[5] http://hpcforge.org/projects/pkdgrav2/
[6] http://www.mpa-garching.mpg.de/gadget/
[7] http://web.mit.edu/~edbert/

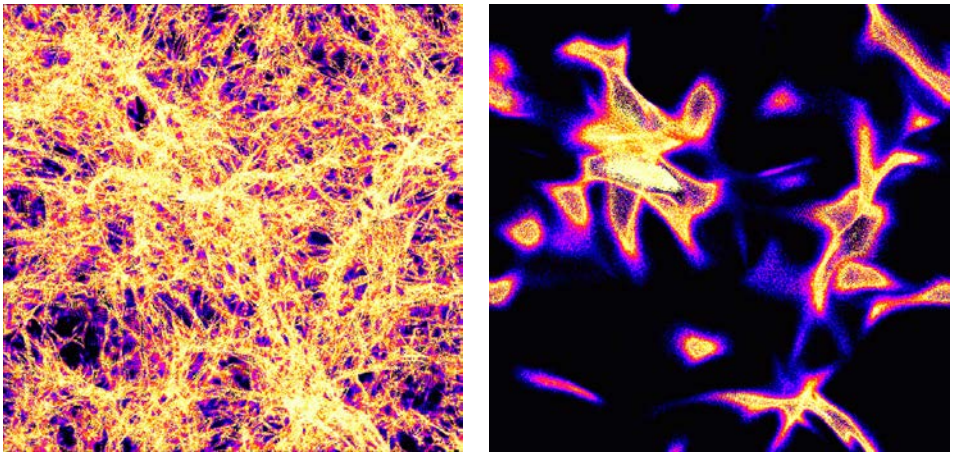

**Figure 2.** Plot of high density regions at redshift 2.3 in a 40 Mpc/h simulation box with CDM particles in the left panel and WDM particles (model WDM2) in the right one, showing major topological differences

collapse first and merge hierarchically into larger systems, as it is obvious in all high resolution simulations (Diemand & Moore 2010, 2011; Stadel et al. 2009). Furthermore, one finds that less massive halos are more concentrated, perhaps reflecting the fact that the density of the universe is higher at earlier epochs, since the CDM particles have an infinite phase space density.

On the other end of the velocities spectrum, for HDM models, the structure formation is essentially top-down up to redshift zero, as can be seen in the right panel of Fig. 1, with just large filaments collapsing into few halos.

As stated in the introduction, in the case of warm dark matter we see from our simulations that the structure formation is more complex, a hybrid mechanism where both long-range and short-range effects are present, from long distance to nearest neighbours, from top-down to bottom-up.

The top-down trend predominant in the early epochs in warm dark matter simulations has been missed in previous works since it is difficult to observe it while analyzing the snapshots of the simulations. For particles with velocities smaller than a few km/s the top-down trend is hidden by the hierarchical growth that dominates at later times. We have been able to see this effect in our simulations while watching movies made with a sufficient large number of snapshots. We stress that only movies convey the complexity of these multiscale hierarchical processes. Several movies of WDM structure formation, filament collapse and halo formation from this study can be found on a youtube playlist (`https://www.youtube.com/playlist?list=PLnGS4wkStJ1aqi3M9hTDaUzuZ-vs-Qg6i`)[8].

As the movies show, in WDM simulations, structures form in a qualitatively different way from CDM models. The hybrid structure formation is more complex than what the traditional top-down/bottom-up dichotomy can categorize, as discussed in the Introduction.

- During the early stages one sees the formation of well contoured filaments. How early is this stage depends on the particle velocity. In our WDM2 simulations this happens in the interval $13 > z > 8$.
- In the higher density regions, usually situated at the intersection of such filaments, the first halos are formed through gravitational collapse. These halos continue growing into larger ones by accreting particles from the disrupted filaments (Fig. C1).
- In medium density regions, halos show a hierarchical formation trend. Small halos collapse first and then merge into bigger halos (Fig. C2).
- In less dense regions, the ones isolated by voids and which have a very slow evolution, we have observed filaments that collapse very late. The top down formed halo survives without any mergers until redshift zero (Fig. C3).
- Finally there is the more complex scenario in which we observe large halos formed earlier which merge together forming a large cluster (Fig. C4).
- The filamentary-like structure is preserved until redshift zero, with new filaments forming in the low density regions as late as redshift $z \sim 4$.

Looking closer, we have analyzed four different regions in our simulations and displayed them in four different movies. The characteristics of these regions are summarized in Table 3.

Our conclusion from analyzing these simulations is that there is only one correlation, between the time of the first collapse and the density reached in a certain region, and that depends only on the network morphology and architecture of that region. The first halos collapse in the region where the density becomes $\sim 2 \times 10^3$ times larger that the average density and almost $\sim 3 \times 10^3$ times larger than the lowest densities present in that region at that epoch. In the simulations with particle velocity of 0.36 km/s (that mimic

[8] All the HD movies are on youtube and can be watched indivadually on this channel `https://www.youtube.com/channel/UCEmQi8hDNW2emqGn-urtvpg`. Remember to adjust your settings to HD quality. Links for direct download can be provided on demand. For a short description of the movies and movies snapshots, see Appendix C.

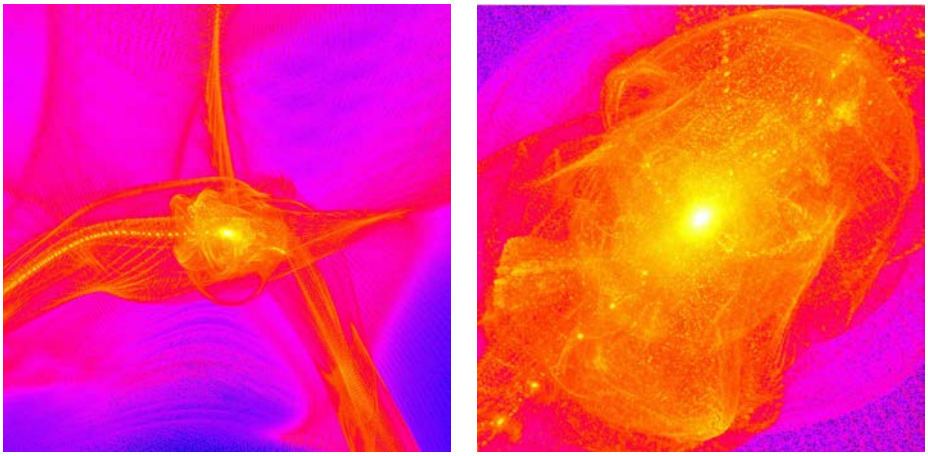

**Figure 3.** Halo formation at the intersection of filaments. A zoom in projection shows that shells and caustics are visible in the not yet virialized WDM halo.

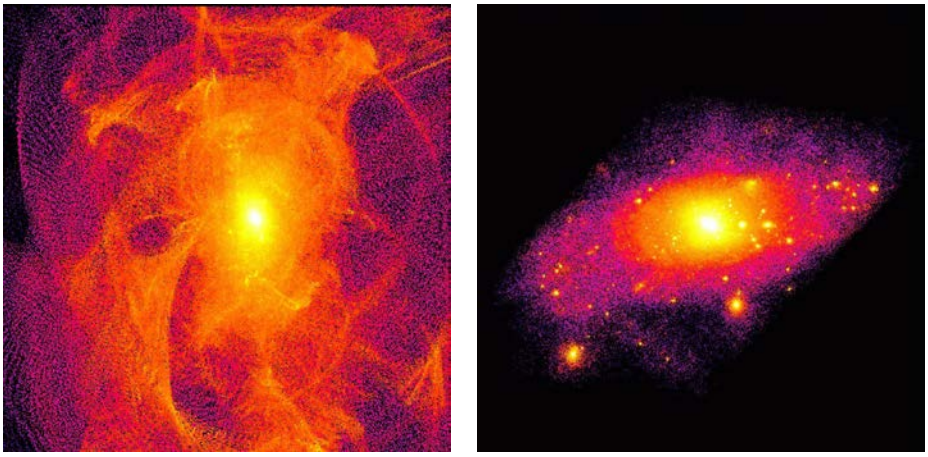

**Figure 4.** A thin slice of the WDM halo formed Top-Down on the left and of a CDM one on the right. Very different internal structure, with shells in caustics in the WDM halo being more apparent

.

**Table 3.** The properties of four different regions of simulation WDM2 displayed in the movies

| Label | size | first collapse | average density | highest density |
|---|---|---|---|---|
| - | box | z | critical | critical |
| lu.avi | 1/4 | 10.13 | 0.264 | 477 |
| ld.avi | 1/4 | 9.45 | 0.258 | 481 |
| ru.avi | 1/4 | 10.77 | 0.268 | 480 |
| rd.avi | 1/4 | 9.78 | 0.258 | 474 |

200 eV), the first collapse appears just after redshift 10 with the first halos forming until redshift 4, while in the simulations with 0.04 km/s (that mimic 1 keV), the first structures would have been already formed by redshift 10. The first halos form at the high density region at the intersection of the filaments and then continue accreting matter. If in a certain region there are many filaments collapsing, then the halos will merge into bigger ones.

Due to the free streaming velocity of the particles, the network configuration and architecture of a certain region is rapidly changing. When the density becomes higher in more isolated regions, the collapse occurs even later, after redshift 4 and some of those halos do not suffer mergers (Fig. C3), so there are halos at redshift zero that have formed via a top-down scenario and did not grow through hierarchical mergers . This is an interesting result, since the observations show that a large fraction of halos in the universe have not suffered any mergers until redshift zero.

Why a certain region has more a top-down or bottom-up formation history depends only on the spatial distribution of the filaments in a certain simulation.

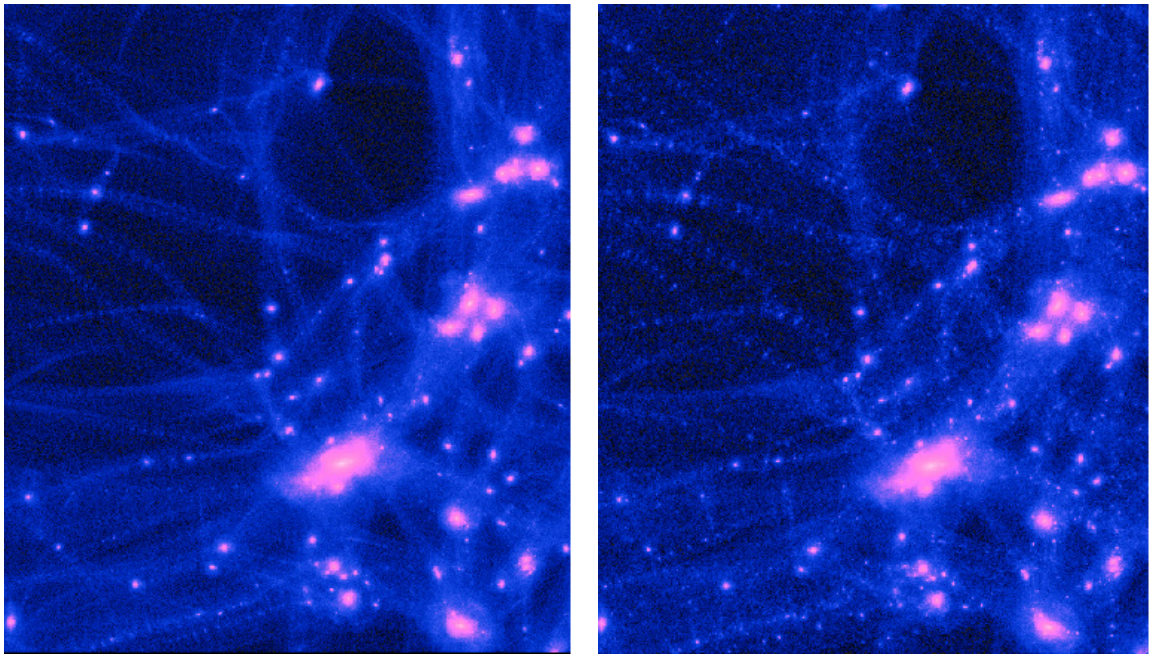

**Figure 5.** A zoom in simulations with the same cutoff in the power spectrum having corresponding thermal velocities - WDM2(left) and no thermal velocities WDM1(right) at z=0

A single halo simulated with different velocities can be seen in the movie halo.avi[9]. The $7 \times 10^{12} M_{\odot}$ halo forms top-down at the intersection of the filaments and has 18 million particles in its $r_{200}$ radius.

These high resolution runs are $8^3$ times more resolved in mass than the initial ones: the dark matter particle mass is $m_d = 2.72 \times 10^5 M_{\odot}$, where each dark matter particle has a spline gravitation softening of 355 pc.

Although the WDM halos on galactic scales contain few bound substructures, one can see shells and caustics inside the virialized region which arise from the coherent infall of material along filaments and from the smooth surrounding regions. As the resolution increases, the presence of shells and caustics becomes more apparent. The early top-down formation of a halo at the intersection filaments is shown in Fig. 3 along with a zoom in its central region. One can clearly see the shells and caustics wrapped inside the 18 million particle halo. A thin slice projection of the warm dark matter halo and a cold dark matter one, clearly illustrates in Fig. 4 how strikingly different is their inner structure.

### 4.2 Impact of thermal velocities on structure formation

As stressed in Section 2, the use of thermal velocities in warm dark matter simulations is crucial, even if their value is comparable with the Zeldovich velocities at a certain redshift.

In Fig. 5 we show the differences at redshift zero between the structures emerging in a region in two similar simulations, WDM1 (without thermal velocities), and WDM2 (with thermal velocities). Both simulations have the same size, the same power spectrum cutoff and the same initial redshift. The structure formation and evolution in these two simulations is shown side by side in movie cosmoboxall.avi[10].

We can see that although the position of the big structures is not affected, below Mpc scales there is a memory of the grid in the simulation without velocities that is smoothed out when adding thermal velocities, as expected. Some of the very small halos formed in the simulation without velocities cannot be found in the simulation where thermal velocities are included. The lack of small halos in WDM simulations with velocities is of course a crucial feature hinting to resolve the discrepancy between the CDM simulations predicting too many subhalos in galaxy-sized halos in comparison with the observed number of dwarf galaxies around large galaxies. Indeed WDM simulations without velocities still suffer from the infinite phase space density problem.

For comparison, we have performed a suit of simulations that start with a cold distribution of particles, no power spectrum cutoff, but have velocities corresponding to 1 km/s, 10 km/s, 200 km/s and 700 km/s. Even the early structure formation is qualitatively different from the warm

[9] The movie can be found on youtube `https://www.youtube.com/watch?v=s_H4dSOP27I`. A zoom in the halo can be watched at `https://www.youtube.com/watch?v=zqVi9SSWmXM`

[10] The movie can be watched here: `https://www.youtube.com/watch?v=5txGwBRNC1U`

dark matter simulations, confirming that the top-down collapse is induced by the damping of the power spectrum at small scales and not the thermal velocities.

### 4.3 Technical aspects in simulating WDM

The resolution limit poses even a more stringent problem in warm dark matter simulations then in cold dark matter ones. Indeed, in order to properly analyze a region of the simulation, multiple refinements of that region with higher resolution particles are used. This implies tracking the particle backwards, from redshift zero to the initial conditions. Due to the large streaming velocities, particles that end up in a virialized halo at redshift zero come from a larger region than in the CDM simulations, making it more difficult to reach high resolution simulations in WDM.

The heavier the effective mass of our simulation particles, the more prominent is the 2-body relaxation effect in small clumps (Eq. (6)). This problem is more stringent in the case of cold dark matter simulations, where an initial zero velocity is used. In the case of warm dark matter, this scales with the velocity of the particle, giving a smaller relaxation time for a smaller velocity. This is why for simulations in the keV range, where the streaming velocity is smaller, the top-down formation history has been barely observed.

As recently shown by Gao, Theuns & Springel (2015), methods like 'FoF' used in analyzing cold dark matter simulations are proved to be insufficient in analyzing warm dark matter halos. We confirm this statement, finding that the artificial fragmentation occurring along the filaments results in a high number of small halos with less than ten particles.

## 5 CONCLUSIONS AND DISCUSSION

We have performed several N-body warm dark matter simulations within a large range of velocity dispersion, for the purpose of pointing out the effects on the formation of structure. We have then focused on a regime where the resolution is better balanced by the velocity distribution. Some of our findings are summarized below.

- In warm dark matter models, as our dark matter only simulations show, the structure formation follows a hybrid scenario in which both top-down and bottom-up scenarios have a saying.
- The early structure formation in this warm dark matter models is essentially top-down, with large halos forming in the highest density regions, tracked at the intersection of filaments. The second level of top down formation of structure is occurring along single isolated filaments.
- The biggest earlier formed halos will accrete matter from the filaments, while in small densities regions the mergers of smaller halos will result in a larger halo.
- Later on, and depending on the morphology of the region in which these halos formed, meaning mainly the density and the layout of the filaments, they merge into bigger halos creating a hierarchical build-up.
- The warm dark matter halos, especially the ones that did not suffer big mergers, show obvious shells and caustics.
- The warmer the dark matter the more pronounced is the top-down effect and the more delayed is the collapse.
- Albeit the numerical limitations we encounter as far as our warm dark matter simulations are concerned, we can conclude that an early top-down structure formation trend would be seen even in dark matter simulations with $v < 0.05$ km/s. For colder particles, this effect is hidden and wiped out by following abundant mergers resulting in a redshift zero distribution that seems in agreement with the hierarchical formation scenario.
- The number of small satellites, as previously found, is visibly reduced in the WDM simulations with respect to the CDM ones.

For a warm dark matter particle, as supported by the arguments adduced in Section 2, the thermal component of the velocity is important for different theoretical and practical considerations. The strong dependence of the mass-velocity relation on the actual particle production model makes it difficult to constrain certain properties of the dark matter particle, including its mass. The impact that a certain velocity dispersion is having on the structure formation and evolution on both small and large scales, as seen in simulations cannot be used as a strong constraint on the mass in the absence of a universal model for particle production. Furthermore, we have shown that there have been some inconsistencies in previous studies with respect to the use of velocities in the simulations, that lead to ambiguous results.

The baryonic physics may play an important role in the actual formation and evolution of halos, hence the necessity of further exploring these effects in simulations. High redshift observations of halos could be used in comparison with complex baryonic warm dark matter simulations in constraining the mass of warm dark matter particles based on their formation and merger history.

The baryonic processes that we have not included in the simulations must play an important role in the structure formation. Previously Gao & Theuns (2007) show a crucial difference in the collapse of a filament that contains both gas and dark matter in a 3 keV simulation, with respect to the cold dark matter case. In the WDM case, the stars form inside the filament, before the halo forms. This trend where stars form in filaments continues for 1.5 keV particles up to redshift $z \approx 2$ resulting in stringy "chain" galaxies that remain to be confirmed by observations (Gao, Theuns & Springel 2015).

The smoother space distribution in the warm dark matter scenario may allow baryons to condense coherently in a smooth potential halo, providing favorable conditions for forming disk-like galaxies. However, a much higher resolution that the one available in present simulations is needed to explore this effect.

## ACKNOWLEDGMENTS

S.P. would like especially to thank Doug Potter and Joachim Stadel for their valuable input and help. Discussions with George Lake, Andrea Macciò, and Ben Moore are acknowledged.

**REFERENCES**


Abazajian, K. & Koushiappas, S. M., 2006, Phy.Rev.D, 74, 023527

Abel, T. and Hahn, O. and Kaehler, R., 2012, MNRAS, 427, 61

Anderhalden, D., Diemand, J., Bertone, G., Macciò, A. V., Schneider, A., 2012,JCAP, 10, 47

Atkins, P., Friedman, R. 2005, Molecular Quantum Mechanics, Oxford Univ. Press

Bertschinger, E., 2001, ApJS, 137, 1

Bode, P., Ostriker, J. P. & Turok, N., 2001, ApJ, 556, 93

Bond, J. R., Efstathiou, G., Silk, J., 1980, Phys. Rev. Let., 45

Boyarsky, A., Ruchayskiy, O., Iakubovskyi, D., France, J., 2014, Phys. Rev. Let., 113, 251301

de Blok, W. J. G., McGaugh, S. S., Bosma, A., & Rubin, V. C. 2001, ApJL, 552, L23

Bulbul, E. and Markevitch, M. and Foster, A. and Smith, R. K. and Loewenstein, M. and Randall, S. W., 2014, ApJ, 789, 13

Chandrasekhar, S., 1942, *Principles of Stellar Dynamics*, The University of Chicago Press

Colombi, S. and Dodelson, S. and Widrow, L. M., 1996, ApJ, 458, 1

Cooper, A. P., Cole S., Frenk, C. S., White, S. D. M., Helly J., Benson, A. J., De Lucia, G., Helmi, A., et al., 2010, MNRAS, 406, 744

Destri, C., de Vega, H. J. and Sanchez, N. G., 2013, New Astronomy 22, 39, arXiv:1204.3090

Diemand, J. & Moore, 2010, B., Particle Dark Matter: Observations, Models and Searches, p. 14, (Cambridge University Press) (2010)

Diemand, J. & Moore, B., 2011, Advanced Science Letters, 4, 297

Gao, L. and Theuns, T., 2007, Science, 317,1527

Gao, L. and Theuns, T. and Springel, V., 2015, MNRAS, 450, 45

Governato, F. and Weisz, D. and Pontzen, A. and Loebman, S. and Reed, D., Brooks, A. M., Behroozi, P., Christensen, C., Madau, P. and Mayer, L. and Shen, S. and Walker, M., Quinn, T., Keller, B. W., Wadsley, J., 2015, MNRAS, 448, 792

Götz, M.,Sommer-Larsen, J., 2002, ApSS, 281, 415

Hahn, O., Angulo, R. E., 2015, arXiv:1501.01959

Hansen, S. H., Lesgourgues, J., Pastor, S. & Silk, J., 2002, MNRAS, 333, 546

Hénon, M., 1973, Dynamical Structure and Evolution of Stellar Systems, (Swiss Society of Astronomy and Astrophysics), p. 183

Huang, K., Statistical Mechanics, 1987, John Wiley & Sons

Kamada, A., Yoshida, N., Kohri, K., Takahashi, T., 2013, JCAP, 3, 8

Klypin, A., Kravtsov, A. V., Valenzuela, O., & Prada, F. 1999, ApJ, 522, 82

Kormendy, J., Drory, N., Bender, R., Cornell, M. E., 2010, ApJ, 723, 54

Kuzio de Naray, R. & Kaufmann, T., 2011, MNRAS, 414, 3617

Lin, C. C. and Mestel, L. and Shu, F. H., 1965, ApJ, 142, 1431

Macciò A. V., Paduroiu S., Anderhalden D., Schneider A., Moore B., 2012, MNRAS, 424, 1105

Marinacci F., Pakmor, R., Springel, V.,2014, MNRAS, 437, 1750

Markovic Katarina,Viel Matteo, 2014, Publications of the Astronomical Society of Australia, 31, 6

Martizzi, D., Teyssier, R., & Moore, B., 2013, MNRAS, 432, 1947

Mashchenko, S., Wadsley, J., Couchman, H. M. P., 2008, Science, 319, 174

Melott, A., L., 2007, arXiv:0709.0745

Miller, R.H., 1964, ApJ, 140, 250

Moore, B., Ghigna, S., Governato, F., Lake, G., Quinn, T., Stadel, J., & Tozzi, P. 1999, ApJL, 524, L19

Muccione, V., Pfenniger, D., 2006, EAS Publications Series, 20,291

Navarro, J. F., Frenk, C. S., & White, S. D. M., 1996, ApJ, 462, 563

Padmanabhan, T., Theoretical Astrophysics, Vol. III (Cambridge University Press)

Peacock, J., Cosmological Physics (Cambridge University Press)

Peebles, P. J. E., 1993, Principles of Physical Cosmology (Princeton Univ. Press)

Pfenniger, D. and Muccione, V., 2006, A&A, 456, 45

Pierpaoli, E. and Borgani, S. and Masiero, A. and Yamaguchi, M., 1998, Phy.Rev.D, 57, 2089

Pontzen A., Governato F., 2012, MNRAS, 421, 3464

Salucci, P., Wilkinson, M. I., Walker, M. G., Gilmore, G. F., Grebel, E. K., Koch, A., Frigerio Martins, C., Wyse, R. F. G., 2012, MNRAS, 420, 2034

de Souza, R. S., Mesinger, A., Ferrara, A., Haiman, Z., Perna, R., Yoshida, N., 2013, MNRAS, 432, 3218

Schneider, A. and Smith, R. E. and Reed, D, 2013, MNRAS, 433, 1573

Seljak, U., Makarov, A., McDonald, P., & Trac, H., 2006, Phys. Rev. Let., 97, 191303

Springel, V., 2005, MNRAS, 364, 1105

Stadel, J., 2001, PhD Thesis, University of Washington

Stadel J., Pooter, D., Moore, B., Diemand, D., Madau, P., Zemp, M., Kuhlen, M. & Quilis, V., 2009, MNRAS, 391, L21

Trodden, M., Carroll, S.M., 2004, arXiv:0401547

de Vega, H. J. and Sanchez, N. G., 2011, arXiv:1109.3187

de Vega, H. J. and Falvella, M. C. and Sanchez, N. G., 2012, arXiv:1203.3562

Viel, M., Lesgourgues, J., Haehnelt, M. G., Matarrese, S., & Riotto, A., 2005, Phy.Rev.D, 71, 063534

Wang, J.,White, S. D. M., 2007, MNRAS, 380, 93

Weinberg, S., 1962, Phys.Rev, 128, 1457

Weinberg, S., 2008, Cosmology, Oxford Univ. Press

Zel'dovich,Y. B., 1970 A&A, 5, 84

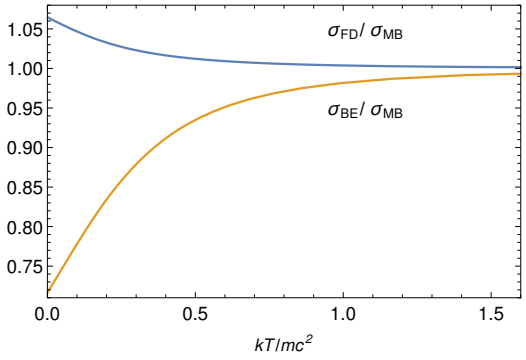


**Figure A1.** The ratios between the velocity dispersions $\sigma_{\rm FD}/\sigma_{\rm MB}$ and $\sigma_{\rm BE}/\sigma_{\rm MB}$ with respect to the temperature

## APPENDIX A: VELOCITY DISPERSION DEPENDENCE ON TEMPERATURE IN FERMI-DIRAC AND BOSE-EINSTEIN DISTRIBUTIONS

As mentioned in Sect. 2.2.1, we check the correction to velocity dispersion that should be applied to a Maxell-Boltzmann distribution when the physical system follows a given quantum statistics.

The energy of a particle as a function of momentum $p$, valid in all regimes (relativistic and non-relativistic), is

$$\epsilon(p) = \sqrt{p^2c^2 + m^2c^4} - mc^2 \ , \tag{A1}$$

and the velocity

$$v(p) = \frac{pc}{\sqrt{m^2c^2 + p^2}} \ . \tag{A2}$$

The corresponding 1D spherical distributions for Fermi-Dirac, Maxwell-Boltzmann and Bose-Einstein cases are:

$$f_{\rm FD} = \frac{4\pi p^2}{\exp\left(\epsilon(p)/kT\right) + 1} \tag{A3}$$

$$f_{\rm MB} = \frac{4\pi p^2}{\exp\left(\epsilon(p)/kT\right)} \tag{A4}$$

$$f_{\rm BE} = \frac{4\pi p^2}{\exp\left(\epsilon(p)/kT\right) - 1} \tag{A5}$$

Integrating over all $p$, we obtain the normalization constant

$$S = \int_0^\infty f dp \ . \tag{A6}$$

For each case respectively the second moment are

$$\sigma^2_{\rm FD} = \frac{1}{S}\int_0^\infty p^2 f_{\rm FD}\, dp \ , \tag{A7}$$

$$\sigma^2_{\rm MB} = \frac{1}{S}\int_0^\infty p^2 f_{\rm MB}\, dp \ , \tag{A8}$$

$$\sigma^2_{\rm BE} = \frac{1}{S}\int_0^\infty p^2 f_{\rm BE}\, dp \ . \tag{A9}$$

Computing these integrals by numerical quadrature, we find the ratios between the velocity dispersions $\sigma_{\rm FD}/\sigma_{\rm MB}$ and $\sigma_{\rm BE}/\sigma_{\rm MB}$ with respect to temperature. The result is plotted in Fig. A1. In any situation the Fermi-Dirac velocity dispersion is not significantly different from Maxwell-Boltzmann's, differing by at most $\sim 6.5\%$, while the Bose-Einstein velocity dispersion differs more, up to $\sim 27\%$. The highest differences occur at low temperature, corresponding to low redshifts. This is not such a dramatic correction as the factor 3.571 invoked in Macciò et al. (2012), but can still be significant for high precision cosmology works.

## APPENDIX B: DETAILED DERIVATION OF THE RESULTS IN SECTION 2.2.2

Using these expressions inserted into Eq. (19), the specific particle entropy becomes

$$\frac{s}{k} = \frac{1}{3}\frac{\int_0^\infty \frac{y^{3/2}\sqrt{2q+y}(5q+4y)}{Z^{-1}\exp(y)\pm 1}}{\int_0^\infty \frac{y^{1/2}\sqrt{2q+y}(q+y)}{Z^{-1}\exp(y)\pm 1}} - \ln(Z) \ , \tag{B1}$$

where $Z \equiv \exp(\mu/kT)$, $q \equiv mc^2/kT$ and $y \equiv (\sqrt{p^2c^2 + m^2c^4} - mc^2)/kT$. Thus $s$ is a function of the reduced dimensionless variables $Z$ and $q$ only, and not of $g$, $m$ and physical constants explicitly.

In the ultra-relativistic regime when the energy of particles is comparable or higher than the rest mass energy, particles and their antiparticles can be created in equal number, so any chemical potential should cancel to a high degree. Then $s/k$ at $\mu = 0$ becomes a constant. The closed form expressions are,

$$\lim_{T\to\infty}\frac{s(T,0)}{k} = \frac{7}{135}\frac{\pi^4}{\zeta(3)} \approx 4.20183245, \tag{B2}$$

for fermions, and

$$\lim_{T\to\infty}\frac{s(T,0)}{k} = \frac{4}{45}\frac{\pi^4}{\zeta(3)} \approx 3.60157071, \tag{B3}$$

for bosons, where $\zeta$ is Riemann's function, and $\zeta(3) \approx 1.20205690$.

The particle velocity at all regimes can be derived from the relativistic particle kinetic energy $\epsilon(T,\mu) = e(T,\mu)/n(T,\mu) = \sqrt{p^2c^2 + m^2c^4} - mc^2$ and that relativistic momentum is related to velocity by $v^2/c^2 = 1/(1+m^2c^2/p^2)$. Eliminating $p$ yields, noting $Y \equiv \epsilon/mc^2$,

$$\frac{v^2(T,\mu)}{c^2} = 1 - \frac{1}{(1+Y)^2} = \frac{Y\,(2+Y)}{(1+Y)^2} \ . \tag{B4}$$

The second form is numerically more precise at low energy. The non-relativistic and ultra-relativistic expansions read, respectively,

$$\frac{v^2}{c^2} \approx 2Y - 3Y^2 + 4Y^3 - \dots \tag{B5}$$

$$\frac{v^2}{c^2} \approx 1 - Y^{-2} + 2Y^{-3} - 3Y^{-4} + \dots \tag{B6}$$

As stated in Section 2.2.2, the conserved particle density $n(T,\mu)$ is related to universal expansion by the scale factor $a = 1/(1+z)$ and therefore

$$n(T(z),\mu(z)) = n_0(1+z)^3 \ , \tag{B7}$$

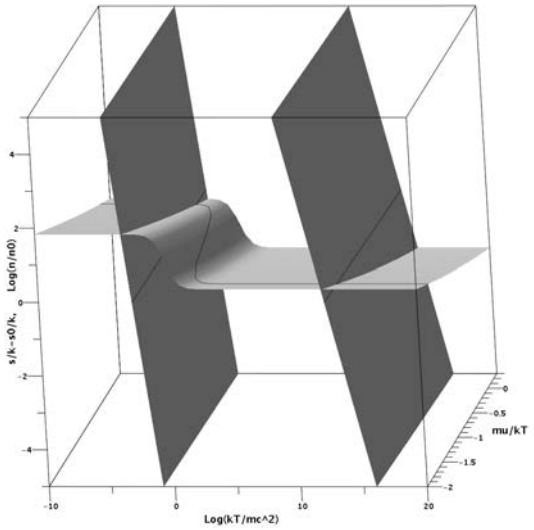


**Figure B1.** Density $n$ and entropy $s/k$ as functions of temperature $T$ and chemical potential $\mu$ as given in Eq. (B7) and (B8). The light-grey surface is the entropy and the dark-grey ones are the density at two redshifts $z = 10^9$ on the left (relativistic), and $z = 0$ on the right (non-relativistic), while $n_0 = 115\,\mathrm{cm}^{-3}$, $g = 1$, and $m = 1\mathrm{keV}/c^2$. The intersection of the level curves yields the solution of Eq. (B7) and (B8).

while the constant particle entropy gives

$$\frac{s(T(z),\mu(z))}{k} = \frac{s(\infty,0)}{k} = 4.20183245\ , \qquad \text{(B8)}$$

For a given particle density $n_0$, redshift $z$ and particle mass $m$ the non-linear Eq. (B7) and (B8) can be solved with a non-linear equation solver for $T$ and $\mu$. The functions are univalued and level curves of $n$ and $s$ intersect once, so any combination of $T$ and $\mu$ gives a single solution (see Fig. B1). Actually the constant level curves $n$ and $s$ expressed with the variables $\log q$ and $Z$ intersect almost at right angle: $n(\log q, Z)$ depends most rapidly on $\log q$, and $s(\log q, Z)$ depends most rapidly on $Z$, so finding a solution for $\log q$ for $n$ at constant $Z$ and then a solution for $Z$ at constant $q$ for $s$, and repeating until satisfaction could be a method to find a solution. Since the thermodynamic functions involve integrals, a fast numerical integrator is handy, since several indefinite integrals must be evaluated at each iteration. To perform this we used Maple 18 which includes a non-linear multidimensional function root solver, and evaluate quickly numerical integrals with the NAG library algorithm D01AMC.[11] When $T$ and $\mu$ are found for a given particle mass and degeneracy factor $g$, all the other quantities like $v^2$ can be derived by plugging these values in the functions, which may require again few numerical integral evaluations. The results are presented in Section 2.2.2.

[11] The Maple script is available on request.

## APPENDIX C: MOVIES CAPTIONS AND SNAPSHOTS

**Table C1.** Description of the movies accompanying the paper

| Label | Description |
|---|---|
| cosmoboxvel.avi | Movie of full-box WDM2 simulation |
| cosmoboxall.avi | WDM1 and WDM2 full-box simulations side-by-side showing the effect of thermal velocities |
| lu.avi ld.avi ru.avi rd.avi | A zoom in the 1/4 of the WDM2 simulation |
| halo.avi | A $7 \times 10^{12} M_{\odot}$ $18 \times 10^{6}$ particles high-resolution refined halo from WDM5 |
| halozoom.avi | A zoom in the refined halo focused on the central region where the shells and caustics can be observed |

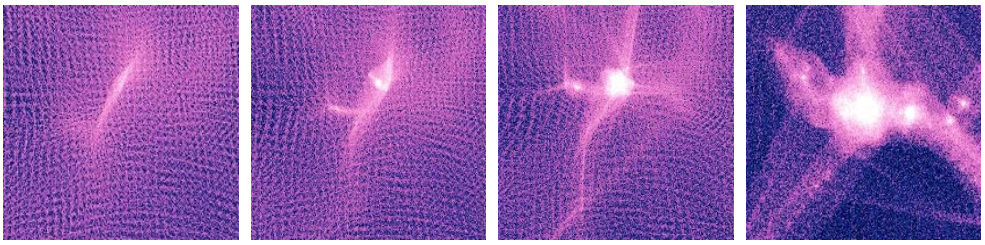

**Figure C1.** A zoom in a region from the WDM2 simulation, showing the evolution of a halo which forms top-down at the intersection of the filaments and then starts accreting matter

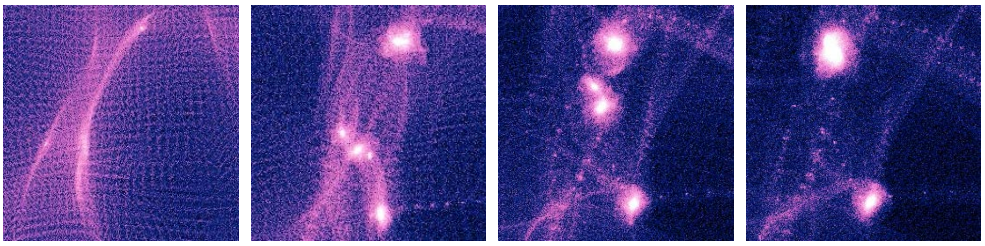

**Figure C2.** A zoom in a region from the WDM2 simulation showing how small halos formed later that merge hierarchically in a larger halo

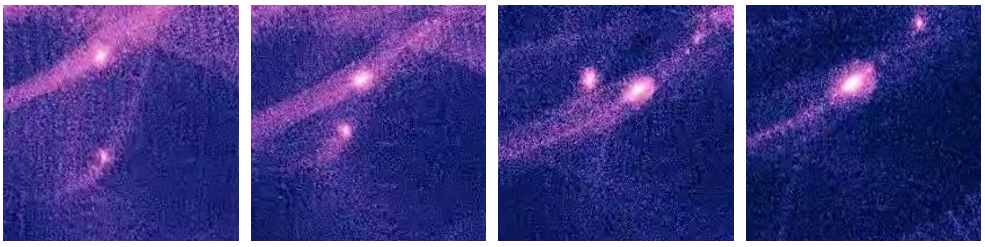

**Figure C3.** An early formed halo which doesn't suffer mergers

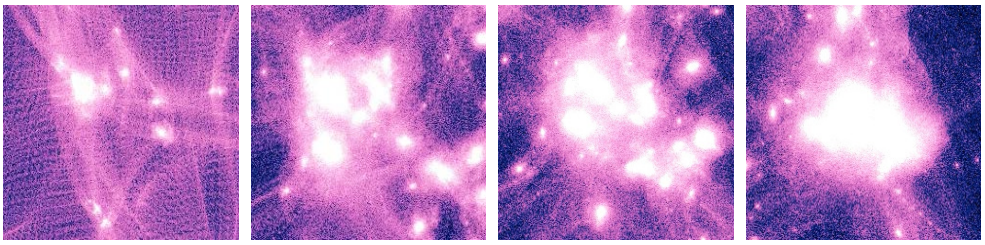

**Figure C4.** A large high density region with many filaments where the halos formed early on via top-down collapse are merging in a violent manner creating a larger cluster

Chapter 4

# Internal structure of warm dark matter halos

The formation of halos is a result of the non-linear dark matter density perturbations. As we have seen in the previous chapter, in the case of CDM, as confirmed by the simulations, the first halos are formed from the smallest scales fluctuations. The large halos are forming later from the merging of the small halos. In the WDM case, as far as pure $N$-body simulations show, the formation mechanism of halos is more complex, a hybrid mechanism, with the first halos forming top-down at the intersection of large filaments. These halos evolve then in several different ways, depending on the morphology of the region where they formed, growing either by accretion, or by mergers. The late stage of structure formation is again different, in the sense that while in cold dark matter, small halos that form late behave like satellites around large halos, in the warm dark matter case, many of these late forming halos are found in more isolated, low density regions. The prevalence of one or another evolution scenario is strongly dependent on the velocity of the simulated particle and it is also influenced by the resolution of the simulation.

Besides the differences found in pure $N$-body simulations, with only one type of dark matter particles, the baryonic physics can bring another degree of complexity in the way in which halos are formed, as we have seen in Gao & Theuns (2007). In order to give an accurate prediction for the formation and evolution of structure in warm dark matter models, more such studies are needed.

Several analyses of halos' structure in warm dark matter simulations and comparisons with the structure of cold dark matter halos will be presented in this chapter.

## 4.1 Halo mass and formation distribution

An important point is to determine statistically how these collapsed halos are distributed in the universe at different times and for different masses. Press & Schechter (1974) proposed a simple

model, based on the assumption that halos are correlated with peaks in the Gaussian random density field of dark matter in the early universe. Following the statistics of the random fields (Press & Schechter 1974) and considering that halos form also in underdense regions, a rough estimation on the number of halos with a mass in a range $M$ to $M + \delta M$ per unit volume, $\delta M(\mathrm{d}n/\mathrm{d}M)$ is given (Bond et al. 1991; Bower 1991; Lacey & Cole 1993) by,

$$\frac{\mathrm{d}n}{\mathrm{d}M}(M,t) = \left(\frac{2}{\pi}\right)^{1/2} \frac{\rho_0}{M^2} \frac{\delta_\mathrm{c}(t)}{\sigma(M)} \left|\frac{\mathrm{d}\ln\sigma}{\mathrm{d}\ln M}\right| \exp\left[-\frac{\delta_\mathrm{c}^2(t)}{2\sigma^2(M)}\right], \tag{4.1}$$

where $\rho_0$ is the mean density in the universe, $\sigma(M)$ is the fractional root variance in the density field smoothed using a filter that contains a mass $M$, on average, and $\delta_\mathrm{c}(t)$ is the critical overdensity for spherical collapse at time $t$ (Eke et al. 1996).

This simple formula does not accurately apply to $N$-body simulations (Sheth, Mo & Tormen 2001). Depending on the parameters used in the simulations, several methods for fitting the mass function have been proposed (Reed et al. 2007; Tinker et al. 2008; Robertson et al. 2009). The estimation of the mass function is given by,

$$\frac{\mathrm{d}n}{\mathrm{d}M} = f(\sigma)\frac{\bar{\rho}}{M}\frac{\mathrm{d}\ln\sigma^{-1}}{\mathrm{d}M}, \tag{4.2}$$

with

$$f(\sigma) = A\left[\left(\frac{\sigma}{b}\right)^{-a} + 1\right]\exp\left(-\frac{c}{\sigma^2}\right), \tag{4.3}$$

and where $A$, $a$, $b$ and $c$ are parameters tuned by the results of $N$-body simulations.

The mass variance is inferred from the power spectrum of density fluctuations,

$$\sigma^2(M) = \frac{1}{2\pi^2}\int_0^\infty P(k)T^2(k)\hat{W}_M^2(k)k^2\mathrm{d}k, \tag{4.4}$$

where $P(k)$ is the initial power spectrum, $T(k)$ is the dark matter transfer function (Eisenstein & Hu 1999) and $\hat{W}_M(k)$ is the Fourier transform.

These fitting parameters depend on redshift, unable to predict a universal mass function and therefore a universal description of the halo mass distribution. In the case of warm dark matter, the mass function also depends on the structure formation mechanism and it is 'contaminated' by the presence of halos formed by artificial fragmentation.

### 4.1.1 Galaxy mergers

The gravitational interaction of two or more halos encountering each other is generally referred to as merging. Yet another distinction is required here. Due to dynamical friction, which is a dissipative process, the orbits of small satellite halos around a large host galaxy are reduced, and the halos may 'fall' towards the center of the more massive halo. This type of interaction, where a large galaxy 'accretes' smaller halos, falls into the category of minor mergers. On the other hand, when two halos or galaxies of similar mass are encountering, their merging results in a new galaxy

with a structure different than that of the preexisting objects. These major mergers are considered responsible for the formation of spheroidal galaxies. The structure of the merger remnant depends however, on the structure of the major mergers. The merging of purely stellar disk halos will produce a spheroidal merger remnant with a central phase space density (PSD) lower than that of the observed ellipticals (Hernquist, Spergel & Heyl 1993), which are produced by the mergers of other types of galaxies.

It has been shown in numerical simulations (Bournaud, Jog & Combes 2005) that mergers with a mass ratio $M_2/M_1 \sim 0.25$ destroy disks in the galaxies forming a spheroidal remnant, while mergers with a lower mass ratio (very minor mergers) may form a thickened disk system. In the pure $N$-body cold dark matter simulations, since mergers are ubiquitous, pure disk galaxies have not been found. It is true, however that the presence of baryons plays in important role and in some exceptional cases, where the major mergers are having a high gas fraction, larger than 50%, the formation of a disk may occur in the remnant galaxy (Barnes 2002; Springel & Hernquist 2005; Robertson et al. 2006).

The sequence of merging events and the masses of the halos involved can be extracted using the mass distribution function at different redshifts (Benson 2010). The distribution function of halo progenitor masses $M_1$ at redshift $z_1$ and $M_2$ at redshift $z_2$ is,

$$\frac{\mathrm{d}N}{\mathrm{d}M_1} = \left(\frac{2}{\pi}\right)^{1/2} \frac{\mathrm{d}\ln\sigma}{\mathrm{d}\ln M}_1 M_2 \frac{\sigma_1^2}{M_1^2} \frac{\delta_{\mathrm{c}1}-\delta_{\mathrm{c}2}}{(\sigma_1^2-\sigma_2^2)^{3/2}} \exp\left[-\frac{(\delta_{\mathrm{c}1}-\delta_{\mathrm{c}2})^2}{(\sigma_1^2-\sigma_2^2)}\right], \tag{4.5}$$

where $\sigma_1 = \sigma(M_1)$, $\sigma_2 = \sigma(M_2)$, $\delta_{\mathrm{c}1} = \delta_{\mathrm{c}}(z_1)$, $\delta_{\mathrm{c}2} = \delta_{\mathrm{c}}(z_2)$. For $z_1 \sim z_2$, this can be interpreted as a merger rate (Benson 2010).

Since in reality, merger rates are not symmetric, as considered in this approach, more accurate rate function formulations have been discussed (Benson, Kamionkowski & Hassani 2005; Benson 2008).

In the case of $N$-body simulations, merger trees can be extracted directly, and several methods have been proposed (Helly et al. 2003; Springel et al. 2005; Hopkins et al. 2010, e.g.). There is, however, a more complex problem that arises in the $N$-body simulations, in the case of substructures, where three body encounters can result in the ejection of halos, as discussed in Sales et al. (2007).

As far as warm dark matter simulations are concerned, in order to compute an accurate mass function for the halos, one needs to compute first the merger trees, since the small halos formed due to the fragmentation may sometimes merge into larger halos that have a mass above the fragmentation scale, as shown in Chapter 5. These halos are difficult to spot without a merger tree analysis.

## 4.2 Shells and caustics in dark matter halos

Dark matter caustic rings and shells are singularities in phase space (Bertschinger 1985; Hogan 1999) formed through the gravitational collapse of dark matter, halos merging and tidal disruption

of satellites. The formation of halos, as described by the Vlasov-Poisson equation, results in the formation of shells or caustics, where the dark matter streams meet at the surface of high density regions (Sikivie & Ipser 1992; Sikivie et al. 1997; Tremaine 1999; Alard & Colombi 2005; Natarajan & Sikivie 2006; Mohayaee & Salati 2008). The tidal tails formed by the satellites falling inside the potential well of the host halos also give rise to high-density caustics. Caustics and shells of stars formed during the mergers of galaxies have been observed in the so-called shell galaxies (Malin & Carter 1980; Carter et al. 1982; Hernquist & Quinn 1988, 1989).

These shells and caustics, once formed, cannot be completely destroyed, making them permanent structures in both real space and phase space. The density in shells and caustics exceeds the density of the neighboring regions, by a factor that depends on the age and history of that particular galaxy (Mohayaee & Salati 2008). Their study is therefore of importance for establishing the mechanism controlling the structure formation and evolution, and hence, the nature of dark matter.

Cold dark matter simulations have not been very successful in reproducing observable caustics and shells. In CDM halos, during the hierarchical evolution, caustics are being wrapped inside earlier generations of the merging history, making them invisible in some cases even at high resolutions. However, Cooper et al. (2010) show using cold dark matter simulations that accretion mechanisms of stars and dark matter clumps and the disruption of the latter can produce concentering shells that resemble those observed in NGC 7600.

As we have shown in Paduroiu et al. (2015), in high resolution warm dark matter simulations, shells and caustics are largely present and highly visible.

From the simulation WDM5 in Table 3.3 we have chosen a region where a large halo forms top-down at the intersection of filaments and we have re-simulated it with high resolution particles. Warm dark matter particles travel longer distances than cold dark matter particles, depending on their velocities, thus a larger region needs to be sampled with high resolution particles. In our simulation, with particles having $\sim 0.36$ km/s velocities at redshift zero, the particles ending in the halo forming region travel a distance almost 15 times larger than the $r_{200} = 630$ kpc of that halo. That means that almost a third of the box had to be refined.

These high resolution runs are $8^3$ times more resolved in mass than the initial ones: the dark matter particle mass is $M_d = 2.72 \times 10^5$ $M_\odot$, where each dark matter particle has a gravitation softening of 355 pc. The $7 \times 10^{12}$ $M_\odot$ halo forms top-down at the intersection of the filaments and then accretes matter, reaching 18 million particles in its $r_{200}$ radius at redshift zero.

In Paduroiu et al. (2015) we show the difference between the same region in a cold dark matter simulation. It is important to mention that the size of the halo is almost three times larger ($r_{200} \sim 630$ kpc) than the same mass halos in the CDM simulations, less concentrated, not virialized by redshift zero and not spherically symmetric. In Fig. 4.1 we show a zoom in projection and a thin slice of the halo.

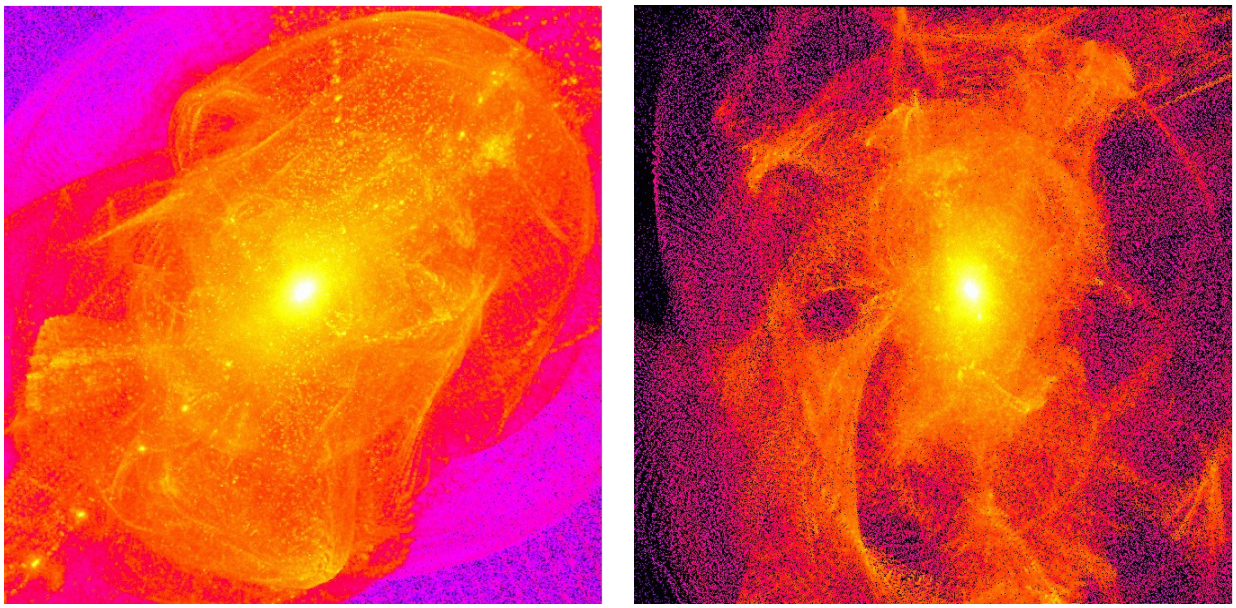

Figure 4.1: A zoom in projection (left panel) and a thin slice (right panel) of the not yet virialized WDM halo formed top-down at the intersection of filaments show the obvious presence of shells and caustics.

Although the WDM halos on galactic scales contain few bound substructures, one can see shells and caustics inside the central region, which arise from the coherent infall of material from the filaments and from the smooth surrounding regions. The tidal tails of small satellites accreted are also visible.

Previous studies signaled the presence of caustics in warm dark matter halos (Lovell et al. 2012; Angulo, Hahn, & Abel 2013; Lovell et al. 2014, e.g.)[1]. These studies, however, do not include thermal velocities. Since the presence of shells is a direct effect of the structure formation mechanism, they can be seen in both simulations, with and without velocities, but their structure is different. In the simulation with velocities, the caustics are thicker, making them more apparent.

In Fig. 4.2 we show a linear plot of the magnitude of the radial velocities in the high resolution region where the halo forms. This is very different to what one would expect in a spherically symmetric halo, since the magnitude of velocities shows a strong correlation with the shells rather than with the distance from the center.

The presence of shells and caustics as features of the warm dark matter halos is very important since it may explain the new found emission line of 3.55 keV (Bulbul et al. 2014). The higher density of such a caustic on the line of sight can translate into a high peak in the detected signal. This may also explain why the line may not be seen in other cases, since it depends on the orientation with respect to the caustic. Also, this can be the case for the detection pointed alongside a filament. Although the filaments are bigger in size then the caustics, we have seen that they do not have a

[1]Lovell et al. use a glass method for the simulations, unlike our study.

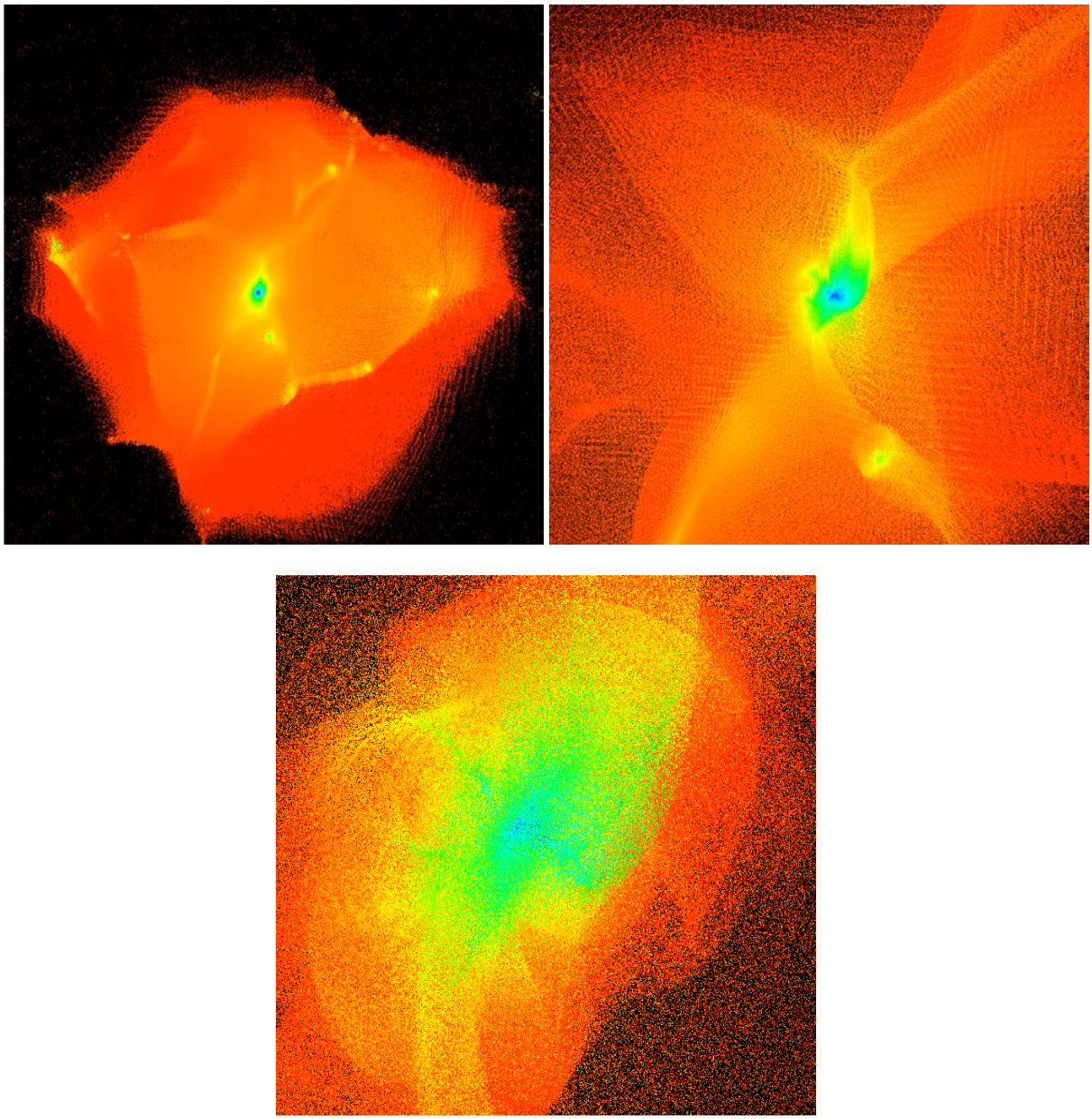

Figure 4.2: A magnitude plot of the radial velocities in the full high resolution region (upper left panel), halo forming region (upper right panel) and halo center (lower panel)

smooth density, the central part of a filament being denser than the outer part.

Indeed, assuming that in such dense regions the weakly interacting species strongly annihilate, a boost can be found in the signal of antiprotons and positrons produced, depending on the dark matter distribution, as shown in Mohayaee & Salati (2008). This study, however, is based on an analytical model which uses the secondary infall mechanism (Fillmore & Goldreich 1984; Bertschinger 1985) with a finite velocity dispersion (Mohayaee & Shandarin 2006), while assuming spherical symmetry and smooth accretion. In the case of cold dark matter caustics, the annihilation signal is not significantly enhanced, as shown in Vogelsberger & White (2011).

More studies, including the results from simulations, are needed in order to estimate the effect of these caustics and use them to constrain dark matter particles.

## 4.3 Density profiles of halos

Considering the simple model of a spherical collapse, it has been shown (Eke et al. 1996) that the overdensity of a collapsed halo with respect to the background density is $\sim 200$, depending slightly on the cosmology. This overdensity corresponds roughly to the virialized region of the halo, hence the virial radius can be defined as (Benson 2010, e.g.)

$$r_{\rm v} = \left( \frac{3M}{4\pi\rho_0\Delta} \right)^{1/3} . \tag{4.6}$$

Cold dark matter $N$-body simulations show that the virial theorem is in most cases obeyed within this radius. Furthermore, the NFW profile (Navarro, Frenk & White 1996, 1997) provides in general a good fit to the cold dark matter halos

$$\rho(r) = 4 \frac{\rho_{\rm s}}{(r/r_{\rm s})[1 + r/r_{\rm s}]^2} , \tag{4.7}$$

where $r_{\rm s}$ is a characteristic scale radius and $\rho_{\rm s}$ is the density at $r = r_{\rm s}$.

More recent $N$-body CDM studies (Navarro et al. 2004; Merritt et al. 2005; Prada et al. 2006) showed that the density profiles are better fitted by the Einasto profile (Einasto 1965)

$$\rho(r) = \rho_{-2} \exp\left( -\frac{2}{\alpha} \left[ \left( \frac{r}{r_{-2}} \right)^{\alpha} - 1 \right] \right) , \tag{4.8}$$

where $r_{-2}$ is a characteristic radius at which the logarithmic slope of the density profile is $-2$ and $\alpha$ is a parameter controlling the variation of the logarithmic slope with the radius. Using the fitting formula provided in Gao et al. (2008), we have for $\alpha$

$$\alpha = \begin{cases} 0.155 + 0.0095\nu^2 & \text{if } \nu < 3.907 \\ 0.3 & \text{if } \nu \geq 3.907 \end{cases} , \tag{4.9}$$

where $\nu(M, z) \equiv \rho_{crit}/\sigma(M, z)$ is a dimensionless 'peak-height' parameter defined as the ratio of the linear density threshold for collapse at $z$ within spheres of mean enclosed mass $M$.

The observations show that the density profiles inferred from galaxy rotation curves provide evidence that structures have a rather constant core (e.g. de Blok et al. 2001; Kuzio de Naray et al. 2009; Oh et al. 2011; Salucci et al. 2012), contrary to the CDM halos from simulations that have a cuspy density profile (Moore 1994; Flores & Primack 1994; Diemand et al. 2005; Macciò et al. 2007; Springel et al. 2008).

This is one of the reasons why warm dark matter has been proposed as a viable alternative. Indeed, in warm dark matter models, the fine grained phase space density is limited by the streaming velocities of the particles. The effects on the final halo structure can be estimated under the assumption that the maximum phase space density value is conserved. This forces the velocity dispersion to become constant and isotropic in the halo center and therefore the density becomes a constant and a core radius can be derived. In reality, the maximum coarse grained phase space density could be significantly lower at the final epoch (due to mixing). Also it is not necessary for the velocities and densities to approach a constant value to limit the maximum phase space density. Velocities may be anisotropic, increase or decrease towards the halo center resulting in rising or falling density slopes.

The Tremaine-Gunn limit (Tremaine & Gunn 1979) on the mass of a neutrino is derived from the maximum phase space density of a homogeneous neutrino background, $2g_\nu h^{-3}$, where $g_\nu$ is the number of allowed helicity states and $h$ is Planck's constant, with the further assumptions that neutrinos form bound structures and that their central regions can be well approximated by isothermal spheres. Assuming that their velocity distribution is Maxwellian we can calculate a maximum phase space density:

$$Q_{max} \equiv \rho_0 m_\nu^{-4} (2\pi\sigma^2)^{-3/2} \, , \tag{4.10}$$

where $\rho_0$ is the central density and $\sigma$ is the one dimensional velocity dispersion. The core radius is then given by

$$r_c^2 = 9\sigma^2 / 4\pi G \rho_0 \, . \tag{4.11}$$

This gives a minimum mass for neutrinos of:

$$m_\nu > (100eV) \left( \frac{100\,\mathrm{km\,s^{-1}}}{\sigma} \right)^{-1/4} \left( \frac{1\mathrm{kpc}}{r_c} \right)^{1/4} g_\nu^{-1/4}. \tag{4.12}$$

In a spherical collapse model, for a halo, the maximum phase space density is given by (Dalcanton & Hogan 2001; Strigari et al. 2006)

$$Q_{max} = 5 \times 10^{-4} \beta \left( \frac{g}{2} \right) \left( \frac{m_x}{1keV} \right)^4 \frac{M_o}{pc^3} (\,\mathrm{km\,s^{-1}})^{-3}. \tag{4.13}$$

The maximum phase space density can be converted in a 'core' size following Hogan & Dalcanton (2000):

$$r_{\mathrm{core,t}}^2 = \frac{\sqrt{3}}{4\pi G Q_{max}} \frac{1}{< \sigma_{halo}^2 >^{1/2}} \, , \tag{4.14}$$

where $\sigma_{halo}$ is the velocity dispersion of the simulated dark matter halo.

In the next section we will study the internal structure of halos from their density and phase space density profiles.

### 4.3.1 Cores and cusps in simulated halos

In order to explore the effect of the maximum phase space density on the internal structures of halos and to test the Tremaine-Gunn limit, several suites of pure $N$-body simulations have been performed.

Firstly, we have run simulations[2] with $160^3$ particles in 40 Mpc boxes. The adopted cosmology is a flat ΛDM cosmology with parameters from the first year WMAP results (Spergel et al. 2003): matter density $\Omega_m = 0.268$, baryon density $\Omega_b = 0.044$, Hubble constant $h = 0.71$, and a scale-invariant, Harrison-Zel'dovich power-spectrum with normalization $\sigma_8 = 0.9$. From these simulations several galaxy mass halos were re-simulated with higher resolution, with and without thermal velocities. The method used for cutting the power spectrum is the same as the one used for the simulations analyzed in the previous chapter, using the fitting formula from Bode et al. (2001),

$$T^2(k) = \frac{P^{WDM}}{P^{CDM}} = [1 + (\alpha k)^{2\nu}]^{-10/\nu} , \tag{4.15}$$

where $\alpha$, the scale of the break, is a function of the WDM parameters, while the index $\nu = 1.12$ is fixed and $\alpha$ is

$$\alpha = 0.049 \cdot \left(\frac{m_X}{1keV}\right)^{-1.11} \cdot \left(\frac{\Omega_\nu}{0.25}\right)^{0.11} \cdot \left(\frac{h}{0.7}\right)^{1.22} h^{-1}\mathrm{Mpc}. \tag{4.16}$$

The streaming velocities were generated using:

$$\frac{v_0(z)}{1+z} = .012 \left(\frac{\Omega_X}{0.3}\right)^{\frac{1}{3}} \left(\frac{h}{0.65}\right)^{\frac{2}{3}} \left(\frac{1.5}{g_X}\right)^{\frac{1}{3}} \left(\frac{keV}{m_X}\right)^{\frac{4}{3}} \mathrm{km\,s^{-1}} \tag{4.17}$$

where $z$ is the redshift and $m_X$ is the mass of the WDM particle X.

From the large cube we selected a $7\times10^{11}$ $M_\odot$ halo and re-simulated this with higher resolution. This halo is two orders of magnitude above the fragmentation scale. The details of the simulations[3] are summarised in Table 4.1.

For particles hotter than 50 eV no halos form by redshift zero. Therefore, in order to study the cores large enough to see with our resolution, we have maintained a 'colder' cutoff in the power spectrum and just increased the velocities. Since the core is mainly due to the presence of the thermal velocities, this method, although not ideal, gives a good approximation.

In Fig. 4.3 we plot the density profiles for this halo from different velocities simulations, while in Fig. 4.4 we plot the corresponding phase space density profiles.

[2]Results from the analysis of these simulations have been published as Paduroiu et al. in the Chalonge Workshop Proceedings de Vega & Sanchez (2011) and Chalonge Colloquium Proceedings de Vega, Falvella & Sanchez (2012). A different set of simulations has been analyzed in Macciò et al. (2012) (Secion 4.5). The conclusions are similar.

[3]Note that chronologically these studies has been done before the ones in Chapter 3, therefore we were referring to the mass of the particles as estimated from Bode et al. (2001) instead of the velocities of the particles. For an easier comparison with the results in Macciò et al. (2012) we keep here the mass parameters.

Table 4.1: Details of the simulations with the mass of particle corresponding to the velocity for which the cutoff is done, the mass corresponding to the thermal velocity, the box size, the softening, the mass of the halo, the value for $r_{200}$ and the number of particles in the $r_{200}$ radius.

| Label | mass | vel | box size | N | softening ($r_{200}$) | $M_{halo}$ | $r_{200}$ | N($<$ r$_{200}$) |
|---|---|---|---|---|---|---|---|---|
| CDM | - | no | 40 Mpc | $160^3$ | $2.6 \times 10^{-3}$ | $7 \times 10^{11} M_\odot$ | 160 | $3.6 \times 10^6$ |
| WDM1 | 200 eV | no | 40 Mpc | $160^3$ | $2.6 \times 10^{-3}$ | $7 \times 10^{11} M_\odot$ | 140 | $2.7 \times 10^6$ |
| WDM2 | 200 eV | 100 eV | 40 Mpc | $160^3$ | $2.6 \times 10^{-3}$ | $7 \times 10^{11} M_\odot$ | 140 | $1.7 \times 10^6$ |
| WDM3 | 200 eV | 20 eV | 40 Mpc | $160^3$ | $2.6 \times 10^{-3}$ | $7 \times 10^{11} M_\odot$ | 132 | $2.7 \times 10^6$ |
| WDM4 | 50 eV | no | 40 Mpc | $160^3$ | $2.6 \times 10^{-3}$ | | | |

The profiles show that the WDM1 (200eV WDM power spectrum but no thermal velocities) halo is already less concentrated than its corresponding CDM halo, as expected (Eke, Navarro & Steinmetz 2001). Once the same WDM halo is simulated with velocities we see a slight flattening of the inner density profile, but this is at the resolution limit which is roughly 0.5% of the virial radius (Diemand, Moore & Stadel 2004). The density profile for the halo simulated with particles that have the velocity corresponding to a 20 eV particle (WDM3) clearly shows a prominent and well resolved constant density core instead of a central cusp.

The density profile of the halo with 20 eV particles was fitted first with a density profile described by the $\alpha$, $\beta$, $\gamma$ law

$$\rho_r = \frac{\rho_0}{\left(\frac{r}{r_s}\right)^\gamma \left(1 + \left(\frac{r}{r_s}\right)^\alpha\right)^{\frac{\beta-\gamma}{\alpha}}} \tag{4.18}$$

using a Monte-Carlo Markov Chain (MCMC) algorithm, which allowed us to easily marginalize over any of the parameters, and to determine the degeneracy in our fit. We found that the transition to the central density core was so sharp that the $\alpha$, $\beta$, $\gamma$ model was a poor fit to the simulation data.

A different parametric description used in Stadel et al. (2009)

$$\rho(r) = \rho_0 \exp(-\lambda[\ln(1 + r/R_\lambda)]^2) \tag{4.19}$$

gives a better fit, as shown in Macciò et al. (2012). In this parameterization the density profile is linear down to a scale $R_\lambda$ beyond which it approaches the central maximum density $\rho_0$ as $r \to 0$. This fitting function is extremely flexible and makes it possible to reproduce at the same time both cuspy profiles like the ones predicted by the CDM theory, and highly cored profiles, like in our case.

Taylor & Navarro (2001) showed that for over two and a half decades in radius the phase space density profiles for CDM halos follow a power law $\rho/\sigma^3 \equiv r^\alpha$ with $\alpha \sim -1.9$. In Fig. 4.4 it is shown that the PSD is constant up to a value of $\approx 6.5$ kpc, and is fitted well with the above power law for larger radii. Thus, the break in the PSD profile corresponds exactly to the break in the density

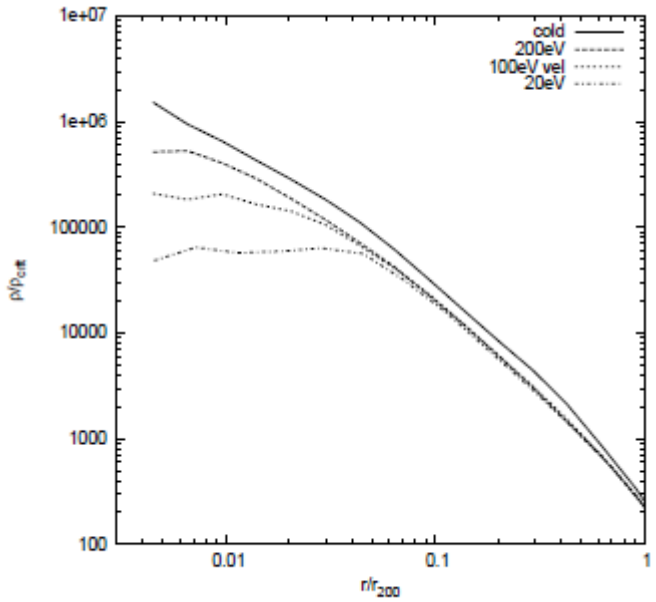


Figure 4.3: The spherically averaged density profiles for CDM, WDM1, WDM2 & WDM3 halos. The resolution limit is at approximately 0.5% of the virial radius (the softening radii are 0.26% of the virial radius).

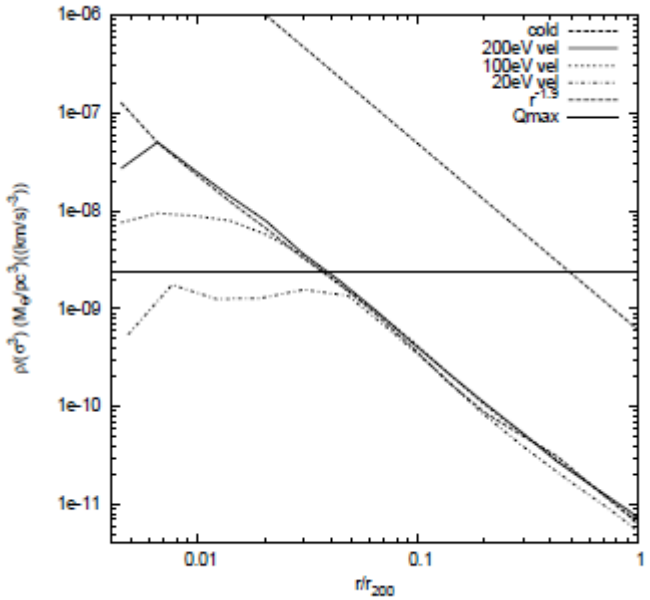


Figure 4.4: Phase-space density (PSD) profiles of the same halos, calculated using $\rho/\sigma^3$. The horizontal line represents the theoretical maximum phase space density. The $r^{-1.9}$ power law fits well the outer slope of the phase space density profile.

profile. The absolute value of the central PSD for this halo is extremely close to that imposed by the initial conditions (the horizontal line in Fig. 4.4).

If we consider the core radius to be the radius where the density starts decreasing from the constant value, a 'by eye' fit gives a radius of 6.5 kpc. If we define the core as the radius at which the density drops by a factor of 2, as in the spherical collapse model (Hogan & Dalcanton 2000), we find a value of 9.4 kpc, in good agreement with the theoretical prediction which gives a value of 9.3 kpc.

The same analysis has been performed for the high resolution halo studied in the previous section. This halo is about one order of magnitude more massive than the ones analyzed before and it has a high resolution 18 million particles in the $r_{200}$. It has been simulated with both velocities consistent with the cutoff in the power spectrum and without velocities, which allows for a quantitative study of how the thermal velocities influence the core and the phase space density profile.

In Fig. 4.5 the density profiles are plotted for this halo in both cases, with and without the thermal velocities. The phase space density is plotted in Fig. 4.6.

One can see that the density profile is shallower in the simulation with velocities. For the phase space density plot, it is obvious that the presence of velocities is making the phase space density have an almost flat behavior towards the center, as expected. It is true that the innermost part of the profile that displays a slight decrease in the PSD is competing with the resolution limit for this simulation, but is nevertheless evident that the contribution of thermal velocities is not negligible.

At this point it is safe to say that the core-like profiles are a consequence of the maximum constant phase space density given by the velocity dispersion, and not of the suppression of small scale power given by the cutoff in the power spectrum, although the latter can soften the abrupt cuspy behavior of cold dark matter density profiles.

In Macciò et al. (2012) (Section 4.5) we show the analysis of a different set of simulations, starting with a cutoff in the power spectrum corresponding to a 2 keV particle and with 'inflated' velocities corresponding to 0.5, 0.2, 0.1 and 0.05 keV respectively. Although all warm dark matter density profiles show a central density lower than the cold dark matter profile, for the 100 eV case, this becomes more pronounced and for the 50 eV case the profile shows a conspicuous core (Fig. 2, Section 4.5). The density profiles for this halo are plotted with redshift and one can see that the core does not evolve much after redshift z=1.6, even though the density increases by more than two orders of magnitude; the profile changes only in the outer part, at radii $r > 50$ kpc (Fig.3, Section 4.5). It is interesting to see that at redshift z=1.6 the profile is almost constant for a much larger radius than at redshift zero, with only a shallow decrease in the outer part.

Plotting the phase space density evolution with time, one can see that after z=1.6 it is decreasing within a factor of 2 from the maximum theoretical value.

For velocities corresponding to masses above 0.3 keV the values for the core size are below the softening of the simulation, meaning below 300 pc; for higher velocity dispersions we get larger

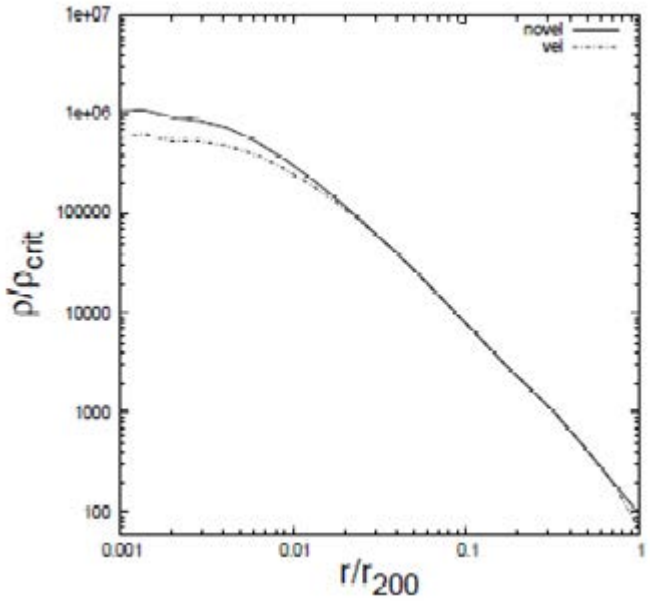


Figure 4.5: Density profiles for a refined halo with 0.36 km/s velocities, corresponding to the same cutoff in the power spectrum (200 eV in Bode et al. (2001)) and without the velocities

cores - several kpc for particles of few tens of eV (Macciò et al. (2012) Erratum Fig.1, Section 4.5).

Similar to our studies, Shao et al. (2013) performed high resolution simulations for 2 keV and 0.03 keV particles in 5 Mpc $h^{-1}$ boxes. Analyzing halos from $2.1 \times 10^{11} h^{-1}$ $M_\odot$ to $1.5 \times 10^{12} h^{-1}$ $M_\odot$, they found that the computed 6 dimensional phase space density of simulated halos is close to the theoretical fine-grained upper bound, while the $Q \sim \rho/\sigma^3$ approximation overestimates the maximum phase space density by up to an order of magnitude. To explain the cores of the dwarf spheroidal satellites of the Milky Way, their model (Shao et al. 2013) estimates a value of 0.5 keV for the mass of the WDM particle, assuming the cores are just the consequence of the particle's free streaming.

To briefly conclude these studies, our findings are summarized below:

- The finite initial fine grained PSD, which sets a maximum of the coarse grained PSD, results in PSD profiles of WDM halos that are similar to CDM halos in the outer regions, but which turn over to a constant value set by the initial conditions, in the inner regions. This is in agreement with previous studies based on simulations (Colín et al. 2008) and theoretical arguments (Villaescusa-Navarro & Dalal 2011).

- The turn over in PSD results in a constant density core with characteristic size that is in agreement with the simplest expectations.

- Finally, for such a warm candidate with velocities high enough as to produce large cores, the free streaming would erase all perturbations on that scale so that the halos would not be able

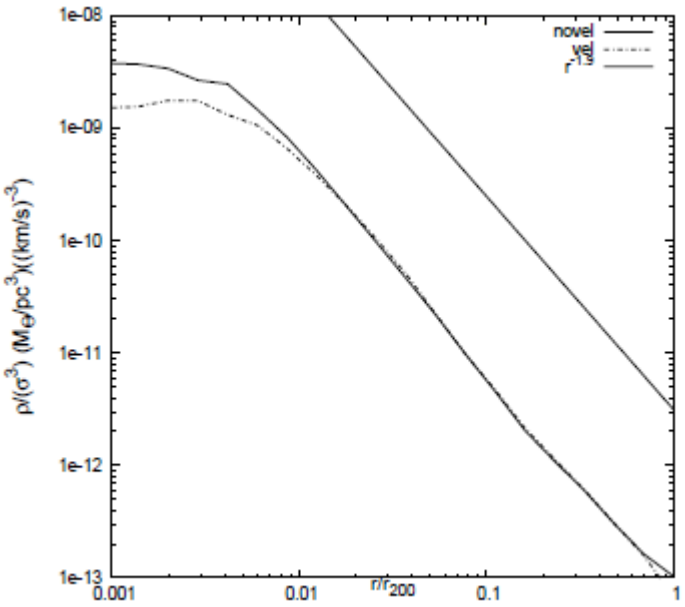


Figure 4.6: Phase space density profiles of the halo with 0.36 km/s velocities, corresponding to the same cutoff in the power spectrum (200 eV in Bode et al. (2001)) and without the velocities

to form in the first place. We called this the 'Catch 22' problem.

- To produce a significant core in a dwarf galaxy, in the kpc scale in agreement with observations (Walker & Penarrubia 2011; Amorisco & Evans 2012; Jardel & Gebhard 2012), one needs primordial velocities corresponding to thermal particles with a mass below 0.1 keV, excluded by independent constraints on large scales (Lyman-$\alpha$ and lensing).

### 4.3.2 'Real' cores - dwarfs and baryons

The results presented in the former section are in agreement with previous studies. Indeed, Strigari et al. (2006) used measurements of the stellar velocity dispersion profile of the Fornax dwarf spheroidal galaxy to constrain the dark matter distribution. While the distribution of the globular clusters inside Fornax may be explained by a large core of $\sim 1.5$ kpc, this is inconsistent with expectations from cold dark matter models as well as plausible warm dark matter ones, i.e. with particles within the limits given by Lyman-$\alpha$ constraints. They give the constraints on the core radius from the central phase space density and the maximum circular velocity derived from the velocity dispersion profile, Fig. 4.7 (Strigari et al. 2006), concluding that the dark matter alone cannot be responsible for the observed distribution of globular clusters in the center of Fornax.

Dwarf galaxies are indeed the best observational candidates for testing different dark matter models, since they are dark matter dominated. The structure and kinematics constraints of Milky Way's dwarf spheroidal satellites may have important implications on the cosmology and the nature of dark matter particles (see Walker (2013) for a review). The dwarf spheroidal satellites in

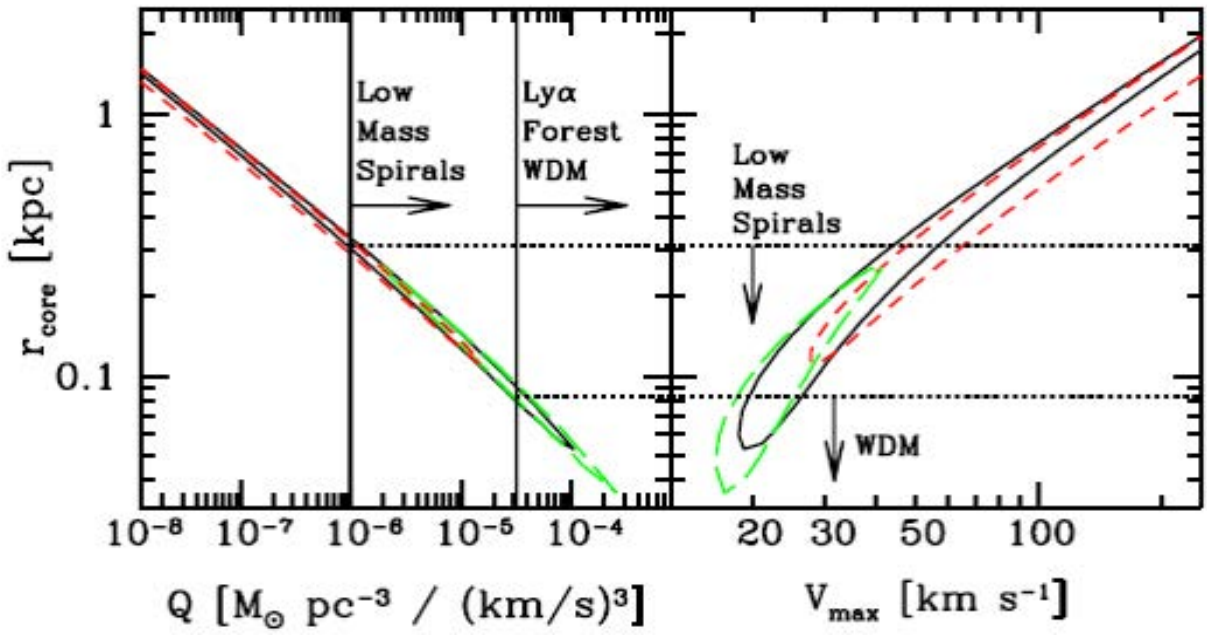


Figure 4.7: Constraints on the core radius of Fornax as a function of the central phase space density (left) and maximum circular velocity derived from the velocity dispersion profile (right) from Strigari et al. (2006)

Milky Way have masses between $10^5$ and $10^7$ $M_\odot$ and are dominated by dark matter at all radii (Walker 2013). Dark matter alone, however, is not able to explain the indication of large constant cores of few hundred pc in Fornax, Sculptor and Ursa Minor.

Several models have been proposed to solve this discrepancy. Using dynamical considerations, several studies argue that the transfer of energy and angular momentum from massive infalling objects, such as black holes, can explain the central density in dwarfs (Sánchez-Salcedo, Reyes-Iturbide & Hernandez 2006; Goerdt et al. 2006, 2010; Cole, Dehnen & Wilkinson 2011). The dynamical coupling of the dark matter to baryonic outflows has also been explored as a possible solution (Read & Gilmore 2005; Mashchenko, Couchman & Wadsley 2006; Mashchenko, Wadsley & Couchman 2008; de Souza et al. 2011). Some of these assumptions are not able to explain some of the other properties of dwarf spheroidals, like luminosity functions, star formation history, etc. (Sawala et al. 2010; Walker & Penarrubia 2011; Parry et al. 2012).

Even though in dwarf galaxies the baryonic content is poor compared to the dark matter content, baryonic processes in general are expected to play a very important role in the galaxy formation and evolution, their effect being dominant in the inner regions of all galaxies. From the panoply of baryonic processes that take place in the universe, several are believed to explain the observed central structure of galaxies and attempts have been made to incorporate them in hydrodynamic simulations:

- Gas radiative cooling will make the gas fall towards the center of the dark matter halo due to the loss of pressure support, making the center denser (Scannapieco et al. 2005, 2006).

- Molecular hydrogen cooling of the gas is crucial for the formation of stars and galaxies (Abel, Bryan, & Norman 2002; Bromm, Coppi & Larson 2009).
- Star formation feedback may explain the cores in dwarf galaxies (Oñorbe et al. 2015) and it is also important for the formation of late-type galaxies (e.g. Okamoto et al. 2005; Scannapieco et al. 2008; Sales et al. 2010; Guedes et al. 2011).
- Supernovae feedback - repetitive outflows from supernova feedback may induce the formation of a core overcoming the adiabatic contraction of the halo (Macciò et al. 2012).
- AGN feedback heats the gas with a much higher energy than the one available from supernova feedback (Matteo, Springel & Hernquist 2005).

Simulations that have incorporated some of these processes have come to different conclusions, sometimes contradictory, as shown in Marinacci, Pakmor & Springel (2014). The ones that claim to solve one problem, like the cored profiles, fail to solve the missing satellite problem, or give unrealistic structure formation predictions. Since the real physical processes are happening on scales below the resolution limit of galaxy simulations, the implementation of these processes is done 'by hand' (Benson 2010) using semi-analytic approaches. Hence, the results are strongly dependent on the fine-tuning of the parameters and the resolution (e.g. Governato et al. 2007; Kaufmann et al. 2007). For example, in contradiction with other previous claims, Marinacci, Pakmor & Springel (2014) find that even when including repeated baryonic outflows, and regardless of the resolution, large cored galaxies are not present in their simulations.

Apart from the attempts made to correlate the observed cores with baryonic processes using hydrodynamic simulations, recently it has been shown (Destri, de Vega & Sanchez 2012) that modeling the quantum pressure of fermionic particles (Weinberg 1962; Muccione & Pfenniger 2006) the expected cores in dwarf galaxies can be reproduced. Applying the Thomas-Fermi semiclassical approach to fermionic WDM, Destri, de Vega & Sanchez (2012) found that the mass, halo radius, phase-space density and velocity dispersion are fully consistent with observations of compact dwarf galaxies for a particle in the 1-2 keV range. This would suggest that dwarf galaxies are 'natural quantum objects for WDM' (Destri, de Vega & Sanchez 2012), hinting towards the fact that dark matter may not be as simple as simulated.

## 4.4 Conclusions and prospects

We have performed several suites of simulations using different codes, different cosmological parameters, different simulation parameters and different resolutions for different types of particles. From these simulations we have analyzed the internal structure of different halos.

One of the first observations is that halos display caustics and shells, very obvious in the high resolution simulations of warm dark matter particles (Paduroiu et al. in de Vega & Sanchez (2011);

de Vega, Falvella & Sanchez (2012); Paduroiu et al. (2015)). These caustics and shells may have important implications for detection, giving an enhancement in the annihilation signal, as well as for the structure formation, when baryonic physics is considered.

Furthermore, when looking at the density profiles of warm dark matter halos in the simulations for which we have the resolution to study the inner part, we find shallower profiles than in the case of cold dark matter halos. Even if in order to solve a core that is well above the resolution limit one needs a hotter, less favored particle, we can conjecture that warm dark matter in general combined with baryonic physics will result in a larger core than in the corresponding cold dark matter case. Although these simulations may not require the extreme and sometimes unrealistic recipes for structure formation (strong feedback, high star formation rate), they do require higher resolution, since in warm dark matter, particles travel larger distances.

The inclusion of quantum effects may prove paramount in accurately describing the effects of warm dark matter particles on the inner part of structures.

From our studies, we have seen that the phase space density is dictating the size of the core, meaning that the thermal velocity dispersion, which is very often neglected in simulations, is crucial for any reasonable comparison between the internal structure of simulated halos and that of the observed galaxies.

As we have seen in the previous section, halos may form in several ways in WDM simulations. The different formation mechanisms may influence the phase space density profiles, therefore comparisons between high resolution simulated halos in different scenarios is an interesting test.

Since dwarf spheroidals are the best testing bed for any dark matter models, careful analysis of similar halos in warm dark matter simulations will be needed. This has been, however, posing some problems since in warm dark matter simulations these small objects are formed on scales affected by the artificial fragmentation. Notwithstanding this difficulty, seeing that there are small halos genuinely forming top-down in warm dark matter simulations, these studies are not impossible to achieve.

Monthly Notices of the ROYAL ASTRONOMICAL SOCIETY

Mon. Not. R. Astron. Soc. **424,** 1105–1112 (2012) doi:10.1111/j.1365-2966.2012.21284.x

# Cores in warm dark matter haloes: a Catch 22 problem

Andrea V. Macciò,[1⋆] Sinziana Paduroiu,[2] Donnino Anderhalden,[3] Aurel Schneider[3] and Ben Moore[3]

[1]*Max-Planck-Institute for Astronomy, Königstuhl 17, D-69117 Heidelberg, Germany*
[2]*Geneva Observatory, University of Geneva, CH-1290 Sauverny, Switzerland*
[3]*Institute for Theoretical Physics, University of Zürich, CH-8057 Zürich, Switzerland*

Accepted 2012 May 10. Received 2012 April 24; in original form 2012 February 11

**ABSTRACT**

The free streaming of warm dark matter particles dampens the fluctuation spectrum, flattens the mass function of haloes and sets a fine-grained phase density limit for dark matter structures. The phase-space density limit is expected to imprint a constant-density core at the halo centre in contrast to what happens for cold dark matter. We explore these effects using high-resolution simulations of structure formation in different warm dark matter scenarios. We find that the size of the core we obtain in simulated haloes is in good agreement with theoretical expectations based on Liouville's theorem. However, our simulations show that in order to create a significant core ($r_c \sim 1$ kpc) in a dwarf galaxy ($M \sim 10^{10}$ M$_\odot$), a thermal candidate with mass as low as 0.1 keV is required. This would fully prevent the formation of the dwarf galaxy in the first place. For candidates satisfying large-scale structure constraints ($m_\nu$ larger than ≈1–2 keV), the expected size of the core is of the order of 10 (20) pc for a dark matter halo with a mass of $10^{10}$ ($10^8$) M$_\odot$. We conclude that 'standard' warm dark matter is not a viable solution for explaining the presence of cored density profiles in low-mass galaxies.

**Key words:** galaxies: haloes – dark matter.

## 1 INTRODUCTION

The formation of structure in the universe is driven by the mysterious dark matter component whose nature is still unknown. Over the last decades, the hierarchical cold dark matter (CDM) model has become the standard description for the formation of cosmic structures. It is in excellent agreement with recent observations, such as measurements of the cosmic microwave background and large-scale surveys (Tegmark et al. 2006; Komatsu et al. 2011). However, there are a number of inconsistencies on subgalactic scales that arise within the CDM scenario. First, the amount of substructure in Milky Way (MW) sized haloes is overpredicted by roughly one order of magnitude (Klypin et al. 1999; Moore et al. 1999). Secondly, the central densities of CDM haloes in simulations show a cuspy behaviour (Flores & Primack 1994; Moore 1994; Diemand et al. 2005; Macciò et al. 2007; Springel et al. 2008), whereas the density profiles inferred from galaxy rotation curves point to a core-like structure (e.g. Kuzio de Naray, McGaugh & Mihos 1999; de Blok et al. 2001; Oh et al. 2011). Furthermore, recent studies (Tikhonov et al. 2009; Zavala et al. 2009; Peebles & Nusser 2010) re-emphasized that also the population of dwarf galaxies within voids is in strong contradiction with CDM predictions.

One possible solution to these issues is that the dark matter particle is a thermal relic with a mass of the order of 1 keV. The most prominent representatives of such warm dark matter (WDM) candidates are the sterile neutrino and the gravitino (Abazajian & Koushiappas 2006; Boyarsky, Ruchayskiy & Shaposhnikov 2009a), whose presence is also motivated by particle theory (e.g. Dodelson & Widrow 1994; Takayama & Yamaguchi 2000; Buchmüller et al. 2007).

Non-zero thermal velocities for WDM particles lead to a strong suppression of the linear matter power spectrum on galactic and subgalactic scales (Bond, Efstathiou & Silk 1980; Pagels & Primack 1982; Dodelson & Widrow 1994; Hogan & Dalcanton 2000; Zentner & Bullock 2003; Viel et al. 2005; Abazajian 2006), and erase all primordial density perturbations smaller than their free-streaming scale $\lambda_{fs}$. Below this scale no structure is expected to form, at least not in the usual bottom-up scenario. However, the effective suppression of halo formation already happens well above $\lambda_{fs}$ and is entirely described by the WDM particle mass (see Smith & Markovic 2011, and references therein).

Recent observational constraints coming from X-ray background measurements and Ly$\alpha$ forest analysis set the allowed mass interval

⋆E-mail: maccio@mpia.de

roughly between 2 and 50 keV (e.g. Viel et al. 2005; Abazajian & Koushiappas 2006; Seljak et al. 2006; Boyarsky et al. 2009b; Boyarsky, Ruchayskiy & Iakubovskyi 2009c).[1] As a complementary study, Macciò & Fontanot (2010, see also Polisensky & Ricotti 2011) compared the subhalo abundance of an MW-like object in different numerical WDM realizations with observed satellite galaxies reported by the Sloan Digital Sky Survey data and set a lower bound for a thermalized particle of $m_{\rm WDM} \gtrsim 2$ keV.

Another important characteristic of a WDM scenario is the possibility to *naturally* obtain cored matter density profiles. According to Liouville's theorem for collisionless systems, the fine-grained phase-space density of the cosmic fluid stays constant through cosmic history. In WDM the dark matter fluid is described by a Fermi–Dirac distribution, whose absolute value is fixed at the time of decoupling when the fluid becomes collisionless. Structure formation then happens through a complex process of distortion and folding of the phase-space sheet. Since it is not possible to measure this fine-grained phase-space density in simulations, one usually defines a coarse-grained or pseudo-phase-space density (e.g. Taylor & Navarro 2001)

$$Q \equiv \frac{\rho}{\sigma^3}, \tag{1}$$

where $\rho$ is the mean density and $\sigma$ is the one-dimensional velocity dispersion within some small patch of the simulation.[2] The quantity $Q$ corresponds to an average density of a small (but not microscopic) phase-space volume and is not constant anymore. However, because of the way the phase-space sheet is distorted, the value of $Q$ in most of the cases can only decrease during structure formation and will not exceed its initial value set at decoupling (Dalcanton & Hogan 2001, see however Boyarsky et al. 2009c for a thorough discussion of the meaning of $Q$ and its evolution with time).

This upper limit for $Q$ also holds for the local pseudo-phase-space density within virialized haloes at redshift 0 and has a direct consequence on the density profile in real space. Since the velocity dispersion does not grow in the inner part of a halo, the real-space density profile must become constant with a core size depending on the specific WDM model (Tremaine & Gunn 1979).

Due to this effect of core formation, the WDM scenario has been suggested as a solution to the long-standing core–cusp problem of dwarf galaxies. In fact, observational measurements favour cored dark matter profiles in low surface brightness galaxies within the Local Group (Kuzio de Naray & Kaufmann 2011; Salucci et al. 2012). However, previous theoretical/analytical studies (e.g. de Vega, Salucci & Sanchez 2010) argue that the cores produced by WDM might be too small to explain the observations. For example, Bode, Ostriker & Turok (2001) argued that the principal effect of the thermal motion in the WDM scenario is to give the particle angular momentum, producing a centrifugal barrier keeping the particle away from $r = 0$; only for radii inside this barrier is the structure of the halo significantly altered with respect to a pure CDM halo. Assuming a flat rotation curve for the halo and spherical collapse, they estimated that for warm particles with masses larger than 1 keV, thermal velocities are not able to modify the structure of haloes on scales of a kiloparsec or above.

More recently, Villaescusa-Navarro & Dalal (2011) have employed the spherical collapse model to study the formation of haloes in WDM cosmologies. They found that the core sizes, for allowed WDM temperatures ($\sim$1 keV), are typically very small, of the order of $10^{-3}$ of the halo virial radius at the time of formation, and considerably smaller following formation. They concluded that for realistic WDM models the core radii of haloes observed at $z = 0$ are generically expected to be far smaller than the core sizes measured in local low surface brightness galaxies. One of the aims of our work is to test these previous analytical results using self-consistent cosmological $N$-body simulations of halo formation in a WDM universe.

Numerical $N$-body simulations have been used to better understand the properties of virialized objects in the WDM scenarios (e.g. Bode et al. 2001; Knebe et al. 2003; Wang & White 2007; Tikhonov et al. 2009; Zavala et al. 2009; Schneider et al. 2011). High-resolution simulations of single objects have studied the suppression of the galactic satellite formation due to free streaming (e.g. Colín, Avila-Reese & Valenzuela 2000; Götz & Sommer-Larsen 2002; Knebe et al. 2008; Macciò & Fontanot 2010), in order to reconcile the observed dwarf galaxy abundance with the prediction from dark matter based theories. More recently, Colín, Valenzuela & Avila-Reese (2008) used $N$-body simulations to study the effects of primordial (thermal) velocities on the inner structure of dark matter haloes, with particular attention on the formation of a possible central density core. They used thermal velocities of the order of 0.1 and 0.3 km s$^{-1}$, without linking them to any particular WDM model, since the aim of their work was to explore the general effect of relic velocities of the dark matter structure. Unfortunately, their combination of resolution and choice for relic velocities was not sufficient to directly test simulation results against core radii predicted by phase-space constraints.

In this work, we want to extend and improve on these previous studies. We will use high-resolution $N$-body simulations to explore the sizes of density cores in WDM and their dependence on the WDM candidate mass.[3] We will explore several models for WDM ranging from 2 to 0.05 keV. We will consider separately the effects of a WDM candidate on the power spectrum and on the relic velocities, trying to disentangle the various consequences of these two different components. Our higher numerical resolution will allow us to directly see the formation of a density core, with a size well above the numerical resolution for the warmer candidates. We will then revise the theoretical arguments for the formation of cored profiles in WDM and perform a direct comparison between the core sizes in our simulations and the ones predicted from phase-space constraints.

This paper is structured as follows. In Section 2, we discuss the set-up of our simulations and the way we implement thermal velocities. Section 3 is dedicated to the presentation of our results in terms of the phase-space limit and its influence on the density

[1] In some of these analyses, the WDM particle is assumed to be a resonantly produced sterile neutrino (Shi & Fuller 1999). We have converted these mass limits into limits for a fully thermalized particle, such as the gravitino, using the formula provided by Viel et al. (2005).

[2] In the context of a non-singular isothermal sphere, the quantity $Q$ is directly proportional to the maximum phase-space density and can be described, as in Tremaine & Gunn (1979), as giving the maximum coarse-grained phase-space density. In a more general context, applicable to simulations, the velocity distribution of the particles is not Maxwellian and hence $Q$ does not really trace the coarse-grained phase-space density and hence we will refer to it as *a pseudo-phase-space density*.

[3] In the present work, we only considered a very simple WDM model; it is worth commenting that there are more complex and physically motivated models discussed in the literature (e.g. warm+cold dark matter: Boyarsky et al. 2009d; Macciò et al. 2012b; or composite dark matter: Khlopov 2006; Khlopov & Kouvaris 2008).

profile of dark matter haloes. A conclusion and summary of our work is finally given in Section 3.

## 2 SIMULATIONS

Numerical simulations have been carried out using PKDGRAV, a treecode written by Joachim Stadel and Thomas Quinn (Stadel 2001). The initial conditions are generated with the GRAFIC2 package (Bertschinger 2001). All simulations start at redshift $z_i = 99$ in order to ensure a proper treatment of the non-linear growth of cosmic structures.

The cosmological parameters are set as follows: $\Omega_\Lambda = 0.727$, $\Omega_m = 0.273$, $\Omega_b = 0.044$, $h = 0.7$ and $\sigma_8 = 0.8$, and are in good agreement with the recent *Wilkinson Microwave Anisotropy Probe* mission results (Komatsu et al. 2011).

We start by running large-scale simulations of a cosmological cube of side 40 Mpc, using $2 \times 256^3$ dark matter particles. This was done for two different models: a standard LCDM and a WDM model with a warm candidate of mass 2 keV produced in thermal equilibrium.

To compute the transfer function for WDM models, we used the fitting formula suggested by Bode et al. (2001):

$$T^2(k) = \frac{P^{\rm WDM}}{P^{\rm CDM}} = [1 + (\alpha k)^{2\nu}]^{-10/\nu}, \quad (2)$$

where $\alpha$, the scale of the break, is a function of the WDM parameters, while the index $\nu$ is fixed. Viel et al. (2005) (see also Hansen et al. 2002), using a Boltzmann code simulation, found that $\nu = 1.12$ is the best fit for $k < 5\,h\,{\rm Mpc}^{-1}$, and they obtained the following expression for $\alpha$:

$$\alpha = 0.049 \left(\frac{m_x}{1\,{\rm keV}}\right)^{-1.11} \left(\frac{\Omega_\nu}{0.25}\right)^{0.11} \left(\frac{h}{0.7}\right)^{1.22} h^{-1}\,{\rm Mpc}. \quad (3)$$

We used the expression given in equation (3) for the damping of the power spectrum for simplicity and generality. More accurate expressions for the damping of sterile neutrinos exist (e.g. Abazajian 2006) and show that the damping depends on the detailed physics of the early universe in a rather non-trivial way. The initial conditions for the two simulations have been created using the same random phases, in order to facilitate the comparison between the different realizations.

We then select one candidate halo with a mass similar to that of our Galaxy ($M \sim 10^{12}\,{\rm M}_\odot$) and resimulated it at higher resolution. These high-resolution runs are $8^3$ times more resolved in mass than the initial ones: the dark matter particle mass is $m_p = 1.38 \times 10^5\,{\rm M}_\odot$, where each dark matter particle has a spline gravitation softening of 355 pc. This single halo has been resimulated in several different models; all simulations are summarized in Table 1 and three of the simulations are shown in Fig. 1.

**Table 1.** Simulation parameters.

| Label | $m_\nu$ (keV) | $m_{\nu,\rm vel}$ (keV) | $v_0(z=0)$ (km s$^{-1}$) | $N_{\rm vir}$ ($\times 10^6$) | $M_{\rm vir}$ ($\times\ 10^{12}\,{\rm M}_\odot$) |
|---|---|---|---|---|---|
| CDM | $\infty$ | – | – | 10.2 | 1.42 |
| WDM1 | 2.0 | 2.0 | $4.8 \times 10^{-3}$ | 8.6 | 1.22 |
| WDM2 | 2.0 | 0.5 | $3.1 \times 10^{-2}$ | 8.4 | 1.20 |
| WDM3 | 2.0 | 0.2 | 0.1 | 8.5 | 1.21 |
| WDM4 | 2.0 | 0.1 | 0.26 | 6.7 | 0.93 |
| WDM5 | 2.0 | 0.05 | 0.66 | 4.9 | 0.71 |

### 2.1 Streaming velocities

Particles that decouple whilst being relativistic are expected to retain a thermal velocity component. This velocity can be computed as a function of the WDM candidate mass ($m_\nu$) according to the following expression (Bode et al. 2001):

$$\frac{v_0(z)}{1+z} = 0.012 \left(\frac{\Omega_\nu}{0.3}\right)^{1/3} \left(\frac{h}{0.65}\right)^{2/3} \left(\frac{1.5}{g_x}\right)^{1/3} \left(\frac{\rm keV}{m_\nu}\right)^{4/3} {\rm km\,s^{-1}}, \quad (4)$$

where $z$ is the redshift. The distribution function is given by the Fermi–Dirac expression until the gravitational clustering begins (Bode et al. 2001).

This formalism is correct for the 'real' dark matter elementary particles (e.g. a sterile neutrino). In the *N*-body approach, we use macro particles (with masses of the order of $10^5\,{\rm M}_\odot$) to describe the density field. These macro particles effectively model a very large number of micro particles. Given that the velocities described in equation (4) have a random direction, the total velocity of the macro (*N*-body) particles should effectively be zero. Hence, it is not fully correct to directly use equation (4) to assign 'thermal' velocities to simulation particles.

On the other hand, the net effect of the thermal velocities is to create a finite upper limit in the phase-space distribution (PSD) due to their initial velocity dispersion ($\sigma$). What we are interested in is to recreate the same PSD limit in our simulation, and then study its effects on the dark matter halo density distribution. In order to achieve this goal, we proceed in the following way. From equation (4), we compute the rms velocity: $\sigma(z) = 3.571 v_0(z)$; we then create a Gaussian distribution centred on zero and with the same rms $\sigma$. Finally, we randomly generate particle velocities from this distribution and assign them to our macro particles. It is worth mentioning that the final results are almost independent of the assumed distribution for the velocities (Fermi–Dirac, Maxwellian, etc.), while they strongly depend on the strength of the velocity field (i.e. $v_0$).

In principle, adding random velocities introduces spurious momentum fluctuations into the initial conditions. For very light particles ($m_\nu \sim 1$ eV), this effect could be important and it could be balanced by introducing particles with opposite momenta (e.g. Gardini, Bonometto & Murante 1999). On the other hand, for the choices of WDM candidate masses in our paper, thermal velocities are quite modest ($\lesssim 0.5$ km s$^{-1}$) and lower than the Zeldovich ones. Hence, no artificial effects are expected.

As detailed in Section 3.1, there is a direct connection between $m_\nu$ and the expected size of the dark matter distribution core. This core is only due to the presence of thermal velocities and not, in the first approximation, to the cut in the power spectrum described by equation (2). Cutting the power spectrum changes the merger history of the dark matter halo but does not affect the density profile significantly (Moore et al. 1999). This implies that in order to study the effect of different values of $m_\nu$ (and hence $v_0$) it is sufficient to '*play*' with equation (4) leaving all other simulation parameters unaltered. Following this approach, we have generated several simulations using the same cut in the power spectrum ($m_\nu$) but different initial thermal velocities ($m_{\nu,\rm vel}$), as detailed in Table 1.

## 3 RESULTS

Density profiles for the CDM run and the five WDM realizations (WDM1–5) are shown in Fig. 2. The profiles show a monotonic decrease of the central density as a function of the temperature of

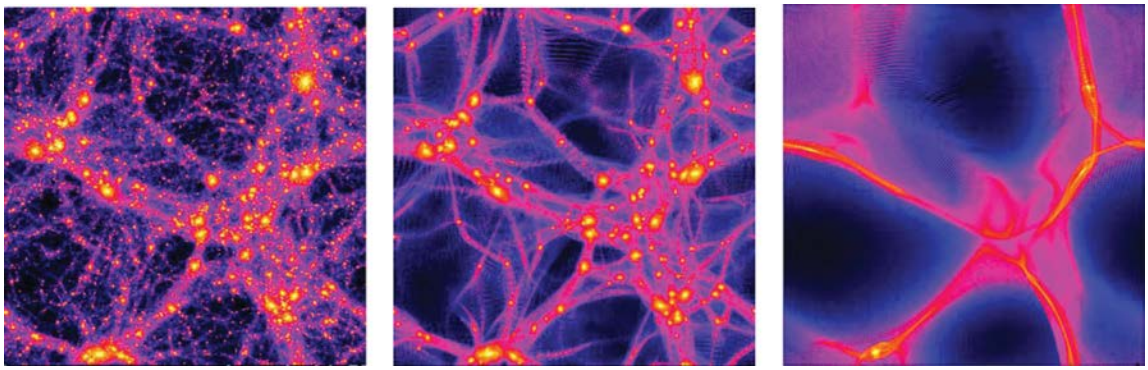

**Figure 1.** Density map of the large-scale (low-resolution) simulations ($L = 40$ Mpc) at redshift 0. From left to right: CDM, and two WDM with a cut in the power spectrum for a mass ($m_\nu$) of 0.2 and 0.05 keV, respectively. The last two simulations have not been used in this paper and are presented only for illustration purposes, see Section 2.1 for more information.

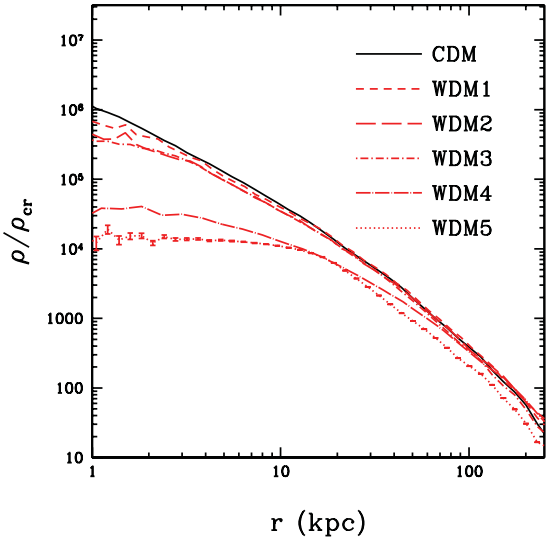


**Figure 2.** The spherically averaged density profiles for CDM, WDM1–5 haloes.

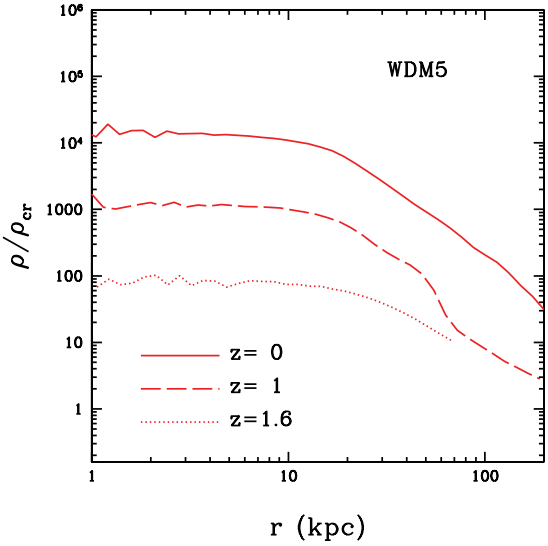


**Figure 3.** Time evolution of the density profiles for the WDM5 halo.

the dark matter candidate. Cold candidates show the usual cuspy behaviour (e.g. Dubinski & Carlberg 1991), while warmer candidates present a lower central density that becomes a clear core for $m_{\nu,\mathrm{vel}} = 0.05$ keV, with a size of several kpc.

Fig. 3 shows the time evolution of the density profile in the WDM5 simulation. The profile is already cored at a high redshift of $z = 1.6$, and the size of the core does not evolve substantially until $z = 0$. The profile only changes at large radii ($r > 50$ kpc) as a consequence of the assembly of the external part of the halo. This smooth mass accretion is also a consequence of the quiet merging history of the halo that does not undergo any merger with a mass ratio larger than 10 after $z = 2$. The assembly of the external part of the halo is consistent with a typical CDM halo in the outer regions.

As already mentioned, the theoretical explanation for the formation of a core is related to the presence of a maximum in the phase-space density distribution. This maximum is clearly visible in Fig. 4, where we plot the pseudo-phase-space density $Q \equiv \rho/\sigma^3$ for three different models, namely CDM, WDM3 and WDM5. For this latter model, the $Q$ shows a large core that extends about 10 kpc. The WDM3 model also shows a strong flattening of the $Q$ profile, consistent with a core distribution. On the other hand, the CDM pseudo-phase-space distribution is well fitted by a single power-law profile on the whole range, in agreement with previous results (Taylor & Navarro 2001; Schmidt, Hansen & Macciò 2008).

Fig. 5 shows the time evolution of the pseudo-PSD for our warmest candidate (i.e. thermal velocities for a 0.05-keV mass particle). The solid (blue) line shows the $Q$ radial profile in the initial conditions ($z = 99$). This value has been calculated using only high-resolution particles that end up within 1.5 times the virial radius of the halo at $z = 0$. The other (red) lines represent the pseudo-PSD profile at different redshifts (from 1.6 to 0) and have been computed using all particles within the virial radius of the halo. All quantities in the plot are in physical units. The phase-space distribution shows very weak evolution with almost no evolution at all from $z = 99$ to 1.6. In the same plot, we also show the theoretical maximum

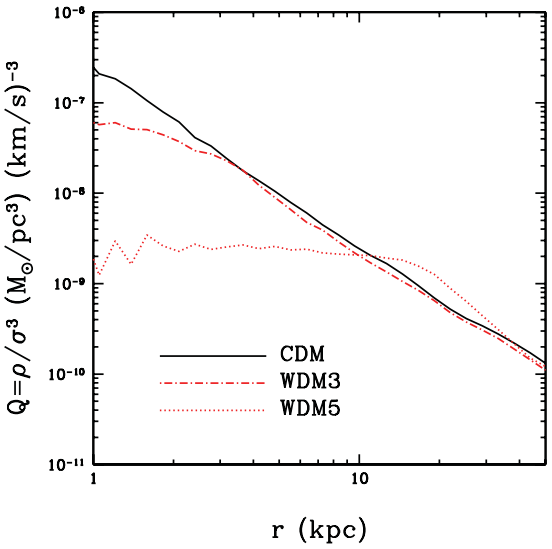


**Figure 4.** Phase-space density profile for the CDM, WDM3 and WDM5 models at $z = 0$.

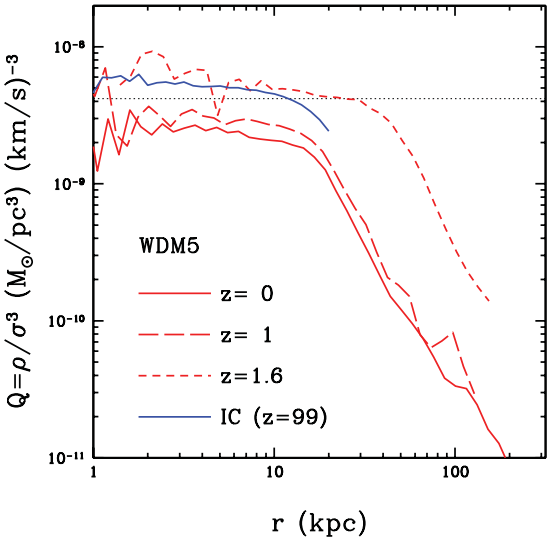


**Figure 5.** Time evolution of the pseudo-PSD radial profile for the WDM5 model. The black dotted line represents the theoretical prediction for the maximum value of $Q$ according to equation (7).

phase-space density achievable by this model (see equation 7 for a rigorous definition of $Q_{\rm max}$).

The dotted (black) lines show predictions for $Q_{\rm max}$ for the *local* value of the matter density, which we measured directly from the simulation initial conditions using dark matter particles in the high-resolution region within a volume of $\approx$1 Mpc$^3$. The local density

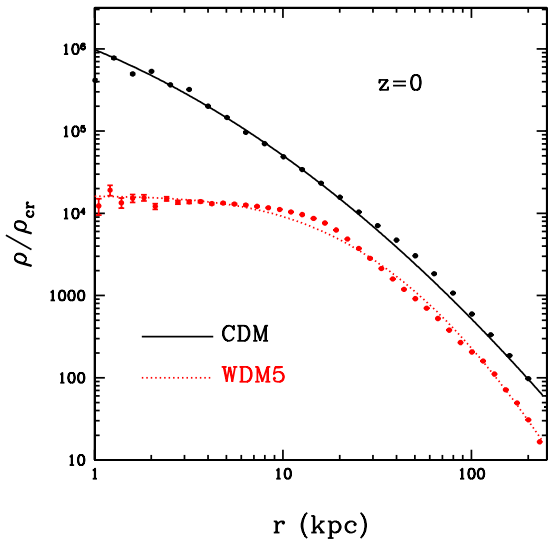


**Figure 6.** Density profiles for CDM and WDM5 and their fit using equation (5).

value turned out to be $\langle\rho\rangle_{\rm local} = 0.31\rho_{\rm cr}$.[4] The theoretical prediction is in quite good agreement with the simulation results.

In order to quantify the flatness (and the core size) of WDM profiles, we have fitted all our density profiles with the following parametric description, originally presented in Stadel et al. (2009):

$$\rho(r) = \rho_0 \exp(-\lambda[\ln(1 + r/R_\lambda)]^2). \quad (5)$$

In this parametrization, the density profile is linear down to a scale $R_\lambda$ beyond which it approaches the central maximum density $\rho_0$ as $r \to 0$. We also note that if one makes a plot of $\mathrm{d}\ln\rho/\mathrm{d}\ln(1 + r/R_\lambda)$ versus $\ln(1 + r/R_\lambda)$ then this profile forms an exact straight line with slope $2\lambda$.

This fitting function is extremely flexible and makes possible to reproduce at the same time both cuspy profiles, like the one predicted by the CDM theory, and highly cored profiles, like in the WDM5 case (as shown in Fig. 6). The values of the parameter are obtained via a $\chi^2$ minimization procedure using the Levenberg–Marquardt method. From now on, we will use the value of the fitting parameter $R_\lambda$ as the fiducial value of the central density core in simulated profiles (hereafter $r_{\rm core,s}$). The $r_{\rm core,s}$ values for all our haloes are reported in the second column of Table 2.

### 3.1 Comparison with theoretical predictions

In Tremaine & Gunn (1979, hereafter TG79) limits on the mass of a neutrino are derived from the maximum phase-space density of a homogeneous neutrino background, with the further assumptions that neutrinos form bound structures and that their central regions can be well approximated by an isothermal sphere.

Assuming a Maxwellian velocity distribution, they obtained the maximum phase-space density:

$$Q_{\rm max} \equiv \frac{\rho}{\sigma^3} \propto m_\nu^4, \quad (6)$$

[4] This local value is slightly higher than the global one since it is computed around an object that will collapse and be fully virialized at $z = 0$.

**Table 2.** Size of density cores using different methods. See the text for a more detailed explanation.

| Label | $r_{\rm core,s}$ (kpc) | $r_{\rm core,Q}$ (kpc) | $r_{\rm core,t}$ (kpc) |
|---|---|---|---|
| CDM | <0.4 | <0.4 | $\infty$ |
| WDM1 | <0.4 | <0.4 | 0.005 |
| WDM2 | <0.4 | <0.4 | 0.075 |
| WDM3 | 0.42 | <1.1 | 0.48 |
| WDM4 | 1.63 | 1.80 | 1.91 |
| WDM5 | 4.56 | 4.85 | 6.98 |

where $m_\nu$ is the mass of the (warm) dark matter candidate. This limit has then been used in several follow-up papers to estimate the size of the density cores in WDM haloes (e.g. Dalcanton & Hogan 2001; Strigari et al. 2006).

Following TG79, we derive the theoretical expectation for the maximum pseudo-phase-space density and the size of the dark matter core for our WDM models adopting a slightly different approach. We can start from the definition of $Q$ assuming to compute the density in some local volume $L$:

$$Q_{\rm max} \equiv \frac{\rho_L}{\sigma^3} = \frac{\frac{\rho_L}{\rho_{\rm cr}} \times \rho_{\rm cr}}{\sigma^3}, \quad (7)$$

where $\rho_{\rm cr} = 2.775 \times 10^{11}\, h^2\, {\rm M}_\odot\, {\rm Mpc}^{-3}$ is the critical density of the Universe and $\rho_L/\rho_{\rm cr}$ is the local density in our volume $L$, expressed in units of the critical density.

The denominator of equation (7) could be expressed as a function of the mass of the WDM candidate using equation (4) and the fact that for a Fermi–Dirac distribution the rms velocity is $\sigma = 3.571 v_0$. Combining equation (4) with equation (7), we get the following expression for $Q_{\rm max}$:

$$Q_{\rm max} = 1.64 \times 10^{-3} \left(\frac{\rho_L}{\rho_{\rm cr}}\right) \left(\frac{m_\nu}{\rm keV}\right)^4 \frac{{\rm M}_\odot\, {\rm pc}^{-3}}{\left({\rm km\, s}^{-1}\right)^3}, \quad (8)$$

where the numerical factor in front of the expression takes into account our choices for $\Omega_{\rm m}$ and $h$. This expression is formally equivalent to the one derived by TG79.

Finally, the maximum phase-space density can be converted in a 'core' size following Hogan & Dalcanton (2000):

$$r^2_{\rm core,t} = \frac{\sqrt{3}}{4\pi G\, Q_{\rm max}} \frac{1}{\left\langle \sigma^2_{\rm halo} \right\rangle^{1/2}}, \quad (9)$$

where $\sigma_{\rm halo}$ is the velocity dispersion (i.e. the mass) of the simulated dark matter halo. Values of $r_{\rm core,t}$ for our simulated haloes are reported in the last column of Table 2.

In the following, we will compare this theoretical value of the core ($r_{\rm core,t}$) with two different core sizes that can be estimated directly from the simulations. The first one is given by the $R_\lambda$ parameter obtained by fitting the numerical density profile (as shown in Fig. 6) and we will refer to this value as $r_{\rm core,s}$. The second one is obtained by computing $Q_{\rm max}$ from the simulated density profile (as shown in Fig. 4) and then inserting this value in equation (9); we name this second parameter $r_{\rm core,Q}$.

Results for the three definitions of the core size for all our simulations are summarized in Table 2. Overall the three different estimators for the core size are in fairly good agreement. $r_{{\rm c},Q_{\rm max}}$ gives on average a larger value for the core, for the WDM4 and WDM5 runs, while for the WDM3 simulation it is only able to give an upper value, since there is not a clear indication of convergence towards a maximum value in the $Q_{\rm max}$ profile, as shown in Fig. 4.

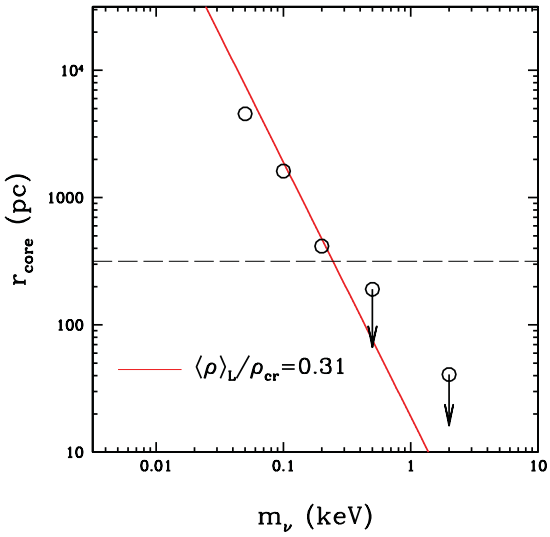


**Figure 7.** Comparison between core size in simulations (open symbols) and the theoretical expectation for an $M = 10^{12}\, {\rm M}_\odot$ halo (solid line). The dashed line is the gravitational softening of our simulations. All points below this line should be considered as upper limits on the core size.

Fig. 7 shows the comparison of the core found directly in simulations ($r_{\rm core,s}$, black symbols) with the core predicted by the above simple theoretical argument ($r_{\rm core,t}$). The solid line is obtained from equations (9) and (8), where, as discussed before, we used $\rho_L/\rho_{\rm cr} = 0.31$ as the value for the local density.

Overall numerical results for WDM3, WDM4 and WDM5 are in very good agreement with the theoretical expectations from equations (9) and (8). The WDM1 and WDM2 simulations only put upper limits on the size of the core, since the values of $R_\lambda$ we obtain from fitting the density profile fall below the simulation softening (the dashed black line in the figure).

Using our determination of the core size as a function of the WDM mass, we compute the expected value of $r_{\rm core}$ for the typical halo mass ($5 \times 10^8\, {\rm M}_\odot$; see Macciò et al. 2010) of dwarf galaxies orbiting the MW. Results are shown in Fig. 8: the grey shaded area takes into account possible different values of the local matter density in the range $\rho/\rho_{\rm cr} = 0.15-0.6$.

From the figure it is clear that a core of $\approx$1 kpc would require a WDM mass of the order of 0.1 keV, well below current observational limits from large scales.

If we assume a WDM particle mass of $m_\nu \sim 2$ keV (represented by the dashed vertical line), in agreement with several astrophysical constraints (e.g. Viel et al. 2008), the maximum core size we can expect ranges from 10 pc for a massive, MW-like halo (see also Fig. 7) to 10–40 pc for a dwarf galaxy like halo. Finally, in predicting the core size for satellite galaxies in the MW halo, the fact that satellites can lose significant mass after accreting into larger haloes due to stripping and tidal forces must also be taken into account (e.g. Penarrubia, Navarro & McConnachie 2008; Macciò et al. 2010). This implies that the halo mass we may infer today for those galaxies is only a lower limit on the mass they had before accretion, which is the one to be used (as $\sigma^2_{\rm halo}$) in equation (9).

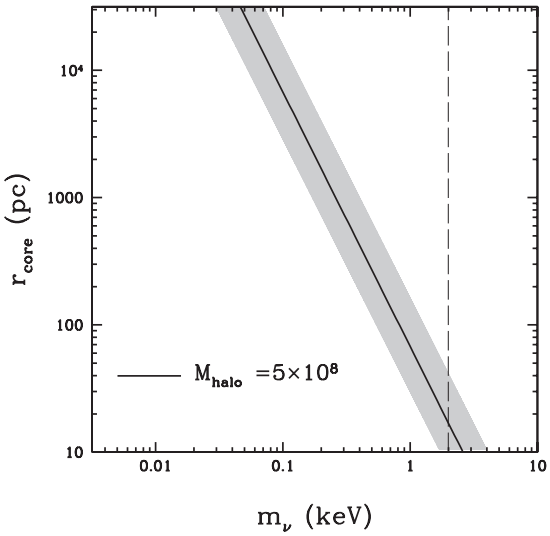


**Figure 8.** Expected core size for the typical dark matter mass of MW satellites as a function of the WDM mass $m_\nu$. The shaded area takes into account possible different values of the local density parameter $0.15 < \Omega_m < 0.6$. The vertical dashed line shows the current limits on the WDM mass from large-scale structure observations.

## 4 CONCLUSIONS

We have used high-resolution *N*-body simulations to examine the effects of free-streaming velocities on halo internal structure in WDM models. We find the following.

(i) The finite initial fine-grained phase-space density (PSD) is also a maximum of the pseudo-PSD, resulting in PSD profiles of WDM haloes that are similar to CDM haloes in the outer regions; however, they flatten towards a constant value in the inner regions. This is in agreement with previous studies based on simulations (Colín et al. 2008) and theoretical arguments (Villaescusa-Navarro & Dalal 2011).

(ii) The finite PSD limit results in a constant density core with characteristic size that is in agreement with theoretical expectations, i.e. following TG79, especially if the value of the local matter density is taken into account.

(iii) The core size we expect for thermal candidates, allowed by independent constraints on large scales (Ly$\alpha$ and lensing, $m_\nu \approx 1$–2 keV), is of the order of 10–50 pc. This is not sufficient to explain the observed cores in dwarf galaxies that are nearly of kpc scale (Walker & Penarrubia 2011; Amorisco & Evans 2012; Jardel & Gebhard 2012).

(iv) Our results show that a core around kpc scale in dwarf galaxies would require a thermal candidate with a mass below 0.1 keV, a mass value ruled out by all large-scale structure constraints (Seljak et al. 2006; Miranda & Macciò 2007; Viel et al. 2008). Moreover, with such a warm candidate, the exponential cut-off of the power spectrum would make impossible to obtain these dwarf galaxies in the first place (e.g. Macciò & Fontanot 2010).

(v) Altogether these results lead to a nice 'Catch 22' problem for WDM: *if you want a large core you won't get the galaxy, if you get the galaxy it won't have a large core*.

We conclude that the solution of the cusp/core problem in Local Group galaxies cannot completely reside in simple models (thermal candidates) of WDM. If cores are required, then it seems that baryonic feedback (e.g. Romano-Díaz et al. 2008; Governato et al. 2010; Macciò et al. 2012a) is still the most likely way to alter the density profile of dark matter and hence reconcile observations with CDM/WDM predictions.

## ACKNOWLEDGMENTS

We acknowledge stimulating discussions with George Lake, Jürg Diemand and Justin Read. We would like to thank A. Boyarsky, O. Ruchayskiy and S. Sergio Palomares-Ruiz for their help with the theory part of this work. Finally, we thank the referee of our paper, Adrian Jenkins, for several comments that improved the presentation and the clarity of our work. Numerical simulations were performed on the THEO and PanStarrs2 clusters of the Max-Planck-Institut für Astronomie at the Rechenzentrum in Garching and on the zBox3. SP would like to thank Joachim Stadel and Doug Potter for their crucial contribution to this project. AVM acknowledges funding by Sonderforschungsbereich SFB 881 'The Milky Way System' (subproject A1) of the German Research Foundation (DFG).

## REFERENCES

Abazajian K., 2006, Phys. Rev. D, 73, 063506
Abazajian K., Koushiappas S. M., 2006, Phys. Rev. D, 74, 023527
Amorisco N. C., Evans N. W., 2012, MNRAS, 419, 184
Bertschinger E., 2001, ApJS, 137, 1
Bode P., Ostriker J. P., Turok N., 2001, ApJ, 556, 93
Bond J. R., Efstathiou G., Silk J., 1980, Phys. Rev. Lett., 45, 1980
Boyarsky A., Ruchayskiy O., Shaposhnikov M., 2009a, Annu. Rev. Nucl. Part. Sci., 59, 191
Boyarsky A., Lesgourgues J., Ruchayskiy O., Viel M., 2009b, J. Cosmol. Astropart. Phys., 5, 12
Boyarsky A., Ruchayskiy O., Iakubovskyi D., 2009c, J. Cosmol. Astropart. Phys., 3, 5
Boyarsky A., Lesgourgues J., Ruchayskiy O., Viel M., 2009d, Phys. Rev. Lett., 102, 201304
Buchmüller W., Covi L., Hamaguchi K., Ibarra A., Yanagida T., 2007, J. High Energy Phys., 3, 37
Colín P., Avila Reese V., Valenzuela O., 2000, ApJ, 542, 622
Colín P., Valenzuela O., Avila Reese V., 2008, ApJ, 673, 203
Dalcanton J. J., Hogan C. J., 2001, ApJ, 561, 35
de Blok W. J. G., McGaugh S. S., Bosma A., Rubin V. C., 2001, ApJ, 552, L23
de Vega H. J., Salucci P., Sanchez N. G., 2010, preprint (arXiv:1004.1908)
Diemand J., Zemp M., Moore B., Stadel J., Carollo M., 2005, MNRAS, 364, 665
Dodelson S., Widrow L. M., 1994, Phys. Rev. Lett., 72, 17
Dubinski J., Carlberg R. G., 1991, ApJ, 378, 496
Flores R. A., Primack J. R., 1994, ApJ, 427, L1
Gardini A., Bonometto S. A., Murante G., 1999, ApJ, 524, 510
Götz M., Sommer-Larsen J., 2002, Ap&SS, 281, 415
Governato F. et al., 2010, Nat, 463, 203
Hansen S. H., Lesgourgues J., Pastor S., Silk J., 2002, MNRAS, 333, 546
Hogan C. J., Dalcanton J. J., 2000, Phys. Rev. D, 62, 063511
Jardel J., Gebhardt K., 2012, ApJ, 746, 89
Khlopov M. Y., 2006, JETP Lett., 83, 1
Khlopov M. Y., Kouvaris C., 2008, Phys. Rev. D, 78, 065040
Klypin A., Kravtsov A. V., Valenzuela O., Prada F., 1999, ApJ, 522, 82
Knebe A., Devriendt J. E. G., Gibson B. K., Silk J., 2003, MNRAS, 345, 1285
Knebe A., Arnold B., Power C., Gibson B. K., 2008, MNRAS, 386, 1029
Komatsu E. (The WMAP Team) et al., 2011, ApJS, 192, 18

Kuzio de Naray R., Kaufmann T., 2011, MNRAS, 414, 3617
Kuzio de Naray R., McGaugh S. S., Mihos J. C., 2009, ApJ, 692, 1321
Macciò A. V., Fontanot F., 2010, MNRAS, 404, L16
Macciò A. V., Dutton A. A., van den Bosch F. C., Moore B., Potter D., Stadel J., 2007, MNRAS, 378, 55
Macciò A. V., Kang X., Fontanot F., Sommerville R. S., Koposov S. E., Monaco P., 2010, MNRAS, 402, 1995
Macciò A. V., Stinson G., Brook C. B., Wadsley J., Couchman H. M. P., Shen S., Gibson B. K., Quinn T., 2012a, ApJ, 744, L9
Macciò A. V., Ruchayskiy O., Boyarsky A., Munoz-Cuartas J. C., 2012b, preprint (arXiv:1202.2858)
Miranda M., Macciò A. V., 2007, MNRAS, 382, 1225
Moore B., 1994, Nat, 370, 629
Moore B., Ghigna S., Governato F., Lake G., Quinn T., Stadel J., Tozzi P., 1999, ApJ, 524, L19
Oh S.-H., de Blok W. J. G., Brinks E., Walter F., Kennicutt R. C., Jr, 2011, AJ, 141, 193
Pagels H., Primack J. R., 1982, Phys. Rev. Lett., 48, 223
Peebles P. J. E., Nusser A., 2010, Nat, 465, 565
Penarrubia J., Navarro J. F., McConnachie A. W., 2008, ApJ, 673, 226
Polisensky E., Ricotti M., 2011, Phys. Rev. D., 83, 043506
Romano-Díaz E., Shlosman I., Hoffman Y., Heller C., 2008, ApJ, 685, L105
Salucci P. et al., 2012, MNRAS, 420, 2034
Schmidt K. B., Hansen S. H., Macciò A. V., 2008, ApJ, 689, L33
Schneider A., Smith R. E., Macciò A. V., Moore B., 2011, preprint (arXiv:1112.0330)
Seljak U., Makarov A., McDonald P., Trac H., 2006, Phys. Rev. Lett., 97, 191303
Shi X., Fuller G. M., 1999, Phys. Rev. Lett., 82, 2832
Smith R. E., Markovic K., 2011, Phys. Rev. D, 84, 063507
Springel V. et al., 2008, MNRAS, 391, 1685
Stadel J., 2001, PhD thesis, Univ. Washington
Stadel J., Pooter D., Moore B., Diemand D., Madau P., Zemp M., Kuhlen M., Quilis V., 2009, MNRAS, 391, L21
Strigari L. E., Bullock J. S., Kaplinghat M., Kravtsov A. V., Gnedin O. Y., Abazajian K., Klypin A. A., 2006, ApJ, 652, 306
Takayama F., Yamaguchi M., 2000, Phys. Lett. B, 485, 388
Taylor J. E., Navarro J. F., 2001, ApJ, 563, 483
Tegmark M. (The SDSS Team) et al., 2006, Phys. Rev. D, 74, 123507
Tikhonov A. V., Gottlöber S., Yepes G., Hoffman Y., 2009, MNRAS, 399, 1611
Tremaine S., Gunn J. E., 1979, Phys. Rev. Lett., 42, 407 (TG79)
Viel M., Lesgourgues J., Haehnelt M. G., Matarrese S., Riotto A., 2005, Phys. Rev. D, 71, 063534
Viel M., Becker G. D., Bolton J. S., Haehnelt M. G., Rauch M., Sargent W. L. W., 2008, Phys. Rev. Lett., 100, 041304
Villaescusa-Navarro F., Dalal N., 2011, J. Cosmol. Astropart. Phys., 1103, 024
Waler M. G., Penarrubia J., 2011, ApJ, 742, 20
Wang J., White S. D. M., 2007, MNRAS, 380, 93
Zavala J., Jing Y. P., Faltenbacher A., Yepes G., Hoffman Y., Gottlöber S., Catinella B., 2009, ApJ, 700, 1779
Zentner A. R., Bullock J. S., 2003, ApJ, 598, 49

This paper has been typeset from a TEX/LATEX file prepared by the author.

Monthly Notices of the ROYAL ASTRONOMICAL SOCIETY

MNRAS **428,** 3715–3716 (2013) doi:10.1093/mnras/sts251

# Erratum: Cores in warm dark matter haloes: a *Catch 22* problem

By Andrea V. Macciò,[1⋆] Sinziana Paduroiu,[2] Donnino Anderhalden,[3] Aurel Schneider[3] and Ben Moore[3]

[1]*Max-Planck-Insitute for Astronomy, Königstuhl 17, D-69117 Heidelberg, Germany*
[2]*Geneva Observatory, University of Geneva, CH-1290 Sauverny, Switzerland*
[3]*Institute for Theoretical Physics, University of Zürich, CH-8057 Zürich, Switzerland*

**Key words:** Errata, addenda: Dark matter: *N*-body simulations – galaxies, haloes.

**Table 1.** Simulations parameters.

| Label | $m_\nu$ (keV) | $m_{\nu,\,\rm vel}$ (keV) | $N_{\rm vir}$ ($10^6$) | $M_{\rm vir}$ ($10^{12}\,{\rm M}_\odot$) |
|---|---|---|---|---|
| CDM | $\infty$ | – | 10.2 | 1.42 |
| WDM1 | 2.0 | 1.32 | 8.6 | 1.22 |
| WDM2 | 2.0 | 0.33 | 8.4 | 1.20 |
| WDM3 | 2.0 | 0.13 | 8.5 | 1.21 |
| WDM4 | 2.0 | 0.15 | 6.7 | 0.93 |
| WDM5-N | 2.0 | 0.05 | 4.9 | 0.71 |
| WDM5 | 2.0 | 0.03 | 5.1 | 0.82 |

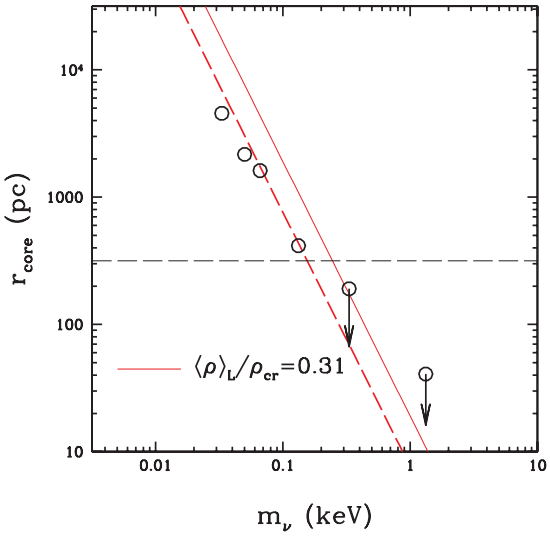


**Figure 1.** Comparison between core size in simulations (open symbols) and the theoretical expectation for a $M = 10^{12}\,{\rm M}_\odot$ halo (solid line). The dashed horizontal line is the gravitational softening of our simulations. All points below this line should be considered as upper limits on the core size. The red dashed line is a linear fit to the simulation results.

The article "Cores in warm dark matter haloes: a *Catch 22* problem" (Macciò et al. 2012) was published in MNRAS, 424, 1105 (2012).

⋆ E-mail: maccio@mpia.de



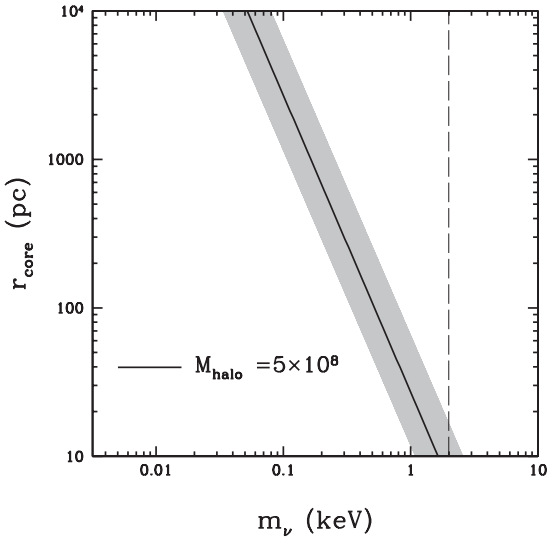


**Figure 2.** Expected core size for the typical dark matter mass of Milky Way satellites as a function of the WDM mass $m_\nu$. The shaded area takes into account possible different values of the local density parameter $0.15 < \Omega_m < 0.6$. The vertical dashed line shows the current limits on the WDM mass from large scale structure observations.

In the code to create the initial conditions we treated the 3D thermal velocity [equation (4) in the original work] as a one dimensional velocity, overestimating then the velocity by a factor $\sqrt{3}$. The main conclusions, however, do not change significantly.

More specifically, given the relation between the mass of the thermal candidate ($m_\nu$) and the thermal velocity, this implies that the velocities we use in the ICs were for a particle mass lower by a factor $3^{3/4} \approx 1.51$. In Table 1 we list the corrected values of the masses, we have also added a new simulation with the corrected velocities for the $m_\nu = 0.05$ keV case. These new masses for the WDM candidates have an effect on the core size-WDM mass relation, which is shown in Fig. 1 (this figure updates fig. 7 in the printed version of the paper). It is clear that simulations results are not well reproduced by our simple analytic argument based on the pseudo phase space density $Q \equiv \rho/\sigma^3$. We need to reduce the 'theoretical' core estimation by 60 per cent in order to fit the simulation points (red dashed line in the figure). This in agreement with recent results

by Shao et al. (2012) that also find that $Q$ overestimates the real maximum phase space density.

This even smaller core makes our original statements even stronger, as shown by Fig. 2, where using our new determination of the core size as a function of the warm dark matter mass we compute the expected value of $r_{\rm core}$ for the typical halo mass ($5 \times 10^8\,{\rm M}_\odot$) of dwarf galaxies orbiting the Milky-Way (fig. 2).

These new, corrected values for the core size in dwarf galaxies make the conclusions of our paper even stronger, and the "Catch 22" problem for warm dark matter still holds:

*If you want a large core you won't get the galaxy, if you get the galaxy it won't have a large core.*

**ACKNOWLEDGMENTS**

We thank Shi Shao and Liang Gao who helped us finding this mistake.

**REFERENCES**

Macciò A. V., Paduroiu S., Anderhalden D., Schneider A., Moore B., 2012, MNRAS, 424, 1105

Shao S., Gao L., Theuns T., Frenk C. S., 2012, arXiv:1209.5563

This paper has been typeset from a TEX/LATEX file prepared by the author.

Chapter 5

# Technical aspects in warm dark matter simulations

Unlike cold dark matter particles, warm dark matter ones have a free streaming length that translates into a suppression of power at small scales and gives a streaming velocity, which allows particles to travel longer distances, delaying the formation of structure and the small scale clumping. These properties produce several effects that make the numerical description more challenging in warm dark matter simulations compared to cold dark matter ones.

First, the resolution studies are more expensive in warm dark matter simulations. Ideally, the structure formation processes as well as the small scale structure studies should be done with high resolution simulations. Since warm dark matter particles possess a velocity dispersion, ascribing the velocity dispersion to a simulated particle that is usually $10^5$ - $10^7$ $M_\odot$, is a procedure highly debated in the literature. Moreover, in order to perform high resolution simulations of a certain region of interest at redshift zero, one needs to trace back the particles to the initial conditions. In the case of warm dark matter, depending on the streaming velocity of the particles, this region is much larger than in cold dark matter simulations.

Furthermore, the artificial fragmentation that occurs in warm dark matter simulations resulting in small spurious halos along the filaments questions the accuracy of halo statistics. The morphology of a certain region is rapidly changing in warm dark matter simulations and this triggers in some cases the growth of spurious halos by mergers, making them difficult to distinguish from genuine halos formed above the fragmentation scales. This results in the contamination of the mass function.

In this chapter we will discuss these issues, present some numerical tests and compare our results with other works in the literature.

## 5.1 High resolution refinements in warm dark matter simulations

In previous chapters we have discussed the properties of a high resolution halo formed top-down at the intersection of filaments. This halo has been chosen from a 30 Mpc box simulation with 0.36 km/s velocity dispersion at redshift zero and the corresponding cutoff in the power spectrum. In the low resolution run we have marked the particles inside the halo at redshift zero and traced them back in the initial conditions. In the case of cold dark matter simulations, the particles inside any given halo at redshift zero are coming from a region of size a few times larger than the virial radius, which can be usually approximated by a sphere.

In the case of warm dark matter simulations, for our chosen velocity, the particles are coming from regions found at large distances from our final halo, regions that have different irregular shapes. Since particles are initially moving in different random directions, those regions are not connected in the initial conditions to the region where the halo eventually forms. When doing a high resolution refinement, we also need to simulate the particles in between these regions, meaning we need a larger box and a larger number of particles.

For our top-down halo, the refinement region is almost a third of the initial box. Because the structure formation in warm dark matter models depends, as shown previously, on the morphology of the region, in regions with many intersecting similar size filaments, few smaller halos may form initially and then rapidly merge. In this case the particles inside the halo resulting from mergers will come from a smaller region then the particles inside our halo formed top-down at the intersection of large filaments. These differences in the structure formation make it difficult to quantify the size of the box needed to be refined for a halo of a certain mass or of a certain radius at redshift zero. Scaling it with the velocity is that much more difficult.

In Fig. 5.1 we plot the evolution of our refined region at different redshifts. To make it less numerically expensive, while still preserving the accuracy in solving the gravitational forces, we have made a progressive refinement[1], where the highest resolution box is embedded in a lower resolution region, embedded in a lower resolution one. The highest resolution box has $8^3$ more particles than the initial box, with intermediate regions having a factor of 2 difference in refinement. These different resolution regions are intertwining by redshift zero, but we have ensured that no low resolution particles will contaminate the halo.

## 5.2 Spurious fragmentation in warm dark matter filaments

The $N$-body method has been proven successful in accurately describing the behavior of cold dark matter particles and have passed many different convergence tests (Heitmann, Lukić, & Fasel 2008; Springel et al. 2008; Stadel et al. 2009; Kim et al. 2014). Several studies, however, point out the effect of discreteness errors on the numerical accuracy, especially on the small scales (Melott et al. 1997; Splinter et al. 1998; Diemand, Moore & Stadel 2004; Binney 2004; Wang & White 2007;

[1]This has been done with a Grafic 2 version modified by Doug Potter

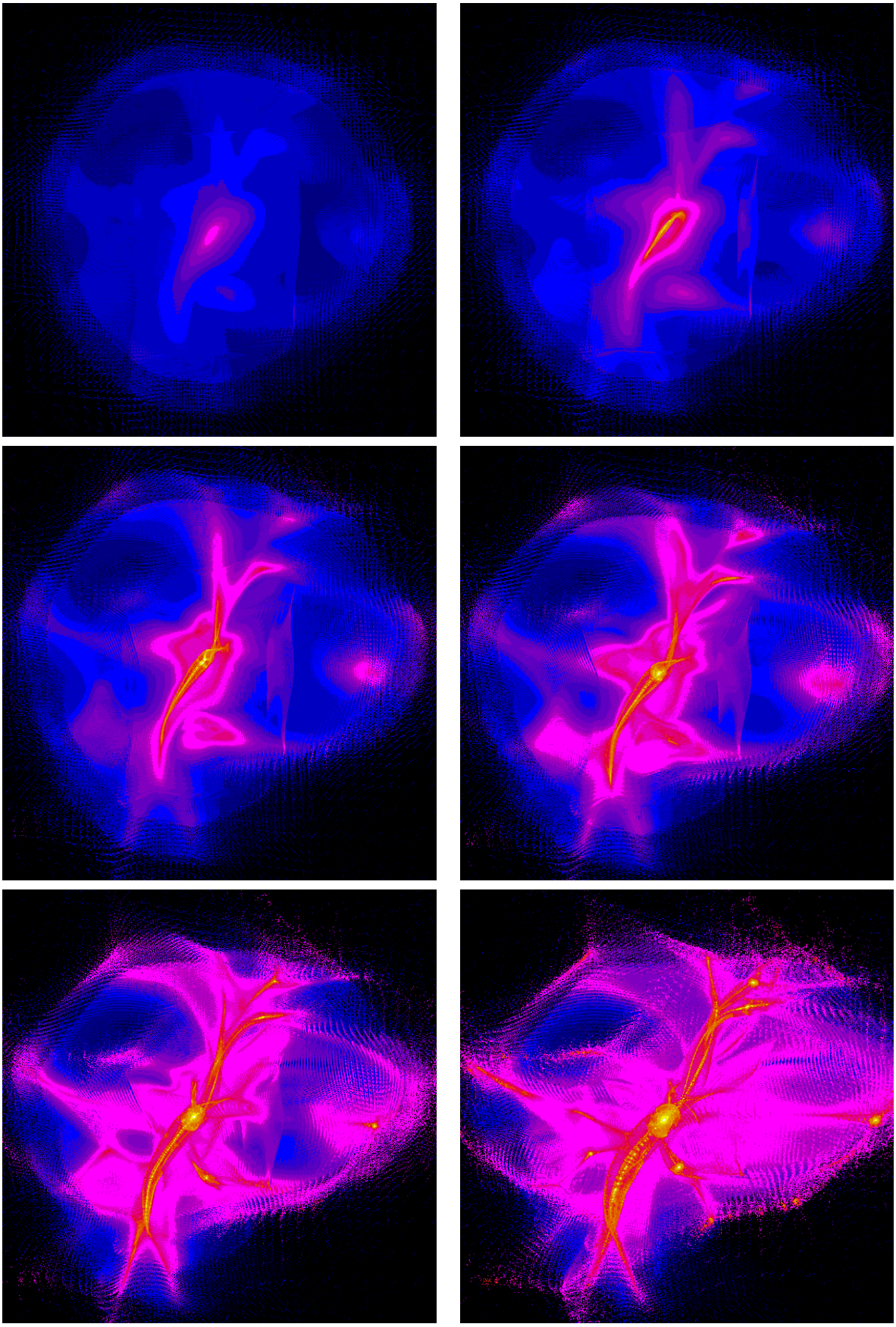

Figure 5.1: High resolution region at redshift 4, 2.5, 1.3, 1, 0.5, 0

Romeo et al. 2008; Joyce, Marcos & Baertschiger 2009, e.g.). For the warm dark matter case, these errors become more problematic (Bode et al. 2001; Avila-Reese et al. 2001).

In warm dark matter simulations, the fragmentation of filaments resulting in similar mass small halos equally spaced inside the filaments, has been observed since the first such simulations (Centrella & Melott 1983; Frenk, White & Davis 1984; Efstathiou et al. 1985; Centrella et al. 1988, e.g.).

It has been believed for a long time that the spurious fragmentation of filaments in warm dark matter simulations is due to the discreteness effects that are influencing the growth of non linear structures below the streaming scale, although in some works (Bode et al. 2001; Knebe et al. 2003) this fragmentation has been considered physical.

Most of the warm dark matter simulations have been performed with the so-called grid method. The grid simulations imply the use of a cubic regular lattice. When imposing perturbations, the preferred directions and the coherence of the lattice can result in numerical artifacts. The glass-like method, as opposed to the grid one, uses the same initial conditions, but with the sign of the peculiar gravitational acceleration reversed, so that each particle is repelled by all others (White et al. 1996; Wang & White 2007). The total force vanishes on each particle, when the system reaches a quasi-equilibrium state, but there are no preferred directions. Since there is no memory of the initial grid in the glass simulations, one would expect no artificial fragmentation in this case.

Götz & Sommer-Larsen (2002) (also Götz & Sommer-Larsen (2003)) found that in the glass simulations the number of spurious halos is reduced compared to the grid simulations. On the contrary, Wang & White (2007) found artificial halos in the glass simulations, with a frequency similar to that found in the grid ones and also regularly spaced. Performing different resolution tests, they saw that this effect depends on and scales with the resolution. In Fig. 5.2 the glass simulations are shown (Wang & White 2007) for different resolutions. One can see the fragmentation of small halos along the filaments with fewer, more massive spurious halos in the low resolution runs. For the same resolution simulation, one can see that in the grid run the fragmentation is more visible than in the glass one, but the fragmentation does occur in all glass simulations. For comparison we plot a fragmented filament from our grid high resolution simulations in Fig. 5.3.

We have performed a similar test[2] as Wang & White (2007) in order to see the correlation between the fragmentation and the resolution used in our grid simulations. While they used a 100 Mpc $h^{-1}$ box and increased the number of particles in the full box, we have done the same test using just a filamentary region where a halo forms top-down. Also, they state that their simulations are done for a 55 eV particle[3], while we have chosen a particle with a 0.36 km/s velocity dispersion at redshift zero, corresponding to 200 eV in Bode et al. (2001).

[2] part of this work has been done in collaboration with Joachim Stadel and Doug Potter

[3] It seems that they use a different power spectrum law, so it is not clear to which velocity their 55 eV corresponds. In our 50 eV (in Bode et al. estimation) simulations, as shown in Chapter 3, halos only begin collapsing at redshift zero and filaments are still smooth, although it is true that we have chosen a much smaller, 40 Mpc $h^{-1}$ box. This shows again that one has to be careful when referring to a particle by its mass and not by its velocity dispersion.

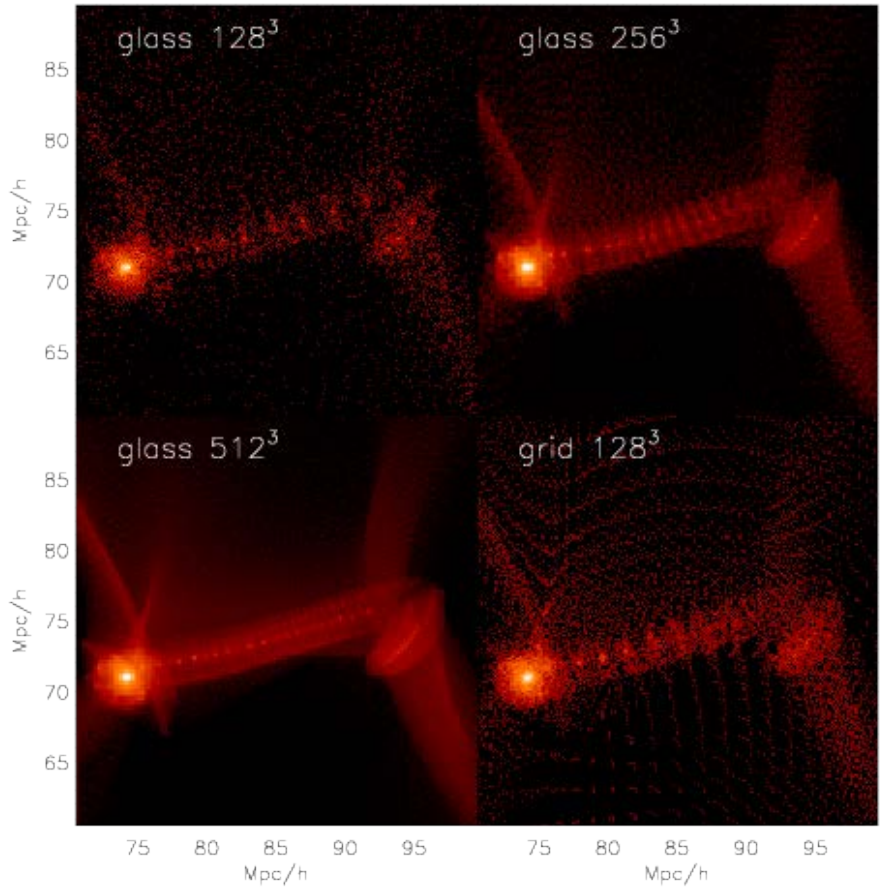


Figure 5.2: A filament fragmenting in simulations performed with the glass method for different resolutions from Wang & White (2007)

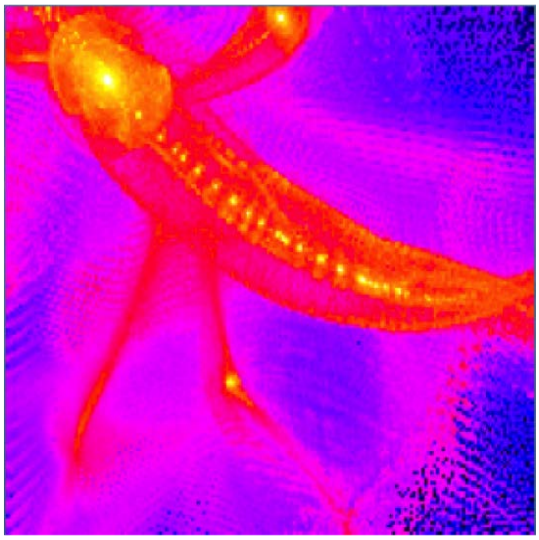

Figure 5.3: The fragmentation occurring along a filament in our high resolution grid simulation

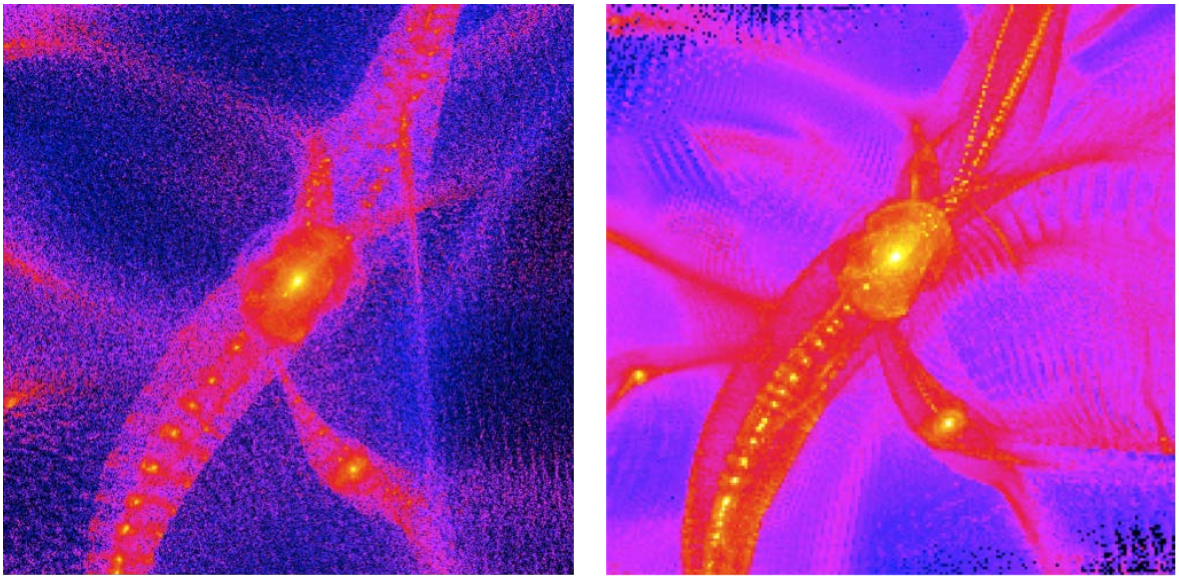

Figure 5.4: Halo forming region at redshift zero in low resolution simulation (left panel), high resolution simulation (right panel)

In Fig. 5.4 we plot the region of interest in low resolution and in $8^3$ higher resolution. The filament we have been analyzing has a diameter[4] of $\sim$ 750 kpc. In the high resolution run we have chosen a softening of 1.5 kpc. One can see in the picture that the number of halos is larger than in the low resolution case and that the spacing between the halos is smaller. While in the low resolution case the fragmentation occurs along its whole width of the filament, in the high resolution case, it occurs just in the central region of the filament, where the density is higher than in the outer part. This inner part of the filament, which fragments has a size of 15 kpc.

To see how the softening is influencing the fragmentation, we have also run the high resolution simulations with larger softening lengths. In Fig. 5.5 we show the difference at redshift 1.5, when the fragmentation first occurs, between the high resolution filament and the high resolution filament with the increased 15 kpc softening. As expected, when the softening is larger than the fragmentation scale, no spurious halos form.

The number of spurious halos is scaling with $N^3$ and the mass of these halos is scaling with $N^{-1}$, thus confirming the results of Wang & White (2007), where N is the number of particles. Also, since these parameters vary with the resolution, it is safe to conclude that the fragmentation is artificial and not physical.

It was only recently shown by Hahn, Abel & Kaehler (2013) that the fragmentation is most likely due to large anisotropic force errors and that with a more accurate force, the number of spurious halos is reduced. For solving the same problem, Hobbs et al. (2015) propose a modified force softening criterion[5], which minimizes the spurious two-body effects, while maintaining high

[4]Since the filament is not perfectly cylindrical, this represents the maximum width

[5]Novel form of Adaptive softening (NovA) implemented in the RAMSES adaptive mesh refinement code.

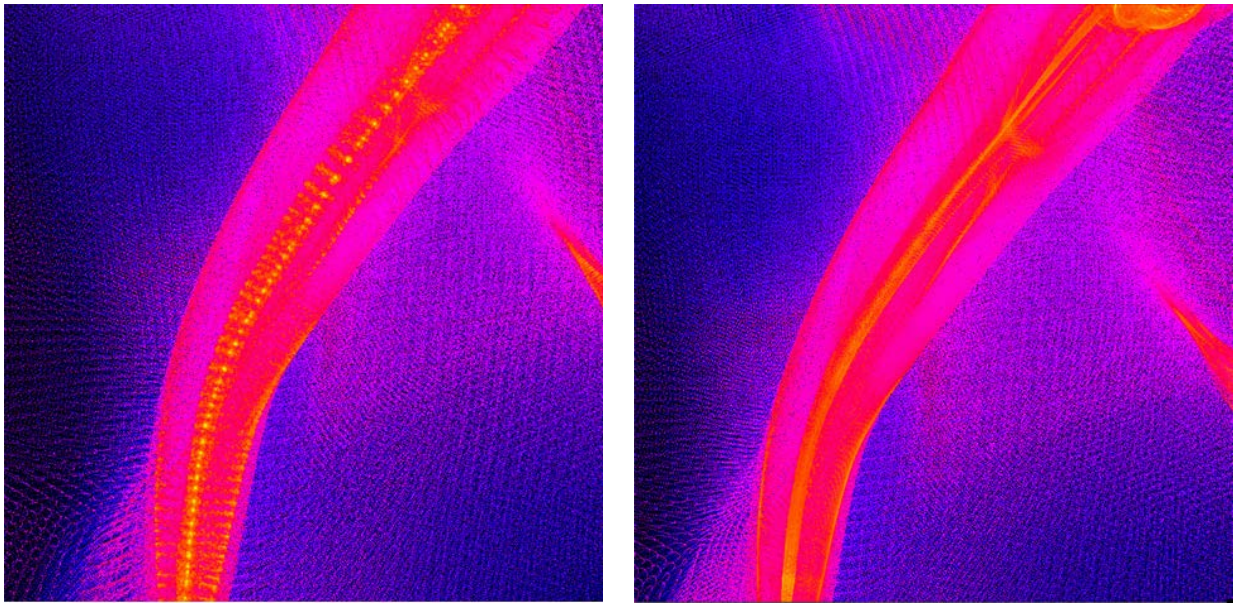

Figure 5.5: The filament at redshift 1.5 in the high resolution run (left panel) and high resolution with large softening (right panel)

force accuracy in collapsed regions.

The question whether or not for some filaments the fragmentation is physical, still remains. It has been shown that infinite self-gravitating cylinders are unstable to fragmentation (Ostriker 1964; Fridman & Poliachenko 1984), but Hobbs et al. (2015) show that even for finite cosmological filaments, in some cases fragmentation occurs regardless of the resolution and the softening criterion used. How this fragmentation is influenced by baryonic physics is another important question.

### 5.2.1 Contamination from the merging of spurious halos

To avoid the contamination by spurious halos when computing the mass function, one method proposed is to simply remove them, since we know the mass scale at which they form (Lovell et al. 2014). There is, however, one caveat to this method. In the warm dark matter simulations, some of the halos, which are artificially forming along the filaments, merge into larger halos, which by redshift zero acquire enough particles to set them above the fragmentation mass scale.

For example, in Fig. 5.6 we show such a merging, where the resulting halo is above the fragmentation scale, that is $\sim 10^{10}$ $M_\odot$ halo for a $\sim 5 \times 10^9$ $M_\odot$ fragmentation scale. While this halo was easy to spot in our simulation, in simulations with colder particles, this becomes more difficult, because the hierarchical growth of structure happens earlier and more rapidly. Therefore, one needs to be extremely cautious when analyzing a halo at redshift zero and make sure that the halo is not the result of spurious halos merging.

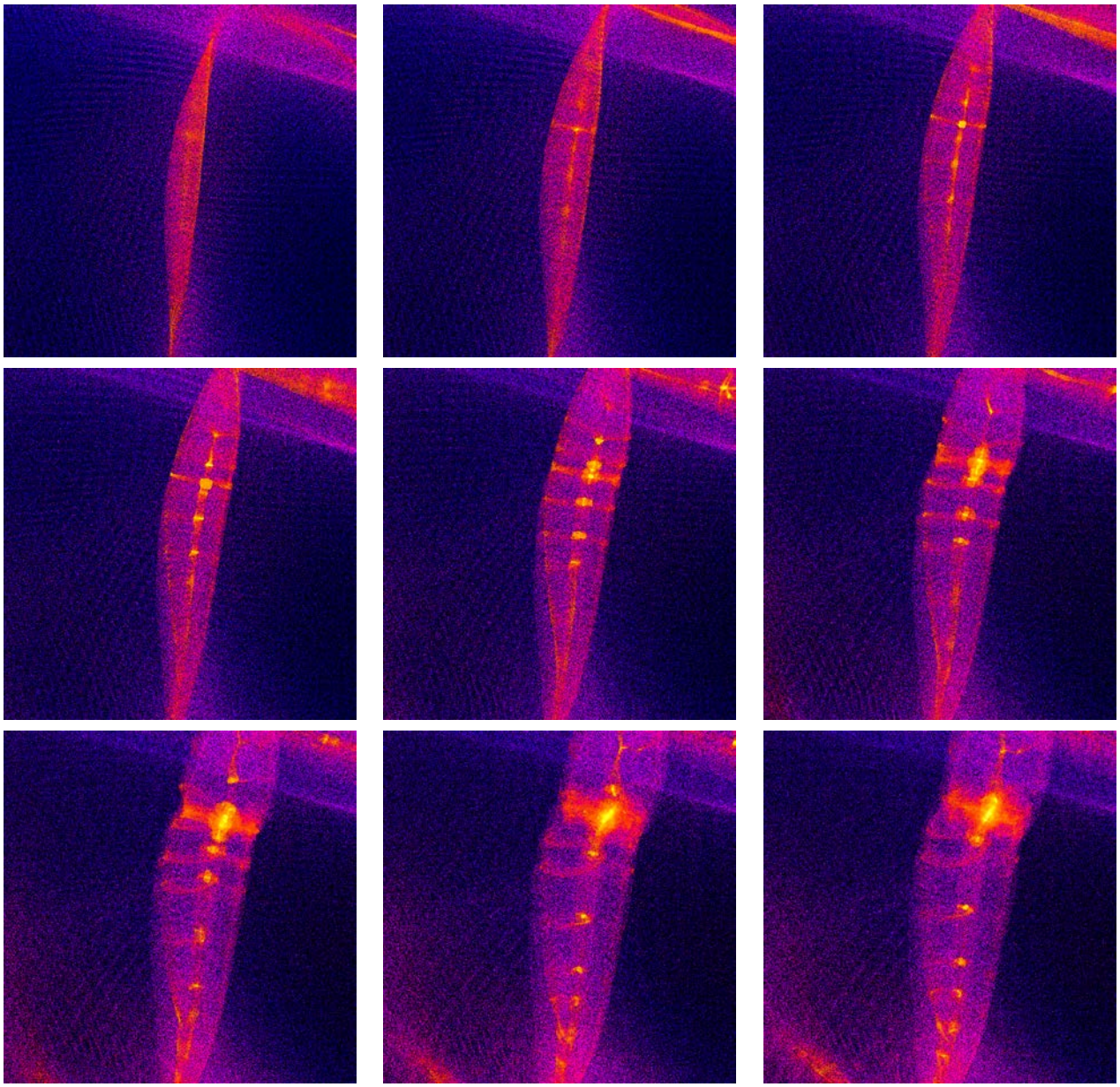

Figure 5.6: Fragmentation of a filament in which small spurious halos merge into a larger halo at redshift 1.77, 1.56, 1.36, 1.27, 1, 0.8, 0.7, 0.6, 0 (from upper left to bottom right)

## 5.3 Conclusions

In this chapter, several technical aspects that need to be considered in warm dark matter simulations have been discussed. We will summarize them below along with other aspects that need to be taken into account in future studies.

- Since warm dark matter particles travel in a given time larger distances than cold dark matter ones, high resolution refinements are more expensive, as they imply larger regions sampled with high energy particles. The size of these regions depends on the streaming velocity of the particle and the morphology of the region that one wants to refine.
- Fragmentation occurs along the filaments in all warm dark matter simulations, resulting in low mass spurious halos. The mass and number of spurious halos is scaling with the resolution.
- In some cases, the fragmentation of filaments may be physical, since it is occurring even for very high resolutions, in simulations that otherwise should prevent the formation of artificial halos.
- Several methods have been proposed in order to solve the fragmentation, with the adaptive softening being highly successful in preventing the formation of spurious halos.
- The baryonic physics may play an important role in the evolution of filaments, as we have seen in Chapter 3, having an important influence on how and when the filaments fragment.
- In many cases, especially for colder particles in the few keV range, artificial halos forming along the filaments merge into larger halos, 'contaminating' the mass function. For an accurate mass function, merger trees should be considered for establishing the origin of halos.
- It was recently shown by Gao, Theuns & Springel (2015) that methods like 'FoF' used in analyzing cold dark matter simulations are proved to be insufficient in analyzing warm dark matter halos. We confirm this statement, finding that the artificial fragmentation occurring along the filaments results in a high number of small halos with less than ten particles.

Chapter 6

# Conclusions

The effects of the free streaming of the warm dark matter particle are expected to manifest themselves on both large scales and small scales. The free streaming exponentially dampens the power spectrum of density fluctuations such that very few structures are formed below the damping scale. Conservation of the fine grained phase space density is expected to set a maximum density that cannot be exceeded during the formation of structures with collisionless particles. After performing numerous warm dark matter simulations and analyzing terabytes of data, in this thesis I have discussed some of the aspects of structure formation and evolution in warm dark matter models. I will summarize below some of our findings.

## 6.1 General Conclusions

Addressing first the theoretical considerations adopted in warm dark matter simulations, we have shown that in the absence of a tested universal mechanism of production for the warm dark matter particle, the relation between the particle mass and its corresponding velocity is strongly dependent on the specific model adopted. Depending on the model adopted this value can vary within one order of magnitude, a fact that is very important when trying to constrain the warm dark matter particles.

Beginning with the effects that warm dark matter particles are having on the structure formation in the universe, we found that these effects are not negligible and that the structure forms qualitatively different in warm dark matter models compared to cold dark matter ones.

- In the case of warm dark matter we see from our simulations that the structure formation is more complex, a hybrid mechanism.
- During the early stages one sees the formation of well contoured filaments. How early this stage is depends on the particle velocity. In our simulations this happens in the interval $13 > z > 8$.

- In the higher density regions, usually situated at the intersection of such filaments, the first halos are formed through gravitational collapse. These halos continue growing into larger ones by accreting particles from the disrupted filaments.
- In medium density regions, halos show a hierarchical formation trend. Small halos collapse first and then merge into bigger halos.
- In less dense regions, the ones isolated by voids and which have a very slow evolution, we have observed filaments that collapse very late. The top-down formed halo survives without any mergers until redshift zero.
- Finally there is the more complex scenario in which we observe large halos formed earlier which merge together forming a large cluster.
- The filamentary-like structure is preserved until redshift zero, with new filaments forming in the low density regions as late as redshift $z \sim 4$.
- The warmer the dark matter the more pronounced is the top-down effect and the more delayed is the initial collapse.
- Despite the numerical limitations we encounter as far as our warm dark matter simulations are concerned, we can conclude that an early top-down structure formation trend would be seen even in dark matter simulations with $v < 0.05$ km/s. For colder particles, this effect is hidden and wiped out by following abundant mergers resulting in a redshift zero distribution that seems to be in agreement with the hierarchical formation scenario.
- The number of small satellites, as previously found, is visibly reduced in the WDM simulations compared to the CDM ones.

Analyzing the internal structure of halos, high resolution $N$-body simulations have been used to examine the effects of free streaming velocities at such scales. The major findings are the following:

- As seen from our simulations, warm dark matter halos display caustics and shells.
- The finite initial fine grained Phase Space Density (PSD) is also a maximum of the pseudo PSD, resulting in PSD profiles of WDM haloes that are similar to CDM haloes in the outer regions, but do flatten towards a constant value in the inner regions. Baryonic processes and quantum effects can influence the profiles in the central region of the halos.
- When testing the Tremaine-Gunn limit, we find that the finite PSD limit results in a constant density core with characteristic size that is in agreement with theoretical expectations from a spherical collapse model.

- In order to explain the cores of order of several kpc observed in dwarf galaxies, one would need, however, a particle that is too light to be in agreement with independent constraints like the ones derived from Lyman-$\alpha$ and lensing.
- Moreover, with such a warm candidate, the exponential cut-off of the power spectrum would make it impossible to obtain these dwarf galaxies in the first place.
- This Catch 22 problem means that warm dark matter alone is not responsible for the large cores observed, although it may provide an important ingredient for the baryonic processes to develop large cores.
- It should be stressed, however, that one important aspect that we do not consider is the quantum effect of the warm dark matter particles.

## 6.2 Outlook and perspectives

In order to better test warm dark matter models, high resolution simulations will be needed, implementing baryonic physics and using techniques that solve problems like artificial fragmentation. In the attempt of reconciling the simulations with observations, one may look at several interesting aspects.

- Since warm dark matter structure forms initially top-down, the effect of baryonic physics may be very important. The stars which form inside the filaments may provide the seeds for growing massive objects, explaining perhaps the very massive black holes observed at high redshift.
- Moreover, observations of regularly spaced supermassive black holes distributed along a 60 Mpc arc (Caramete & Biermann 2011) may be explained in the WDM scenario.
- The smoother space distribution in the warm dark matter scenario may allow baryons to condense coherently in a smooth potential halo, providing favorable conditions for forming disk-like galaxies.
- The same effect may produce large cores like the ones observed in dwarf galaxies.
- The high resolution analysis of the small halos that we find in our simulations and which do not suffer mergers may shed some light on the difference between the properties of these halos and other halos in simulations. These differences can be tested against observations.
- Estimating the enhancement in the annihilation signal that can be due to the shells we find in warm dark matter simulations and comparing it with detected signals may be an important test for warm dark matter.

- Measuring the phase space density for simulated halos in the mass range of dwarf galaxies and comparing them with observations can be yet again a test for the model.

Appendix A

# Other work

Your theory is crazy
but is it crazy enough to be true?

*paraphrasing* NIELS BOHR*'s alleged remark*

## A.1 What if the black hole event horizon has a quantum thickness?

Jack Sarfatti[1], Sinziana Paduroiu[2]

[1] ISEP, San Francisco, CA 94133, USA

[2] Geneva Observatory, University of Geneva, CH-1290 Sauverny, Switzerland

**Abstract**

Considering that the black hole has a quantum thickness, L, the radiation predicted by Hawking, with a peak wavelength for distant observers $\sim A^{1/2}$ for the area A should be corrected by a second asymptotic redshifted higher Unruh temperature component with peak wavelength proportional to the proper quantum thickness of the horizon. The radiation power and the emitted flux from a black hole that include these correction terms are presented in the paper. The two Hawking surface and thickness radiations form a Carnot limited heat engine. $L = Lp$ corresponds to random black body gravity waves. $L \sim h/mc$ for virtual electron-positron pairs stuck to the horizon corresponds to far field thermal photons. Although our results show that the flux from the black hole in the galactic center is too small to be detected by current gravitational wave detectors, the thermal Hawking thickness radiation $hc/L_p^2 A$ gives a prediction for the observed dark energy density if we use the future de Sitter horizon entropy.

**Introduction**

At the beginning of the seventies, Hawking (Hawking 1971, 1974, 1975) and Bekenstein (Bekenstein 1973a,b) calculated the black body radiation emitted by a black hole including the quantum

gravitational effects. Hawking's black body radiation from the horizon surface area-entropy A peaks at wavelength $\sim A^{1/2}$ for distant observers. This is not the complete story. Classically the event horizon is approximated as infinitely thin. Heisenberg tells us this is not possible. We know that the event horizon of a black hole must have some effective thickness of quantum origin.

Ever since Stephen Hawking suggested information is lost in an evaporating black hole once it passes through the event horizon and is inevitably destroyed at the singularity, turning pure quantum states into mixed states, some physicists have wondered if a complete theory of quantum gravity might be able to conserve information with a unitary time evolution. But how can this be possible if information cannot escape the event horizon without traveling faster than light? This seems to rule out Hawking radiation as the carrier of the missing information. It also appears as if information cannot be "reflected" at the event horizon as there is nothing special about it locally.

Leonard Susskind (Susskind, Thorlacius & Uglum 1993) proposed a radical resolution to this problem by claiming that the information is both reflected at the event horizon and passes through the event horizon and cannot escape, with the catch being no observer can confirm both stories simultaneously. According to an external observer, the extremely large time dilation at the horizon itself makes it appear as if it takes an infinite amount of time to reach the horizon. He also postulated a stretched horizon, which is a membrane hovering about a Planck length outside the event horizon and which is both physical and hot. According to the external observer, infalling information heats up the stretched horizon, which then re-radiates it as Hawking radiation, with the entire evolution being unitary. However, according to an infalling observer, nothing special happens at the event horizon itself, and both the observer and the information will hit the singularity. This is not to say there are two copies of the information lying about - one at or just outside the horizon, and the other inside the black hole - as that would violate the no cloning theorem. Instead, an observer can only detect the information at the horizon itself, or inside, but never both simultaneously. Complementarity is a feature of the quantum mechanics of noncommuting observables, and Susskind proposed that both stories are complementary in the quantum sense. Interestingly enough, an infalling observer will see the point of entry of the information as being localized on the event horizon, while an external observer will notice the information being spread out uniformly over the entire stretched horizon before being re-radiated. To an infalling observer, information and entropy passes through the horizon with nothing strange happening. To an external observer, the information and entropy is absorbed into the stretched horizon which acts like a dissipative fluid with entropy, viscosity and electrical conductivity. See the membrane paradigm for more details. The stretched horizon is conducting with surface charges which rapidly spread out over the horizon.

In this paper, we calculate the radiation coming from a black hole, considering Susskind's assumption (Susskind, Thorlacius & Uglum 1993) that the horizon has a quantum thickness $L = Lp$. Hence, there should be a second asymptotic redshifted higher Unruh temperature component with peak wavelength proportional to the proper quantum thickness of the horizon $\sim$ geometric mean

L of IR cutoff i.e., $\sqrt{L\sqrt{A}}$ with an energy density $T^4 \sim hc/L^2A$. Our result shows that the power emitted is independent of the mass of the black hole and its area-entropy. Considering as examples the black hole at the center of the Milky Way and the one in M87, we find that although the radiation is very high at the surface, the flux on Earth is undetectable by our current gravitational waves detectors.

The Unruh effect (Fulling 1973; Davies 1975; Unruh 1976) suggests that the $w = +1/3$ black body radiation (gravity or EM) for accelerating detectors corresponds to $w = -1$ for the distant local inertial frame detectors, where $w$ is the pressure over the energy density.

All this leads up to Susskind's holographic principle: the universe filled with galaxies, stars, planets, people is a hologram, an image of reality coded on a distant two-dimensional surface.

In the last few years, several works (Biermann & Harms 2012, 2013) were proposing models that link dark energy to the gravitational waves bursts ejected during the birth of super-massive black holes.

Our prediction for dark energy differs in that it takes into account the blue-shifted radiation from our future cosmologic horizon. The two Hawking surface and thickness radiations form a Carnot limited heat engine. $L = Lp$ corresponds to random black body gravity waves. $L \sim h/mc$ for virtual electron-positron pairs stuck to the horizon corresponds to far field thermal photons. These back of the envelope heuristic shortcuts apply both to observer independent black hole horizons as well as observer-dependent past and future cosmological horizons bounding the causal diamond. In the case of gravity wave thermal Hawking thickness radiation $hc/L_p^2A$ is the observed dark energy density if we use the future deSitter horizon entropy A.

**New radiation predicted**

Leonard Susskind in his work on stretched horizons suggests that the event horizon should be one Planck length thick, which is in the realm of quantum gravity. According to Susskind, a thermometer lowered to the vicinity of a black hole will report a very high temperature at the stretched horizon (1 Planck length thick above the horizon). To a free-falling observer it is normal empty space and a non event. According to black hole complementarity model, the maximum amount of information that can fill a region of space is equal to the area of the region (not the volume). Adding one bit of information to a black hole of any size will increase the area of the horizon by one square Planck unit (Planck unit of area). The entropy of a black hole, measured in bits, is proportional to the area of the horizon, measured in Planck units (information = area). The maximum amount of information that can possibly be contained in any region of space can be stored in the boundary of the region using no more than one quarter bit per Planck area. We conjecture that virtual Planck scale black holes become real, like in the electron-positron case, and they quickly evaporate emitting gravity wave Hawking radiation. For an arbitrary 'coordinate thickness' IR cutoff L, the physically measurable local 'proper length' thickness line element for

the Schwarzschild black hole metric in the static Local Non-Inertial Frame (LNIF) representation is, to first order Taylor series expansion

$$\tilde{L} \approx \frac{L}{\sqrt{1-\frac{\sqrt{A}}{L+\sqrt{A}}}} \rightarrow \sqrt{L\sqrt{A}}, for \frac{L}{r_s} \ll 1 \tag{A.1}$$

Therefore, the radial horizon proper thickness is the geometric mean of the IR cutoff with the square root of the area of the horizon. The random radial vibrations of the virtual electron-positrons, or the virtual black holes as the case may be, have a peak wavelength in their black body radiation that is this geometric mean as seen by the distant observer.[1]

The new radial quantum thickness modes are

$$g_{tt}(receiver) \approx 1 \tag{A.2}$$

and

$$g_{tt}(source) = 1 - \frac{r_s}{L + r_s} \approx \frac{L}{r_s}, \tag{A.3}$$

for a far away observer.

For quantum thickness radial modes, the flux at the source is $f(source) \sim 1/L$, therefore

$$(1+z) = \sqrt{\frac{r_s}{L}} = \frac{f(source)}{f(receiver)}. \tag{A.4}$$

Considering the geometric mean rule,

$$f(receiver) \approx \sqrt{\frac{r_s}{L}} = \frac{1}{\sqrt{L\sqrt{A}}}. \tag{A.5}$$

On the other hand, for Hawking's radiation, the surface modes give

$$f(source) \approx \frac{1}{r_s} \tag{A.6}$$

$$f(receiver) \approx \sqrt{g_{tt}} f(source) \approx \frac{c^2}{r_s} \tag{A.7}$$

The Hawking black body temperature corresponding to this new mode of random vibrations is

$$T \approx \frac{hc}{k_B \sqrt{L\sqrt{A}}} \tag{A.8}$$

The Stefan-Boltzmann law gives the energy density

$$\rho \approx \frac{hc}{L^2 A}. \tag{A.9}$$

[1]The proper acceleration of the hovering non-inertial observer near the horizon that describes the virtual particles is huge because of the square root of the $g_{00}$ in the denominator multiplying the Newtonian surface gravity in the numerator. However, the high energy radiation from this accelerating source is redshifted for the distant observer, by the same square root of the $g_{00}$ that is now in the numerator. The two factors cancel out and this is why it is only the Newtonian surface gravity that is relevant for the distant observer in Hawking's original model.

The total power emitted isotropically at the event horizon from these hitherto ignored random quantum thickness vibrations is

$$P = \frac{2}{\pi \times 15360}\frac{hc^2}{L^2} \approx 4 \times 10^{-5}\frac{hc^2}{L^2}. \tag{A.10}$$

Therefore, the universal total power for Hawking horizon thickness[2] gravity blackbody radiation is

$$P_{gravity} \approx 4 \times 10^{-5}\frac{hc^2}{L_g} \approx 4 \times 10^{51} W \tag{A.11}$$

In contrast, Hawking's original surface gravity radiation has

$$\rho_H \approx \frac{hc}{A^2}, \tag{A.12}$$

with non-universal total radiated power for photons

$$P_H \approx 4 \times 10^{-5}\frac{hc^2}{A}. \tag{A.13}$$

The ratio of the two modes of Hawking radiation is, within the limits of our Taylor series expansion:

$$\frac{P}{P_H} = \frac{A}{L^2} \tag{A.14}$$

$$\frac{T}{T_H} = \frac{\frac{1}{\sqrt{L\sqrt{A}}}}{\frac{1}{\sqrt{A}}} = \sqrt{\frac{\sqrt{A}}{L}} \tag{A.15}$$

The flux coming from a black hole can be calculated using:

$$f = \frac{6.582 \times 10^{-16}}{(L \times r_s)^2} eVs \tag{A.16}$$

$$f = \frac{1.054 \times 10^{-34}}{(L \times r_s)^2} Js \tag{A.17}$$

in the approximation in which the source is at an infinite distance from the detector.

A spherically symmetric static Schwarzschild black hole of one solar mass will have the peak of the high freaquency gravitational waves (HFGW) at the surface of the Earth will be $\sim 10^{24}$ Hz after the enormous gravity redshift from a Planck length distance of the classical horizon. In contrast, the indirect electromagnetic black body radiation from the stuck electron-positron plasma at the horizon has a much lower temperature corresponding to a $10^{12}$ Hz peak.

Let us consider the super-massive black hole at the center of our galaxy of about four million solar masses (e.g Reid 2009; Sofue 2013) with a Schwarzschild radius of ten billion meters. The

[2]We need to distinguish direct emission of our new horizon thickness Hawking radiation from indirect emission. All zero rest mass bosons (transverse polarized far field photons and gravitons in Glauber macro-quantum coherent states of maximally sharp amplitude and phase - displaced Gaussians in their phase spaces) have infinite L, and therefore, zero direct emission rate in contrast to the indirect emission of photons from escaping electric charges and indirect emission of gravitons from rapidly decaying Planck scale mini black holes at the horizon.

peak black body frequency will be $\sim 10^{20}$ Hz, at the boundary between the values for X-rays and Gamma rays.

The HFGW power flux hitting the Earth will be[3]

$$f_{gravity} \approx 4 \times 10^{-5} \frac{hc^2}{4\pi r^2 L^2} \approx 1.7 \times 10^3 1 \frac{W}{m^2} \tag{A.18}$$

In contrast, if we were to suppose that the cutoff is the Compton wavelength of the electron $2.4 \times 10^{-12}$ m, the peak black body photon wavelength would be $\sim 30$ cm corresponding to 1000 MHz. Since, as mentioned above, Hawking's basic argument invokes virtual electron-positron pairs stuck on the horizon as hovering static objects with enormous proper accelerations, hence a very hot Unruh temperature that provides enough energy from the gravitational field to make a plasma of real electron-positron pairs, it seems then plausible to use the electron Compton wave length as the 'high-pass filter' (coordinate thickness IR cutoff) for the electromagnetic Hawking radiation. This is $10^{22}$ times larger than the Planck length and it gives reasonable predictions for the photon flux at Earth as well for the peak frequency of the newly predicted component of the Hawking radiation.

$$f(L_C) \approx 1.4 \times 10^{-5} \frac{hc^2}{4\pi r^2 L_C^2} \approx 10^{18} \frac{W}{m^2} \tag{A.19}$$

In the case of Sgr A* (our GC BH), there is a mysterious absence of the high energy emission (X-rays and UV radiation) often observed from active galactic nuclei. The values are summarized in Table A.1.

These examples strongly suggest that the photon flux at Earth will not be detectable by gravitational waves detectors like LISA, that have a sensitivity for frequencies in the 0.1 mHz-0.1 Hz range (Prince et al. 2006), though the graviton flux perhaps will be detected if HFGW detectors can be built. On the other hand, the gravity wave emissions near the black hole horizons from their quantum thickness might have observable effects from scatterings with matter in the accretion disks.

The coupling of the hotter horizon quantum thickness temperature with the cooler orthodox Hawking surface temperature is a Carnot heat engine capable to doing work, with a maximal efficiency approaching $100\%$,

$$\zeta = \frac{W}{Q_{hot}} = 1 - \frac{T_{cold}}{T_{hot}} = 1 - \frac{\frac{1}{\sqrt{A}}}{\frac{1}{\sqrt{L\sqrt{A}}}} \approx 1 - \sqrt{\frac{L}{\sqrt{A}}} \tag{A.20}$$

**Evaporation time**

When including the contribution to the emitted radiation from the quantum thickness of the black holes the evaporation time becomes smaller. We only consider non-rotating Schwarzschild

[3]We do not take into account Eq. 3.15 (Boughn & Rothman 2006) for absorption of gravity waves to matter give an estimate in hydrogen However, that estimate relies on the dipole approximation, which is not adequate for $\sim 10^{20}$ Hz gravity waves.

Table A.1: Black hole flux and peak frequency (P) for radiation coming from different mass sources, considering three different values for the quantum thickness, Planck length, Compton length and the weak scale length respectively

| Label | $r_s$ | $f(L_p)$ | $P(L_p)$ | $f(L_c)$ | $P(L_c)$ | $f(L_{ws})$ | $P(L_{ws})$ |
|---|---|---|---|---|---|---|---|
| | $m$ | $W/m^2$ | Hz | $W/m^2$ | Hz | $W/m^2$ | Hz |
| $1M_\odot$ | $2.95 \times 10^3$ | $1.7 \times 10^{31}$ | $10^{24}$ | $7 \times 10^{-16}$ | $10^{12}$ | $0.4$ | $1$ |
| Sgr $A^*$ | $1.2 \times 10^{10}$ | $10^{18}$ | $10^{20}$ | $4.6 \times 10^{-29}$ | $10^9$ | $2.7 \times 10^{-14}$ | $10^{13}$ |
| Hubble | $1.3 \times 10^{26}$ | $8.9 \times 10^{13}$ | $10^{15}$ | $3.9 \times 10^{-33}$ | 17 | $2.3 \times 10^{-18}$ | $8 \times 10^5$ |

black holes here to show the basic new physics in as simplest a setting as possible. In Hawking's description, where he neglected the quantum gravity fluctuations in the position $g_{00} = 0$ of the black hole horizon we have:

$$\frac{dM}{dt} = \frac{a}{L^2} + \frac{b}{M^2} \tag{A.21}$$

Hawking's term is $b/M^2$ which is analogous to Einstein's B-coefficient for stimulated emission of horizon surface vibrational quanta with distant observer gravity redshifted black body radiation of very low temperature

$$T_H \approx \frac{hc}{A^{1/2}k_B} \tag{A.22}$$

where A is the area entropy of the black hole horizon.

Our new quantum gravity zero point vacuum term, analogous to Einstein's A-coefficient for spontaneous emission is $a/L^2$ with distant observer gravity redshifted relatively higher temperature:

$$T_S \approx \frac{hc}{LA^{1/2}k_B} \tag{A.23}$$

The solution of the Eq. (A.21) is:

$$\tau = \int \frac{1}{\frac{a}{L^2} + \frac{b}{M^2}} dM \tag{A.24}$$

that is:

$$\tau = 10^{69} \int \frac{1}{\frac{1}{L^2} + \frac{1}{r_s^2}} dr_s \tag{A.25}$$

with the solution:

$$\tau = 10^{69} L^2 (r_s - Ltan^{-1}(\frac{r_s}{L}) \tag{A.26}$$

**Dark Energy Prediction**

With respect to the black holes, we are outside observer-independent black hole horizons so that the inverse square law applies. In contrast, we are inside our observer-dependent cosmological horizons at the exact center where the Hawking radiation from it converges. Curiously, using the asymptotic area $\sim 10^{52}\ m^2$ of our future dark energy de Sitter horizon, and $L \sim 10^{35}$ m for indirect Hawking-Unruh horizon thickness, gravity waves emission corresponds very roughly to a peak blackbody wavelength

$$\lambda_{peak} \approx 10^{13-17.5} m \approx 1/3 \times 10^{-4} m \approx 3 \times 10^{12} Hz^{-1} \tag{A.27}$$

with Stefan-Boltzmann HFGW energy density

$$\frac{hc}{{L_p}^2 A} \approx 10^{-8} J/m^3 \approx 10^{-28} g/cm^3 \tag{A.28}$$

corresponding for a $k = 0$ flat universe to the dark energy density. It is important to stress that these are black body gravity waves not electromagnetic waves. However, dark energy comes from virtual bosons with $w = -1$ negative quantum pressure causing the expansion of 3D space to accelerate rather than slow down. Blackbody radiation, in contrast, has $w = +1/3$ positive quantum pressure causing gravity universal attraction rather than anti-gravity universal repulsion. Nevertheless, the Unruh effect's Bogoliubov transformation says that the Local Inertial Frame (LIF) observer sees virtual bosons with $w = -1$ whilst the physically coincident LNIF observer sees real blackbody bosons with $w = +1/3$. We are only concerned with the distant observer far away from the horizon, which limits to a LIF for both the Schwarzschild black hole and the de Sitter cosmological toy model metrics. So this is a clue as to what may really be going on, ratherthan a rigorous argument.

Even more problematical is that we, most likely, must use classical causality in describing where the past and future light cones intersect both the past particle and future event cosmological horizons of the detector. One can see that the area of our past particle horizon is smaller than the area of our future event horizon at the corresponding light cone intersections. The ball park numerical agreement with the actually observed dark energy density from Type 1a supernovae anomalous redshift data in our past light cones will only work if the gravity waves that are advanced Wheeler-Feynman waves propagating back to us along our future light cone.

This is reminiscent of Yakir Aharonov's (Aharonov, Albert & Vaidman 1988) 'destiny' post-selected quantum waves that interfere with pre-selected 'history waves' to form the 'weak measurements' in the intermediate time. John Cramer's (Cramer 1986) 'transactional interpretation' also uses advanced quantum waves. Of course, quantum waves for subluminal massive particles travel outside the classical light cones. Furthermore, the hologram conjecture is that a conformal 2D + 1 anyonic fractional quantum statistical heat resistant topological computer quantum

field theory on both our past and future cosmological horizons provide a 3D + 1 quantum gravity geometrodynamics in the interior bulk of this causal diamond observable piece of a 'Level 1' multiverse in the sense of Max Tegmark's (Tegmark 2009) classification.

Thus, it is plausible that the dark energy density is an advanced Wheeler-Feynman hologram influence and that we live in a kind of virtual 'weak measurement' computed reality. Fred Hoyle (Hoyle 1984) anticipated this picture in his book 'The Intelligent Universe'. On the other hand, the hologram conjecture predicts that the Planck area pixels on our past and future cosmological quantum computing horizon screens have Fermi-scale voxels (Susskind 2008). This would mean a strong short-range Abdus Salam (Salam & Strathdee 1976) f-gravity 'quantum foam' which may be disproved by the high-energy gamma ray experiments looking for violations of Lorentz invariance in deviations from the special relativity mass shell constraint. If so, that would disprove the hologram conjecture [4].

**Conclusions**

If the event horizon has a quantum thickness L, there is a qualitative change in the total power. The original Hawking result can be derived quite simply intuitively in the spirit of the old quantum theory of Bohr and later de Broglie, i.e. simply fitting quantum waves into finite box or in this case, a two dimensional spherical shell. Hawking's result above can be pictured as random surface waves in a virtual electron-positron plasma, combined with the Unruh effect. This describes the pairs stuck to the horizon as having huge proper acceleration proportional to the Hawking-Unruh temperature.

The flux coming to earth from the black hole at the center of our galaxy is too small to be sensed by our present-day gravitational waves detectors.

Furthermore, our new term added to the Hawking's equation has the same functional dependence as the dark energy whose anti-gravity is accelerating the expansion of space. Furthermore, when we insert the Planck length $10^{-33}$ cm for L and the square of the cosmological Hubble radius $\approx 10^{28}$ cm we get the right ballpark number for the observed dark energy density from the anomalous redshifts of Type 1a Supernovae. However, the only way that numerical coincidence makes sense, is if the dark energy is advanced Wheeler-Feynman radiation back from our future de Sitter cosmological event horizon with the mirror image Feynman boundary condition that advanced waves propagate negative energy forward in time.

[4]The above is for advanced black body gravity waves from our future cosmological horizon. If we consider the advanced black body electromagnetic waves from the electron-positron plasma confined within a Compton wavelength of our future cosmological horizon, the peak wavelength is $\sim 10^7\ m \sim 10\ Hz^{-1}$ in the same range as our EEG human brain waves relevant to our waking consciousness and other vital brain activity.

# Acknowledgements

Firstly, I would like to thank the members of my committee.

I am profoundly grateful to Peter L. Biermann for the enormous help, advice, assistance and continuous encouragement during the writing of my thesis. Our many days of discussions on various scientific topics have generated many of the ideas presented in this thesis. My special thanks are due to Joanna Biermann for her understanding and her motivational support.

I appreciate immensely the ongoing help of Michael Joyce, his comments and suggestions. I am very thankful for organizing my visits to LPNHE, where we had many stimulating discussions.

I would like to express my gratitude to Georges Meylan for his interest in my work and for his encouraging feedback.

I am extremely grateful to Héctor J. de Vega and Norma G. Sanchez for inviting me to the Chalonge meetings and for their interest in my work. These meetings provided me with a unique opportunity to share my work and to exchange ideas with many experts in my field.

In this laboratory of ideas I had the immense pleasure and honour of meeting Héctor de Vega, a distinguished scientist and a remarkable human being. His insightful feedback meant a lot to me and his enthusiasm was always inspiring. Sadly, he left us way too soon - a tremendous loss for the scientific community. He will be missed.

I am in debt to Norma Sanchez for her inestimable help and stimulating discussions. Her extraordinary support, as well as Héctor's kept me motivated throughout my Ph.D. journey.

Extensive discussions with Daniel Boyanovsky, Claudio Destri and Paolo Salucci were extremely valuable for this work and I highly appreciate them.

I would like to convey my sincere thanks to Andrzej Drukier, Christopher Tully, Casey Watson and many others for their appreciative feedback.

For his technical help in juggling with codes I want to thank Yves Revaz. I am also grateful to Doug Potter and Joachim Stadel for their instrumental help in coding and for the many ideas connected to this work.

I am thankful to Thierry Courvoisier for insightful discussion and a great course in high-energy astrophysics. My gratitude is extended to Stéphane Udry for his support.

Many thanks are due to the patient, helpful and resourceful in crisis management administrative staff at the Observatory, Livia Schnell, Myriam Burgener, Chantal Tacoy, Françoise Page, Claire Schatzmann.

I am also grateful to the technical department, especially to Olivier Genevay and Gilles Simond for their assistance and for providing me with a working laptop - essential for writing my thesis.

Last but not least, I would like to thank Mircea Rusu, my first astrophysics professor, for his many enthusiastic lessons in life and the universe.

# Rolling Credits

Many thanks to the many people who made a difference:

My mother for being my pillar of strength amidst chaos!

My parents and grandparents for providing me with an education that no university can provide;

Björn, my best friend, for saving me whenever needed, for putting up with a lot of drama and for his help, without which this work would not have been completed - I hope the investment will pay off;

Jack Sarfatti, my amazing friend, for saving physics, for his constant reminders of why I began this journey and for his fascinating ideas 'back to the future' and into the 'destiny matrix';

Lynn Picknett and Clive Prince, my fantastic friends and fellow travellers down the rabbit hole, for taking care of me after being hit by a car and for their ever-elevating humour and brilliance.

Bonnie Ora Sherk, my inspiring friend who helped me navigate over troubled waters for her insights and adversity training;

Dr. Mohamad Morad for fixing my broken ankle so I can walk again and my physiotherapist Isaline Henry for making me dance again;

Daniel Gitnacht for his valuable support and advice;

Emil Rivera-Thorsen, who sent me a video of the last 17 minutes from Tarantino's 'Death Proof' while I was writing my thesis - it kept me focused and inspired;

Elisa and Leo, Stefano, Monica, Tina, Kat, Csaba, Jean, Tilman, Lea, Claudia and Richard for their help, friendship and advice - thank you so much!

And...my Dragons, always there to be.

The Soundtrack for this work has been mostly NIGHTWISH and a weird and wicked combination of (amongst others) HIM, Muse, Leonard Cohen, Wilco, The Gaslight Anthem, Editors, Elbow, Meat Loaf, Wagner, Beethoven, The Baseballs, Verdi, One Republic, Neil Diamond, The National, Alanis Morissette, Hozier, Florence and the Machine, U2, Within Temptation and Hans Zimmer's Pirates of the Caribbean - I know, right?!

# Bibliography


Abazajian, K., Koushiappas, S. M., 2006, Phys. Rev. D, 74, 023527

Abazajian, K. 2006, Phys. Rev. D, 73, 063506

Abel, T., Bryan, G. L., Norman, M. L. 2002, Science, 295, 93

Abel, T., Hahn, O., Kaehler, R., 2012, MNRAS, 427, 61

Aharonov, Y, Albert, D. Z., Vaidman, L., 1988, Phys. Rev. Lett., 60, 1351

Alard C., Colombi S., 2005, MNRAS, 359, 123

Albrecht, A., Steinhardt, P. J., 1982, Phys. Rev. Lett., 48, 1220

Alexeyev, E. N., Alexeyeva, L. N., Krivosheina, I. V., Volchenko, V. I., 1988, Phys. Lett. B, 205, 209

Amorisco, N. C., Evans, N. W., 2012, MNRAS, 419, 184

Anderhalden, D., Diemand, J., Bertone, G., Macciò, A. V., Schneider, A., 2012, JCAP, 10, 47

Angulo, R. E., Hahn, O., Abel, T., 2013, MNRAS, 434, 3337

Aprile, E., Alfonsi, M., Arisaka, K., Arneodo, F., Balan, C., Baudis, L., Bauermeister, B., Behrens, A.,Beltrame, P., Bokeloh, K., Brown, E., Bruno, G., Budnik, R., Cardoso, J. M. R., Chen, W.-T., Choi, B., Cline, D., Colijn, A. P., Contreras, H., Cussonneau, J. P., Decowski, M. P., Duchovni, E., Fattori, S., Ferella, A. D., Fulgione, W., Gao, F., Garbini, M., Ghag, C., Giboni, K.-L., Goetzke, L. W., Grignon, C., Gross, E., Hampel, W., Kaether, F., Kish, A., Lamblin, J., Landsman, H., Lang, R. F., Le Calloch, M., Levy, C., Lim, K. E., Lin, Q., Lindemann, S., Lindner, M., Lopes, J. A. M., Lung, K., Marrodán Undagoitia, T., Massoli, F. V., Melgarejo Fernandez, A. J., Meng, Y., Molinario, A., Nativ, E., Ni, K., Oberlack, U., Orrigo, S. E. A., Pantic, E., Persiani, R., Plante, G., Priel, N., Rizzo, A., Rosendahl, S., dos Santos, J. M. F., Sartorelli, G., Schreiner, J., Schumann, M., Scotto Lavina, L., Scovell, P. R., Selvi, M., Shagin, P., Simgen, H., Teymourian, A., Thers, D., Vitells, O., Wang, H., Weber, M., Weinheimer, C., 2012, Phys. Rev. Lett., 109, 181301

Asaka, T., Laine, M., Shaposhnikov, M., 2007, JHEP, 01, 91

Asztalos, S. J., Carosi, G., Hagmann, C., Kinion, D., van Bibber, K., Hotz, M., Rosenberg, L. J., Rybka, G., Hoskins, J., Hwang, J., Sikivie, P., Tanner, D. B., Bradley, R., Clarke, J., ADMX Collaboration, 2010, Phys. Rev. Lett., 104, 041301

Atkins, P., Friedman, R., 2005, Molecular Quantum Mechanics, Oxford University Press

Avila-Reese V., Colín P., Valenzuela O., D'Onghia E., Firmani C., 2001, ApJ, 559, 516

Barnes, J. E., 2002, MNRAS, 333, 481

Baugh, C. M., 2006, Reports on Progress in Physics, 69, 3101

Beane, S. R., Davoudi, Z., Savage, M. J., 2014, EPJA, 50, 9

Bekenstein, J. D., 1973a, Phys. Rev. D, 7, 949

Bekenstein, J. D., 1973b, Phys. Rev. D, 7, 2333

Bentley, J. L., 1979, IEEE Transactions on Software Engineering, SE-5(4), 333

Benson, A. J., Kamionkowski, M., Hassani, S. H., 2005, MNRAS, 357, 847

Benson, A. J., 2008, MNRAS, 388, 1361

Benson, A. J., 2010, Phys. Rep., 495, 33

Bergström, L., 2012, Annalen der Physik, 524, 479

Bernabei, R., Belli, P., Cappella, F., Caracciolo, V., Cerulli, R., Dai, C. J., d'Angelo, A.,d'Angelo, S., Di Marco, A., He, H. L., Incicchitti, A., Kuang, H. H. and Ma, X. H., Montecchia, F., Sheng, X. D.,Wang, R. G., Ye, Z. P., 2015, EPJWC Proc., 95, 3001

Bertone, G., Hooper, D., Silk, J., 2005, Phys. Rep., 405, 279

Bertone, G., 2010, Particle Dark Matter: Observations, Models and Searches, Cambridge University Press

Bertschinger E., 1985, ApJS, 58, 39

Bertschinger, E., 1995, COSMICS software release, arXiv:astro-ph/9506070

Bertschinger, E., 2001, ApJS, 137, 1

Biermann, P. L., Kusenko, A., 2006, Phys. Rev. Lett., 96, 091301

Biermann, P. L., Harms, B. C., 2012, arXiv:1205.4016

Biermann, P. L., Harms, B. C., 2013, arXiv:1305.0498

Bilenky, S., 2010, Lecture notes in physics, Springer, 817

Binney J., 2004, MNRAS, 350, 939

de Blok, W. J. G., McGaugh, S. S., Bosma, A., Rubin, V. C., 2001, ApJL, 552, L23

Blumenthal, G.R., Faber, S.M., Primack, J.R., Rees, M.J., 1984, Nature, 311, 517

Bode, P., Ostriker, J. P., Turok, N., 2001, ApJ, 556, 93

Boehm, C. B., Dolan, M. J., McCabe, C., 2012, JCAP, 12, 27

Boi, L., 2011, The Quantum Vacuum, John Hopkins University Press

Bond, J. R., Efstathiou, G., Silk, J., 1980, Phys. Rev. Lett., 45

Bond, J. R., Centrella, J., Szalay, A. S., Wilson, J. R., 1984, Dark Matter And Shocked Pancakes, NATO ASI C, 117, 87

Bond, J. R., Szalay, A. S., Turner, M. S., 1982, Phys. Rev. Lett., 48, 1636

Bond, J. R., Cole, S., Efstathiou, G., Kaiser, N., 1991, ApJ, 379, 440

Bond, J. R., Kofman, L., Pogosyan, D., 1996, Nature, 380, 603

Bottino, A., Fornengo, N., 1998, Dark matter and its particle candidates, Non-accelerator particle astrophysics, Proc., Trieste, 241

Boughn, S., Rothman, T., 2006, Classical and Quantum Gravity, 23, 5839

Bournaud, F., Jog, C. J., Combes, F., 2005, A&A, 437, 69

Bower, R. G., 1991, MNRAS, 248, 332

Boyarsky, A., Lesgourgues, J., Ruchayskiy, O., Viel, M., 2009, JCAP, 5, 12

Boyarsky, A., Ruchayskiy, O., Shaposhnikov, M., 2009a, Annual Review of Nuclear and Particle Science, 59, 191

Boyarsky, A., Ruchayskiy, O., Iakubovskyi, D., 2009b, JCAP, 3, 5

Boyarsky, A., Ruchayskiy, O., Iakubovskyi, D., France, J., 2014, Phys. Rev. Lett., 113, 251301

Boylan-Kolchin, M., Bullock, J. S., Kaplinghat, M., 2011, MNRAS, 415, 40

Bromm, V., Coppi, P. S., Larson, R. B., 2002, ApJ, 564, 23

Brownstein, J. R., Moffat, J. W., 2006, ApJ, 636, 721

Buchmüller, W., Covi, L., Hamaguchi, K., Ibarra, A., Yanagida, T., 2007, JHEP, 03, 037

Bulbul, E., Markevitch, M., Foster, A., Smith, R. K., Loewenstein, M., Randall, S. W., 2014, ApJ, 789, 13

Caramete, L. I., Biermann, P. L., 2011, arXiv:1107.2244

Carter, D., Allen, D. A., Malin, D. F., 1982, Nature, 295, 126

Centrella, J., Melott, A. L., 1983, Nature, 305, 196

Centrella, J. M., Gallagher III, J. S., Melott, A. L., Bushouse H. A., 1988, ApJ, 333, 24

Challinor, A., Lewis, A., 2005, Phys. Rev. D, 71, 103010

Chandrasekhar, S., 1942, Principles of Stellar Dynamics, The University of Chicago Press

Cirkovic, M. M., 2012, The Astrobiological Landscape, Cambridge University Press

Cole, D. R., Dehnen, W., Wilkinson, M. I., 2011, MNRAS, 416, 1118

Colless, M., Dalton, G., Maddox, S., Sutherland, W., Norberg, P., Cole, S., Bland-Hawthorn, J., Bridges, T., Cannon, R., Collins, C., Couch, W., Cross, N., Deeley, K., De Propris, R., Driver, S. P., Efstathiou, G., Ellis, R. S., Frenk, C. S., Glazebrook, K., Jackson, C., Lahav, O., Lewis, I., Lumsden, S., Madgwick, D., Peacock, J. A., Peterson, B. A., Price, I., Seaborne, M., Taylor, K., 2001, MNRAS, 328, 1039

Colín, P., Avila-Reese, V., Valenzuela, O., 2000, ApJ, 542, 622

Colín, P., Valenzuela, O., Avila-Reese, V., 2008, ApJ, 673, 203

Colombi, S., Dodelson, S., Widrow, L. M., 1996, ApJ, 458, 1

Cooper, A. P., Cole S., Frenk, C. S., White, S. D. M., Helly J., Benson, A. J., De Lucia, G., Helmi, A., et al., 2010, MNRAS, 406, 744

Cramer, J. G., 1986, Rev. Mod. Phys., 58, 647

Dalcanton, J. J., Hogan, C. J., 2001, ApJ, 561, 35

Dasgupta, B., Beacom, J. F., 2011, Phys. Rev. D, 83, 113006

Davies, P. C. W., 1975, Jr. Phys. A, 8, 609

Dehnen, W., 2001, MNRAS, 324, 273

Dekel, A., Aarseth, S. J., 1984, ApJ, 283, 1

Dekel, A., Ostriker, J. P., 1999, Formation of structure in the universe, Cambridge University Press

Destri, C., 2014, Phys. Rev. D, 90, 123531

Destri, C., de Vega, H. J., Sanchez, N. G., 2013, New Astronomy 22, 39

Diemand, J., Moore, B., Stadel, J., 2004, MNRAS, 353, 624

Diemand, J., Zemp, M., Moore, B., Stadel, J., Carollo, M., 2005, MNRAS, 364, 665

Diemand, J., Moore, B., 2010, Particle Dark Matter: Observations, Models and Searches, Cambridge University Press, 14

Diemand, J., Moore, B., 2011, Advanced Science Letters, 4, 297

Dodelson, S., Widrow, L. M., 1994, Phys. Rev. Lett., 72, 17

Dolgov, A. D., Hansen, S. H., 2002, Astropart. Phys., 16, 339

Donato, F., Fornengo, N., Scopel, S., 1998, Astropart. Phys., 247

Drukier, A., Stodolsky, L., 1984, Phys. Rev. D, 30

Drukier, A. K., Freese, K., Spergel, D. N., 1986, Phys. Rev. D, 33, 3495

Drukier, A., Freese, K., Lopez, A., Spergel, D., Cantor, C., Church, G., Sano, T., 2012, arXiv:1206.6809

Dubinski, J., Carlberg, R. G., 1991, ApJ, 378, 496

Efstathiou G., Davis M., White S. D. M., Frenk C. S., 1985, ApJS, 57, 24

Eggen, O. J., Lynden-Bell, D. Sandage, A. R., 1962, ApJ, 136, 748

Einasto, J., 1965, Trudy Inst. Astrofiz. Alma-Ata, 51, 87

Eisenstein, D. J., Hu, W., 1999, ApJ, 511, 5

Eke, V. R., Cole, S., Frenk, C. S., Navarro, J. F., 1996, MNRAS, 281, 703

Eke, V. R., Navarro, J. F., Steinmetz, M., 2001, ApJ, 554, 114

Erken, O., Sikivie, P.,Tam, H., Yang, Q., 2012, Phys. Rev. D, 85, 063520

Ewald, P. P., 1921, Annalen der Physik, 369, 253

Feng, J. L., Grivaz, J. F., Nachtman, J., 2010, Rev. Mod. Phys., 82, 699

Fialkov, A., 2014, International Journal of Modern Physics D, 23,30017

Fillmore J. A., Goldreich P., 1984, ApJ, 281, 1

Flores, R. A., Primack, J. R., 1994, ApJL, 427, L1

Fontana, G., 2006, STAIF, 813, 1402

Freese, K., 2014, The cosmic cocktail: three parts dark matter, Princeton University Press

Frenk C. S., White S. D. M., Davis M., 1984, Elementary Particles and the Large-Scale Structure of the Universe - Short Contributions, Setti G., Van Hove L., 257

Fridman A. M., Poliachenko V. L., 1984, Physics of gravitating systems. II - Nonlinear collective processes: Nonlinear waves, solitons, collisionless shocks, turbulence. Astrophysical applications

Fulling, S. A., 1973, Phys. Rev. D, 7, 2850

Fuller, G. M. and Kishimoto, C. T. and Kusenko, A., 2011, arXiv:1110.6479

Gao, L., Theuns, T., 2007, Science, 317,1527

Gao, L., Navarro, J. F., Cole, S., Frenk, C. S., White, S. D. M., Springel, V.,Jenkins, A., Neto, A. F., 2008, MNRAS, 387, 536

Gao, L. and Theuns, T. and Springel, V., 2015, MNRAS, 450, 45

Gardini, A., Bonometto, S. A., Murante, G., 1999, ApJ, 524, 510

Geller, M. J.,Huchra, J. P., 1989, Science, 246, 897

Geringer-Sameth, A., Walker, M. G., Koushiappas, S. M., Koposov, S. E., Belokurov, V., Torrealba, G., Evans, N. W., 2015, Phys. Rev. Lett., 115, 081101

Gheller, C., Moscardini, L., Pantano, O., 1996, MNRAS, 283, 1184

Goerdt, T., Moore, B., Read, J. I., Stadel, J., Zemp, M., 2006, MNRAS, 368, 1073

Goerdt, T., Moore, B., Read, J. I., Stadel, J., 2010, ApJ, 725, 1707

Goldman, I., Aharonov, Y., Alexander, G., Nussinov, S., 1988, Phys. Rev. Lett., 60, 1789

Goodman, M. W., Witten, E., 1985, Phys. Rev. D, 31, 3059

Gott, III, J. R., Jurić, M., Schlegel, D., Hoyle, F., Vogeley, M., Tegmark, M., Bahcall, N., Brinkmann, J., 2005, ApJ, 624, 463

Götz, M.,Sommer-Larsen, J., 2002, Ap&SS, 281, 415

Götz, M., Sommer-Larsen, J., 2003, Ap&SS, 284, 341

Governato, F., Willman, B., Mayer, L., Brooks, A., Stinson, G., Valenzuela, O., Wadsley, J., Quinn, T., 2007, MNRAS, 374, 1479

Governato, F., Brook, C., Mayer, L., Brooks, A., Rhee, G., Wadsley, J., Jonsson, P., Willman, B., Stinson, G., Quinn, T., Madau, P., 2010, Nature, 463, 203

Governato, F., Weisz, D. Pontzen, A., Loebman, S., Reed, D., Brooks, A. M., Behroozi, P., Christensen, C., Madau, P., Mayer, L., Shen, S., Walker, M., Quinn, T., Keller, B. W., Wadsley, J., 2015, MNRAS, 448, 792

Guedes, J., Callegari, S., Madau, P., Mayer, L., 2011, ApJ, 742, 76

Gunn, J. E., Tinsley, B. M., 1975, Nature, 257, 454

Guth, A. H., 1981, Phys. Rev. D, 23, 347

Hagiwara, K., Hikasa, K., Nakamura, K., Tanabashi, M. Aguilar-Benitez, M., Amsler, C., Barnett, R. M., Burchat, P. R., Carone, C. D., Caso, C., Conforto, G.,Dahl, O., Doser, M., Eidelman, S., Feng, J. L., Gibbons, L., Goodman, M., Grab, C., Groom, D. E., Gurtu, A. Hayes, K. G. Herna'Ndez-Rey, J. J., Honscheid, K., Kolda, C., Mangano, M. L., Manley, D. M., Manohar, A. V., March-Russell, J., Masoni, A., Miquel, R., Mönig, K., Murayama, H., Navas, S., Olive, K. A., Pape, L.,Patrignani, C., Piepke, A., Roos, M., Terning, J., Törnqvist, N. A., Trippe, T. G., Vogel, P., Wohl, C. G.,Workman, R. L., Yao, W. M., Armstrong, B., Gee, P. S., Lugovsky, K. S., Lugovsky, S. B., Lugovsky, V. S., Artuso, M., Asner, D., Babu, K. S.,Barberio, E., Battaglia, M., Bichsel, H., Biebel, O., Bloch, P., Cahn, R. N., Cattai, A., Chivukula, R. S., Cousins, R. D., Cowan, G.,Damour, T., Desler, K., Donahue, R. J., Edwards, D. A., Elvira, V. D., Erler, J., Ezhela, V. V., Fasso', A., Fetscher, W., Fields, B. D., Foster, B., Froidevaux, D., Fukugita, M., Gaisser, T. K., Garren, L., Gerber, H. J., Gilman, F. J., Haber, H. E., Hagmann, C., Hewett, J., Hinchliffe, I., Hogan, C. J., Höhler, G., Igo-Kemenes, P., Jackson, J. D., Johnson, K. F., Karlen, D., Kayser, B.,Klein, S. R., Kleinknecht, K., Knowles, I. G., Kreitz, P., Kuyanov, Y. V., Lua, R., Langacker, P., Littenberg, L., Martin, A. D.,Nakada, T., Narain, M., Nason, P., Peacock, J. A., Quinn, H. R., Raby, S., Raffelt, G., Razuvaev, E. A., Renk, B., Roli, L., Ronan, M. T., Rosenberg, L. J., Sachrajda, C. T., Sa, A. I., Sarkar, S., Schmitt, M., Schneider, O., Scott, D., Seligman, W. G., Shaevitz, M. H., Sjöstr, T., Smoot, G. F., Spanier, S., Spieler, H., Spooner, N. J. C., Srednicki, M., Stahl, A., Stanev, T., Suzuki, M. Tkachenko, N. P., Valencia, G., van Bibber, K., Vincter, M. G., Ward, D. R., Webber, B. R., Whalley, M., Wolfenstein, L., Womersley, J., Woody, C. L., Zenin, O. V., 2002, Phys. Rev. D, 66, 010001

Hahn, O., Abel, T., 2011, MNRAS, 415, 2101

Hahn, O., Abel, T., Kaehler, R., 2013, MNRAS, 434, 1171

Hahn, O., Angulo, R. E., 2015, arXiv:1501.01959

Hansen, S. H., Lesgourgues, J., Pastor, S., Silk, J., 2002, MNRAS, 333, 546

Hawking, S. W., 1971, Phys. Rev. Lett., 26, 1344

Hawking, S. W., 1974, Nature, 248, 30

Hawking, S. W., 1975, Comm. Math. Phys., 43, 199

Heitmann, K., Lukić, Z., Fasel, P., 2008, Computational Science and Discovery, 1, 1, 015003

Helly, J. C., Cole, S., Frenk, C. S., Baugh, C. M., Benson, A., Lacey, C., 2003, MNRAS, 338, 903

Hénon, M., 1973, Saas-Fee Advanced Course 3: Dynamical Structure and Evolution of Stellar Systems, Swiss Society of Astronomy and Astrophysics, 183

Herant, M., Colgate, S. A., Benz, W., Fryer, C., 1997, Los Alamos Science, 25, 64

Hernquist, L., 1987, ApJS, 64, 715

Hernquist, L., Quinn, P. J., 1988, ApJ, 331, 682

Hernquist, L., Quinn, P. J., 1989, ApJ, 342, 1

Hernquist, L., Katz, N., 1989, ApJ, 70, 419

Hernquist, L., Spergel, D. N., Heyl, J. S., 1993, ApJ, 416, 415

Hinshaw, G., Larson, D., Komatsu, E., Spergel, D. N., Bennett, C. L., Dunkley, J., Nolta, M. R., Halpern, M., Hill, R. S.,Odegard, N., Page, L., Smith, K. M., Weiland, J. L., Gold, B., Jarosik, N., Kogut, A., Limon, M., Meyer, S. S., Tucker, G. S., Wollack, E., Wright, E. L., 2013, ApJS, 208, 19

Hobbs, A., Read, J., Agertz, O., Iannuzzi, F., Power, C., 2015, arXiv:1503.02689

Hogan, C. J., 1999, ApJ, 527, 42

Hogan, C. J., Dalcanton, J. J., 2000, Phys. Rev. D, 62, 063511

Hopkins, P. F., Croton, D., Bundy, K., Khochfar, S., van den Bosch, F., Somerville, R. S., Wetzel, A., Keres, D., Hernquist, L., Stewart, K., Younger, J. D., Genel, S., Ma, C., 2010, ApJ, 724, 915

Hoyle, F., 1984, The Intelligent Universe, Holt, Rinehart & Winston, New York

Huang, K., 1987, Statistical Mechanics, John Wiley & Sons

Hubble, E., 1926, ApJ, 64, 321

Hubble, E., 1929, Proc. Nat. Acad. Sci., 15, 168

The IceCube Collaboration, Aartsen, M. G., Abraham, K., Ackermann, M., Adams, J., Aguilar, J. A., Ahlers, M., Ahrens, M., Altmann, D., Anderson, T., et al., 2015, PoS ICRC2015, 23

Jardel, J., Gebhardt, K., 2012, ApJ, 746, 89

Jones, T. W., 1994, Supernova Neutrinos: A Summary, Philosophical Transactions: Physical Sciences and Engineering, Royal Society, 346, 85

Joyce, M., Marcos, B., Baertschiger, T., 2009, MNRAS, 394, 751

Jungman, G., Kamionkowski, M., Griest, K., 1996, Phys. Rev. D, 267, 195

Kaufmann, T., Mayer, L., Wadsley, J., Stadel, J., Moore, B., 2007, MNRAS, 375, 53

Khlopov, M. Y., 2006, JETP Lett., 83, 1

Khlopov, M. Y., Kouvaris, C., 2008, Phys. Rev. D, 78, 065040

Kim, J.-h., Abel, T., Agertz, O., Bryan, G. L., Ceverino, D., Christensen, C., Conroy, C., Dekel, A., Gnedin, N. Y., Goldbaum, N. J., Guedes, J., Hahn, O., Hobbs, A., Hopkins, P. F., Hummels, C. B., Iannuzzi, F., Keres, D., Klypin, A., Kravtsov, A. V., Krumholz, M. R., Kuhlen, M., Leitner, S. N., Madau, P., Mayer, L.,Moody, C. E., Nagamine, K., Norman, M. L., Onorbe, J., O'Shea, B. W., Pillepich, A., Primack, J. R., Quinn, T., Read, J. I., Robertson, B. E.,Rocha, M., Rudd, D. H., Shen, S., Smith, B. D., Szalay, A. S., Teyssier, R., Thompson, R., Todoroki, K., Turk, M. J., Wadsley, J. W., Wise, J. H.,Zolotov, A., AGORA Collaboration29, 2014, ApJS, 210, 14

Klypin, A., Kravtsov, A. V., Valenzuela, O., Prada, F. 1999, ApJ, 522, 82

Knebe, A., Devriendt, J. E. G., Gibson, B. K., Silk, J., 2003, MNRAS, 345, 1285

Knebe, A., Arnold, B., Power, C., Gibson, B. K., 2008, MNRAS, 386, 1029

Komatsu, E., Smith, K. M., Dunkley, J., & The WMAP Team, 2011, ApJS, 192, 18

Kormendy, J., Drory, N., Bender, R., Cornell, M. E., 2010, ApJ, 723, 54

Kormendy, J., 2016, Galactic Bulges, Springer, 418, 431

Kravtsov, A. V., Gnedin, O. Y., Klypin, A. A., 2004, ApJ, 609, 482

Kuzio de Naray, R., McGaugh, S. S., Mihos, J. C., 2009, ApJ, 692, 1321

Kuzio de Naray, R., Martinez, J. D., Bullock, J. S., Kaplinghat, M., 2010, ApJL, 710, L161

Kuzio de Naray, R., Kaufmann, T., 2011, MNRAS, 414, 3617

Lacey, C., Cole, S., 1993, MNRAS, 262, 627

Larson, R.B., 1975, MNRAS, 173, 671

Lello, L., Boyanovsky, D., 2015, Phys. Rev. D, 91, 063502

Lemaître, G., 1927, Annales de la Société Scientifique de Bruxelles, 47, 49

Lemaître, G., 1931a, Nature, 127, 706

Lemaître, G., 1931b, MNRAS, 41, 483

Lin, C. C., Mestel, L., Shu, F. H., 1965, ApJ, 142, 1431

Linde, A., 1982, Phys. Lett. B, 108, 389

Linde, A., 1983, Phys. Lett. B, 129, 177

Lovell, M. R., Eke, V., Frenk, C. S., Gao, L., Jenkins, A., Theuns, T., Wang, J., White, S. D. M., Boyarsky, A., Ruchayskiy, O., 2012, MNRAS, 420, 2318

Lovell, M. R., Frenk, C. S., Eke, V. R., Jenkins, A., Gao, L.,Theuns, T., 2014, MNRAS, 439, 300

Luminet, J. P., 2015, arXiv:1503.08304

LUX Collaboration, Akerib, D. S., Araujo, H. M., Bai, X., Bailey, A. J., Balajthy, J., Bedikian, S., Bernard, E., Bernstein, A., Bolozdynya, A., Bradley, A., Byram, D., Cahn, S. B., Carmona-Benitez, M. C., Chan, C., Chapman, J. J., Chiller, A. A., Chiller, C., Clark, K., Coffey, T., Currie, A., Curioni, A., Dazeley, S., de Viveiros, L., Dobi, A., Dobson, J., Dragowsky, E. M., Druszkiewicz, E., Edwards, B., Faham, C. H., Fiorucci, S., Flores, C., Gaitskell, R. J., Gehman, V. M., Ghag, C., Gibson, K. R., Gilchriese, M. G. D., Hall, C., Hanhardt, M., Hertel, S. A., Horn, M., Huang, D. Q., Ihm, M., Jacobsen, R. G., Kastens, L., Kazkaz, K., Knoche, R., Kyre, S., Lander, R., Larsen, N. A., Lee, C., Leonard, D. S., Lesko, K. T., Lindote, A., Lopes, M. I., Lyashenko, A., Malling, D. C., Mannino, R., McKinsey, D. N., Mei, D.-M., Mock, J., Moongweluwan, M., Morad, J., Morii, M., Murphy, A. S. J., Nehrkorn, C., Nelson, H., Neves, F., Nikkel, J. A., Ott, R. A., Pangilinan, M., Parker, P. D., Pease, E. K., Pech, K., Phelps, P., Reichhart, L., Shutt, T., Silva, C., Skulski, W., Sofka, C. J., Solovov, V. N., Sorensen, P., Stiegler, T., O'Sullivan, K., Sumner, T. J., Svoboda, R., Sweany, M., Szydagis, M., Taylor, D., Tennyson, B., Tiedt, D. R., Tripathi, M., Uvarov, S., Verbus, J. R., Walsh, N., Webb, R., White, J. T., White, D., Witherell, M. S., Wlasenko, M., Wolfs, F. L. H., Woods, M., Zhang, C., 2014, Phys. Rev. Lett., 112, 091303

Macciò, A. V., Dutton, A. A., van den Bosch, F. C., Moore, B., Potter, D., Stadel, J., 2007, MNRAS, 378, 55

Macciò, A. V., Kang, X., Fontanot, F., Sommerville, R. S., Koposov, S. E., Monaco, P., 2010, MNRAS, 402, 1995

Macciò, A. V., Fontanot, F., 2010, MNRAS, 404, L16

Macciò, A. V., Stinson, G., Brook, C. B., Wadsley, J., Couchman, H. M. P., Shen, S., Gibson, B. K., Quinn, T., 2012, ApJ, 744, L9

Macciò, A. V., Paduroiu, S., Anderhalden, D., Schneider, A., Moore, B., 2012, MNRAS, 424, 1105

Macciò, A. V., Ruchayskiy, O., Boyarsky, A., Munoz-Cuartas, J. C., 2013, MNRAS, 428, 882

Malin, D. F., Carter, D., 1980, Nature, 285, 643

Marinacci, F., Pakmor, R., Springel, V., 2014, MNRAS, 437, 1750

Markovic, K., Viel, M., 2014, Publications of the Astronomical Society of Australia, 31, 6

Martin, S. P., 1998, A Supersymmetry Primer, Perspectives On Supersymmetry, 18, 1

Martizzi, D., Teyssier, R., Moore, B., 2013, MNRAS, 432, 1947

Mashchenko, S., Couchman, H. M. P., Wadsley, J., 2006, Nature, 442, 539

Mashchenko, S., Wadsley, J., Couchman, H. M. P., 2008, Science, 319, 174

Matteo, T. D., Springel, V., Hernquist, L., 2005, 433, 604

May, R. M., 1976, Nature, 261, 459

Melott, A., L., 1982, Phys. Rev. Lett., 48, 894

Melott, A., L., 1983, ApJ, 264, 59

Melott, A. L., Shandarin, S. F., Splinter, R. J., Suto, Y., 1997, ApJL, 479, L79

Melott, A., L., 2007, arXiv:0709.0745

Merritt, D., Navarro, J. F., Ludlow, A., Jenkins, A., 2005, ApJ, 624, L85

Milgrom, M., 1983, ApJ, 270, 365

Miller, R.H., 1964, ApJ, 140, 250

Miranda, M., Macciò, A. V., 2007, MNRAS, 382, 1225

Moffat, J. W., 2006, JCAP, 3, 4

Mohayaee, R., Salati, P., 2008, MNRAS, 390, 1297

Mohayaee, R., Shandarin, S. F., 2006, MNRAS, 366, 1217

Monaghan, J. J., Lattanzio, J. C., 1985, A&A, 149, 135

Moore, B. 1994, Nature, 370, 629

Moore, B., Ghigna, S., Governato, F., Lake, G., Quinn, T., Stadel, J., Tozzi, P., 1999, ApJL, 524, L19

Morselli, A., Lionetto, A., Cesarini, A., Fucito, F., Ullio, P., 2002, Nuclear Physics B Proceedings Supplements, 113, 213

Muccione, V., Pfenniger, D., 2006, EAS Publications Series, 20,291

Natarajan, A., Sikivie, P., 2006, Phys. Rev. D, 73, 023510

Navarro, J. F., Frenk, C. S., White, S. D. M., 1996, ApJ, 462, 563

Navarro, J. F., Frenk, C. S., White, S. D. M., 1997, ApJ, 490, 493

Navarro, J.F., Hayashi, E., Power, C., Jenkins, A. R., Frenk, C. S., White, S. D. M., Springel, V., Stadel, J., Quinn, T. R., 2004, MNRAS, 349, 1039

Okamoto, T., Eke, V. R., Frenk, C. S., Jenkins A., 2005, MNRAS, 363, 1299

Oh, S.-H., de Blok, W. J. G., Brinks, E., Walter, F., Kennicutt, R. C., Jr., 2011, AJ, 141, 193

Oñorbe, J., Boylan-Kolchin, M., Bullock, J. S., Hopkins, P. F., Kerěs, D., Faucher-Giguère, C. A., Quataert, E., Murray, N., 2015, arXiv:1502.02036

Ostriker, J., 1964, ApJ, 140, 1529

Padmanabhan, T., 2002, Theoretical Astrophysics, Vol. III, Cambridge University Press

Paduroiu, S., 2014, The Dark-Files: Dark Matter, Roostergnn Global News Network, Web

Paduroiu, S., Revaz, Y., Pfenniger, D., 2015, arXiv:1506.03789

Paduroiu, S., 2015, The Dark Side of the Universe, Brown Bear Books, Windmill Books Ltd., Kindle Edition

Pagels, H., Primack, J. R., 1982, Phys. Rev. Lett., 48, 223

Parry, O. H., Eke, V. R., Frenk, C. S., Okamoto, T., 2012, MNRAS, 419, 3304

Peacock, J., 1999, Cosmological Physics, Cambridge University Press

Peccei, R., Quinn, H. R., 1977a, Phys. Rev. Lett., 16, 1791

Peccei, R., Quinn, H. R., 1977b, Phys. Rev. D, 38, 1440

Peebles, P. J. E., 1982, ApJL, 263, L1

Peebles, P. J. E., 1993, Principles of Physical Cosmology, Princeton University Press

Peebles, P. J. E., Nusser, A., 2010, Nature, 465, 565

Pen, U. L., 1997, ApJ, 490, L127

Penarrubia, J., Navarro, J. F., McConnachie, A. W., 2008, ApJ, 673, 226

Peter, A. H. G., 2012, arXiv:1201.3942

Pfenniger, D., Muccione, V., 2006, A&A, 456, 45

Pierpaoli, E., Borgani, S., Masiero, A., Yamaguchi, M., 1998, Phys. Rev. D, 57, 2089

Planck Collaboration, Ade, P. A. R., Aghanim, N., Arnaud, M. , Ashdown, M., Aumont, J., Baccigalupi, C., Banday, A. J., Barreiro, R. B., Bartlett, J. G., et al., 2015, arXiv:1502.01589

Polisensky, E., Ricotti, M., 2011, Phys. Rev. D, 043506

Pontzen, A., Governato, F., 2012, MNRAS, 421, 3464

Prada, F., Klypin, A. A., Simonneau, E., Betancort-Rijo, J., Patiri, S., Gottlöber, S., Sanchez-Conde, M. A., 2006, ApJ, 645, 1001

Press, W. H., Schechter, P., 1974, ApJ, 187, 425

Primack, J. R., Blumenthal, G. R., 1984, What Is The Dark Matter?, NATO ASI C, 117, 163

Primack, J. R., 1997, arXiv:astro-ph/9707285

Primack, J. R., Gross, M. A. K., 2001, Current Aspects Of Neutrino Physics, Springer, 287

Prince, T. A., Binetruy, P., Centrella, J., Finn, L. S., Hogan, C., Nelemans, G., Phinney, E. S., Schutz, B., & LISA International Science Team, 2006, American Astronomical Society Meeting Abstracts, 38, 990

Raffelt, G. G., 1996, Stars as laboratories for fundamental physics: the astrophysics of neutrinos, axions and other weakly interacting particles, Chicago University Press

Raffelt, G. G., 2004, Phys. Lett. B592, 1, 391

Read, J. I., Gilmore, G., 2005, MNRAS, 356, 107

Reed, D. S., Bower, R., Frenk, C. S., Jenkins, A., Theuns, T., 2007, MNRAS, 374, 2

Reed, D. S., Smith, R. E., Potter, D., Schneider, A., Stadel, J., Moore, B., 2013, MNRAS, 431, 1866

Reid, M. J., 2009, Int. Jr. Mod. Phys. D, 18, 889

Ringwald, A., Wong, Y. Y. Y., 2004, JCAP, 12, 5

Robertson, B., Bullock, J. S., Cox, T. J., Matteo, T. D., Hernquist, L., Springel, V., Yoshida, N., 2006, ApJ, 645, 986

Robertson, B. E., Kravtsov, A. V., Tinker, J., Zentner, A. R., 2009, ApJ, 696, 636

Romano-Díaz, E., Shlosman, I., Hoffman, Y., Heller, C., 2008, ApJL, 685, L105

Romeo, A. B., Agertz, O., Moore, B., Stadel, J., 2008, ApJ, 686, 1

Roszkowski, L., 1993, arXiv:hep-ph/9302259

Rubin, V. C., Ford, Jr., W. K., 1970, ApJ, 159, 379

Rubin, V. C., Ford, W. K. J., . Thonnard, N., 1980, ApJ, 238, 471

Salam, A., Strathdee, J., 1976, Phys. Lett., 61B, 449

Sales, L. V., Navarro, J. F., Abadi, M. G., Steinmetz, M., 2007, MNRAS, 379, 1475

Sales, L. V., Navarro, J. F., Schaye, J., Dalla Vecchia, C., Springel, V., Booth, C. M., 2010, MNRAS, 409, 1541

Salmon, J., 1996, ApJ, 460, 59

Salucci, P., Wilkinson, M. I., Walker, M. G., Gilmore, G. F., Grebel, E. K., Koch, A., Frigerio Martins, C., Wyse, R. F. G., 2012, MNRAS, 420, 2034

Sánchez-Salcedo, F. J., Reyes-Iturbide, J., Hernandez, X., 2006, MNRAS, 370, 1829

Sawala, T., Scannapieco, C., Maio, U., White, S. 2010, MNRAS, 402, 1599

Scannapieco, C., Tissera, P. B., White, S. D. M., Springel, V., 2005, MNRAS, 364, 552

Scannapieco, C., Tissera, P. B., White, S. D. M., Springel, V., 2006, MNRAS, 371, 1125

Scannapieco, C., Tissera, P. B., White, S. D. M., Springel, V., 2008, MNRAS, 389, 1137

Schneider, A., Anderhalden, D., Macciò, A. V., Diemand, J., 2014, MNRAS, 441, L6

Schmidt, K. B., Hansen, S. H., Macciò, A. V., 2008, ApJL, 689, L33

Schneider, A., Smith, R. E., Macciò, A. V., Moore, B., 2012, MNRAS, 424, 684

Schneider, A., Smith, R. E., Reed, D, 2013, MNRAS, 433, 1573

Seljak, U., Zaldarriaga, M., 1996, ApJ, 469, 437

Seljak, U., Makarov, A., McDonald, P., Trac, H., 2006, Phys. Rev. Lett., 97, 191303

Shao, S., Gao, L., Theuns, T., Frenk, C. S., 2013, MNRAS, 430, 2346

Shapiro, P. R., Struck-Marcell, C., Melott, A. L., 1983, 275, 413

Shaposhnikov, M., Tkachev, I., 2006, Phys. Rev. B, 639, 414

Shaposhnikov, M., 2008, Lecture from the Eleventh Marcel Grossmann Meeting, 1006

Sheth, R. K., Mo, H. J., Tormen, G., 2001, 323, 1

Shi, X., Fuller, G. M., 1999, Phys. Rev. Lett., 82, 2832

Sikivie, P., Ipser, J. R., 1992, Phys. Lett. B, 291, 288

Sikivie, P., Tkachev, I. I., Wang, Y., 1997, Phys. Rev. D, 56, 1863

Smith, R. E., Markovic, K., 2011, Phys. Rev. D, 84, 063507

Sofue, Y., 2013, PASJ, 65, 118

de Souza, R. S., Rodrigues, L. F. S., Ishida, E. E. O., Opher, R. 2011, MNRAS, 415, 2969

de Souza, R. S., Mesinger, A., Ferrara, A., Haiman, Z., Perna, R., Yoshida, N., 2013, MNRAS, 432, 3218

Splinter, R. J., Melott, A. L., Shandarin, S. F., Suto, Y., 1998, ApJ, 497, 38

Springel, V., 2005, MNRAS, 364, 1105

Springel, V., White, S. D. M., Jenkins, A., Frenk, C. S., Yoshida, N., Gao, L., Navarro, J., Thacker, R., Croton, D., Helly, J., Peacock, J. A., Cole, S., Thomas, P., Couchman, H., Evrard, A., Colberg, J., Pearce, F., 2005, Nature, 435, 629

Springel, V., Hernquist, L., 2005, ApJ, 622, L9

Springel, V., Frenk, C. S., White, S. D. M., 2006, Nature, 440, 1137

Springel, V., Wang, J., Vogelsberger, M., Ludlow, A., Jenkins, A., Helmi, A., Navarro, J. F., Frenk, C. S., White, S. D. M., 2008, MNRAS, 391, 1685

Stadel, J., 2001, PhD Thesis, University of Washington

Stadel, J., Potter, D., Moore, B., Diemand, D., Madau, P., Zemp, M., Kuhlen, M., Quilis, V., 2009, MNRAS, 391, L21

Steffen, F. D., 2007, arXiv:0711.1240

Strigari, L. E., Bullock, J. S., Kaplinghat, M., Kravtsov, A. V., Gnedin, O. Y., Abazajian, K., Klypin, A. A., 2006, ApJ, 652, 306

Susskind, L., Thorlacius, L., Uglum, J., 1993, Phys. Rev. D, 48, 3743

Susskind, L., 2008, The Cosmic Landscape: String Theory and the Illusion of Intelligent Design, Little & Brown

Takayama, F., Yamaguchi, M., 2000, Phys. Lett. B, 485, 388

Taylor, J. E., Navarro, J. F., 2001, ApJ, 563, 483

Tegmark, M., & The SDSS Team., 2006, Phys. Rev. D, 74, 123507

Tegmark, M., 2009, Universe or Multiverse?, Cambridge University Press

Tikhonov, A. V., Gottlöber, S., Yepes, G., Hoffman, Y., 2009, MNRAS, 399, 1611

Tinker, J., Kravtsov, A. V., Klypin, A., Abazajian, K., Warren, M., Yepes, G., Gottlöber, S., Holz, D. E., 2008, 688. 709

Tinsley, B.M., Gunn, J.E., 1976, ApJ, 203, 52

Tremaine, S., Gunn, J. E., 1979, Phys. Rev. Lett., 42, 407

Tremaine, S., 1999, MNRAS, 307, 877

Trodden, M., Carroll, S.M., 2004, arXiv:0401547

Turner, M. S., 2001, arXiv:0108103

Turner, M. S., 2002a, Int. Journ. of Mod. Phys. A, 17, 180

Turner, M. S., 2002b, ApJL, 576, L101

Unruh, W. G., 1976, Phys. Rev. D, 14, 870

Valageas, P., 2012, Phys. Rev. D, 86, 123501

de Vega, H. J., Sanchez, N. G., 2011, arXiv:1109.3187

de Vega, H. J., Falvella, M. C., Sanchez, N. G., 2012, arXiv:1203.3562

de Vega, H. J., Salucci, P., Sanchez, N. G., 2012, New Astronomy, 17, 653

Viel, M., Lesgourgues, J., Haehnelt, M. G., Matarrese, S., Riotto, A., 2005, Phys. Rev. D, 71, 063534

Viel, M., Becker, G. D., Bolton, J. S., Haehnelt, M. G., Rauch, M., Sargent, W. L. W., 2008, Phys. Rev. Lett., 100, 041304

Villaescusa-Navarro, F., Dalal, N., 2011, JCAP, 1103, 024

Vissani, F., Pagliaroli, G., 2011, A&A, 528, L1

Vogelsberger, M., White, S. D. M., 2011, MNRAS, 413, 1419

Walker, M. G., Penarrubia, J., 2011, ApJ, 742, 20

Walker, M., 2013, Planets, Stars and Stellar Systems: Galactic Structure and Stellar Populations, Springer, 5, 1039

Wang, J.,White, S. D. M., 2007, MNRAS, 380, 93

Wasserman, I., 1986, Phys. Rev. D, 33, 271

Weinberg, S., 1962, Phys.Rev, 128, 1457

Weinberg, S., 1972, Gravitation and Cosmology, Wiley

Weinberg, S., 2008, Cosmology, Oxford University Press

West, R. M., Lauberts, A., Jorgensen, H. E., Schuster, H. E., 1987, A&A, 177, L1

White, S. D. M., Frenk, C. S., Davis, M., 1983, ApJL, 274, L1

White S. D. M., 1996, Cosmology and Large Scale Structure, Formation and Evolution of Galaxies, Schaeffer R., Silk J., Spiro M., Zinn-Justin J., 349

York, D. G., Adelman, J., Anderson, Jr., J. E., Anderson, S. F., Annis, J., Bahcall, N. A., Bakken, J. A., Barkhouser, R., Bastian, S., Berman, E., Boroski, W. N., Bracker, S., Briegel, C., Briggs, J. W., Brinkmann, J., Brunner, R., Burles, S., Carey, L., Carr, M. A., Castander, F. J., Chen, B., Colestock, P. L., Connolly, A. J., Crocker, J. H., Csabai, I., Czarapata, P. C., Davis, J. E., Doi, M. , Dombeck, T., Eisenstein, D. , Ellman, N., Elms, B. R. , Evans, M. L., Fan, X. , Federwitz, G. R., Fiscelli, L. , Friedman, S., Frieman, J. A., Fukugita, M., Gillespie, B., Gunn, J. E., Gurbani, V. K., de Haas, E. , Haldeman, M., Harris, F. H., Hayes, J., Heckman, T. M., Hennessy, G. S., Hindsley, R. B., Holm, S., Holmgren, D. J. , Huang, C. H., Hull, C., Husby, D. , Ichikawa, S. I., Ichikawa, T., Ivezić, Ž., Kent, S., Kim, R. S. J., Kinney, E., Klaene, M., Kleinman, A. N., Kleinman, S., Knapp, G. R., Korienek, J., Kron, R. G., Kunszt, P. Z., Lamb, D. Q., Lee, B., Leger, R. F., Limmongkol, S., Lindenmeyer, C., Long, D. C., Loomis, C., Loveday, J., Lucinio, R., Lupton, R. H., MacKinnon, B., Mannery, E. J., Mantsch, P. M., Margon, B., McGehee, P., McKay, T. A., Meiksin, A., Merelli, A., Monet, D. G., Munn, J. A., Narayanan, V. K., Nash, T., Neilsen, E., Neswold, R., Newberg, H. J., Nichol, R. C., Nicinski, T., Nonino, M., Okada, N., Okamura, S., Ostriker, J. P., Owen, R., Pauls, A. G., Peoples, J., Peterson, R. L., Petravick, D., Pier, J. R., Pope, A., Pordes, R., Prosapio, A., Rechenmacher, R., Quinn, T. R., Richards, G. T., Richmond, M. W., Rivetta, C. H., Rockosi, C. M., Ruthmansdorfer, K., Sandford, D., Schlegel, D. J., Schneider, D. P. , Sekiguchi, M., Sergey, G., Shimasaku, K., Siegmund, W. A., Smee, S., Smith, J. A., Snedden, S., Stone, R., Stoughton, C., Strauss, M. A., Stubbs, C., SubbaRao, M., Szalay, A. S., Szapudi, I., Szokoly, G. P., Thakar, A. R., Tremonti, C., Tucker, D. L., Uomoto, A., Vanden Berk, D., Vogeley, M. S., Waddell, P., Wang, S. I., Watanabe, M., Weinberg, D. H., Yanny, B., Yasuda, N. & SDSS Collaboration, 2000, AJ, 120, 1579

Zavala, J., Jing, Y. P., Faltenbacher, A., Yepes, G., Hoffman, Y., Gottlöber, S., Catinella, B., 2009, ApJ, 700, 1779

Zel'dovich, Y. B., 1970, A&A, 5, 84

Zolotov, A., Brooks, A. M., Willman, B., Governato, F., Pontzen, A.,Christensen, C., Dekel, A., Quinn, T., Shen, S., Wadsley, J., 2012, ApJ, 761, 71

Zentner, A. R., Bullock, J. S., 2003, ApJ, 598, 49

Zwicky, F., 1933, Helvetica Physica Acta, 6, 110

Zwicky, F., 1937, ApJ, 86, 217

SINZIANA PADUROIU

Email: sinziana.paduroiu@unige.ch
sinziana.paduroiu@gmail.com

## Education and Training

2008 - 2015 **Observatory of Geneva, University of Geneva**
Ph.D. Thesis: Structure Formation in Warm Dark Matter Cosmologies

2006 - 2008 **Institute for Theoretical Physics, University of Zürich**
Postgraduate Research – Cosmology and Computational Astrophysics Group

2004 - 2006 **University of Bucharest, Romania**
M.Sc. in Physics – Department of Atomic and Nuclear Interactions, Astrophysics, Elementary Particles and Applications

2005 - 2006 **Max Planck Institute for Radio Astronomy, Bonn**
Erasmus – Socrates scholarship – Theory Group

2000 - 2004 **Faculty of Physics, University of Bucharest**
B.Sc. in Physics - Department of Atomic and Nuclear Interactions
Specialization: Astrophysics

2000 - 2004 **Faculty of Philosophy, University of Bucharest**

## Publications

- **S. Paduroiu**, Y. Revaz, D. Pfenniger, Structure formation in warm dark matter cosmologies: Top - Bottom Upside - Down, 2015, arXiv:1506.03789, submitted to MNRAS
- J. Sarfatti & **S. Paduroiu,** What if the black hole event horizon has a quantum thickness?, 2015, in preparation
- A.V. Maccio, **S. Paduroiu**, D. Anderhalden, A. Schneider, B. Moore, Cores in warm dark matter haloes: a Catch 22 problem 2012, MNRAS, 424, 1105
- **S. Paduroiu** et al., 2015, 14$^{th}$ Marcel Grossmann Meeting proceedings, in preparation
- **S. Paduroiu** et al. 2012 Towards the Chalonge 16th Paris Cosmology Colloquium 2012: Highlights and Conclusions of the Chalonge 15th Paris Cosmology Colloquium 2011 H. J. de Vega, M. C. Falvella, and N. G. Sanchez, arXiv:1203.3562, proceedings
- **S. Paduroiu** et al. 2011, Warm dark matter in the galaxies: theoretical and observational progresses, Highlights and conclusions of the Chalonge Meudon workshop 2011 H. J. de Vega and N. G. Sanchez, arXiv:1109.3187, proceedings

- **Sinziana Paduroiu,** The Dark Side of the Universe, E-book, 2015, Brown Bear Books - Windmill Books Ltd., Kindle Edition
- **Sinziana Paduroiu,** The Dark Files: Dark Matter, 2014, ROOSTERGNN Global News Network, Web

## Invited lectures, contributed talks and posters

- 19th Paris Cosmology Colloquium, 2015, **invited lecture**
- 14th Marcel Grossmann Meeting, Rome, 2015, **invited talk**
- Ecole Internationale Daniel Chalonge, Meudon Workshop, 2015, **invited lecture**
- EWASS – European Week of Astronomy and Space Science, Geneva, 2014, **contributed talk**
- Ecole Internationale Daniel Chalonge, Meudon Workshop, 2014, **invited lecture**
- NASA Ames Research Center, Mountain View CA, 2013, **invited seminar**
- Ecole Internationale Daniel Chalonge Meudon Workshop 2013, **invited lecture**
- Laboratoire de physique nucléaire et de hautes énergies LPNHE, Paris, 2013, **invited seminar**
- SU workshop – Galaxy Formation & Large Scale Structures: Theory vs Observations, Paris, 2012, **invited lecture**
- 15th Paris Cosmology Colloquium, 2011, **contributed talk & poster**
- Ecole Internationale Daniel Chalonge, Meudon Workshop CIAS, 2011, **contributed talk & poster**
- UNESCO Invisible Universe International Conference – Towards A New Cosmological Paradigm, Paris, 2009, **contributed talk**
- Astrophysics, Dynamical Systems and Fractals - Past and Future, a conference to mark the formal retirement of Prof. Mircea V. Rusu, Bucharest, 2007, **co-organizer & talk**
- 15th International Conference on Control Systems and Computer Science (CSCS), 2nd Symposium on Interdisciplinary Approaches in Fractal Analysis, Bucharest, 2005, **contributed talk**
- British-Romanian-Hungarian N+N+N Workshop on Plasma and Astrophysics: from laboratory to outer space, Cluj-Napoca, 2005, **contributed talk**

## Schools, Conferences and Workshops

- CADMOS – Center for Advanced Modeling Science, Activity Days, Leysin, Switzerland, 2013
- 16th Paris Cosmology Colloquium, The New Standard Model Of The Universe: Lambda Warm Dark Matter Theory And Observations, 2012
- Ecole Internationale Daniel Chalonge, Meudon Workshop CIAS, Warm Dark Matter Galaxy Formation In Agreement With Observations, 2012
- 4th International Workshop DICE, From Quantum Mechanics through Complexity to Spacetime: the role of emergent dynamical structures, Toscana, 2008
- Next Generation of Computational Models of Baryonic Physics in Galaxy Formation: from Protostellar Cores to Disk Galaxies, Zürich, 2007

- 37th Saas-Fee Advanced Course of the Swiss Society for Astrophysics and Astronomy - Origin of the Galaxy and the Local Group , Mürren, 2007
- 3rd Aegean Summer School, The Invisible Universe: Dark Matter and Dark Energy, Karfas, 2005
- Carpatian Summer School of Physics, Exotic Nuclei and Nuclear/Particle Astrophysics, Mamaia-Constanta, 2005
- International School on AstroParticle Physics, European Doctorate School (ISAPP), L.N.G.S. L'Aquila, 2004

## Teaching Experience

2009 - 2013 Mentoring undergraduate students - supervising projects, University of Geneva
2007 T.A., An Overview of Modern Astrophysics - Prof. V. Tran, University of Zürich
2006 T.A., Astrophysics and Cosmology - Prof. Ph. Jetzer, University of Zürich
2000 - 2004 Pedagogical Module - University of Bucharest

## Scholarships and Grants

2013 Fondation Ernst et Lucie Schmidheiny conference travel grant
2012 Swiss Society for Astronomy and Astrophysics (SSAA) conference travel grant
2005 - 2006 Erasmus - Socrates Scholarship, Max Planck Institute for Radio Astronomy, Bonn
2005 - 2006 High Performance Scholarship for scientific activity, University of Bucharest
2000 - 2004 Yearly Merit Scholarship, University of Bucharest

## Public Outreach

Science and Culture Contributor for ROOSTERGNN Global News Network
Public visits and sessions at the Observatory of Geneva
Editor-in-chief for Faculty of Physics, University of Bucharest Newspaper